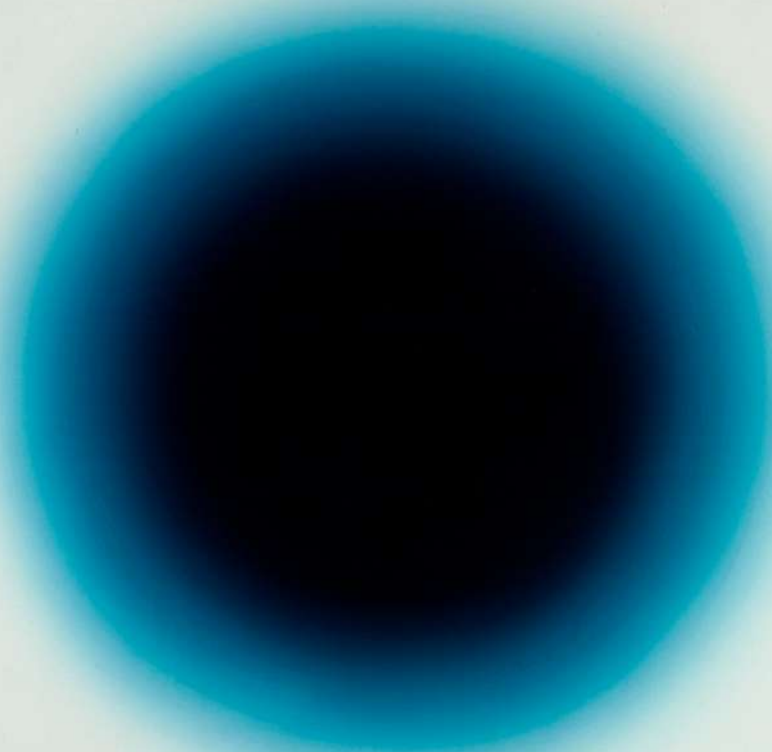
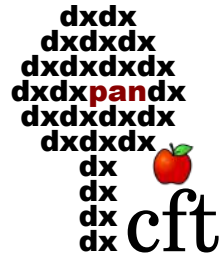


Jakub Kopyciński

**Low-dimensional Bose gases with competing interactions:
Non-linear effects in beyond-mean-field frameworks**



Centre for Theoretical Physics
of the Polish Academy of Sciences



Low-dimensional Bose gases with competing interactions: Non-linear effects in beyond-mean-field frameworks

Author
Jakub Kopyciński, MScEng

Supervisor
Krzysztof Pawłowski, DSc

Thesis submitted to the Centre for Theoretical Physics of the Polish Academy of Sciences
in accordance with the requirements for the degree of Doctor of Philosophy in Physics

Warsaw, 2024

The cover contains a reproduction of the following art piece:

E19, oil on canvas, 1966

by Wojciech Fangor (1922-2015)

on the sublicense for the use of the reproduction obtained from the National Museum in Warsaw (Muzeum Narodowe w Warszawie), the licence holder for the works of Wojciech Fangor.

This thesis contains the following publications reprinted in full:

J. Kopyciński, M. Łebek, M. Marciniak, R. Ołdziejewski, W. Górecki, K. Pawłowski

Beyond Gross-Pitaevskii equation for 1D gas: Quasiparticles and solitons,

SciPost Phys. **12**, 023 (2022)

on the CC BY 4.0 licence.

© J. Kopyciński *et al.*

J. Kopyciński, M. Łebek, W. Górecki, K. Pawłowski

Ultrawide dark solitons and droplet-soliton coexistence in a dipolar Bose gas with strong contact interactions,

Phys. Rev. Lett. **130**, 043401 (2023)

with the permission from American Physical Society.

© American Physical Society

J. Kopyciński, L. Parisi, N.G. Parker, K. Pawłowski

Quantum Monte Carlo-based density functional for one-dimensional Bose-Bose mixtures,

Phys. Rev. Res. **5**, 023050 (2023)

on the CC BY 4.0 licence.

© J. Kopyciński *et al.*

J. Kopyciński, B. Tüzemen, W. Górecki, K. Pawłowski, M. Łebek

Propagation properties and stability of dark solitons in weakly interacting Bose-Bose droplets,

J. Phys. B: At. Mol. Opt. Phys. **57** 035302 (2024)

on the CC BY 4.0 licence.

© J. Kopyciński *et al.*

*and that water these words what can they do what can they do prince*¹

¹Z. Herbert, 'Elegy of Fortinbras', *Selected Poems*, translated by Cz. Miłosz and P. Dale Scott, The Ecco Press, New York 1986, p. 99. ISBN 0-88001-099-1.

ACKNOWLEDGEMENTS

First of all, I would like to thank my whole family, especially the very best Mum in the world and my lovely Grannies. An enormous ‘thank you’ goes to Tosia for her constant love and support.

Let me also thank all my friends; Wiola, Aga, Gabi, Martyna, Karo, Paweł, and Fryderyk in particular – you have been invaluable over the past years!

I would like to express my gratitude to Krzysiek. If not for his ideas, I would have probably written a memoir (a dull one, without any great Proustian panache) titled *In Search of Lost Time* instead of this thesis. I would not have done it all without the help from my Varsovian collaborators Maciek Ł., Wojtek, Maciek M., Rafał, and Buğra.

I cannot forget about all the bonny lads and lasses I met when I ran to the Toon. Nick, Holly, Tom, Ryan, Sri, and Luca – ’twas a canny time spent there.

I must appreciate the work of all my teachers throughout the whole education period, particularly my very first academic mentor, Prof. Gabriel Wlazłowski, who showed me the world of ultracold gases in late 2017 and has supported me since then.

Last but not least, I would like to thank His Barking Fourpawness Jimin the Fluffiest, King of the Armchair and His other Blankets, Defensor of Treats, for his unrestrained joy of life and interspecies friendship.

This research was supported by
the (Polish) National Science Centre (Grant No. 2019/34/E/ST2/00289).

ABSTRACT

This Thesis focuses on the investigation of dark solitons and quantum droplets in systems with competing interactions. The scope of the studies is narrowed down to quasi-one-dimensional dipolar Bose gases and one-dimensional two-component bosonic mixtures.

The properties of solitons are shown, including their stability and propagation, especially the possibility of a dark soliton-quantum droplet coexistence. A benchmark of the models, which are later used to reveal the presence of ultrawide solitons with peculiar properties and dispersion relation, is done. Furthermore, a connection between the stability and dispersion relation is established.

The theoretical treatment of bosonic gases presented here, offers ground-state energies, chemical potentials, and droplet bulk densities quantitatively agreeing with *ab initio* analytical models or quantum Monte Carlo data.

STRESZCZENIE

Niskowymiarowe gazy bozonowe z konkurującymi oddziaływaniami: Efekty nieliniowe powyżej przybliżenia pola średniego.

Niniejsza rozprawa skupia się na badaniu ciemnych solitonów i kropli kwantowych w układach z konkurującymi oddziaływaniami. Zakres pracy został ograniczony do quasi-jednowymiarowych gazów Bosego i jednowymiarowych dwuskładnikowych mieszanin bozonowych.

Pokazane są własności solitonów, w tym dotyczące ich stabilności i propagacji, a w szczególności możliwości współistnienia ciemnych solitonów z kroplami kwantowymi. Modele te zostały przetestowane i użyte potem, by pokazać obecność ultraszerokich solitonów mających specyficzne właściwości i relację dyspersyjną. Co więcej, ustanowione zostało połączenie między stabilnością solitonów a relacją dyspersyjną właśnie.

Zaprezentowane tu narzędzia teoretyczne do opisu gazów bozonowych zapewniają energie stanu podstawowego, potencjał chemiczny i gęstość równowagową kropli ilościowo zgodne z modelami *ab initio* – rozwiązywalnymi analitycznie czy danymi uzyskanymi za pomocą metod Monte Carlo.

RÉSUMÉ

Gaz de bosons en réduite dimension avec des interactions concurrentes : Effets non linéaires au-dessus du champ moyen.

Cette thèse se concentre sur l'étude des solitons sombres et gouttes quantiques dans les systèmes avec des interactions concurrentes. La portée des études est réduite aux gaz de Bose dipolaires quasi-unidimensionnels et aux gaz à deux composant bosoniques unidimensionnels.

On étudie les propriétés des solitons, leur stabilité et propagation, notamment la possibilité de coexistence de solitons sombres avec des gouttes quantiques. On teste des modèles au-dessus de champs moyen et puis les utilise pour montrer la présence de solitons ultra-larges qui ont des propriétés spécifiques et une relation de dispersion avec deux sous-branches. De plus, on établit une connexion de stabilité avec les sous-branches d'excitation.

Ce traitement théorique des gaz bosoniques offre des énergies d'état de base, le potentiel chimique et la densité des gouttes en accord quantitatif avec les modèles *ab initio* analytiques ou les données obtenues avec des méthodes Monte Carlo.

CONTENTS

Acknowledgements	vii
Abstract	ix
Streszczenie	xi
Résumé	xiii
Part I. Commentary on the collection of publications	1
1. Broad context, basic description of the scientific problem and its significance	3
2. Introduction to Bose-Einstein condensation	9
3. General framework and methods	15
3.1. Single-component gases with contact interactions in 1D	15
3.2. Two-component gases with competing contact interactions	18
3.3. Single-component gases with dipolar interactions	21
4. Dark solitons in ultracold matter	23
5. Quantum droplets in dipolar and two-component gases	29
6. Description of the main results	31
6.1. Overview of Ref. [J. Kopyciński <i>et al.</i> , SciPost Phys. 12 , 023 (2022)]	31
6.2. Overview of Ref. [J. Kopyciński <i>et al.</i> , Phys. Rev. Lett. 130 , 043401 (2023)]	34
6.3. Overview of Ref. [J. Kopyciński <i>et al.</i> , Phys. Rev. Res. 5 , 023050 (2023)]	37
6.4. Overview of Ref. [J. Kopyciński <i>et al.</i> , J. Phys. B: At. Mol. Opt. Phys. 57 , 035302 (2024)]	42
6.5. Concluding remarks	46
References	49
Part II. Publications	61
1. [J. Kopyciński <i>et al.</i> , Beyond Gross-Pitaevskii equation for 1D gas: Quasiparticles and solitons, SciPost Phys. 12 , 023 (2022)]	63
2. [J. Kopyciński <i>et al.</i> , Ultrawide dark solitons and droplet-soliton coexistence in a dipolar Bose gas with strong contact interactions, Phys. Rev. Lett. 130 , 043401 (2023)]	87
3. [J. Kopyciński <i>et al.</i> , Quantum Monte Carlo-based density functional for one-dimensional Bose-Bose mixtures, Phys. Rev. Res. 5 , 023050 (2023)]	93
4. [J. Kopyciński <i>et al.</i> , Propagation properties and stability of dark solitons in weakly interacting Bose-Bose droplets, J. Phys. B: At. Mol. Opt. Phys. 57 , 035302 (2024)]	103
Complete list of PhD candidate's publications	111

Part I.

Commentary on the collection of publications

[T1] J. Kopyciński, Maciej Łebek, Maciej Marciniak, Rafał Ołdziejewski, Wojciech Górecki, and Krzysztof Pawłowski, Beyond Gross-Pitaevskii equation for 1D gas: quasiparticles and solitons, *SciPost Phys.* **12**, 023 (2022).

[T2] J. Kopyciński, Maciej Łebek, Wojciech Górecki, and Krzysztof Pawłowski, Ultrawide dark solitons and droplet-soliton coexistence in a dipolar Bose gas with strong contact interactions, *Phys. Rev. Lett.* **130**, 043401 (2023).

[T3] Jakub Kopyciński, Luca Parisi, Nick G. Parker, and Krzysztof Pawłowski, Quantum Monte Carlo-based density functional for one-dimensional Bose-Bose mixtures, *Phys. Rev. Res.* **5**, 023050 (2023).

[T4] J. Kopyciński, Maciej Łebek, Maciej Marciniak, Rafał Ołdziejewski, Wojciech Górecki, Krzysztof Pawłowski, Propagation properties and stability of dark solitons in weakly interacting Bose–Bose droplets, *J. Phys. B: At. Mol. Opt. Phys.* **57**, 035302 (2024).

1. Broad context, basic description of the scientific problem and its significance

‘It starts with an earthquake and the tension rises.’ Not only can this sentence describe the scheme of a Hitchcockian film but, alas, also the birth and lifetime of a disastrous tsunami wave. Before the tsunami reaches the shallows and builds up to even a 30-metre-high wall of water, it remains an almost completely inconspicuous shape-preserving wave of an amplitude of sometimes less than a single metre, yet moving at a high pace of a few hundred kilometres per every hour [1, 2].

One of these features will remain crucial throughout this Thesis as it characterizes a class of waves called *solitons*. We shall follow the definition of a soliton, which is common in the ultracold gas community, i.e. of a localized disturbance propagating without changes in its shape. Unlike in mathematics, we will not demand solitons to preserve their shape upon collisions [3]. Thus, we will use the names *solitons* and *solitary waves* synonymously.

Speaking of other branches, solitons have been created in classical fluids by natural phenomena in the form of a tsunami² or a harmless wave like the one observed in 1834 in the Scottish Union Canal and later pioneeringly described by J. Scott Russell. He subsequently recreated solitary waves in his laboratory [5]. The theoretical research on the phenomenon in question was crowned by the Korteweg-de Vries equation describing waves in shallow waters [6]. An exemplary soliton induced in water is shown in Fig. 1.

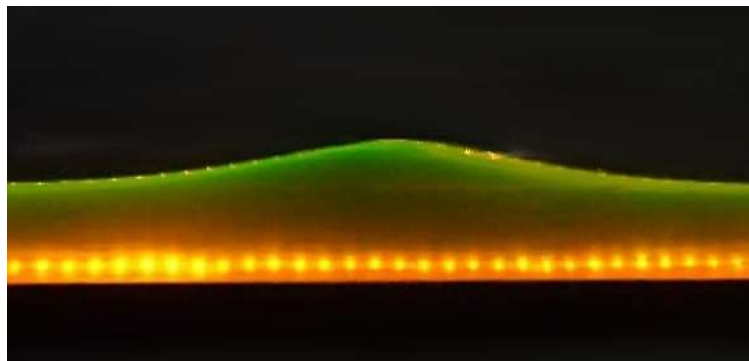


FIG. 1. Soliton induced in water, colouring due to the use of fluorescein.

Figure reprinted on CC-BY SA 2.5 licence.

© 2009 by Ch. Finot and K. Hammani (Univ. of Bourgogne)

<https://commons.wikimedia.org/w/index.php?curid=5776418>

The notion of solitons appeared also in the physics of plasma in the late 1950s. The presence of collisionless hydromagnetic waves was predicted in low-density plasma [7, 8] at that time and detected almost five decades later in the Earth's magnetopause [9]. Optical fibres are yet another example of a medium, where we can deal with soliton propagation [10]. Optics enables us to look into solitary waves at distances thousand times larger than the width of the wave itself [11]. Solitons can even appear in field theory as solutions of non-linear models [12].

² Although the theory of solitons does not necessarily have to be employed to study the propagation of tsunamis as there are alternative approaches proposed, e.g. in Ref. [4].

This Thesis will not illuminate either the solitons in non-linear optics or the ones in classical fluids. As timidly suggested a bit earlier, we shall put our focus on ultracold gases instead.

At an extremely low temperature, low density and in high vacuum, we can produce a state of matter, called Bose-Einstein condensate (BEC), in which the quantum properties play a crucial role [13]. Practically all atoms gather in a single state [14]. In systems at low temperatures the interactions between atoms are tunable. We may say that these interactions translate to non-linearities in the mathematical equations.

When the non-linear terms happen to compensate for the dispersion term (arising from quantum pressure), we have stable solitary waves as solutions of the equations [3]. The question is – have we got any reality which stands behind these equations?

Well, indeed, the solitons are present in cold gases [15], as we can see in Fig. 2. A rarefaction, visible as a dark fringe, is induced in the gas. Then, it separates into two solitary waves, which propagate in the system. **The soliton is, in this case, a depletion of the gas density. This type of solitary waves, called dark solitons³, will be the focal point of our interest throughout this Thesis.**

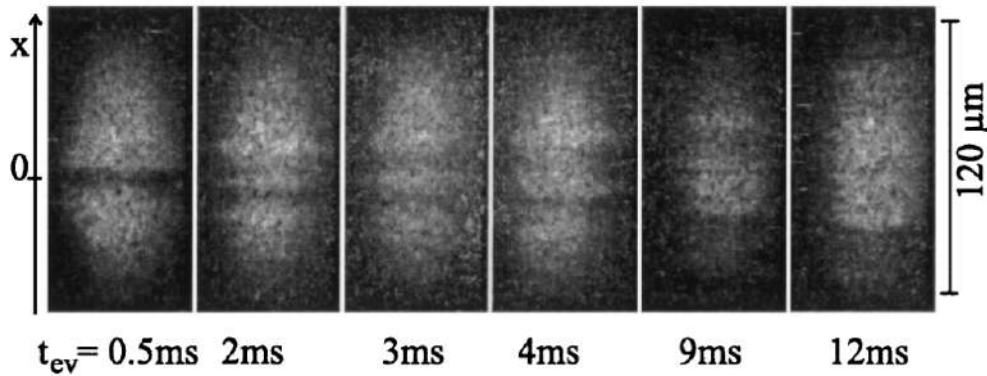


FIG. 2. Images of dark solitons travelling through an ultracold gas of rubidium-87 atoms at different evolution times t_{ev} .

Figure reprinted with permission from [S. Burger *et al.*, Phys. Rev. Lett. **83**, 5198 (1999)].

© 1999 by the American Physical Society.

The size of the two dark fringes is of the order of $5 \mu\text{m}$. They are only visible thanks to the expansion of the gas from a trap, where it is initially produced and kept. During such a procedure, the gas increases its size (and so do the solitons), and an absorption image can be taken. On one hand, it enables us to reveal tiny traits of the gas density profile, on the other one, such a free expansion causes noise and changes the geometry of the system [3]. The solitons become longer and more prone to bending and decaying into other structures like vortices [16, 17].

If only we had a system with interactions compensating the dispersion, still enabling the existence of wide solitary waves, though, we would be able to take an *in situ* image of a soliton. A rough intuition behind the soliton width tells us that the stronger the interaction

³ Dark solitons owe their name to optics. The density depletion in ultracold atoms corresponds to the lack of light, a dark spot in the non-linear optical medium.

between the atoms is, the smaller the width we can expect. Strongly interacting atoms will try to ‘jostle’ to get some space at the cost of the soliton size. Therefore, one needs some softening of the interatomic repulsion. Another type of interaction, an attractive one, might be a good candidate to effectively widen the soliton. First and foremost, it is essential to check if the solitons exist in systems with competing interactions or not. Such systems display attention-drawing properties, which we shall see in a moment. The quest for solitons in this case is one of the crucial points of this Thesis.

Let us, for instance, look at gases of highly magnetic atoms. In principle, the dipolar interaction potential in such gases is anisotropic, we can make it effectively attractive, though [18, 19]. If we employ the most commonly used equation, called the Gross-Pitaevskii equation (GPE), the predictions given by this equation is usually consistent with experiments [20, 21]. It is true even when the dynamics is violent, e.g. if we have shock waves travelling in the BEC [22, 23]. According to the GPE, the dipolar gas should be either stable (when the overall interaction is repulsive) or collapse and later explode (in the attractive overall interaction case), just like supernovae do. An example of a dipolar Bose-nova, is shown in Fig. 3. However, in a small interaction range, the results of experiments with highly dipolar gases do not always match the predictions made with the GPE [24, 25]. Well, in the GPE derivation, we use the macroscopic occupation of the BEC only to assume that literally all atoms are in a single state. Whereas, it is not entirely true – the GPE needs amendments to work in a broader spectrum of interactions.

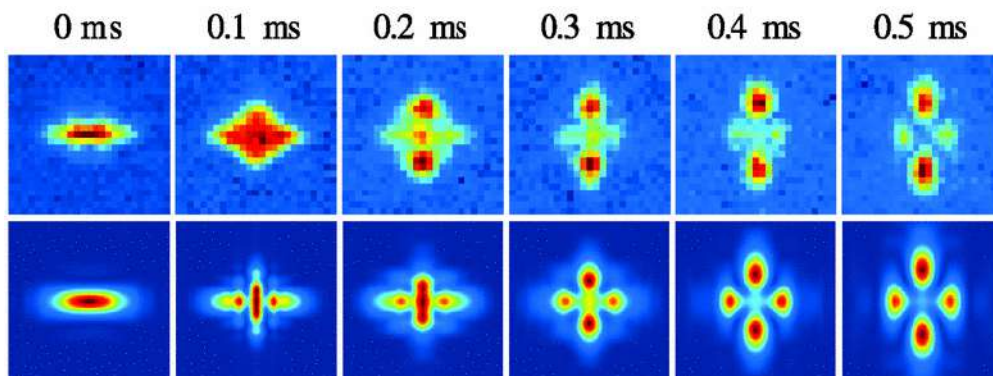


FIG. 3. Dipolar Bose-nova. The explosion of a chromium-52 condensate with anisotropic dipolar interactions. Experiment (top row) and GPE simulations (bottom row) results for different times of evolution. The characteristic d -wave shape is exactly due to anisotropy of the interaction potential. Each panel represents an area of $130 \mu\text{m} \times 130 \mu\text{m}$.

Figure reprinted with permission from [T. Lahaye *et al.*, Phys. Rev. Lett. **101**, 080401 (2008)].

© 2008 by the American Physical Society.

An analogous failure of the GPE is present in yet another system with competing interactions, namely Bose-Bose mixtures [26]. In these systems, we have two types of atoms, which interact with each other. We will be interested in a specific scenario. Namely, we want the interactions between the atoms of the same type to be repulsive. Atoms of different kinds ought to attract each other. This system was also thought to be either stable or to form a Bose-nova.

The key to a qualitatively correct equation is the inclusion of the term describing quantum fluctuations [27]. In other words, we say that the macroscopically occupied state is influenced by a small perturbation coming from atoms being in other, i.e. excited, states. This additional part of the equation is called the Lee-Huang-Yang (LHY) term [28, 29] and it prevents the gas from collapsing in a narrow range of interactions.

What happens with the gas then? In simple terms, we observe its liquefaction to droplets. In the very first experiment with ultracold droplets, the scientists obtained self-bound atomic clusters of highly magnetic dysprosium with $\sim 5x$ higher density than the BEC and a lifetime of around 100 ms [24]. Each droplet contains approx. 2000 atoms and by regulating the total number of atoms in the system, one can produce droplet arrays with different numbers of clusters, just like in Fig. 4.

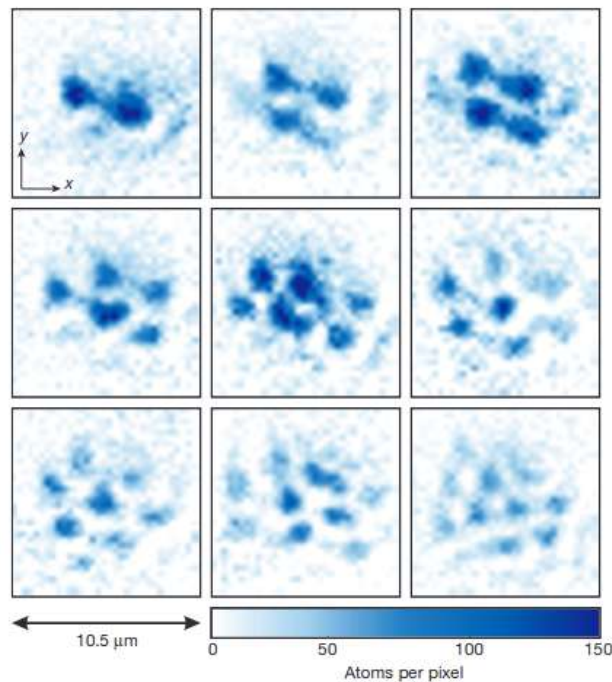


FIG. 4. *In situ* images of dysprosium-164 droplet arrays with the number of droplets varying from two to ten.

Figure reprinted with permission from Springer Nature [H. Kadau *et al.*, *Nature* **530**, 194 (2016)].

© 2016 by Springer Nature Limited.

Moreover, if we finely tune the interactions, the isolated droplets may become slightly connected and form a *supersolid* state, which has properties characteristic of solids and *superfluids*, i.e. the substances lacking viscosity, BECs included [30]. In such a state the density is modulated; we deal with a broken translational symmetry just like in crystals. Yet, the matter stays phase coherent, which is typical of superfluids [31].

It is high time I introduced the last general remark on the subject of solitons, now that we know what system we will be interested in. Namely, one may think that a many-body approach is sufficient. There would be no need to add corrections, as the problem would be solved exactly.

Up until now, there is no direct link between the solitons appearing in the non-linear equations like the GPE and the solutions of linear many-body Schrödinger equation. Despite

trying different approaches [32–34], the connection between many-body calculations and non-linear models has not been fully understood yet.

All in all, in the remaining part of this Thesis, **I will try to give a prediction of whether or not dark (and possibly wide) solitons exist in atomic systems with competing interactions. If so, we will also try to obtain stable solitonic solutions coexisting with quantum droplets.**

Beforehand, I will present the necessary theoretical introduction to the subject. In Chap. 2, we will encounter basic mechanisms ruling the Bose-Einstein condensation, with some insights into experimental realisations. Chapter 3 is devoted to theoretical tools used in the collection of publications, like the Bogoliubov transformation. We will see how to obtain a description of a low-dimensional gas when we freeze some of the degrees of freedom. The analysis of solitons is presented in Chap. 4. I show the method for finding solitary-wave solutions there too. Chapter 5 thoroughly describes quantum droplets, their properties, and excitations. Finally, we shall pass to Chap. 6 with the description and summary of the collection of publications, which is included in pt. II.

2. Introduction to Bose-Einstein condensation

Let us look into a system of non-interacting integer-spin particles at temperature T . We denote the chemical potential of such a system, regulating the total number of bosons⁴, with μ . They occupy different states ordered with i by the value of energy ϵ_i (from the lowest, ground-state energy ϵ_0) and obey the Bose distribution function [14]

$$f_B(\epsilon_i) = \left[\exp\left(\frac{\epsilon_i - \mu}{k_B T}\right) - 1 \right]^{-1}, \quad (1)$$

with k_B being the Boltzmann constant. Equation (1) gives us the mean occupation of the i^{th} energy level.

We now stocktake N atoms in the system, which can either occupy the ground state (N_0 of them) or the excited states ($N_x = N - N_0$). Instead of writing a sum, we will assume there is a continuous spectrum of excited states distributed with a certain density of states $g(\epsilon)$ (dependent on the system dimensionality and confinement) and

$$N = N_0 + N_x = N_0 + \int_0^\infty d\epsilon g(\epsilon) f_B(\epsilon). \quad (2)$$

We can introduce the critical temperature T_c corresponding to a state, in which all atoms can be stored in the excited states. The critical temperature depends on the particle density $\rho^{(3D)}$ and atomic mass m as $T_c \propto (\rho^{(3D)})^{2/3} / m$. To avoid molecule formation due to three-body interactions, the gas has to be dilute with $\rho^{(3D)} \sim 10^{14} \text{ cm}^{-3}$, i.e. 5 orders of magnitude less dense than air. This gives us a rough estimation of T_c at the level of one-tenth of a microkelvin. High above T_c , the ground state occupation is less than a single atom. Below the critical temperature, the relative mean ground state occupation $\langle N_0/N \rangle$ as a function of the system temperature is given by the following formula:

$$\left\langle \frac{N_0(T)}{N} \right\rangle = 1 - \left(\frac{T}{T_c} \right)^v, \quad (3)$$

where the exponent v depends on the system dimensionality and trapping potential. For example, in a three-dimensional system of harmonically trapped atoms $v = 3$ whereas in the case without the trap, we get $v = 3/2$. Such a macroscopic occupation of a single orbital is called *Bose-Einstein condensation* [14, 37].

In lower-dimensional gases, the situation is quite different. The condensate in 1D exists only at $T = 0$. At higher temperature, we have a quasi-condensate, a state in which the phase coherence is small in comparison to the system size but large when compared to the typical microscopic distance [38].

The first BEC with dilute atomic vapours was achieved in 1995 [13]. Atomic BECs are most frequently obtained with bosonic isotopes of alkali, alkaline earth and rare metals as shown in Fig. 5. From our point of view, the most important will be (i) the highly magnetic erbium and dysprosium with the magnetic moments of 7 and 10 Bohr magnetons respectively [39] and (ii) potassium-39 in two hyperfine states [26, 40] or a potassium-rubidium mixture [41].

⁴ For the sake of simplicity, we will use the grand canonical ensemble to describe the BEC. If we wanted to relate to current experiments, however, one would have to use the microcanonical ensemble instead, as it was shown on the example of condensate fluctuations [35, 36].

FIG. 5. Periodic table of elements with highlighted Bose-condensed species. Based on Refs. [13, 42–53].

Other, a bit more exotic examples of BECs have been achieved using, for instance, exciton polaritons [54, 55], bosonic quasiparticles made of electron-hole pairs, which are strongly coupled to electromagnetic field. We have had BECs consisting of magnetic excitation quanta, called magnons [56], and photons [57] as well.

The non-interacting picture is an incomplete model, though. For instance, alkali atoms interact via a short-range van der Waals potential. Assuming low-energy collisions in the s -wave channel, the interaction between atoms can be described with a single quantity, namely the scattering length a . Effectively, the self-interaction potential between two atoms of mass m separated by \mathbf{r} is approximated⁵ with [58]

$$V_{\text{int}}^{(3D)}(\mathbf{r}) = \frac{4\pi\hbar^2 a}{m} \delta(\mathbf{r}). \quad (4)$$

The scattering length can be regulated using a magnetic field via Fano-Feshbach resonances [59–61]. The interaction can be tuned to be repulsive (positive a) or attractive (negative a) [43]. By changing the magnetic field B , one can steer the scattering length

$$a(B) = a_{\text{nr}} \left(1 - \frac{\Delta B}{B - B_0} \right), \quad (5)$$

where a_{nr} is the non-resonant scattering length, B_0 – the resonant magnetic field, and ΔB is the resonance width.

Atoms of chromium, dysprosium and erbium need some special treatment due to their non-negligible magnetic moments μ_D . In their cases, we need to consider d -wave scattering as well. The dipole-dipole interaction (DDI) between two magnetic atoms separated by \mathbf{r} can be expressed as [18]

$$V_{\text{dd}}^{(3D)}(\mathbf{r}) = \frac{\mu_0 \mu_D^2}{4\pi r^3} \left[1 - 3 \left(\frac{\mathbf{r} \cdot \boldsymbol{\mu}_D}{r \mu_D} \right)^2 \right], \quad (6)$$

where μ_0 is the magnetic constant. The DDI, in contrast to the contact interaction, is anisotropic. We have already seen the consequences of this anisotropy in Fig. 3.

⁵ The δ -potential in two and three dimensions has to be properly regularized as it was shown in Ref. [28].

Thanks to the advances in cooling techniques, atomic gases can be now cooled up to a record $T = 38_{-7}^{+6}$ pK [62], that is eleven orders of magnitude less than the typical temperature in the outer space⁶.

In a while, I will shortly present how experimental setups used to produce BEC look like. The methods of both cooling and trapping the atomic vapours base on the interactions of the electromagnetic field with atoms and we shall focus on it now.

Let us now consider a laser beam and a single atom in a magnetic field, which makes two Zeeman-splitted states appear. The separation between the ground state $|g\rangle$ and the excited state $|e\rangle$. These two levels are separated by the energy $\hbar\omega_{g\rightarrow e}$.

The laser frequency is red-detuned from $\omega_{g\rightarrow e}$. The transfer from $|g\rangle$ to $|e\rangle$ is most probable when the atom moves at a certain velocity (dependent on the value of detuning) in the direction opposite to the propagation of the laser beam. Certainly, this is due to the Doppler shift. Let us assume such a transfer occurs. The atom in the state $|e\rangle$ spontaneously relaxes back to the state $|g\rangle$ emitting a recoil photon. The laser photon transfers also momentum in the direction of light propagation to the atom. The recoil photon on the other hand is emitted in a random direction. Thus, after many such events, the atom is slowed down in the direction parallel to the laser [65].

Experimenters use this effect in Zeeman slower. This piece of equipment consist of a set of coils and a laser counterpropagating to the atoms. While the atoms are slowed down, one has to compensate for the change in velocity. To do this, the coils produce a magnetic field varying (and therefore changing $\omega_{g\rightarrow e}$) along the flow of atoms [66]. With the use of six laser beams, we are able to both trap and further cool the atoms. Analogous phenomena take place in such a configuration too. This appliance is called a magneto-optical trap (MOT). To achieve a BEC, another cooling stage is necessary. The atoms are transferred to a yet another trap. The pre-cooled gas is gathered in a focal point of a laser beam inducing dipole moments of the atoms. They are consequently attracted to the laser focal point. Next, the trap strength, i.e. laser power, is lowered and the warmest fraction of atoms escapes the trap. This procedure is called evaporative cooling [67].

Now, we can assemble the setup. Not literally, of course. First, as most condensed atomic species are metals, we need an oven to produce vapour at 300-1500 K, depending on the species [52, 68]. Next, the gas is cooled a few orders of magnitude down with a half a metre long Zeeman slower [69]. Then, the atoms gather in a science chamber with a MOT and a subsequent dipole trap performing evaporative cooling. The science chamber also provides the experimenters with the possibility of imaging the BEC (as previously shown in Figs. 2 and 4). Figure 6 presents an exemplary setup scheme of an erbium experiment [70].

So-produced BECs manifest properties, which are not present in the day-to-day human experience. For instance, by stirring an ultracold gas, one can induce a regular lattice of many quantum vortices (cf. Fig. 7) with a long lifetime of a several dozen seconds [71]. The presence of these vortices is a visible signature of *superfluidity* – the lack of energy dissipation.

⁶For instance, the cosmic microwave background temperature equals to 2.73 K [63] and the temperature of the Boomerang nebula – to ~ 1 K [64].

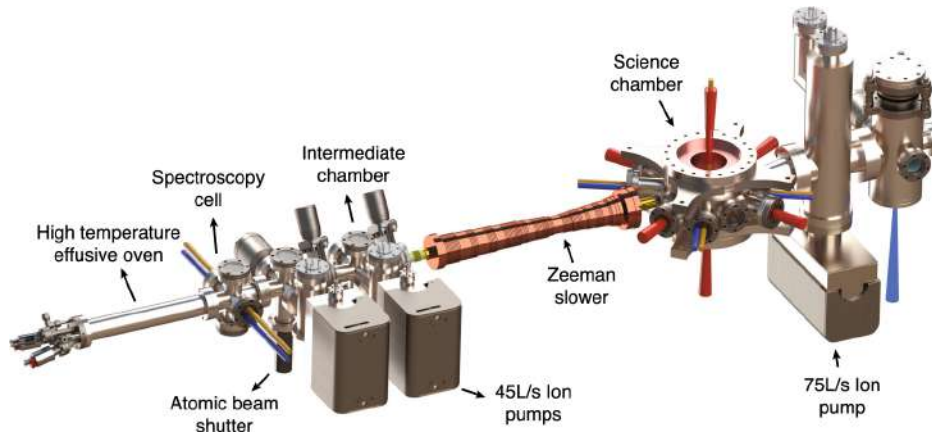


FIG. 6. Experimental setup for erbium-168 BEC production. The setup starts with an oven and ends up with the so-called science chamber.

Figure reprinted with permission from Springer Nature
 [B. Seo *et al.*, J. Korean Phys. Soc. **82**, 901–906 (2023)]
 © 2023 by the Korean Physical Society.

According to the Landau criterion, if collective excitations are not energetically favourable when the fluid flows at a velocity v lower than the critical velocity, in our case equal to the speed of sound c , the medium is superfluid [72, 73]. It is worth mentioning here that BECs are not the only superfluid state of matter. Helium-4 becomes inviscid below approx. 2 K and we can directly observe the presence of quantized vortices there [74]. Superfluidity is present also in fermionic systems like helium-3 [75], superconducting materials [76], degenerate Fermi gases [77], nuclei [78], and most probably in the crusts of neutron stars [79]. In all these phenomena we deal with Cooper pair creation and condensation via the Bardeen-Cooper-Schrieffer mechanism [80].

Apart from vortices, experimenters have witnessed different collective excitations called monopole and scissors mode (we will encounter the former when discussing quantum droplets in Chap. 5) [81, 82], also in dipolar supersolids [83]. They have constructed BEC-based coherent

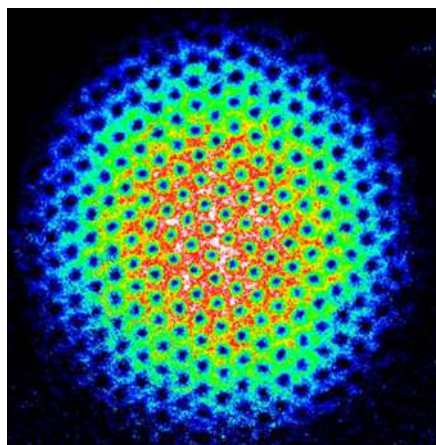


FIG. 7. Quantum vortex lattice with over 300 vortices nucleated in a BEC.

Public domain. Courtesy: National Science Foundation.

atom sources dubbed atom lasers [84–86]. Ultracold quantum gases are applicable in, *inter alia*, quantum metrology [87–89], thermodynamics [90–93], simulators [94, 95], and possibly computing [96–99]. BECs can be also used for modelling in cosmology, e.g. the tests of models of dark matter [100], or in astrophysics to simulate pulsar glitches [101] and analogues of black holes emitting the Hawking radiation [102–104].

3. General framework and methods

3.1. Single-component gases with contact interactions in 1D

In this Thesis, I focus on low-dimensional Bose gases. Our everyday intuition tells us that the space around us has three dimensions. How to make the ultracold gas behave like a one-dimensional system?

We start by considering a gas at $T = 0$ consisting of N non-magnetic bosonic atoms trapped in an external harmonic confinement $V_{\text{ext}}(\mathbf{r}_i)$, where \mathbf{r}_i is the i^{th} atom position. The many-body wave function describing the gas $\Psi^{(3D)}(\{\mathbf{r}_i\}, t)$ is symmetric and obeys the Schrödinger equation

$$i\hbar\partial_t\Psi^{(3D)}(\{\mathbf{r}_i\}, t) = \sum_{i=1}^N \left[-\frac{\hbar^2}{2m}\nabla_i^2 + V_{\text{ext}}(\mathbf{r}_i) \right] \Psi^{(3D)}(\{\mathbf{r}_i\}) + \frac{1}{2} \sum_{i \neq j} V_{\text{int}}^{(3D)}(|\mathbf{r}_i - \mathbf{r}_j|) \Psi^{(3D)}(\{\mathbf{r}_i\}, t). \quad (7)$$

Now, let the external potential distinguish one direction, i.e. $V_{\text{ext}}(\mathbf{r}_i) = \frac{1}{2}m\omega_{\perp}^2(y_i^2 + z_i^2)$ and the energy spacing $\hbar\omega_{\perp}$ be much larger than the chemical potential. We assume the wave function has the form

$$\Psi^{(3D)}(\{\mathbf{r}_i\}, t) = \Psi(\{x_i\}, t) \prod_{i=1}^N \Phi_G(y_i; l_{\perp}) \Phi_G(z_i; l_{\perp}) \exp\left(-\frac{iE_{\perp}t}{\hbar}\right), \quad (8)$$

where $\Phi_G(\alpha; l_{\perp})$ is the Gaussian being the ground state of a non-interacting gas confined in the direction α , in a harmonic potential with oscillatory length $l_{\perp} = \sqrt{\hbar/m\omega_{\perp}}$ and E_{\perp} is the energy associated with the perpendicular directions. This approach enables us to integrate out y and z and get the one-dimensional Schrödinger equation

$$i\hbar\partial_t\Psi(\{x_i\}, t) = -\frac{\hbar^2}{2m} \sum_{i=1}^N \partial_{x_i}^2 \Psi(\{x_i\}) + \frac{g}{2} \sum_{i \neq j} \delta(x_i - x_j) \Psi(\{x_i\}, t) \quad (9)$$

with $g \equiv 2\hbar^2 a/m l_{\perp}^2$ being the interaction coupling constant [38].

We have just assumed that the whole dynamics of the system is effectively one-dimensional and described by the wave function Ψ . All the particles in the perpendicular degrees of freedom occupy the non-interacting ground state. The energy necessary to excite the gas in the perpendicular direction is much higher than the one needed to create an excitation in the longitudinal one. Thus, in the limit of low-lying elementary excitations, such a suppression ought to be valid [105].

The one-dimensional Schrödinger equation (9) is quite special as it is analytically solvable in an exact manner. The case of an unconfined gas with periodic boundary conditions is known as the Lieb-Liniger model [106]. The interaction regime in 1D is described by a dimensionless Lieb parameter⁷ $\gamma \equiv mg/\hbar^2\rho$, where ρ is the 1D particle density. For instance, one can derive the ground-state energy of the system

$$E_{\text{GS}} = \frac{\hbar^2}{2m} N \rho^2 e_{\text{LL}}(\gamma), \quad (10)$$

⁷ As one can see, γ can be interpreted as a ratio of two typical energy scales – interaction energy scale to the kinetic energy scale.

where e_{LL} is a function, which can be numerically approximated⁸ by [107]

$$e_{\text{LL}}(\gamma) \stackrel{\gamma \leq 2}{=} \gamma - \frac{4}{3\pi}\gamma^{3/2} + \frac{\pi^2 - 6}{6\pi^2}\gamma^2 - \frac{4 - 3\zeta(3)}{8\pi^3}\gamma^{5/2} + \mathcal{O}(\gamma^3) \quad (11)$$

in the weakly interacting regime and [108, 109]

$$e_{\text{LL}}(\gamma) \stackrel{\gamma \geq 2}{=} \frac{\pi^2}{3} \left(1 - \frac{4}{\gamma} + \frac{12}{\gamma^2} - \frac{10.9448}{\gamma^3} \right) + \mathcal{O}(\gamma^{-4}) \quad (12)$$

for intermediate and strong interactions.

An alternative approach is to assume that all particles in the longitudinal direction occupy a single orbital. The depletion is disregarded, which applies basically to weakly interacting systems only [110–112]. In such a case, the wave function $\Psi(\{x_i\}, t)$ in Eq. (8) becomes

$$\Psi(\{x_i\}, t) = \frac{1}{\sqrt{N}} \prod_{i=1}^N \psi(x_i, t). \quad (13)$$

The particle density is defined as $\rho = |\psi|^2$.

The principle of least action yields the following non-linear differential equation

$$i\hbar\partial_t\psi(x, t) = \left[-\frac{\hbar^2}{2m}\partial_x^2 + g|\psi(x, t)|^2 \right] \psi(x, t), \quad (14)$$

which is the one-dimensional version of the time-dependent Gross-Pitaevskii equation (GPE), already mentioned in Chap. 1. Its stationary form can be derived by plugging the so-called Hartree ansatz (13) in the Schrödinger equation (9).

The GPE has been widely used in ultracold matter physics to look into systems with, e.g. different dimensionalities, confining potentials, and interactions [23, 113–120].

The Lieb-Liniger model is complex in comparison to the simplicity of the GPE. On the other hand, the GPE is bound to describe weakly interacting systems only. What if we wanted to have an equation for a single-particle function in the other limiting case?

In general, knowing the energy density functional (EDF) of a system $\mathcal{E}[\rho]$, one, using the local density approximation [121, 122], can generate an equation of the form

$$i\hbar\partial_t\psi(x, t) = \left(-\frac{\hbar^2}{2m}\partial_x^2 + \frac{\delta\mathcal{E}[\rho]}{\delta\rho} \right) \psi(x, t). \quad (15)$$

When we are outside the regime of weak interactions, the function ψ is not a wave function *stricto sensu*. Thus, we will call it a pseudo-wave function⁹.

When the bosons are impenetrable (Tonks-Girardeau limit of $\gamma \rightarrow \infty$), we can make use of a one-to-one correspondence between the bosonic and a fermionic system of non-interacting particles, i.e. the Fermi-Bose mapping [123, 124]. The EDF of the non-interacting Fermi gas equals to $\mathcal{E}_{\text{TG}}[\rho] = \hbar^2\pi^2\rho^3/6m$, which for bosons yields

$$i\hbar\partial_t\psi(x, t) = \frac{\hbar^2}{2m} \left[-\partial_x^2\psi(x, t) + \pi^2|\psi(x, t)|^4 \right] \psi(x, t), \quad (16)$$

that is, a single-orbital equation describing the dynamics of a one-dimensional gas of (by virtue of the Fermi-Bose mapping) impenetrable bosons, which I will call Kolomeisky equation [125]. The solution of Eq. (16) with an addition of an external harmonic potential agrees very well

⁸ For brevity, I only show here the first few terms of the series.

⁹ In the density functional theory, such a function is called an orbital [122].

with the many-body solution [125] but it does not reproduce Friedel oscillations [126]. The application to violent dynamics when, for example, an excited gas is released from the trap has been a subject of debate [127, 128].

There is, of course, a possibility to use the EDF based on the Lieb-Liniger model $\mathcal{E}_{\text{LL}}[\rho] = \frac{\hbar^2}{2m}\rho^3 e_{\text{LL}}(\gamma)$ and obtain the following equation

$$i\hbar\partial_t\psi(x,t) = \left\{ -\frac{\hbar^2}{2m}\partial_x^2\psi(x,t) + \mu_{\text{LL}}[\rho;\gamma] \right\} \psi(x,t), \quad (17)$$

where $\mu_{\text{LL}}[\rho;\gamma] = \delta\mathcal{E}_{\text{LL}}/\delta\rho = \frac{\hbar^2}{2m}\rho^2 [3e_{\text{LL}}(\gamma) - \gamma e'_{\text{LL}}(\gamma)]$.

I will consistently use the name Lieb-Liniger Gross-Pitaevskii equation (LLGPE) for Eq. (17) although one may encounter the nomenclature of the modified or generalized non-linear Schrödinger equation [129, 130]. The LLGPE is investigated at length in Ref. [T1] from the collection of publications.

It is also interesting that in the limit of weak interactions $\gamma \ll 1$, the LLGPE transforms into the GPE and in the Tonks-Girardeau limit $\gamma \rightarrow \infty$, it turns into the Kolomeisky equation. In these limits, we use the first term in Eqs. (11) (for $\gamma \ll 1$) and (12) (for $\gamma \rightarrow \infty$) to calculate the EDFs¹⁰. We will return to the LLGPE at length in Chap. 6.

One can see that $\psi(x,t) = \psi_0 \exp(-i\mu t/\hbar)$ is a solution of the non-linear equation (15) [having in mind we shall mostly focus on the (LL)GPE or the Kolomeisky equation] by means of e.g. propagation in imaginary time [131]. It satisfies the stationary equation

$$\mu\psi_0 = \left(-\frac{\hbar^2}{2m}\partial_x^2 + \mu[\rho_0] \right) \psi_0, \quad (18)$$

where $\mu[\rho_0] \equiv \delta\mathcal{E}[\rho]/\delta\rho|_{\rho=|\psi_0|^2}$. We will always use square brackets in the notation to mark the derivative of the energy functional with respect to the density $\mu[\rho]$ so that it cannot be confused with the chemical potential μ when the density profile is inhomogeneous.

Let us now consider a slightly perturbed state $\psi(x,t) = \psi_0 + \delta\psi(x,t)$ and insert it into Eq. (15). Using the property that ψ_0 satisfies Eq. (18), we obtain an equation describing the dynamics of the small perturbation $\delta\psi$. After linearizing it in $\delta\psi$, we assume a plane-wave form [3, 132]

$$\delta\psi(x,t) = \left\{ u_q \exp \left[i \left(qx - \frac{\epsilon}{\hbar}t \right) \right] + v_q^* \exp \left[-i \left(qx - \frac{\epsilon}{\hbar}t \right) \right] \right\} \exp \left(\frac{i\mu t}{\hbar} \right), \quad (19)$$

where coefficients $|u_q|^2 - |v_q|^2 = 1$, $\hbar q$ is the momentum of the perturbation, and ϵ – its energy.

We can finally write the Bogoliubov equations in a matrix form¹¹

$$\begin{pmatrix} \frac{\hbar^2 q^2}{2m} + \mu[\rho_0] & \mu[\rho_0] \\ -\mu[\rho_0] & -\left\{ \frac{\hbar^2 q^2}{2m} + \mu[\rho_0] \right\} \end{pmatrix} \begin{pmatrix} u_q \\ v_q \end{pmatrix} = \epsilon \begin{pmatrix} u_q \\ v_q \end{pmatrix}. \quad (20)$$

The excitation energy ϵ is the eigenvalue of the problem given by Eq. (20) and equals to

$$\epsilon = \pm \sqrt{c^2 \hbar^2 q^2 + \left(\frac{\hbar^2 q^2}{2m} \right)^2} \quad (21)$$

with c being the speed of sound. The relation between the speed of sound and chemical potential μ reads $c^2 = (\rho/m)d\mu[\rho]/d\rho|_{\rho=|\psi_0|^2}$.

¹⁰ Then, we get $\mathcal{E}_{\text{LL}}[\rho] \stackrel{\gamma \ll 1}{\cong} g\rho^2/2$ and $\mathcal{E}_{\text{LL}}[\rho] \stackrel{\gamma \rightarrow \infty}{\cong} \hbar^2 \pi^2 \rho^3 / 6m$, which are the EDFs of a weakly and strongly interacting Bose gases correspondingly.

¹¹ Had we not assumed the uniformity of the ground state, the resulting Bogoliubov equations would be much more complicated [133]. We will deal with such a system later on.

In the limit of low momenta, the spectrum is linear with $\epsilon \stackrel{\hbar q \ll mc}{\approx} c\hbar q$. In Chap. 2, we have encountered the Landau criterion for superfluidity, i.e. the existence of a critical velocity v_c , below which the collective excitations are not favourable. This critical velocity is given by [72]

$$v_c = \min \frac{\epsilon}{\hbar q} \stackrel{\hbar q \ll mc}{\approx} c, \quad (22)$$

which, at the end of the day, is the speed of sound. If not for the linear start of the excitation spectrum, the BEC would not be superfluid. When the momentum is high, the spectrum becomes quadratic $\epsilon \stackrel{\hbar q \gg mc}{\approx} \hbar^2 q^2 / 2m$, typical of a free particle.

Sometimes, the speed of sound is imaginary, meaning the excited mode will exponentially grow (or decay) in time. This behaviour (in low momenta) is called phonon instability. For example, it happens when we have a weakly attractive Bose gas. The uniform-density state is unstable and every small perturbation leads to violent dynamics [3, 134]. When the excitation energy gets imaginary in the intermediate momentum range, we have a roton instability, occurring e.g. in dipolar gases [135, 136].

The Bogoliubov analysis of a weakly interaction system, described by the GPE (14), provides us also with an energy correction to the mean-field term $E_{\text{GS}}^{(\text{MF})} = \hbar^2 N \gamma \rho^2 / 2m$ and overall we get [28, 29]

$$E_{\text{GS}}^{(\text{MF+BdG})} = \frac{\hbar^2}{2m} N \gamma \rho^2 - \frac{2\hbar^2}{3\pi m} N \gamma^{3/2} \rho^2, \quad (23)$$

where we identify the so-called Lee-Huang-Yang (LHY) correction to be the same as the second term in the expansion of the Lieb-Liniger function e_{LL} [see Eq. (11)]. When the interactions are low ($\gamma \ll 1$), the LHY term is negligible compared to the mean-field one.

3.2. Two-component gases with competing contact interactions

Let us now consider a gas of bosons occupying two different hyperfine states $|\sigma\rangle$ denoted with $\sigma = \{\uparrow, \downarrow\}$ and interacting with strengths $g_{\sigma\sigma}$ (repulsive intracomponent interactions) and $g_{\uparrow\downarrow}$ (attractive intercomponent interaction). In principle, one can use an analogous form of the many-body wave function, the Hartree ansatz (13), that is [137]

$$\Psi(\{x_i^\sigma\}, t) = \prod_{\sigma=\{\uparrow, \downarrow\}} \prod_{i_\sigma=1}^{N_\sigma} \psi_\sigma(x_i^\sigma, t), \quad (24)$$

where N_σ is the number of bosons in the state σ .

As a result, we obtain a set of coupled Gross-Pitaevskii equations for wave functions describing both components

$$\begin{cases} i\hbar\partial_t\psi_\uparrow(x, t) = \left[-\frac{\hbar^2}{2m}\partial_x^2 + g_{\uparrow\uparrow}|\psi_\uparrow(x, t)|^2 - g_{\uparrow\downarrow}|\psi_\downarrow(x, t)|^2 \right] \psi_\uparrow(x, t), \\ i\hbar\partial_t\psi_\downarrow(x, t) = \left[-\frac{\hbar^2}{2m}\partial_x^2 + g_{\downarrow\downarrow}|\psi_\downarrow(x, t)|^2 - g_{\uparrow\downarrow}|\psi_\uparrow(x, t)|^2 \right] \psi_\downarrow(x, t). \end{cases} \quad (25)$$

The Bogoliubov analysis shows that a low-energy excitation of the system will keep the ratio $\rho_\downarrow/\rho_\uparrow = \sqrt{g_{\uparrow\uparrow}/g_{\downarrow\downarrow}}$. Thus, when the spatial density profile of the system is a smooth, although not homogeneous, and the temporal evolution sufficiently slow, one can encode the whole dynamics using the following scaling [27, 138]

$$\psi_\sigma(x, t) = \sqrt{\frac{\sqrt{g_{\sigma'\sigma'}}}{\sqrt{g_{\sigma\sigma}} + \sqrt{g_{\sigma'\sigma'}}}} \psi(x, t) \quad (26)$$

with $\sigma \neq \sigma'$.

When $\delta g = g_{\uparrow\downarrow} - \sqrt{g_{\uparrow\uparrow}g_{\downarrow\downarrow}} < 0$ the mean-field theory predicts an instability, a collapse. In Chap. 1, we have encountered an experimental proof that falsifies the presence of collapse in a tiny range of parameters [23]. To fill this gap, one needs to, e.g. include the correction for quantum fluctuations in the system, which yields a generalized Gross-Pitaevskii equation (GGPE) (also called extended Gross-Pitaevskii equation, EGPE) [138, 139]

$$i\hbar\partial_t\psi(x,t) = -\frac{\hbar^2}{2m}\partial_x^2\psi(x,t) + \frac{2\delta g\sqrt{g_{\uparrow\uparrow}g_{\downarrow\downarrow}}}{(\sqrt{g_{\uparrow\uparrow}} + \sqrt{g_{\downarrow\downarrow}})^2}|\psi(x,t)|^2\psi(x,t) - \frac{\sqrt{m}(g_{\uparrow\uparrow}g_{\downarrow\downarrow})^{3/4}}{\hbar\pi}|\psi(x,t)|\psi(x,t). \quad (27)$$

To find the validity regime of the GGPE, one has to compare it with an *ab initio* solution. Sadly, the Lieb-Liniger analogue for a bosonic mixture, i.e. the Yang-Gaudin model [140–142] is solvable only in the case when all the interactions, two intraspecies and the interspecies one, are the same, which is not useful in the case we are considering here.

It is the moment when quantum Monte Carlo (QMC) methods lend us a hand, with diffusion Monte Carlo in particular. The basic principle of this QMC method is to propagate an initial guess of the state in imaginary time. Each propagation step consists at first of a random walk in position space, similar to the classical diffusion. Then, one decides whether or not to keep the configuration system. The lower the system energy gets, the more copies of the configuration we will create. Sometimes, highly energetic states will be deleted. Every one of them will be changed randomly and independently in the iterative diffuse-copy/delete procedure. The particle configuration will gradually converge to the ground state [143].

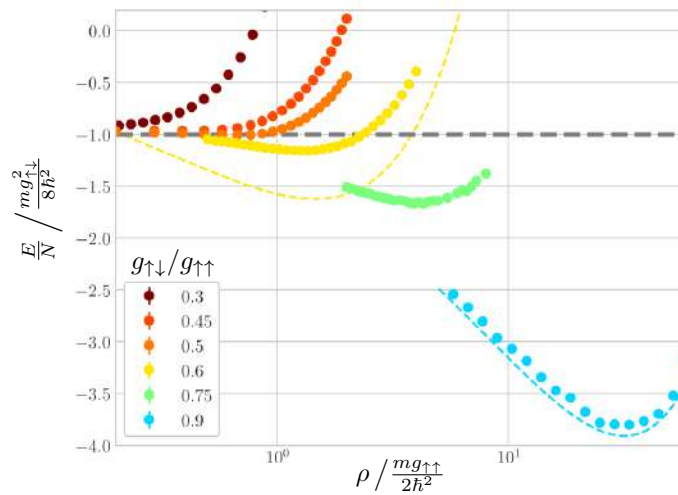


FIG. 8. Energy per particle as a function of the density for different interaction ratios $g_{\uparrow\downarrow}/g_{\uparrow\uparrow}$. The intraspecies interactions are symmetric $g_{\uparrow\uparrow} = g_{\downarrow\downarrow}$. Markers: QMC results (uncertainty bars smaller than the marker size); dashed lines: GGPE predictions.

Figure reprinted with permission from [L. Parisi *et al.*, Phys. Rev. Lett. **122**, 105302 (2019)].

© 2019 by the American Physical Society.

QMC methods have been successfully used to investigate homogeneous Bose-Bose mixtures with symmetric intraspecies interactions $g_{\uparrow\uparrow} = g_{\downarrow\downarrow}$. Figure 8 shows us the energy per particle as a function of the total density $\rho = |\psi_{\uparrow}|^2 + |\psi_{\downarrow}|^2$, providing also with a comparison between

the GGPE and QMC outcomes. In the high-density region (weakly interacting regime), the two methods give qualitatively agreeing results. In the low-density region, they become not only quantitatively but also qualitatively different. When the interaction ratio becomes lower than $g_{\uparrow\downarrow}/g_{\uparrow\uparrow} = 0.47(2)$, the QMC data, unlike GGPE, lack a local minimum in E/N [144]. As we will see in Chap. 5, the consequences of this fact are essential for the formation of quantum droplets.

The study of inhomogeneous systems is a tough nut to crack. Dark solitons have not been investigated with the use of QMC yet. In spite of that, the already mentioned quantum droplets have been analyzed with QMC methods. With the use of linear-response theory, it was even possible to make a prediction about some basic dynamics like the breathing mode [145].

After a careful look at Fig. 8, one sees that when the density of the system goes down, the energy per particle for all interaction strengths goes to the value of half the binding energy $\varepsilon_b = -mg_{\uparrow\downarrow}^2/4\hbar^2$. This feature is not captured by the GGPE (see also Fig. 9). It means that in the limit $\rho \rightarrow 0$, the mixture forms a weakly interacting gas of dimers. Therefore, an inclusion of a pairing field Δ (like in Fermi systems [80]) was one of the ideas on how to obtain a simple model, which would fit the QMC results. The energy of a uniform state in the symmetric case $g_{\uparrow\uparrow} = g_{\downarrow\downarrow}$ is given by

$$E_0^{(\text{pair})}[\mu, \Delta] = -\frac{(\mu + \Delta)^2}{g_{\uparrow\uparrow}} - \frac{\Delta^2}{g_{\uparrow\downarrow}} - \frac{2\sqrt{m}}{3\pi\hbar}(\mu + \Delta)^{3/2}\mathcal{G}_1\left(\frac{\Delta}{\mu + \Delta}\right), \quad (28)$$

where $\mathcal{G}_1(s) \equiv (1+s)^{3/2} + 3\int_0^\infty dt \left[t^2 + \frac{1}{2}(1+s) - \sqrt{(t^2+1)(t^2+s)} \right]$. The relation between the chemical potential and the density reads $\rho = -\partial E_0^{(\text{pair})}/\partial\mu$. Equation (28) gives a qualitative agreement with the QMC data, including the disappearance of the local minimum in E/N function [146].

Another idea was to include a higher-order correction into the GGPE. The EDF corresponding to the GGPE in the symmetric case $g_{\uparrow\uparrow} = g_{\downarrow\downarrow}$ looks as follows [145]

$$\mathcal{E}_{\text{GGP}}[\rho] = \frac{\delta g}{4}\rho - \frac{\sqrt{m}g_{\uparrow\uparrow}^{3/2}\rho^{3/2}}{3\sqrt{2}\pi\hbar} \left[\left(1 - \frac{g_{\uparrow\downarrow}}{g_{\uparrow\uparrow}}\right)^{3/2} + \left(1 + \frac{g_{\uparrow\downarrow}}{g_{\uparrow\uparrow}}\right)^{3/2} \right]. \quad (29)$$

One can modify it using the approach from Ref. [147], include a correction of an order higher than LHY, and eventually obtain

$$\mathcal{E}_{\text{BMF}}[\rho] = \frac{\delta g}{4}\rho - \frac{2m^2}{3\pi\hbar}c_{\text{BMF}}^3(\rho; g_{\uparrow\uparrow}, g_{\uparrow\downarrow}), \quad (30)$$

and c_{BMF}^3 being

$$\begin{aligned} c_{\text{BMF}}^3(\rho; g_{\uparrow\uparrow}, g_{\uparrow\downarrow}) = & \left(\frac{\rho}{2m}\right)^{3/2} \left(\left\{ \delta g - \frac{g_{\uparrow\uparrow}^{3/2}\sqrt{m}}{2\sqrt{2}\pi\hbar\sqrt{\rho}} \left[\left(1 - \frac{g_{\uparrow\downarrow}}{g_{\uparrow\uparrow}}\right)^{3/2} + \left(1 + \frac{g_{\uparrow\downarrow}}{g_{\uparrow\uparrow}}\right)^{3/2} \right] \right\}^{3/2} \right. \\ & \left. + \left\{ (g_{\uparrow\uparrow} + g_{\uparrow\downarrow}) \left[1 + \frac{\sqrt{m}g_{\uparrow\uparrow}\delta g}{\pi\sqrt{2}\hbar g_{\uparrow\downarrow}\sqrt{\rho}} \left(\sqrt{1 - \frac{g_{\uparrow\downarrow}}{g_{\uparrow\uparrow}}} + \sqrt{1 + \frac{g_{\uparrow\downarrow}}{g_{\uparrow\uparrow}}} \right) \right] \right\}^{3/2} \right), \end{aligned} \quad (31)$$

also leads to a qualitative agreement with the QMC description. We can see that in Fig. 9. If one wants to obtain a qualitatively agreeing equation for mixtures, it is necessary to form an EDF based on the QMC data. We shall see such an approach in Ref. [T3] from the collection of publications.

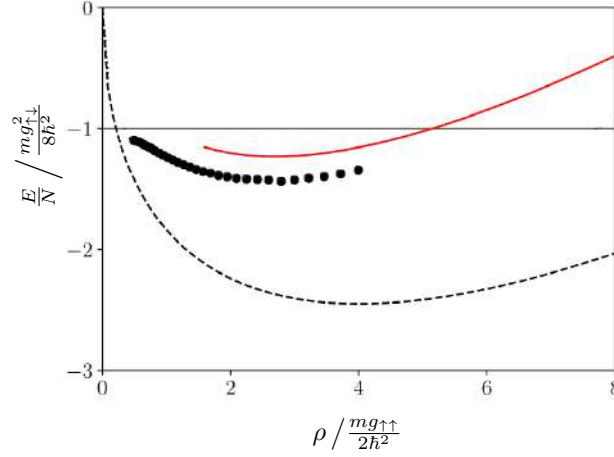


FIG. 9. Energy per particle as a function of the density for $g_{\uparrow\downarrow}/g_{\uparrow\uparrow} = 0.7$. The intraspecies interactions are symmetric $g_{\uparrow\uparrow} = g_{\downarrow\downarrow}$. Markers: QMC results (uncertainty bars smaller than the marker size); solid line: beyond-mean-field result from Ref. [147], cf. Eqs. (30) and (31); dashed line: GGPE prediction.

Figure reprinted from [M. Ota and G.E. Astrakharchik, SciPost Phys. 9, 020 (2020)]
on the CC BY 4.0 licence.

© 2020 by M. Ota and G. E. Astrakharchik.

3.3. Single-component gases with dipolar interactions

We have already seen how to obtain an effectively one-dimensional equation describing a three-dimensional system (as well as the necessary conditions, which allow us to do so) in the case of contact interactions. When we consider a system with long-range and anisotropic DDI potential (6), this procedure is slightly more complicated. We also assume Gaussian profiles in the perpendicular dimension. We add another condition because we look for quantum droplets and we need competing interactions. Namely, we consider a situation when the external magnetic field aligns all magnetic moments μ_D along the longitudinal direction x . The head-to-tail configuration makes the effective non-local interaction purely attractive. The resulting form of the potential (6) after integrating out the perpendicular degrees of freedom reads [18, 19]

$$\tilde{V}_{\text{dd}}(u) = -\frac{g_{\text{dd}}}{4l_{\perp}} \left[-2|u| + \sqrt{2\pi}(1+u^2)e^{u^2/2}\text{Erfc}\left(\frac{|u|}{\sqrt{2}}\right) + \frac{8}{3}\delta(u) \right], \quad (32)$$

where $u = x/l_{\perp}$ and $g_{\text{dd}} = \mu_0\mu_D^2/2l_{\perp}^2$. We can identify two parts in Eq. (32) – the contact and non-local ones. We will merge the Dirac delta coming from the DDI with the ‘standard’ contact interactions. Thus, since now, whenever we write the contact interaction coupling constant g , we have to remember it contains a part coming from the DDI as well. We shall use the name dipolar potential (or DDI) to the non-local part

$$V_{\text{dd}}(u) = -\frac{g_{\text{dd}}}{4l_{\perp}} \left[-2|u| + \sqrt{2\pi}(1+u^2)e^{u^2/2}\text{Erfc}\left(\frac{|u|}{\sqrt{2}}\right) \right]. \quad (33)$$

It is important to realize the perpendicular oscillatory length l_{\perp} is also the effective interaction range. Please note that the DDI (33) is no longer divergent at the origin as we can see in Fig. 10.

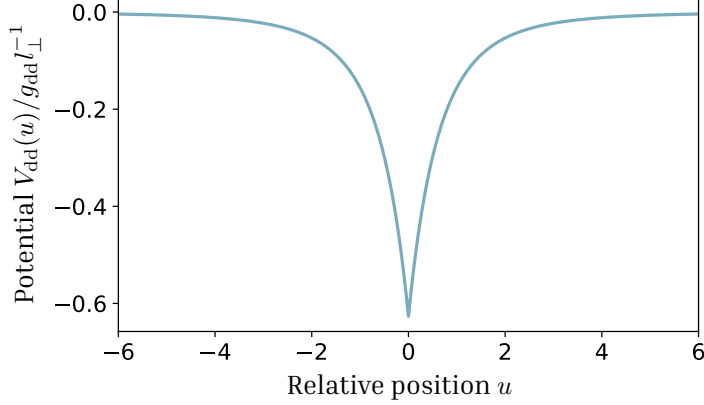


FIG. 10. Effective dipole-dipole interaction in a quasi-one-dimensional configuration.

In the mean-field approach, the quasi-one-dimensional non-local GPE has the following form

$$i\hbar\partial_t\psi(x,t) = \left[-\frac{\hbar^2}{2m}\partial_x^2 + g|\psi(x,t)|^2 + \int dx' |\psi(x',t)|^2 V_{\text{dd}}(|x-x'|) \right] \psi(x,t). \quad (34)$$

Having performed the Bogoliubov analysis, one can use a naïve approach and get quantum corrections from both contact and dipolar terms [148, 149]

$$\mathcal{E}^{(\text{LHY, DDI})}[\rho] = \frac{16l_{\perp}^2}{\pi\sqrt{2}\hbar^3} \left(1 + \frac{3}{2}\varepsilon_{\text{dd}} \right) m^{3/2} g^{5/2} \rho^{5/2}, \quad (35)$$

where $\varepsilon_{\text{dd}} \equiv g_{\text{dd}}/3\pi g$.

The LHY term here is calculated under the assumption that the system is three-dimensional and subsequently the perpendicular degrees of freedom are integrated out. In the case of mixtures, that procedure would give an opposite sign if the LHY correction, not stabilising the gas at all. Therefore, one has to very carefully approach the issue of dimensional crossovers in beyond-mean-field frameworks [150, 151].

One way to flee from that problem is to assume that the dipolar interaction strength $\gamma_{\text{dd}} \equiv mg_{\text{dd}}/\hbar^2\rho$ is much smaller than the contact interaction strength γ . We will say that the correction for quantum fluctuations resulting from the dipolar interaction is negligible at a price of employing a beyond-LHY description of the contact interactions. Eventually, we get the non-local LLGPE

$$i\hbar\partial_t\psi(x,t) = \left[-\frac{\hbar^2}{2m}\partial_x^2 + \mu_{\text{LL}}[\rho;\gamma] + \int dx' |\psi(x',t)|^2 V_{\text{dd}}(|x-x'|) \right] \psi(x,t). \quad (36)$$

Another possibility to make this approach work, is to consider a case where the interaction range is much larger than the interparticle spacing $l_{\perp} \gg \rho^{-1}$ [152, 153].

As a matter of fact, it is also possible to merge the properties of the two system described above and consider a dipolar mixture of atoms. It probably offers rich physics but is beyond the scope of this Thesis [154–156].

4. Dark solitons in ultracold matter

As we have already seen in Chap. 1, non-linear systems, like ultracold atomic gases, can host localized waves travelling without any change of their shape, i.e. solitons¹². We can group them in two kinds: bright solitons being a localized concentrations of matter [20, 157, 158] and dark solitons, which are gas rarefactions [15, 114]. This part of the Thesis is devoted to the latter.

Dark solitons are thought to spontaneously appear in thermal gas [159]. In experiments, the most common technique to induce a soliton is phase imprinting [15, 160, 161].

Firstly, we shall use Eq. (15) to show the solitonic solution derivation in a general case. A shape-preserving wave moving with velocity v is given by the following (pseudo-)wave function

$$\Phi_s(x, t) \equiv \psi_s(x - vt) \exp\left(-\frac{i\mu t}{\hbar}\right) \quad (37)$$

with the ψ_s in the density-phase representation being

$$\psi_s(\zeta) = \sqrt{\rho(\zeta)} e^{i\varphi(\zeta)}, \quad (38)$$

where $\zeta = x - vt$ is the comoving coordinate.

We plug the solitonic ansatz (37) to Eq. (15) and obtain

$$\mu\psi_s(\zeta) - iv\psi_s'(\zeta) = -\frac{\hbar^2}{2m}\psi_s''(\zeta) + \mu[|\psi_s(\zeta)|^2]\psi_s(\zeta) \quad (39)$$

with $\mu[|\psi_s(\zeta)|^2] = \delta\mathcal{E}[\rho]/\delta\rho|_{\rho=|\psi_s(\zeta)|^2}$. Next, we use the density-phase representation and separate the resulting equation into the real

$$\mu\sqrt{\rho} + \hbar v\varphi'\sqrt{\rho} + \frac{\hbar^2}{2m}(\sqrt{\rho})'' - \frac{\hbar^2}{2m}(\varphi')^2\sqrt{\rho} - \mu[\rho]\sqrt{\rho} = 0 \quad (40a)$$

and imaginary part

$$\frac{\hbar}{m}\varphi''(\sqrt{\rho})^2 + \frac{2\hbar}{m}\varphi'(\sqrt{\rho})'\sqrt{\rho} - 2v(\sqrt{\rho})'\sqrt{\rho} = 0, \quad (40b)$$

where $(\cdot)' = d(\cdot)/d\zeta$.

The two equations above are equivalent to the continuity and Euler equations in the classical hydrodynamics complimented with the quantum pressure term [3, 162].

Equation (40b) can be contracted to the following form

$$\left(\frac{\hbar}{m}\varphi'\rho - v\rho\right)' = 0, \quad (41)$$

which we integrate with an integration constant Q and after a simple rearrangement get

$$\varphi' = \frac{m}{\hbar}\left(v + \frac{Q}{\rho}\right). \quad (42)$$

Consecutively, Eq. (40a) can be rewritten as¹³

$$\left(\mu + \frac{mv^2}{2}\right)\sqrt{\rho}(\sqrt{\rho})' + \frac{\hbar^2}{2m}(\sqrt{\rho})''(\sqrt{\rho})' - \frac{mQ^2}{2}\frac{(\sqrt{\rho})'}{\rho} - \mu[\rho](\sqrt{\rho})' = 0 \quad (43)$$

¹² As also mentioned in Chap. 1, we will not demand shape preservation upon collisions from solitons.

¹³ Please notice we eliminate plane waves as we have multiplied Eq. (40a) by $(\sqrt{\rho})'$, which for $\rho(\zeta) = \text{const}$ equals 0.

Again, we can integrate this equation and obtain

$$\frac{1}{2} \left(\mu + \frac{mv^2}{2} \right) \rho + \frac{\hbar^2}{4m} [(\sqrt{\rho})']^2 + \frac{mQ^2}{4\rho} - \mathcal{M}[\rho] = V, \quad (44)$$

where V is another integration constant and \mathcal{M} being the antiderivative of $\mu[\rho] (\sqrt{\rho})'$, i.e. $d\mathcal{M}[\rho(\zeta)]/d\rho = \mu[\rho] (\sqrt{\rho})'$, and fulfilling $\mathcal{M}[\rho \equiv 0] = 0$.

In a more compact form, Eq. (44) looks as follows

$$\left(\frac{\rho'}{2} \right)^2 + \frac{m}{\hbar} U(\rho) = 0 \quad (45)$$

with

$$U(\rho) = -4\rho\mathcal{M}[\rho] + 2 \left(\mu + \frac{mv^2}{2} \right) \rho^2 - 4V\rho + mQ^2. \quad (46)$$

After this short mathematical journey, let us stop for a moment and look at the physical consequences of the two equations above. Namely, roots of $U(\rho)$ correspond to extrema (or else inflection points) of the solitonic density profile. Therefore, the analysis of the function $U(\rho)$ can give us some information about the soliton shape.

We shall assume the following boundary conditions – far away from the soliton, the density and phase have constant¹⁴ values $\lim_{\zeta \rightarrow \pm\infty} \rho(\zeta) = \rho_\infty$ and $\lim_{\zeta \rightarrow \pm\infty} \varphi(\zeta) = \pm\varphi_\infty$. It enables us to find the chemical potential $\mu = \mu[\rho_\infty]$ and integration constants to be $Q = -v\rho_\infty$ and $V = -\mathcal{M}[\rho_\infty] + \mu[\rho_\infty]\rho_\infty/2 + mv^2\rho_\infty/2$.

Now, one can integrate Eq. (45)

$$\int_0^\zeta d\tilde{\zeta} = \int_{\rho_{\min}}^{\rho(\zeta)} \frac{d\tilde{\rho}}{2\sqrt{-\frac{m}{\hbar^2}U(\tilde{\rho})}}, \quad (47)$$

which yields the density profile of the soliton centred at $\zeta = 0$. The minimum density ρ_{\min} can be evaluated from $U(\rho)$ as it is one of its zeros.

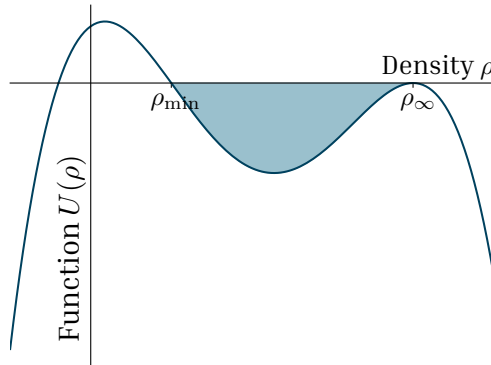


FIG. 11. Schematic representation of $U(\rho)$ function. We see two non-negative roots corresponding to the minimum density ρ_{\min} and the maximum density ρ_∞ (double root). The shaded area shows $U(\rho) \leq 0$ region.

¹⁴ Non-zero in the case of density $\rho_\infty \neq 0$.

Once we get the density profile, we are able to integrate Eq. (42) to obtain the phase profile $\varphi(\zeta)$.

It is time we took a look at two remarks. Firstly, $\forall \rho \in [\rho_{\min}, \rho_{\infty}]$, the function $U(\rho) \leq 0$. It prevents the radicand on the right-hand side of Eq. (47) from being negative. The other condition is slightly more subtle. Namely, when ζ on the left-hand side of Eq. (47) goes to infinity, $\rho(\zeta)$ goes to ρ_{∞} . The integral on the left-hand side is divergent and so has to be the one on the right-hand side. Such a divergence is possible when ρ_{∞} is at least a double root of $U(\rho)$. A scheme of $U(\rho)$ is shown in Fig. 11.

This method enables us to analytically find the soliton density and phase profiles for a wide class of energy density functionals, like in Refs. [T2, T4] from the collection of publications. Otherwise, one can use numerical schemes like in the case of a weakly repulsive dipolar gas [163] or a Bose-Bose mixture [164].

In Chap. 3, we have seen how the energy of a small perturbation depends on its momentum. Now, we will try to obtain the dispersion (energy-momentum) relation for a dark soliton.

Let us start with a soliton ψ_s in a finite box of size L . The soliton consists of N atoms, i.e. $N = \int_{-L/2}^{L/2} |\psi_s(x)|^2 dx$. The excitation energy of the soliton is a difference between the energy of the soliton and a constant density profile with $\rho_0 \equiv N/L$. The total energy of a soliton equals to

$$E_s^{(L)} = \int_{-L/2}^{L/2} \left(\frac{\hbar^2}{2m} \left| \frac{d\psi_s(x)}{dx} \right|^2 + \mathcal{E} [|\psi_s(x)|^2] \right) dx \quad (48)$$

and the energy of a constant profile $E_0^{(L)} = \mathcal{E}[\rho_0]L$.

In the last step, we go to the thermodynamic limit and obtain a general formula for the soliton excitation energy

$$\epsilon_s = \lim_{\substack{N \rightarrow \infty \\ L \rightarrow \infty \\ N/L = \text{const}}} E_s^{(L)} - E_0^{(L)}. \quad (49)$$

The solitonic momentum is given by [157]

$$p_s = \frac{i\hbar}{2} \int_{-\infty}^{\infty} \left(\psi_s(x) \frac{d\psi_s^*(x)}{dx} - \psi_s^*(x) \frac{d\psi_s(x)}{dx} \right) dx - 2\hbar\rho_{\infty}\varphi_{\infty}. \quad (50)$$

Interestingly, the Lieb-Liniger model also provides us with the description of many-body elementary excitations [165]. There are two elementary excitation branches: type I, reproducing the BdG spectrum, and type II, which is usually called the solitonic branch due to its energy spectrum coinciding with the solitonic one [166–168].

In the case of a weakly interacting single-component gas described by the GPE (14), the solution looks as follows [3]:

$$\rho(\zeta) = \rho_{\infty} - \frac{\rho_{\infty} - \rho_{\min}}{\cosh^2 \left(\frac{\zeta}{\sqrt{2}\xi} \sqrt{1 - \frac{v^2}{c^2}} \right)}, \quad (51a)$$

where in this particular case $\rho_{\min} = \rho_{\infty}v^2/c^2$, the speed of sound $c = \sqrt{g\rho_{\infty}/m}$, and $\xi = \hbar/\sqrt{2mg\rho_{\infty}}$ is the healing length.

The phase profile reads

$$\varphi(\zeta) = \arctan \left[\frac{v}{\sqrt{c^2 - v^2} \tanh \left(\frac{\zeta}{\sqrt{2}\xi} \sqrt{1 - \frac{v^2}{c^2}} \right)} \right]. \quad (51b)$$

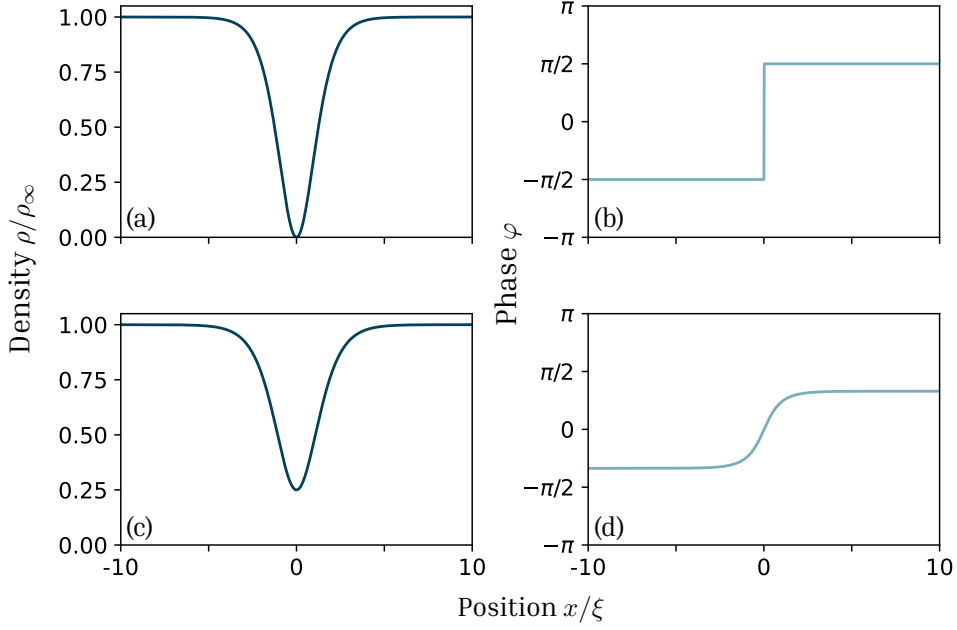


FIG. 12. (a) Density of a motionless dark (black) soliton and (b) its phase profile. (c) Grey soliton density and (d) phase profiles; its speed equals to $v = 0.5c$. All profiles correspond to the weakly interacting regime and have been evaluated using Eqs. (51a) and (51b).

In Fig. 12, we show the density and phase profiles of two solitons given by Eqs. (51a) and (51b). The motionless [$v = 0$, Fig. 12(a)] soliton density is fully depleted, i.e. black. The phase profile has got a characteristic π -jump and is discontinuous as we can see in Fig. 12(b). The motionless dark soliton in a weakly interacting Bose gas is thus a topological defect in 1D [169], just like a quantum vortex is in higher dimensionalities [170]. Moving solitons are non-topological defects with non-zero density minimum. That is why they are called grey solitons. An example of a grey soliton density profile is shown in Fig. 12(c). Its phase profile, visible in Fig. 12(d), is smoothly varying along space. Dark solitons in the strongly interacting regime share the features mentioned above [125].

Next, type-II excitation spectra are shown in Fig. 13 alongside the dispersion relation of a strongly interacting Bose gas from Ref. [125] based on the procedure involving Eqs. (49) and (50). In the weakly interacting regime, the shape of this branch is basically the same. The spectrum from Fig. 13 is quantitatively agreeing for low momenta and qualitatively in the whole momentum range (at most $\sim 25\%$ difference for momentum $p_s = \pi\hbar\rho_\infty$).

Can one connect the solitons appearing in non-linear equations and the many-body solutions of the Schrödinger equation? The answer remains unclear until now, yet there have been some trials of tackling this issue.

Firstly, one may construct an N -particle state $|X\rangle$ out of type-II excitations, called here also *grast* states¹⁵ [32, 172]

$$|X\rangle = \sum_p c_p |p\rangle_{\text{yr}}, \quad (52)$$

¹⁵ In a 1D gas, an yrast state $|p\rangle_{\text{yr}}$ is the lowest-energy state for a given momentum p . The name *grast* was first introduced in nuclear physics [171].

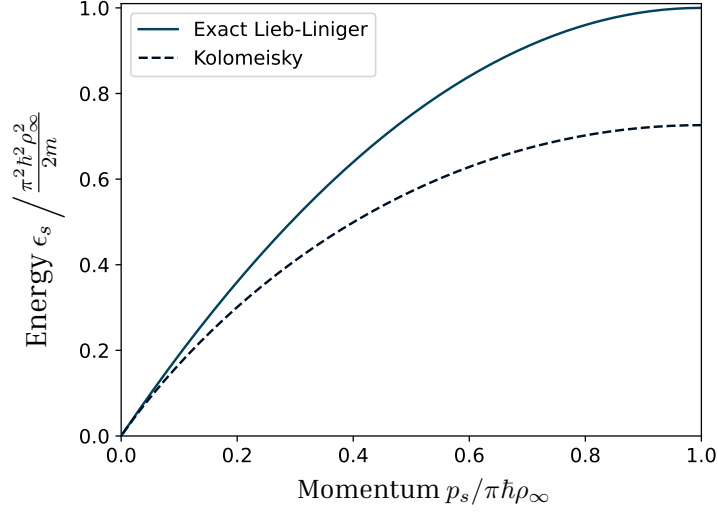


FIG. 13. Solitonic dispersion relation in the strongly interacting limit $\gamma \rightarrow \infty$. Type-II excitation branch (blue, solid line) and the result of the procedure involving Eqs. (49) and (50) from Ref. [125] (navy, dashed).

where c_p is a coefficient defining the superposition. Such states, with specific c_p coefficients, correspond to density rarefactions travelling at a constant pace, yet slowly dispersing [32, 34].

Another proposal concerns particle position measurements. Type-II eigenstates have a uniform single-particle probability density, however, consecutive measurements (or equivalently single-particle particle losses) lead to solitonic profiles appearing, in both weakly and strongly interacting gases [33].

We compare the solitons in LLGPE with these many-body approaches in Ref. [T1] from the collection of publications.

5. Quantum droplets in dipolar and two-component gases

It is said that the result of the first experiment, in which quantum droplets were obtained, has left both experimenters and theorists flabbergasted. It took some time until they found out that dipolar and two-component gases have something in common – competing interactions causing the LHY term not to be negligible [24, 25, 27].

The first proposal mentioning a possibility of creating a droplet state in ultracold matter used Efimov physics to stabilize the collapse by three-body interactions [173]. This increases losses in the system [174, 175], which are already limiting the droplet lifetime [176]. Thus, this idea has not been implemented, yet we have seen quantum droplets stabilized by quantum fluctuations in both dipolar systems and Bose-Bose mixtures. So far, quantum droplets have been obtained in dipolar systems of dysprosium [24, 25] and erbium [177] as well as mixtures of potassium-39 (in two hyperfine states) [26, 40] and potassium-rubidium [41].

In Chap. 3, I wrote that the presence of a minimum in the energy per particle function $E/N(\rho)$ has a link to the formation of quantum droplets. Let us say that the minimum is achieved when $\rho = \rho_{\text{eq}} > 0$, which we will call the equilibrium density from now on. In order to minimize its energy, the system will tend to reach the equilibrium density. With N particles in a 1D system, this density can be achieved at a distance $W = N/\rho_{\text{eq}}$. What will happen to the remaining space? It will be empty. We will have a localized state, a candidate for a quantum droplet as the ground state, whenever there is a local minimum in E/N function [27, 144]. It is visible in Fig. 14, where we have droplets with different N , but the same bulk density ρ_{eq} . When the equilibrium density is reached, the pressure vanishes, i.e. $P = -dE/dL|_{\rho=\rho_{\text{eq}}} = 0$ [150]. In the limit of large number of particles¹⁶ $N \gg 1$, the chemical potential of a one-dimensional

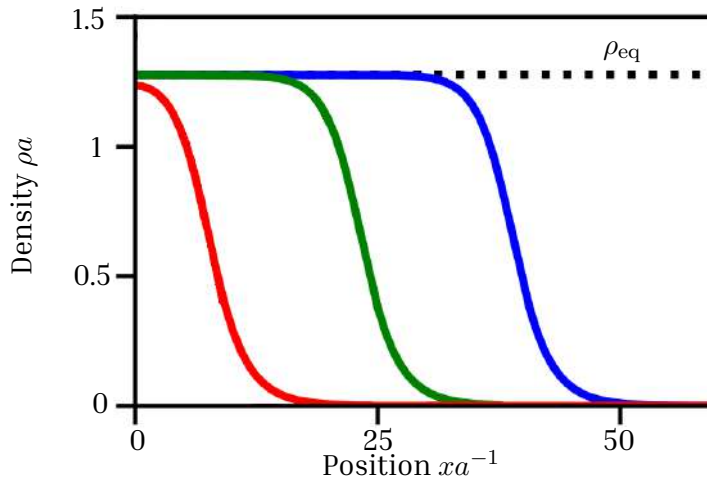


FIG. 14. Density profiles of two-component quantum droplets with different numbers of particles $N = 20, 60, 100$ (red, green, and blue correspondingly) at interaction ratio $g_{\uparrow\downarrow}/g_{\uparrow\uparrow} = 0.6$. The equilibrium density ρ_{eq} is shown with a dashed line; a is the scattering length.

Figure reprinted from [J. Kopyciński *et al.*, Phys. Rev. Res. 5, 023050 (2023)]

on the CC BY 4.0 licence.

© 2023 by J. Kopyciński *et al.*

¹⁶ This condition is necessary to neglect the influence of surface energy.

droplet is constant and its width is proportional to N . Unlike bright solitons, droplets widen with the increasing number of particles [178]

There are numerous studies of quantum droplets in different systems and dimensionalities. A particular attention has been drawn to excitations. With the use of Bogoliubov analysis, it was possible to find excitation spectra of Bose-Bose droplets in one, two, and three dimensions [27, 138, 179]. Similar research has been done in the dipolar case [180–182]. Even more complex phenomena, like droplet collisions were studied [149, 183, 184] (cf. Fig. 15), revealing scenarios analogous to low-energy nuclear collisions [185, 186].

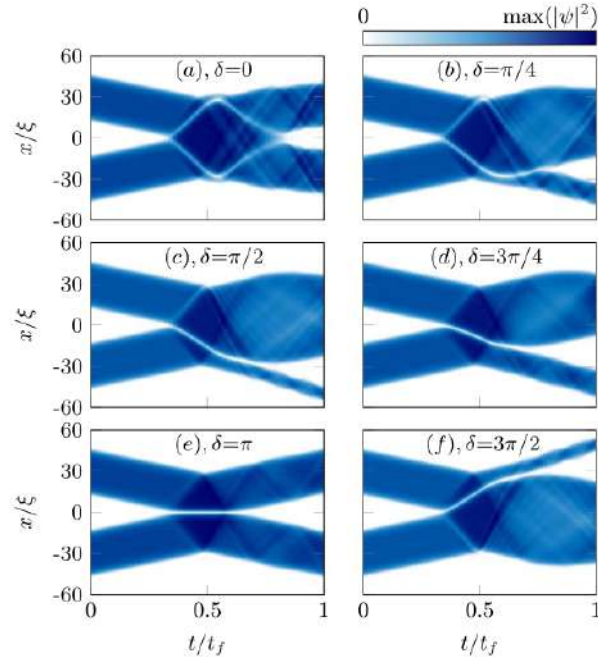


FIG. 15. Space-time diagrams of quasi-one-dimensional dipolar droplet collisions for interdroplet phase differences δ from 0 to $3\pi/2$. Time t_f is an arbitrary integration time.

Figure reprinted from [M. Edmonds *et al.*, J. Phys. Commun. **4**, 125008 (2020)]

on the CC BY 4.0 licence.

© 2020 by M. Edmonds *et al.*

I will focus here on a quite simple excitation called the monopole mode. It is also known as the breathing mode. As a careful reader might notice, I promised to return to this matter in Chap. 2. The monopole mode is an excitation when a droplet (or a BEC) alternately expands and contracts. In the case of a weakly-interacting single-component BEC confined in a spherical harmonic potential with angular frequency ω_{ho} , the monopole mode changes the density as [3]

$$\delta\rho(\mathbf{r}, t) \propto r^2 \cos(\omega_{ho}t). \quad (53)$$

To investigate the monopole mode in quantum droplets, one can, for instance, use linear response theory to extract the monopole mode frequency from Monte Carlo data [145] or perform variational calculations [187]. In Ref. [T3] from the collection of publications, we extract this value from a real time evolution of a slightly perturbed droplet. We shall see a discussion of this subject in the next chapter 6.

6. Description of the main results

6.1 Overview of Ref. [T1]

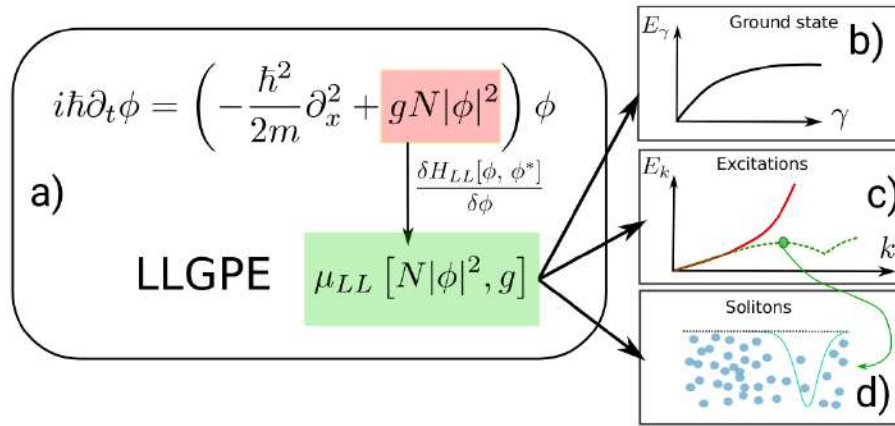


FIG. 16. Graphical abstract of Ref. [T1]: Investigation of Bose gas beyond mean field. (a) We derive the Lieb-Liniger Gross-Pitaevskii equation. It is GPE-like with a more complicated non-linear term in it. (b) From construction, the ground-state energy is the very same as in the Lieb-Liniger model. (c) We look into type-I excitations using Bogoliubov analysis. (d) We also investigate dark solitons, which are thought to be connected to type-II excitations.

Figure reprinted from [J. Kopyciński *et al.*, *SciPost Phys.* **12**, 023 (2022)]

on the CC BY 4.0 licence.

© 2022 by J. Kopyciński *et al.*

The very first theoretical proposal concerning the production of strongly correlated dipolar quantum droplets in a quasi-1D configuration used a prototype of the non-local LLGPE (36) [178]. An analogous state in the weakly interacting regime had been studied a bit earlier [188]. Instead of accurate approximations of the e_{LL} function like the ones given in Refs. [107, 108], i.e. Eqs. (11) and (12), a simplified form was used. Despite having been employed earlier, **the LLGPE still needed a proper derivation and benchmarks with many-body approaches** as one can see in Fig. 16.

The derivation of the LLGPE starts from hydrodynamic equations, which I have briefly mentioned in Chap. 4:

$$\frac{\partial \rho(x, t)}{\partial t} + \frac{\partial}{\partial x} [\rho(x, t)v(x, t)] = 0, \quad (54a)$$

that is the continuity equation and the Euler equation

$$\frac{\partial v(x, t)}{\partial t} + v(x, t) \frac{\partial v(x, t)}{\partial x} = \frac{1}{m\rho(x, t)} \frac{\partial P(x, t)}{\partial x}, \quad (54b)$$

where ρ is the particle density, m is a single-particle mass, v is the velocity field, and P stands for pressure [162].

Once we use the pressure term from the Lieb-Liniger model and connect the velocity field with the phase of our pseudo-wave function via $v = (i\hbar/m)\partial\varphi/\partial x$, we can merge the two real-valued equations (54a) and (54b) into one but complex-valued Lieb-Liniger Gross-Pitaevskii equation (17).

The use of such a derivation has its limits, though. One has to demand that the system consists of infinitesimal volumes containing many particles, which are in local equilibrium [189]. In other words, this approach may not be fully accurate while dealing with violent phenomena like shock waves [127, 190] or narrow dark solitons like in the strongly interacting Bose gas [125]. In these cases we may expect a qualitative agreement only.

The LLGPE provides us with the correct chemical potential, ground-state energy value, and the speed of sound in the all regimes from weak to strong interactions. In the case of the usual GPE, we can rely on it only to study the weakly interacting Bose gas.

I would like to draw particular attention to solitonic solutions of the LLGPE. I have significantly developed a numerical toolkit¹⁷ based on programs used earlier in Refs. [163, 178, 191]. The toolkit enabled us to obtain black soliton density profiles using the ordinary GPE (14), the LLGPE (17), and the Kolomeisky equation (16). It has been done by applying a phase-imprinting procedure throughout the evolution in imaginary time. The density profiles for different interaction strengths γ are shown in Fig. 17.

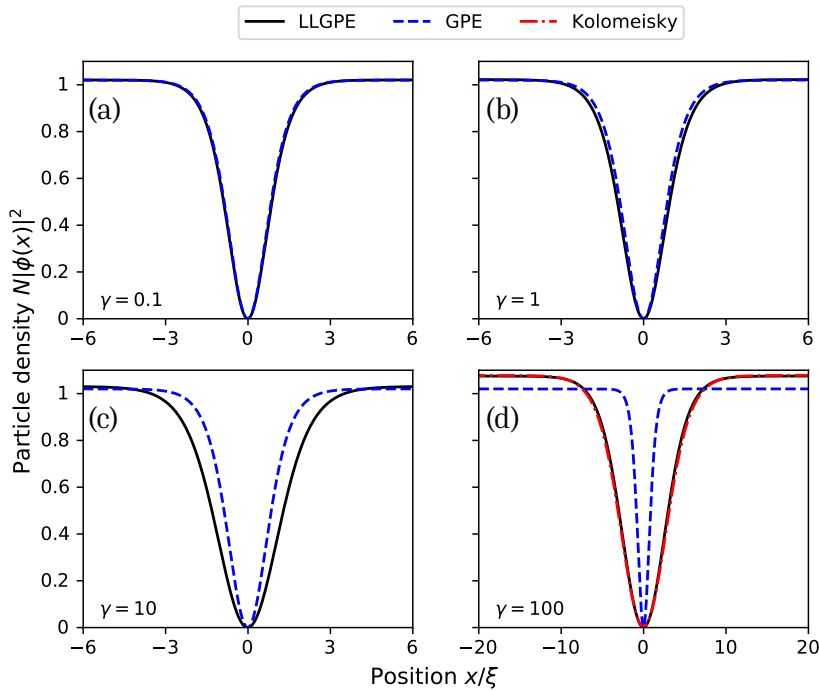


FIG. 17. Solitonic profiles for different interactions $\gamma = \{0.1, 1, 10, 100\}$. The solutions of the GPE and the LLGPE for $\gamma = 0.1$ (weak interactions) as well as the ones of the LLGPE and Kolomeisky equation for $\gamma = 100$ (strong interactions) overlap each other. Box size $L = 100\xi$, where ξ is the healing length (or equivalently $N = 100\sqrt{1/\gamma}$).

Figure reprinted from [J. Kopyciński *et al.*, *SciPost Phys.* **12**, 023 (2022)]

on the CC BY 4.0 licence.

© 2022 by J. Kopyciński *et al.*

The LLGPE results agree with the GPE profiles in the weakly interacting regime. Slight differences are seen when the interaction strength is increased and, finally, are significant

¹⁷ MUDGE toolkit, <https://gitlab.com/jakkop/mudge/-/releases>.

in the case of strongly interacting gas. Then, the LLGPE is consistent with the Kolomeisky equation. The profile obtained from the GPE gets unphysically narrow despite the fact that the gas becomes fermionized.

Another thing, which was quite natural to do, was a comparison between the density profiles extracted from many-body solitonic (type-II) excitations obtained with methods (described in Chap. 4) with the LLGPE solitonic solutions. We show it in Fig. 18.

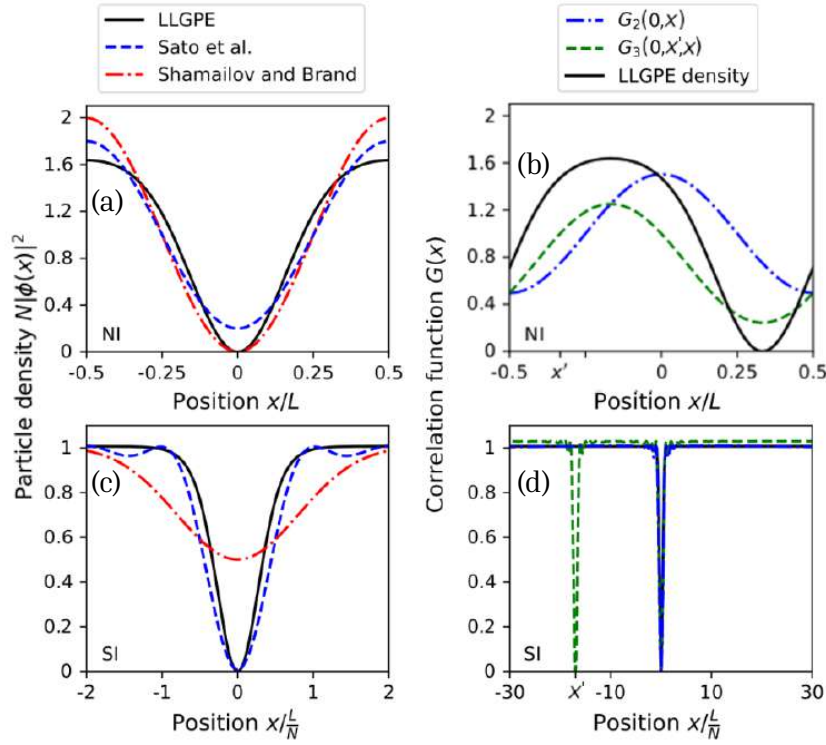


FIG. 18. Left panels: Single-particle density of yrast state superpositions (Sato et al. - based on Ref. [172], Shamailov and Brand - based on Ref. [34]). Right panels: $G_2(0, x)$ and $G_3(0, x', x)$ correlation functions evaluated for the yrast state with the total momentum $\pi N/L$. NI – non-interacting gas ($\gamma \rightarrow 0$), SI – strongly interacting gas ($\gamma \rightarrow \infty$). The G_2 function, one dip in G_3 and the LLGPE solution overlap each other in the strong interaction limit. The length scales used on the horizontal axes reflect that the soliton width depends only on L in the non-interacting regime, and only on L/N in the strongly interacting regime. The value of x' is chosen randomly.

Figure reprinted from [J. Kopyciński *et al.*, SciPost Phys. **12**, 023 (2022)]

on the CC BY 4.0 licence.

© 2022 by J. Kopyciński *et al.*

We can see the approach based on Eq. (52) is superposition dependent. Different choices of the coefficients c_p give very different results. The correlation-function-based approach works well in the weakly interacting limit. The more particles we measure, the more the density dip resembles the LLGPE profile. Yet, when we enter the limit $\gamma \rightarrow \infty$, more measurements mean more solitonlike dips. Therefore, it is still not clear how to reconcile the non-linear solitonic solution and the yrast state superpositions. Although, one has to emphasize the similarity of

the $G_2(0, x)$ function and the solitonic profile for $\gamma \rightarrow \infty$, quite an unexpected feature, having in mind the hydrodynamic origin of the LLGPE.

We have also compared how the excitation energy of black solitonic solutions obtained with the (LL)GPE looks like compared to the yrast state excitation energy. We have checked it for different interaction strengths γ . The three energies are the same up until $\gamma \approx 10$, when the GPE solitonic energy does not saturate and increases, while the other two – the LLGPE and yrast state energies – become constant. The saturation energy difference is at most $\sim 25\%$ (cf. solitons with $p_s = \pi\hbar\rho$ for $\gamma = \infty$ in Fig. 13).

All in all, the LLGPE has proven to give results coherent with the Lieb-Liniger model if it goes for the ground-state energy, chemical potential, and the speed of sound. The black soliton energies qualitatively agree with the yrast state energies in a wide interaction range, yet we are unable to provide any conclusive results concerning the comparison of the LLGPE solitonic solutions with many-body solitonlike states in the strongly interacting limit. The solitons there are quite narrow and thus not consistent with the assumptions of our hydrodynamics-based model.

Authorship statement – The PhD candidate’s contribution to this article consists of performing the study of dark solitons, their comparison to the results of many-body methods provided by M. Marciniak, and preparing the numerical toolkit MUDGE. The PhD candidate has also visualised the results and has taken part in writing and editing the manuscript.

6.2 Overview of Ref. [T2]

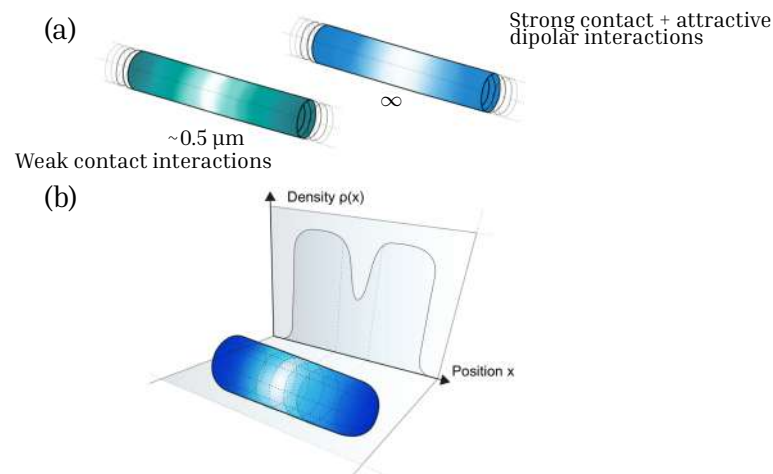


FIG. 19. Graphical abstract: (a) We demonstrate that in a dipolar gas, there are solutions of infinitely wide dark solitons due to an interplay between short- and non-local interactions. (b) Artistic vision of a dark soliton existing inside a quantum droplet.

Figure reprinted with permission from [J. Kopyciński *et al.*, Phys. Rev. Lett. **130**, 043401 (2023)]

© 2023 by American Physical Society.

Having benchmarked the LLGPE, it is high time we looked for solitons in dipolar systems and, more importantly, in quantum droplets, as we show it in Fig. 19. We shall use numerics and the non-local LLGPE (36) as well as its approximate form to get an analytical formula for solitary waves in Bose systems with strong contact interactions and weak dipolar ones.

We shall assume that the contact interactions are infinitely strong ($\gamma \rightarrow \infty$) and the effective range of the dipolar interaction is negligible ($l_{\perp} \rightarrow 0$). The non-local LLGPE (36) simplifies to

$$i\hbar\partial_t\psi = \frac{\hbar^2}{2m} (-\partial_x^2 + \pi^2|\psi|^4) \psi - g_{\text{dd}}|\psi|^2\psi. \quad (55)$$

One can see it contains competing non-linearities. The one corresponding to local repulsion is the same as in the Kolomeisky equation (16), the other one – responsible for dipolar attraction – the same as in the GPE (14) with $g < 0$. I have solved Eq. (55) using the method described in Chap. 4, i.e. Eqs. (37)-(46).

The final formulas for the density and phase profile read

$$\rho(\zeta) = \rho_{\infty} - \frac{(\rho_{\infty} - \rho_{\min})(1 + D)}{1 + D \cosh(W\zeta)} \quad (56a)$$

and

$$\varphi(\zeta) = \frac{2mv(D+1)(\frac{\rho_{\min}}{\rho_{\infty}} - 1)}{\hbar DW\sqrt{1-a^2}} \arctan\left(\frac{(a-1)\tanh\left(\frac{W\zeta}{2}\right)}{\sqrt{1-a^2}}\right), \quad (56b)$$

where $a \equiv \frac{\rho_{\min}}{\rho_{\infty}} + \frac{\rho_{\min}}{D\rho_{\infty}} - 1$, $D \equiv \frac{\rho_{\min} - \rho_1}{2\rho_{\infty} - \rho_1 - \rho_{\min}}$, and $W \equiv 2\sqrt{\frac{\pi^2}{3}(\rho_{\infty} - \rho_{\min})(\rho_{\infty} - \rho_1)}$. Constant $\rho_{\min} = \frac{3mg_{\text{dd}}}{2\hbar^2\pi^2} - \rho_{\infty} + \frac{\sqrt{\Delta}}{2}$ with $\Delta = \left(2\rho_{\infty} - \frac{3mg_{\text{dd}}}{\hbar^2\pi^2}\right)^2 + \frac{12m^2v^2}{\hbar^2\pi^2}$ is the soliton density minimum and ρ_{∞} is the background density ($\lim_{\zeta \rightarrow \pm\infty} \rho(\zeta) = \rho_{\infty}$). There is no clear interpretation for $\rho_1 = \frac{3mg_{\text{dd}}}{2\hbar^2\pi^2} - \rho_{\infty} - \frac{\sqrt{\Delta}}{2}$, though.

It is quite handy to use the dipolar interaction strength $\gamma_{\text{dd}} \equiv mg_{\text{dd}}/\hbar^2\rho$ and the speed relative to the speed of sound $\beta = v/c$, where $c = \sqrt{\frac{\hbar^2\rho_0^2}{m^2}(\pi^2 - \gamma_{\text{dd}})}$ comes from the Bogoliubov analysis. As one can see, above $\gamma_{\text{dd}} > \pi^2$, the gas is unstable and thus cannot host a soliton.

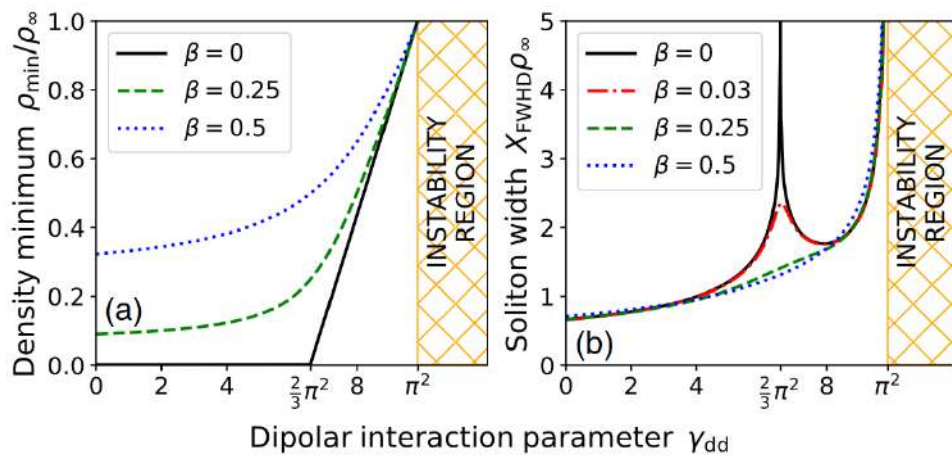


FIG. 20. (a) Soliton density minima ρ_{\min} as functions of the dipolar interaction strength γ_{dd} for different relative velocities β . (b) Soliton full width at half depth X_{FWHD} as functions of the dipolar interaction strength γ_{dd} for different relative velocities β .

Figure reprinted with permission from [J. Kopyciński *et al.*, Phys. Rev. Lett. **130**, 043401 (2023)]

© 2023 by American Physical Society.

Figure 20(a) shows us the solitonic density minimum ρ_{\min} as a function of the dipolar interaction strength. If we look at the line corresponding to the motionless soliton ($\beta = 0$), we can clearly see that, above $\gamma_{\text{dd}} = 2\pi^2/3$, it starts to behave oddly compared to the standard motionless solitons, which are fully depleted (black).

Let us now take a look at Fig. 20(b), which shows us the soliton full width at half depth $X_{\text{FWHD}} = 2\text{arccosh}[(1 + 2D)/D]/W$ such that $\rho(X_{\text{FWHD}}/2) = (\rho_{\infty} + \rho_{\min})/2$. There are two critical points, in which the width is diverging. The instability threshold $\gamma_{\text{dd}} = \pi^2$ and the other one for $\gamma_{\text{dd}} = 2\pi^2/3$. What is so special about the other critical point? The pressure P vanishes there. It is the very point, which corresponds to the conditions of quantum droplet existence.

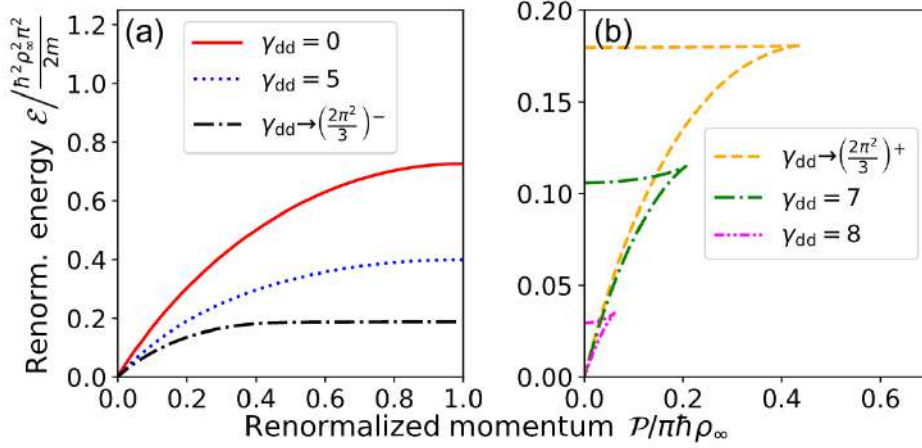


FIG. 21. (a) Soliton dispersion relation for $\gamma_{\text{dd}} < 2\pi^2/3$. (b) Soliton dispersion relation for $\gamma_{\text{dd}} > 2\pi^2/3$.

Figure reprinted with permission from [J. Kopyciński *et al.*, Phys. Rev. Lett. **130**, 043401 (2023)]

© 2023 by Americal Physical Society.

The motionless soliton width diverges logarithmically when $\gamma_{\text{dd}} \rightarrow \frac{2}{3}\pi^2$. On the other hand, when $\gamma_{\text{dd}} \rightarrow \pi^2$, the width diverges like $X_{\text{FWHD}} \propto |\gamma_{\text{dd}} - \pi^2|^{-\nu}$ with the critical exponent $\nu = 1/2$.

With the use of renormalization procedures as in Eqs. (49) and (50), we have plotted the dispersion relation for different γ_{dd} in Fig. 21. In the range $0 \leq \gamma_{\text{dd}} < \frac{2}{3}\pi^2$, the dispersion relation behaves qualitatively the same as the one coming from the Kolomeisky solution ($\gamma_{\text{dd}} = 0$) [125] (cf. Fig. 13), whereas, when $\gamma_{\text{dd}} > \frac{2}{3}\pi^2$, we observe a new subbranch formed. We have named these solutions *anomalous solitons*.

We complete our analysis with a simulation of droplet dynamics with a soliton induced via phase imprinting, which is a standard experimental method. Figure 22 shows us the time evolution of the droplet. We imprint a phase difference of $\Delta\varphi = \pi/2$ on a quarter of the droplet. From this moment on, we can observe a dark soliton moving with a relative velocity $\beta \approx 0.37$ and accompanied by shock waves. The droplet consists of $N = 20$ atoms so that it can be compared with the experiment described in Ref. [192].

Finally, I would like to briefly comment on the existence of a dark soliton inside the quantum droplet. I have written above that the droplet exists when $\gamma_{\text{dd}} = 2\pi^2/3$ or, more precisely, when the local interaction strength calculated for the bulk density equals to the critical value $m\gamma_{\text{dd}}/\hbar^2\rho_{\text{bulk}} = 2\pi^2/3$. For $\gamma_{\text{dd}} = 2\pi^2/3$, dark solitons do not exist. How is that possible then to

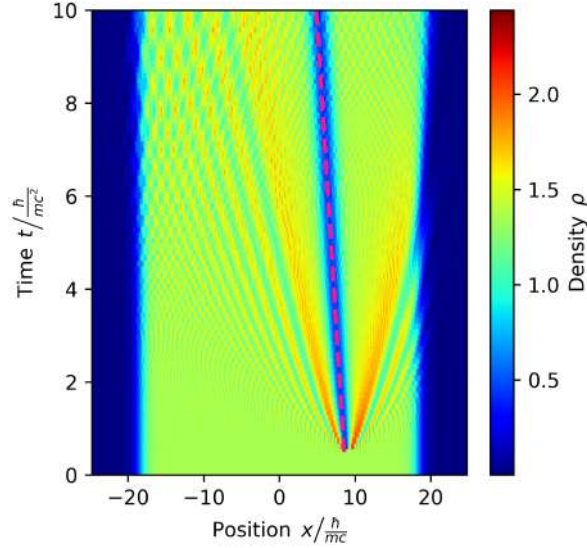


FIG. 22. Evolution of a quantum droplet given by Eq. (55) with dipolar interaction strength $\gamma_{dd} = 9$ after a phase imprint $\Delta\varphi = \pi/2$ at $t \approx \frac{mc^2}{\hbar}$. The dashed line marks a trajectory of an object moving with velocity $\beta = 0.3684(4)$, which was predicted from the shape of the soliton. The visible emerging high-density structures are the shock waves induced in the phase-imprinting process.

Figure reprinted with permission from [J. Kopyciński *et al.*, Phys. Rev. Lett. **130**, 043401 (2023)]

© 2023 by American Physical Society.

obtain a result like shown in Fig. 22? We owe it to finite-size effects. For a finite-size droplet the surface tension changes slightly the local γ_{dd} , which equals to $\frac{2}{3}\pi^2 \left[1 - \text{sech}\left(\pi\sqrt{N/3}\right)\right]^{-1}$ and in this regime, dark solitons do exist.

Our analytical calculations predict that dark solitons exist in the dipolar Bose gas with strong contact interactions. The solitons have a steerable width, which may be used to take an *in situ* image of them. Moreover, we have found a family of solitons with unusual properties and a peculiar dispersion relation.

Authorship statement – The PhD candidate has contributed to this article by performing all numerical calculations. The analytical ones have been also done by the candidate, although the linearization together with M. Łebek and the energy renormalization with W. Górecki. The PhD candidate has also written the first draft of the article and visualised the results.

6.3 Overview of Ref. [T3]

This time we will investigate a two-component Bose gas, in lieu of the single-component dipolar one. Our goal will be to prepare an easy-to-use GPE-like equation enabling to study non-linear phenomena beyond LHY.

To this end, we have taken QMC data from Ref. [144] and fitted them to get a numerical representation of the EDF $\mathcal{E}_{\text{mLLGP}}$. We use the density locking $\rho_{\downarrow}/\rho_{\uparrow} = \sqrt{g_{\uparrow\uparrow}/g_{\downarrow\downarrow}}$, introduced

already in Chap. 3 and an additional assumption of symmetric intraspecies interactions $g_{\uparrow\uparrow} = g_{\downarrow\downarrow}$. The equation we got reads

$$i\hbar\partial_t\psi(x,t) = \left(-\frac{\hbar^2}{2m}\partial_x^2 + \frac{\delta\mathcal{E}_{\text{LLGP}}[\rho; g_{\uparrow\downarrow}/g_{\uparrow\uparrow}]}{\delta\rho} \right) \psi(x,t), \quad (57)$$

where $\mathcal{E}_{\text{LLGP}}$ is encoded in the form of a spline and $g_{\uparrow\downarrow}/g_{\uparrow\uparrow}$ is the inter-to-intraspecies interaction ratio. We will refer to Eq. (57) as the Lieb-Liniger Gross-Pitaevskii equation for mixtures (mLLGPE).

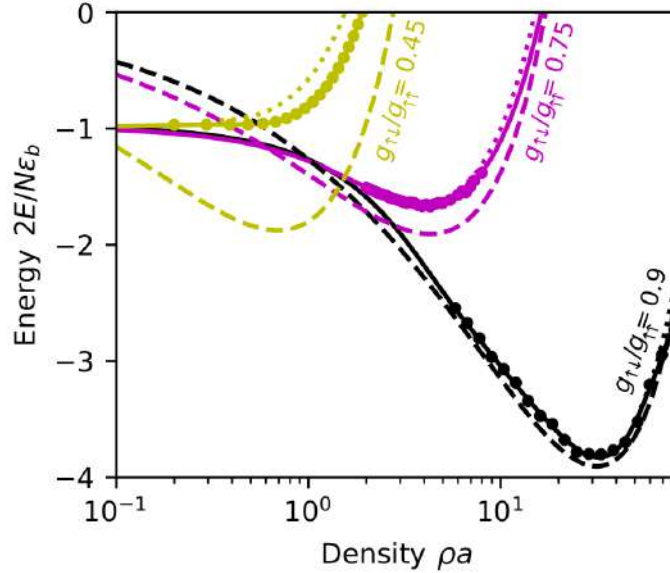


FIG. 23. Energy per particle as a function of density – comparison of different models: QMC from Ref. [144] (markers), our density functional dubbed mLLGPE (solid line), GGPE [139] (dashed line), pairing theory [146] (dotted line) - and interaction ratios $g_{\uparrow\downarrow}/g_{\uparrow\uparrow} = 0.45$ (yellow), 0.75 (magenta) and 0.9 (black). The QMC error bars are smaller than the marker sizes.

$\varepsilon_b = -(mg_{\uparrow\downarrow}^2/4\hbar^2)$ is the binding energy of an atomic pair in vacuum.

Figure reprinted from [J. Kopyciński *et al.*, Phys. Rev. Res. 5, 023050 (2023)]

on the CC BY 4.0 licence.

© 2023 by J. Kopyciński *et al.*

Figure 23 shows us the energy per particle of a homogeneous Bose-Bose mixture. When interaction ratios $g_{\uparrow\downarrow}/g_{\uparrow\uparrow} \simeq 1$ all three approaches (GGP, pairing theory and mLLGP) align well with QMC calculations. However, when the ratio decreases, a discrepancy shows up in the case of the GGP and pairing theory. At a ratio of $g_{\uparrow\downarrow}/g_{\uparrow\uparrow} = 0.45$, the GGP model exhibits a noticeable minimum in the energy per particle, in contrast to QMC, mLLGPE, and the pairing theory, which do not predict such a minimum. The pairing theory deviates from QMC data, providing only a qualitative match in this region. The liquid-to-gas transition occurs at $g_{\uparrow\downarrow}/g_{\uparrow\uparrow} = 0.47(2)$ [144].

As we have said in Chap. 5, the presence and position of the energy per particle minimum play a vital role in the context of quantum droplets. Namely, the equilibrium density ρ_{eq} , where $d(E/N)/d\rho = 0$, is the value of the density in the droplet bulk, assuming the droplet is sufficiently large, i.e. $N \gg 1$ and possesses a flat-top profile.

Based on this knowledge, we may see whether at a given density and interaction ratio we have a gaseous state (no minimum in E/N), liquid stable (minimum in E/N and $c^2 > 0$) or a liquid unstable state (minimum in E/N and $c^2 < 0$). We present it on a phase diagram in Fig. 24. The GGPE approach does not predict the gaseous state in such a system. Therefore, our approach gives a qualitative difference compared to the state-of-the-art mean-field+LHY model and agrees with *ab initio* QMC methods.

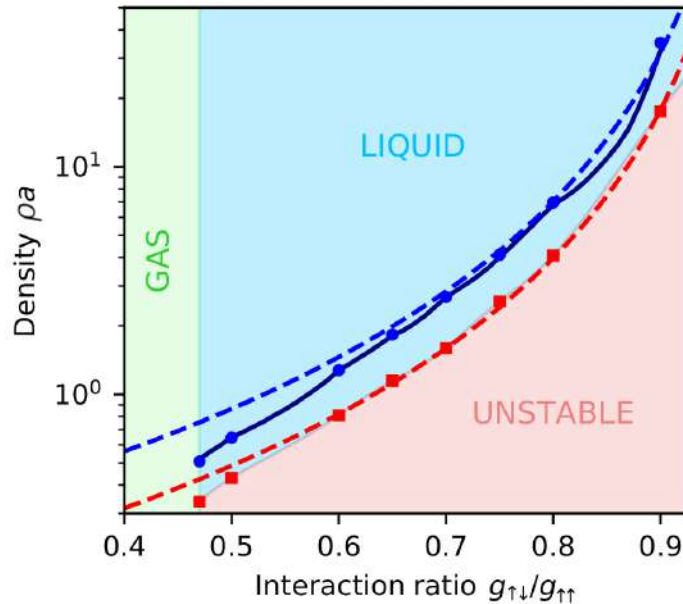


FIG. 24. Phase diagram of a homogeneous two-component mixture: the unstable region is demarcated by spinodal densities, predicted from GGPE (red dashed line) and QMC (square markers). Equilibrium density given by the mLLGP (navy solid line), GGPE (blue dashed line) and QMC from Ref. [144] (round markers).

Figure reprinted from [J. Kopyciński *et al.*, Phys. Rev. Res. 5, 023050 (2023)]
on the CC BY 4.0 licence.

© 2023 by J. Kopyciński *et al.*

Next, we study the monopole mode. We start a simulation with a slightly perturbed quantum droplet and extract the frequency of breathing. We show the results of this numerical analysis in Fig. 25 altogether with the monopole mode frequencies evaluated with the GGP [193] and linear response theory predictions based on QMC data [145], i.e. the data which were not used in to fit $\mathcal{E}_{\text{mLLGP}}$. In the limit of a large number of particles, all three approaches give consistent results. In this regime, the monopole mode frequency follows a scaling of $\omega \propto N^{-1}$ [193]. Remarkably, the QMC data aligns with the results obtained from the GGP, despite the GGP equation not being anticipated to be accurate for small N , due to the local density approximation, which typically requires the condition $N \gg 1$ to be satisfied.

The mLLGPE simulations generally exhibit agreement within a range of 2 uncertainties in most cases. The primary contributor to uncertainties stems from the form of $\mathcal{E}_{\text{mLLGP}}$ in low-density regions $\rho \ll \rho_{\text{eq}}$. Since there is a lack of Monte Carlo data in these regions, we

basically cannot control the quality of the fit below the equilibrium density. This becomes particularly important when the number of particles in the droplet is low. During the study of the monopole mode, the bulk density frequently falls below ρ_{eq} , especially following a slight expansion triggered by the perturbation we introduce. It might be one of the causes of why the frequency coming from mLLGPE slightly differs from QMC results for $N \simeq 1$. The number of particles seems to play an important role in shaping the breathing mode frequency [194].

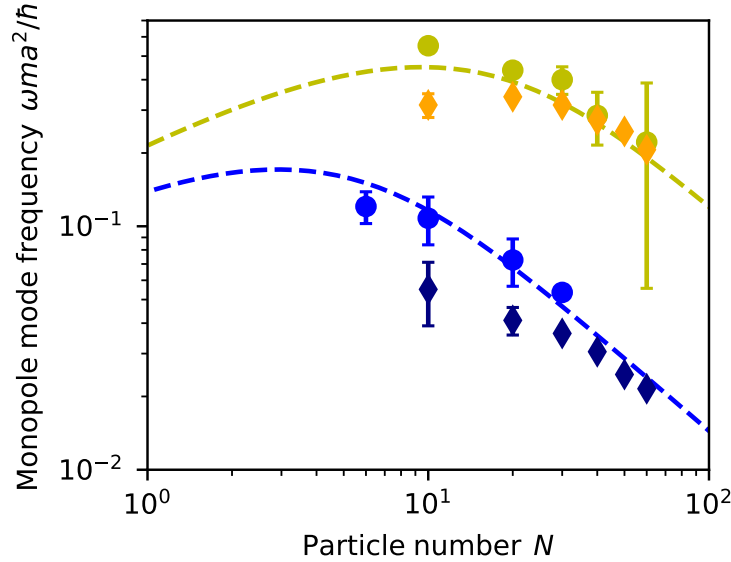


FIG. 25. Monopole mode frequency as a function of the number of particles in the droplet. Round markers correspond to the linear response theory prediction based on QMC data from Ref. [145], diamonds – to the mLLGPE, and the dashed lines – to the GGPE predictions. Frequencies evaluated at ratios $g_{\downarrow}/g_{\uparrow} = 0.6$ (blue) and 0.8 (yellow).

Figure reprinted from [J. Kopyciński *et al.*, Phys. Rev. Res. 5, 023050 (2023)]

on the CC BY 4.0 licence.

© 2023 by J. Kopyciński *et al.*

Until now, we have used the mLLGPE basically to reproduce the results obtained with exact methods. On the other hand, there are phenomena, for instance the non-linear ones, which are extremely difficult to investigate with *ab initio* methods. The mLLGPE might become useful here. We solved numerically Eq. (57) for solitons using the ansatz (37). The analytical method described in Chap. 4 was not available due to a purely numerical form of $\mathcal{E}_{\text{mLLGP}}$.

The results are quite similar to what we have already seen in Fig. 20. Motionless solitons there become wide when they approach to the instability region and a particular γ_{dd} , which is connected to the equilibrium density of dipolar droplets. Also, we have encountered an analogous situation with density minima there.

In the gaseous phase, solitons exhibit standard behavior, where the motionless soliton is fully depleted with a π -jump in its phase [see Fig. 26(a)]. However, as we transition to the liquid phase, motionless solitons are observed to be ultrawide and not black, as depicted in Fig. 26(c, e).

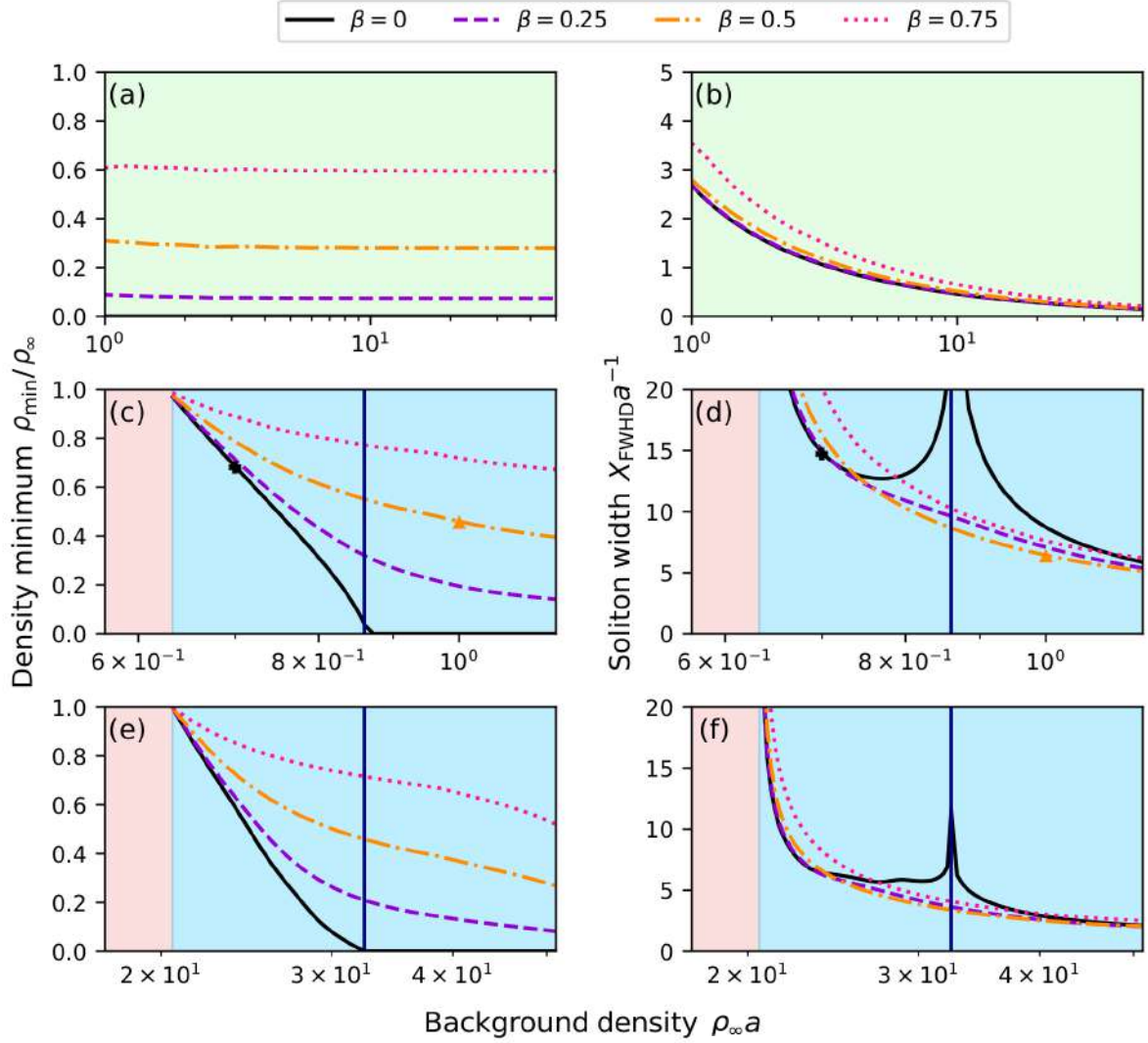


FIG. 26. Minimum densities ρ_{\min} (a, c, e) and full widths at half depth X_{FWHD} (b, d, f) of dark solitons for different relative velocities of the soliton β and interaction ratios $g_{\downarrow}/g_{\uparrow} = 0.4$ (a, b), 0.55 (c, d), and 0.9 (e, f). Green shading corresponds to gaseous phase, blue – to the liquid one and red – to the unstable regime (cf. Fig. 24). The vertical blue line marks the equilibrium density value; a is the scattering length.

Figure reprinted from [J. Kopyciński *et al.*, Phys. Rev. Res. 5, 023050 (2023)]

on the CC BY 4.0 licence.

© 2023 by J. Kopyciński *et al.*

In the weakly interacting regime, the soliton's minimum density is zero. However, below ρ_{eq} , we observe a region where the minimum density starts to increase, as shown in Fig. 26(c,e). This implies greying of motionless solitons. We have previously witnessed a similar phenomenon in Fig. 20, where motionless solitons widen upon approaching the instability region and a specific γ_{dd} linked to the equilibrium density of dipolar droplets. This behavior is reminiscent of the density minima encountered in that scenario.

Grey solitons also become shallower with decreasing density ρ_∞ . For $\beta > 0$, it is a gradual change though [cf. Fig. 26(c,e)]. Another difference is that the grey soliton width does not diverge when $\rho_\infty \rightarrow \rho_{\text{eq}}$, it does so in the vicinity of the unstable regime only [cf. Fig. 26(d,f)].

We have introduced a single-orbital energy density functional based on QMC data for a one-dimensional two-component bosonic mixture, i.e. the mLLGPE. Our method ensures quantitative agreement in the energy and chemical potential of a homogeneous state with the *ab initio* QMC model. To validate our approach, we have compared it against original QMC data, demonstrating the mLLGPE accurately predicts bulk density, monopole mode frequency ($\omega \propto N^{-1}$ for large particle numbers), and the correct phase diagram. Additionally, we explore solitonic solutions of the mLLGPE, unveiling ultrawide solitons and anomalous motionless solitons characterized by a non-zero density minimum and the absence of a π -jump in the phase.

Authorship statement – The PhD candidate conducted all numerical simulations. The PhD candidate has also written the first draft of the article and visualised the results.

This research has resulted from a collaboration with Joint Quantum Centre Durham-Newcastle. A two-month stay of the candidate in Newcastle upon Tyne was financed by the (Polish) National Science Centre.

6.4 Overview of Ref. [T4]

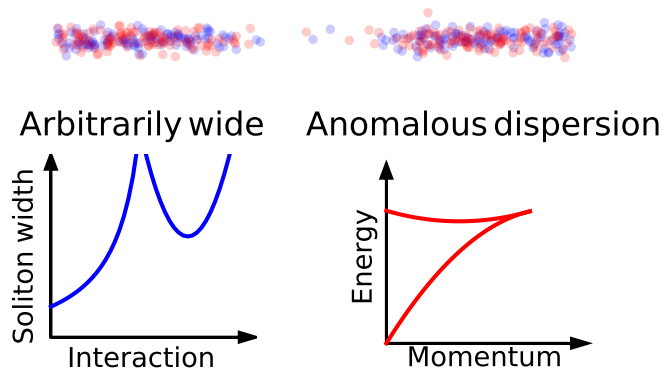


FIG. 27. Graphical abstract: We look again into dark solitons in two-component Bose gases (species coloured red and blue) with a beyond mean-field approach but focusing on weak interactions. Our analytical studies confirm that dark solitons can be arbitrarily wide in such systems. Moreover, we find a class of solutions with an anomalous dispersion relation and perform a stability analysis of these solutions. We predict the moving solitons can exist in the quantum droplets as their excitations.

Figure reprinted from [J. Kopyciński *et al.*, *J. Phys. B: At. Mol. Opt. Phys.* **57**, 035302 (2024)]
on the CC BY 4.0 licence.

© 2024 by J. Kopyciński *et al.*

Until now, we have seen anomalous solitons appearing in dipolar gases and mixtures described with beyond-LHY models. Quite unexpectedly, they are also present in the weakly interacting regime. Thus, we have decided to investigate a two-component gas with weak interactions, using the well known GGPE. We have chosen to check the stability of the solitons and find the interpretation of the two excitation subbranches.

We introduce a scaling $t = t_0\tilde{t}$, $x = x_0\tilde{x}$, $\psi = \psi_0\tilde{\psi}$, where we define the units of length $x_0 \equiv \frac{\pi\hbar^2}{m} \frac{\sqrt{2\delta g}}{\sqrt{g_{\uparrow\uparrow}g_{\downarrow\downarrow}}(\sqrt{g_{\uparrow\uparrow}} + \sqrt{g_{\downarrow\downarrow}})}$, time $t_0 = \hbar/mx_0^2$, energy $E_0 = \hbar/t_0$, and the normalization factor of the wave function $\psi_0 = \frac{(\sqrt{g_{\uparrow\uparrow}} + \sqrt{g_{\downarrow\downarrow}})^{3/2}}{\sqrt{\pi x_0 (2\delta g)^{3/4}}}$ [138]. For brevity, we skip the tildes and obtain the dimensionless GGPE

$$i\partial_t\psi(x,t) = -\frac{1}{2}\partial_x^2\psi(x,t) + |\Phi(x,t)|^2\psi(x,t) - |\psi(x,t)|\psi(x,t). \quad (58)$$

Using the method shown in Chap. 4, we obtain a function $U(\rho)$, which can be used to find the density and phase profiles of the solitons

$$U(\rho) = (\rho - \rho_\infty)^2 \left[v^2 - \rho + \frac{2\rho(2\sqrt{\rho} + \sqrt{\rho_\infty})}{3(\sqrt{\rho} + \sqrt{\rho_\infty})^2} \right]. \quad (59)$$

In principle, it is possible to proceed with the analytical calculations. Nevertheless, the solution is very complex and does not give much insight into the problem. The profiles $\rho(\zeta)$ and $\varphi(\zeta)$ were found numerically using Eq. (47) and (42).

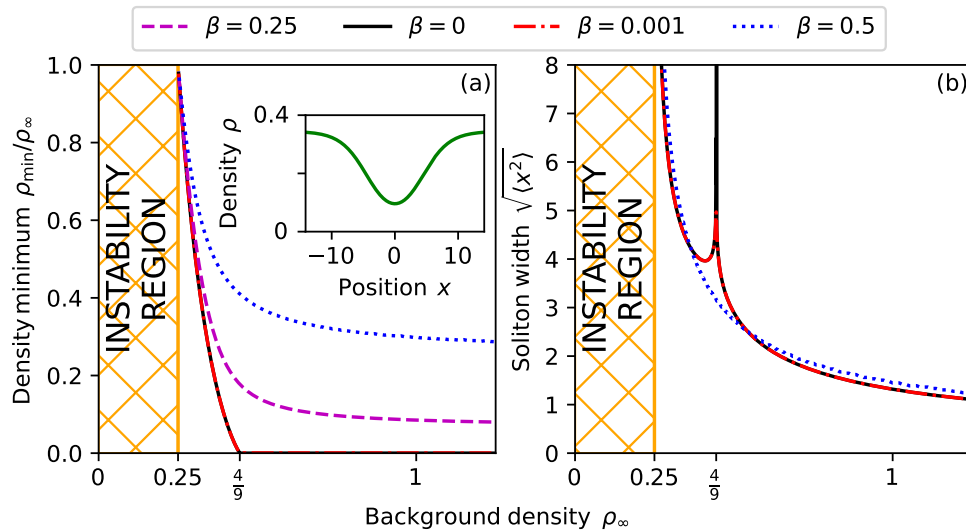


FIG. 28. Dark soliton (a) density minima and (b) root mean square widths as functions of the background density ρ_∞ for different relative velocities $\beta = \{0, 0.001, 0.25, 0.5\}$. Inset in (a): density profile of an anomalous soliton ($\beta = 0$ and $\rho_\infty = 0.345$). The solitonic properties of $\beta = 0.001$ will be important when we consider the coexistence of a quantum droplet and a dark soliton.

Figure reprinted from [J. Kopyciński *et al.*, J. Phys. B: At. Mol. Opt. Phys. **57**, 035302 (2024)]

on the CC BY 4.0 licence.

© 2024 by J. Kopyciński *et al.*

Figure 28 illustrates the density minimum ρ_{\min} and root mean square width $\sqrt{\langle x^2 \rangle - \langle x \rangle^2}$ of solitonic excitations based on the background density. Three distinct regions emerge: (i) the unstable liquid, (ii) anomalous, and (iii) the standard regime.

In the unstable region, we have no solitonic solutions. For $\rho_{\text{ins}} < \rho_{\infty} < \rho_{\text{eq}}$, we are in the anomalous regime. Conditions for anomalous soliton existence are satisfied, as detailed in [195, 196], marked by $0 < \rho_{\text{min}} < \rho_{\infty} < \rho_{\text{eq}}$ and stable uniform system conditions [$U(\rho_{\text{min}}) = U(\rho_{\infty}) = 0, U(\rho) < 0, \forall, \rho_{\text{min}} \leq \rho \leq \rho_{\infty}$, and $c^2 > 0$]. An inset in Fig. 28(a) displays a motionless anomalous soliton, characterized by partial density depletion and a constant phase profile ($\beta \equiv v/c = 0$). In the regime $\rho_{\infty} > \rho_{\text{eq}}$, solitons exhibit standard properties, featuring a black ($\beta = 0$) soliton with zero density and a typical π -jump in the phase.

Figure 28(b) reveals that motionless solitons, whether anomalous or standard, become ultrawide as $\rho_{\infty} \rightarrow \rho_{\text{eq}}$. This enables size control based on the number of atoms and interaction strengths $g_{\sigma\sigma'}$, just as we have seen it in earlier works.

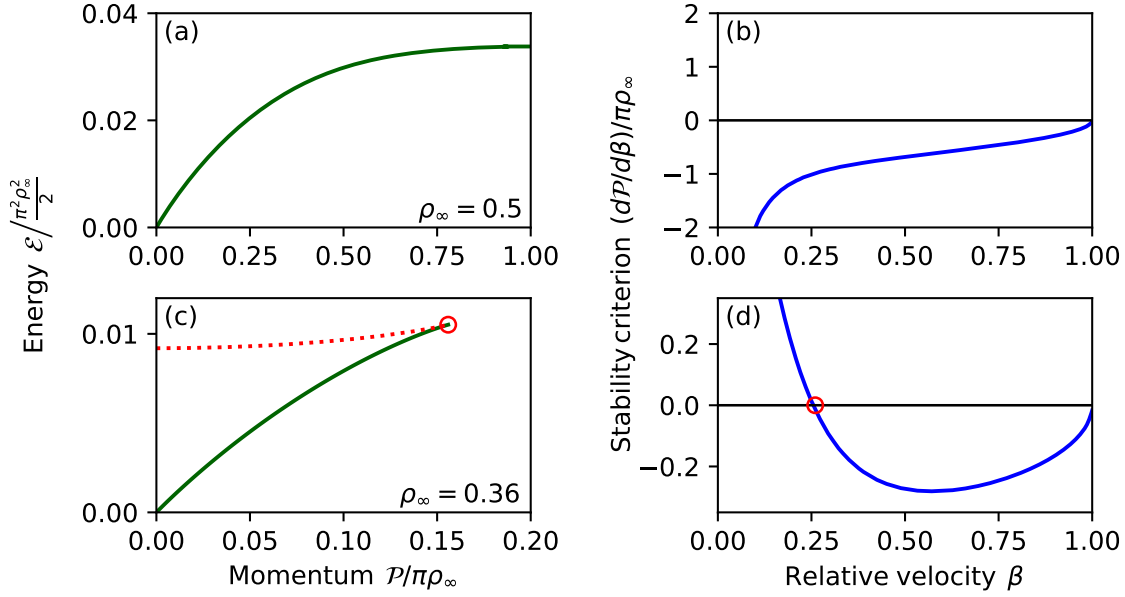


FIG. 29. (a,c) Dispersion relation of solitons (standard – top row, anomalous – bottom row). The red dashed line shows the upper subbranch. (b,d) Soliton stability criterion. Solitons are stable when $d\mathcal{P}/d\beta < 0$. In the standard regime, the solitons are stable everywhere. In the anomalous one – only above the critical velocity, which in this case of $\rho_{\infty} = 0.36$ is numerically evaluated to be $\beta_{\text{cr}} = 0.2550(29)$. [Red circles in panels (c,d) mark the place where the velocity of solitons equals the critical velocity β_{cr}].

Figure reprinted from [J. Kopyciński *et al.*, J. Phys. B: At. Mol. Opt. Phys. **57**, 035302 (2024)]
on the CC BY 4.0 licence.
© 2024 by J. Kopyciński *et al.*

Another distinctive feature of anomalous solitons, as previously discussed, is the emergence of a subbranch in the dispersion relation. In Fig. 29(a,c), we illustrate the relationship between the renormalized energy ϵ and momentum p .

A notable change in the energy spectrum occurs upon crossing $\rho_{\infty} = 4/9$ from above, entering the anomalous region. Specifically, an additional subbranch with a cusp becomes apparent, rendering the effective mass $m_{\text{eff}} = (d^2\epsilon/dp^2)^{-1}$ undefined due to the lack of derivative.

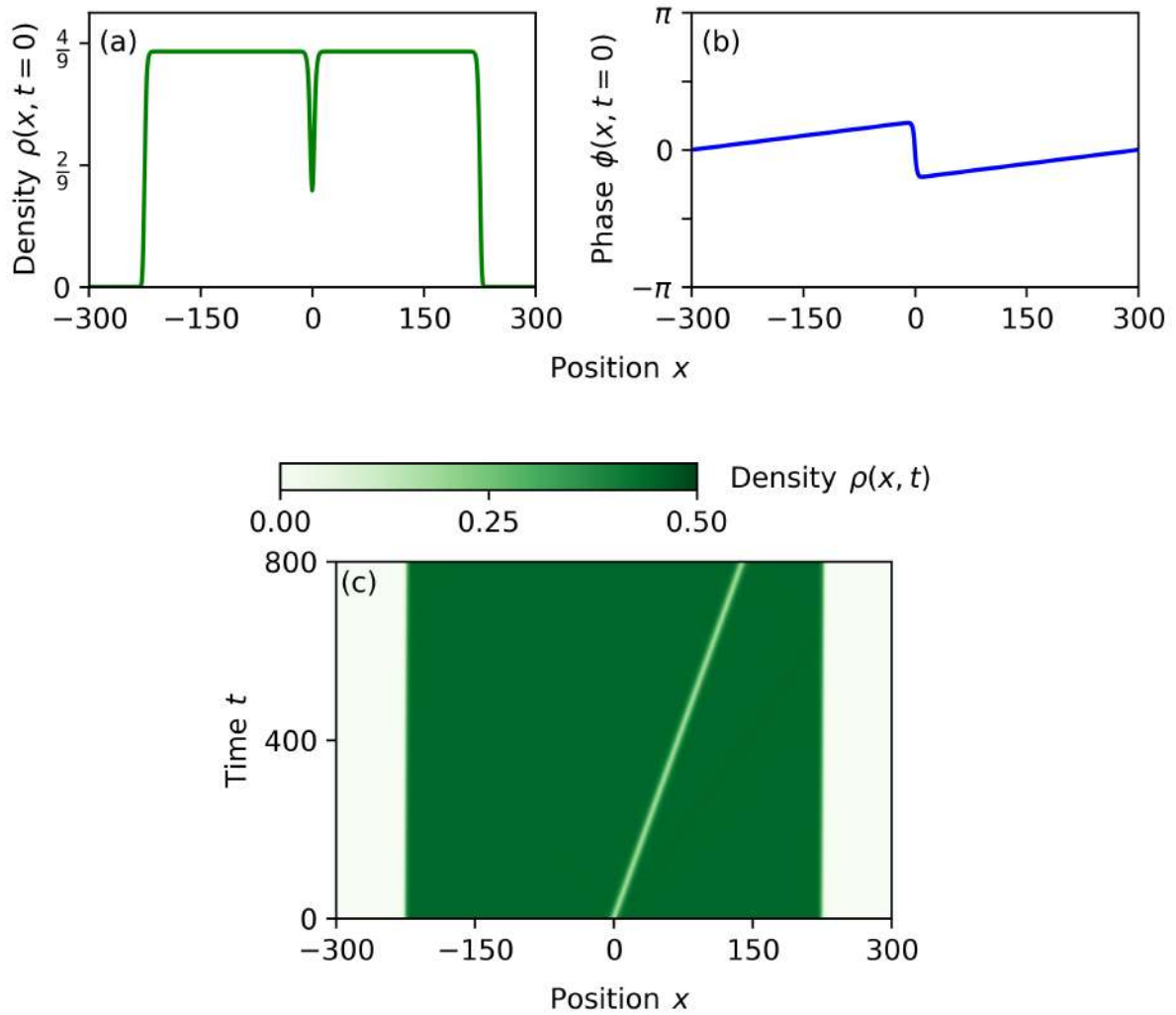


FIG. 30. Dark soliton in a quantum droplet. Initial density (a) and phase (b) profiles as well as a space-time diagram of evolution (c) of a quantum droplet with a grey ($\beta = 0.5$) soliton inside. The number of particles in the system $N = 198.079$.

Figure reprinted from [J. Kopyciński *et al.*, *J. Phys. B: At. Mol. Opt. Phys.* **57**, 035302 (2024)]

on the CC BY 4.0 licence.

© 2024 by J. Kopyciński *et al.*

Further insights arise from the stability analysis, where stability is ensured when $dp/d\beta < 0$ [133]. For our case, this criterion is met only for the lower branch of anomalous solitons, implying a critical velocity β_{cr} below which the anomalous soliton becomes unstable.

In Fig. 29(d), the stability criterion reveals that solitons are stable only above a specific velocity β_{cr} , as indicated by a red circle. A comparison with Fig. 29(c) shows that the upper subbranch corresponds to solitons moving with $\beta \leq \beta_{cr}$ (also marked with a red circle), revealing the upper branch as unstable. In contrast, standard solitons with $\rho_{\infty} > \rho_{eq}$ are consistently stable, as illustrated in Fig. 29(b), where $\beta_{cr} = 0$.

To corroborate the soliton stability, we conduct a numerical Bogoliubov-de Gennes analysis of solitonic wave functions, yielding results qualitatively consistent with the stability criterion from [133].

In Fig.30(a,b), we show an overall wave function $\psi(x)\psi_{\text{QD}}(x)$, where $\psi(x)$ is the solitonic wave function and

$$\psi_{\text{QD}}(x) = \frac{\sqrt{\rho_{\text{eq}}\mu/\mu_{\text{eq}}}}{1 + \sqrt{1 - \mu/\mu_{\text{eq}}} \cosh(\sqrt{-2\mu}x)} \quad (60)$$

is the wave function of a quantum droplet – an initial state to be evolved in real time dynamics. The parameter $\mu_{\text{eq}} = \rho_{\text{eq}} - \sqrt{\rho_{\text{eq}}}$ is the chemical potential corresponding to a homogeneous density profile with density $\rho = \rho_{\text{eq}}$ and the number of particles in the droplet N as a function of the chemical potential μ is given by [138]:

$$N = \rho_{\text{eq}} \sqrt{-\frac{2}{\mu_{\text{eq}}}} \left[\ln \left(\frac{1 + \sqrt{\mu/\mu_{\text{eq}}}}{\sqrt{1 - \mu/\mu_{\text{eq}}}} \right) - \sqrt{\mu/\mu_{\text{eq}}} \right]. \quad (61)$$

The space-time diagram in Fig. 30(c) shows us how the anomalous moving soliton behaves in a quantum droplet. The dynamics are very stable. We do not see any phonons or shock waves appearing.

This time, we have uncovered a relation between the dispersion relation and stability of the solitons. Namely, the upper subbranch corresponds to unstable solitonic solutions and the lower one – to the stable ones. Last but not least, we have shown a stable propagation of a soliton inside a quantum droplet.

Authorship statement – The PhD candidate has conducted all numerical simulations and literature review necessary to apprehend the meaning of two excitation subbranches. The analytical calculations have been done together with M. Łebek and W. Górecki. The candidate and B. Tüzemen have performed the stability analysis of solitons. The PhD candidate has also written the first draft of the article and visualised the results.

6.5. Concluding remarks

All four publications focus on non-linear phenomena in (quasi-)1D Bose gases beyond the mean-field approximation. Both dark solitons and quantum droplets in systems with competing interactions are present in each of the articles, although implicitly in the case of Ref. [T1]. Yet, it provides us with benchmark which has allowed us to adapt the model and use it to investigate dipolar systems with strong contact interaction. That article has also shown the need to experimentally realize dark solitons in strongly interacting systems. It would certainly help theorist to understand the link between non-linear and many-body methods to describe dark solitons.

Refs. [T2] and [T4] have shown us the possibilities of coexistence of quantum droplets and dark solitons. We have seen quite unusual dispersion relations and established a connection to the stability of solitons. The large width of these objects in systems with competing interactions might be useful in experiments to take *in situ* images of this special type of wave.

In the dipolar case, when the strength of the contact interactions is substantial, there is still an open question on the possibility of an experimental realization. Namely, we neglect the perpendicular degrees of freedom, which may be important in an experiment like the one done in Ref. [192]. There is a lack of many-body calculations, which would help us answer the question on whether or not strong contact interactions cause a substantial depletion to higher states in the perpendicular directions. The only clue so far is an analysis showing a sub-one-dimensionality of dipolar quantum droplets [197], an analogue of magnetostriction [198].

The theoretical descriptions of the two systems, which we investigate, produce qualitatively similar solitonic solutions. Even though two-component gases and dipolar ones are physically two distinct systems. One may expect that these features might be also present in a wider class of systems with competing interactions.

Finally, in Ref. [T3], we have created a novel equation, which gives e.g. droplet bulk densities qualitatively agreeing with QMC data. The mLLGPE ought to be a simple method providing with a correct phase diagram and the properties of both droplets and solitons. This awaits an experimental corroboration, though.

References

- [1] V. Titov, A. B. Rabinovich, H. O. Mofjeld, R. E. Thomson, and F. I. González, The global reach of the 26 December 2004 Sumatra tsunami, *Science* **309**, 2045 (2005).
- [2] A. Constantin and D. Henry, Solitons and tsunamis, *Z. Naturforsch. A* **64**, 65 (2009).
- [3] C. Pethick and H. Smith, Bose-Einstein condensation in dilute gases (Cambridge University Press, Cambridge, UK, 2008) Chap. 7. Dynamics of the condensate, 2nd ed.
- [4] A. Constantin and R. S. Johnson, Modelling tsunamis, *J. Phys. A Math. Gen.* **39**, L215 (2006).
- [5] J. E. Allen, The early history of solitons (solitary waves), *Phys. Scr.* **57**, 436 (1998).
- [6] D. J. Korteweg and G. de Vries, On the change of form of long waves advancing in a rectangular canal, and on a new type of long stationary waves, *Phil. Mag.* **39**, 422 (1895).
- [7] J. H. Adlam and J. E. Allen, The structure of strong collision-free hydromagnetic waves, *Phil. Mag.* **3**, 448 (1958).
- [8] M. Kono and M. M. Škorić, Solitons in plasmas, in *Nonlinear Physics of Plasmas* (Springer Berlin Heidelberg, Berlin, Heidelberg, 2010) pp. 151–195.
- [9] K. Stasiewicz, P. K. Shukla, G. Gustafsson, S. Buchert, B. Lavraud, B. Thidé, and Z. Klos, Slow magnetosonic solitons detected by the cluster spacecraft, *Phys. Rev. Lett.* **90**, 085002 (2003).
- [10] A. Hasegawa and F. Tappert, Transmission of stationary nonlinear optical pulses in dispersive dielectric fibers. I. Anomalous dispersion, *Appl. Phys. Lett.* **23**, 142 (1973).
- [11] J. K. Jang, M. Erkintalo, S. G. Murdoch, and S. Coen, Ultraweak long-range interactions of solitons observed over astronomical distances, *Nat. Photonics* **7**, 657 (2013).
- [12] Y. Yang, *Solitons in Field Theory and Nonlinear Analysis* (Springer New York, 2001).
- [13] M. H. Anderson, J. R. Ensher, M. R. Matthews, C. E. Wieman, and E. A. Cornell, Observation of Bose-Einstein condensation in a dilute atomic vapor, *Science* **269**, 198 (1995).
- [14] C. Pethick and H. Smith, Bose-Einstein condensation in dilute gases (Cambridge University Press, Cambridge, UK, 2008) Chap. 2. The non-interacting Bose gas, 2nd ed.
- [15] S. Burger, K. Bongs, S. Dettmer, W. Ertmer, K. Sengstock, A. Sanpera, G. V. Shlyapnikov, and M. Lewenstein, Dark solitons in Bose-Einstein condensates, *Phys. Rev. Lett.* **83**, 5198 (1999).
- [16] Y. S. Kivshar and D. E. Pelinovsky, Self-focusing and transverse instabilities of solitary waves, *Phys. Rep.* **331**, 117 (2000).
- [17] J. Brand and W. P. Reinhardt, Solitonic vortices and the fundamental modes of the “snake instability”: Possibility of observation in the gaseous Bose-Einstein condensate, *Phys. Rev. A* **65**, 043612 (2002).
- [18] F. Deuretzbacher, J. C. Cremon, and S. M. Reimann, Ground-state properties of few dipolar bosons in a quasi-one-dimensional harmonic trap, *Phys. Rev. A* **81**, 063616 (2010).
- [19] F. Deuretzbacher, J. C. Cremon, and S. M. Reimann, Erratum: Ground-state properties of few dipolar bosons in a quasi-one-dimensional harmonic trap [*Phys. Rev. A* **81**, 063616 (2010)], *Phys. Rev. A* **87**, 039903 (2013).
- [20] K. E. Strecker, G. B. Partridge, A. G. Truscott, and R. G. Hulet, Formation and propagation of matter-wave soliton trains, *Nature* **417**, 150–153 (2002).

- [21] I. Coddington, P. Engels, V. Schweikhard, and E. A. Cornell, Observation of Tkachenko oscillations in rapidly rotating Bose-Einstein condensates, *Phys. Rev. Lett.* **91**, 100402 (2003).
- [22] M. A. Hoefer, M. J. Ablowitz, I. Coddington, E. A. Cornell, P. Engels, and V. Schweikhard, Dispersive and classical shock waves in Bose-Einstein condensates and gas dynamics, *Phys. Rev. A* **74**, 023623 (2006).
- [23] T. Lahaye, J. Metz, B. Fröhlich, T. Koch, M. Meister, A. Griesmaier, T. Pfau, H. Saito, Y. Kawaguchi, and M. Ueda, d -wave collapse and explosion of a dipolar Bose-Einstein condensate, *Phys. Rev. Lett.* **101**, 080401 (2008).
- [24] H. Kadau, M. Schmitt, M. Wenzel, C. Wink, T. Maier, I. Ferrier-Barbut, and T. Pfau, Observing the Rosensweig instability of a quantum ferrofluid, *Nature* **530**, 194 (2016).
- [25] I. Ferrier-Barbut, H. Kadau, M. Schmitt, M. Wenzel, and T. Pfau, Observation of quantum droplets in a strongly dipolar Bose gas, *Phys. Rev. Lett.* **116**, 215301 (2016).
- [26] C. R. Cabrera, L. Tanzi, J. Sanz, B. Naylor, P. Thomas, P. Cheiney, and L. Tarruell, Quantum liquid droplets in a mixture of Bose-Einstein condensates, *Science* **359**, 301 (2018).
- [27] D. S. Petrov, Quantum mechanical stabilization of a collapsing Bose-Bose mixture, *Phys. Rev. Lett.* **115**, 155302 (2015).
- [28] T. D. Lee and C. N. Yang, Many-body problem in quantum mechanics and quantum statistical mechanics, *Phys. Rev.* **105**, 1119 (1957).
- [29] T. D. Lee, K. Huang, and C. N. Yang, Eigenvalues and eigenfunctions of a Bose system of hard spheres and its low-temperature properties, *Phys. Rev.* **106**, 1135 (1957).
- [30] E. Poli, T. Bland, C. Politi, L. Klaus, M. A. Norcia, F. Ferlaino, R. N. Bisset, and L. Santos, Maintaining supersolidity in one and two dimensions, *Phys. Rev. A* **104**, 063307 (2021).
- [31] L. Tanzi, E. Lucioni, F. Famà, J. Catani, A. Fioretti, C. Gabbanini, R. N. Bisset, L. Santos, and G. Modugno, Observation of a dipolar quantum gas with metastable supersolid properties, *Phys. Rev. Lett.* **122**, 130405 (2019).
- [32] J. Sato, R. Kanamoto, E. Kaminishi, and T. Deguchi, Exact relaxation dynamics of a localized many-body state in the 1D Bose gas, *Phys. Rev. Lett.* **108**, 110401 (2012).
- [33] A. Syrwid and K. Sacha, Lieb-Liniger model: Emergence of dark solitons in the course of measurements of particle positions, *Phys. Rev. A* **92**, 032110 (2015).
- [34] S. S. Shmailov and J. Brand, Quantum dark solitons in the one-dimensional Bose gas, *Phys. Rev. A* **99**, 043632 (2019).
- [35] P. Navez, D. Bitouk, M. Gajda, Z. Idziaszek, and K. Rzażewski, Fourth statistical ensemble for the Bose-Einstein condensate, *Phys. Rev. Lett.* **79**, 1789 (1997).
- [36] M. B. Christensen, T. Vibel, A. J. Hilliard, M. B. Kruk, K. Pawłowski, D. Hryniuk, K. Rzażewski, M. A. Kristensen, and J. J. Arlt, Observation of microcanonical atom number fluctuations in a Bose-Einstein condensate, *Phys. Rev. Lett.* **126**, 153601 (2021).
- [37] K. Sacha, *Kondensat Bosego-Einsteina* (Instytut Fizyki im. M. Smoluchowskiego, Uniwersytet Jagielloński, 2004).
- [38] C. Pethick and H. Smith, Bose-Einstein condensation in dilute gases (Cambridge University Press, Cambridge, UK, 2008) Chap. 15. Lower dimensions, 2nd ed.

- [39] J. Ulitzsch, D. Babik, R. Roell, and M. Weitz, Bose-Einstein condensation of erbium atoms in a quasielectrostatic optical dipole trap, *Phys. Rev. A* **95**, 043614 (2017).
- [40] G. Semeghini, G. Ferioli, L. Masi, C. Mazzinghi, L. Wolswijk, F. Minardi, M. Modugno, G. Modugno, M. Inguscio, and M. Fattori, Self-bound quantum droplets of atomic mixtures in free space, *Phys. Rev. Lett.* **120**, 235301 (2018).
- [41] C. D’Errico, A. Burchianti, M. Prevedelli, L. Salasnich, F. Ancilotto, M. Modugno, F. Minardi, and C. Fort, Observation of quantum droplets in a heteronuclear bosonic mixture, *Phys. Rev. Res.* **1**, 033155 (2019).
- [42] K. B. Davis, M. O. Mewes, M. R. Andrews, N. J. van Druten, D. S. Durfee, D. M. Kurn, and W. Ketterle, Bose-Einstein condensation in a gas of sodium atoms, *Phys. Rev. Lett.* **75**, 3969 (1995).
- [43] C. C. Bradley, C. A. Sackett, and R. G. Hulet, Bose-Einstein condensation of lithium: Observation of limited condensate number, *Phys. Rev. Lett.* **78**, 985 (1997).
- [44] D. G. Fried, T. C. Killian, L. Willmann, D. Landhuis, S. C. Moss, D. Kleppner, and T. J. Greytak, Bose-Einstein condensation of atomic hydrogen, *Phys. Rev. Lett.* **81**, 3811 (1998).
- [45] G. Modugno, G. Ferrari, G. Roati, R. J. Brecha, A. Simoni, and M. Inguscio, Bose-Einstein condensation of potassium atoms by sympathetic cooling, *Science* **294**, 1320 (2001).
- [46] F. Pereira Dos Santos, J. Léonard, J. Wang, C. J. Barrelet, F. Perales, E. Rasel, C. S. Unnikrishnan, M. Leduc, and C. Cohen-Tannoudji, Bose-Einstein condensation of metastable helium, *Phys. Rev. Lett.* **86**, 3459 (2001).
- [47] Y. Takasu, K. Maki, K. Komori, T. Takano, K. Honda, M. Kumakura, T. Yabuzaki, and Y. Takahashi, Spin-singlet Bose-Einstein condensation of two-electron atoms, *Phys. Rev. Lett.* **91**, 040404 (2003).
- [48] T. Weber, J. Herbig, M. Mark, H.-C. Nägerl, and R. Grimm, Bose-Einstein condensation of cesium, *Science* **299**, 232 (2003).
- [49] A. Griesmaier, J. Werner, S. Hensler, J. Stuhler, and T. Pfau, Bose-Einstein condensation of chromium, *Phys. Rev. Lett.* **94**, 160401 (2005).
- [50] S. Kraft, F. Vogt, O. Appel, F. Riehle, and U. Sterr, Bose-Einstein condensation of alkaline earth atoms: ^{40}Ca , *Phys. Rev. Lett.* **103**, 130401 (2009).
- [51] S. Stellmer, M. K. Tey, R. Grimm, and F. Schreck, Bose-Einstein condensation of ^{86}Sr , *Phys. Rev. A* **82**, 041602 (2010).
- [52] M. Lu, N. Q. Burdick, S. H. Youn, and B. L. Lev, Strongly dipolar Bose-Einstein condensate of dysprosium, *Phys. Rev. Lett.* **107**, 190401 (2011).
- [53] K. Aikawa, A. Frisch, M. Mark, S. Baier, A. Rietzler, R. Grimm, and F. Ferlaino, Bose-Einstein condensation of erbium, *Phys. Rev. Lett.* **108**, 210401 (2012).
- [54] H. Deng, G. Weihs, C. Santori, J. Bloch, and Y. Yamamoto, Condensation of semiconductor microcavity exciton polaritons, *Science* **298**, 199 (2002).
- [55] J. Kasprzak, M. Richard, S. Kundermann, A. Baas, P. Jeambrun, J. M. J. Keeling, F. M. Marchetti, M. H. Szymańska, R. André, J. L. Staehli, V. Savona, P. B. Littlewood, B. Deveaud, and L. S. Dang, Bose-Einstein condensation of exciton polaritons, *Nature* **443**, 409–414 (2006).

- [56] S. O. Demokritov, V. E. Demidov, O. Dzyapko, G. A. Melkov, A. A. Serga, B. Hillebrands, and A. N. Slavin, Bose–Einstein condensation of quasi-equilibrium magnons at room temperature under pumping, *Nature* **443**, 430–433 (2006).
- [57] J. Klaers, J. Schmitt, F. Vewinger, and M. Weitz, Bose–Einstein condensation of photons in an optical microcavity, *Nature* **468**, 545–548 (2010).
- [58] C. Pethick and H. Smith, Bose-Einstein condensation in dilute gases (Cambridge University Press, Cambridge, UK, 2008) Chap. 5. Interactions between atoms, 2nd ed.
- [59] U. Fano, Effects of configuration interaction on intensities and phase shifts, *Phys. Rev.* **124**, 1866 (1961).
- [60] H. Feshbach, A unified theory of nuclear reactions. II, *Ann. Phys.* **19**, 287 (1962).
- [61] W. C. Stwalley, Stability of spin-aligned hydrogen at low temperatures and high magnetic fields: New field-dependent scattering resonances and predissociations, *Phys. Rev. Lett.* **37**, 1628 (1976).
- [62] C. Deppner, W. Herr, M. Cornelius, P. Stromberger, T. Sternke, C. Grzeschik, A. Grote, J. Rudolph, S. Herrmann, M. Krutzik, A. Wenzlawski, R. Corgier, E. Charron, D. Guéry-Odelin, N. Gaaloul, C. Lämmerzahl, A. Peters, P. Windpassinger, and E. M. Rasel, Collective-mode enhanced matter-wave optics, *Phys. Rev. Lett.* **127**, 100401 (2021).
- [63] A. Grant, Water reveals the universe’s temperature 12.9 billion years ago, *Phys. Today* **2/22**, 0215a (2022).
- [64] R. Sahai, W. H. T. Vlemmings, and L. Å. Nyman, The coldest place in the universe: Probing the ultra-cold outflow and dusty disk in the Boomerang nebula, *Astrophys. J.* **841**, 110 (2017).
- [65] C. Pethick and H. Smith, Bose-Einstein condensation in dilute gases (Cambridge University Press, Cambridge, UK, 2008) Chap. 4. Trapping and cooling of atoms, 2nd ed.
- [66] W. D. Philips, Nobel lectures in physics (1996-2000) (World Scientific Publishing, Singapore, 2002) Chap. Laser cooling and trapping of neutral atoms.
- [67] M. D. Barrett, J. A. Sauer, and M. S. Chapman, All-optical formation of an atomic Bose-Einstein condensate, *Phys. Rev. Lett.* **87**, 010404 (2001).
- [68] D. S. Durfee and W. Ketterle, Experimental studies of Bose–Einstein condensation, *Opt. Express* **2**, 299 (1998).
- [69] R. Grimm, Laser cooling and trapping basics (Innsbruck, 2022), talk at Introductory Course on Ultracold Quantum Gases.
- [70] B. Seo, Z. Chen, M. Huang, M. K. Parit, Y. He, P. Chen, and G.-B. Jo, Apparatus for producing a ^{168}Er Bose–Einstein condensate, *J. Korean Phys. Soc.* **82**, 901–906 (2023).
- [71] J. R. Abo-Shaeer, C. Raman, J. M. Vogels, and W. Ketterle, Observation of vortex lattices in Bose-Einstein condensates, *Science* **292**, 476 (2001).
- [72] C. Pethick and H. Smith, Bose-Einstein condensation in dilute gases (Cambridge University Press, Cambridge, UK, 2008) Chap. 10. Superfluidity, 2nd ed.
- [73] A. V. Kavokin, J. J. Baumberg, G. Malpuech, and F. P. Laussy, Derivation of the Landau Criterion of Superfluidity and Landau Formula, in *Microcavities* (Oxford University Press, 2017).

- [74] E. Fonda, D. P. Meichle, N. T. Ouellette, S. Hormoz, and D. P. Lathrop, Direct observation of Kelvin waves excited by quantized vortex reconnection, *Proc. Natl. Acad. Sci.* **111**, 4707 (2014).
- [75] N. D. Mermin and D. M. Lee, Superfluid helium 3, *Sci. Am.* **235**, 56–71 (1976).
- [76] A. A. Abrikosov, Nobel Lecture: Type-II superconductors and the vortex lattice, *Rev. Mod. Phys.* **76**, 975 (2004).
- [77] M. W. Zwierlein, A. Schirotzek, C. H. Schunck, and W. Ketterle, Fermionic superfluidity with imbalanced spin populations, *Science* **311**, 492 (2006).
- [78] D. M. Brink and R. A. Broglia, *Nuclear Superfluidity: Pairing in Finite Systems*, Cambridge Monographs on Particle Physics, Nuclear Physics and Cosmology (Cambridge University Press, 2023).
- [79] P. W. Anderson and N. Itoh, Pulsar glitches and restlessness as a hard superfluidity phenomenon, *Nature* **256**, 25–27 (1975).
- [80] J. Bardeen, L. N. Cooper, and J. R. Schrieffer, Microscopic theory of superconductivity, *Phys. Rev.* **106**, 162 (1957).
- [81] D. S. Jin, J. R. Ensher, M. R. Matthews, C. E. Wieman, and E. A. Cornell, Collective excitations of a Bose-Einstein condensate in a dilute gas, *Phys. Rev. Lett.* **77**, 420 (1996).
- [82] M.-O. Mewes, M. R. Andrews, N. J. van Druten, D. M. Kurn, D. S. Durfee, C. G. Townsend, and W. Ketterle, Collective excitations of a Bose-Einstein condensate in a magnetic trap, *Phys. Rev. Lett.* **77**, 988 (1996).
- [83] M. A. Norcia, E. Poli, C. Politi, L. Klaus, T. Bland, M. J. Mark, L. Santos, R. N. Bisset, and F. Ferlaino, Can angular oscillations probe superfluidity in dipolar supersolids?, *Phys. Rev. Lett.* **129**, 040403 (2022).
- [84] M. R. Andrews, C. G. Townsend, H.-J. Miesner, D. S. Durfee, D. M. Kurn, and W. Ketterle, Observation of interference between two Bose condensates, *Science* **275**, 637 (1997).
- [85] M.-O. Mewes, M. R. Andrews, D. M. Kurn, D. S. Durfee, C. G. Townsend, and W. Ketterle, Output coupler for Bose-Einstein condensed atoms, *Phys. Rev. Lett.* **78**, 582 (1997).
- [86] I. Bloch, T. W. Hänsch, and T. Esslinger, Atom laser with a cw output coupler, *Phys. Rev. Lett.* **82**, 3008 (1999).
- [87] M. F. Riedel, P. Böhi, Y. Li, T. W. Hänsch, A. Sinatra, and P. Treutlein, Atom-chip-based generation of entanglement for quantum metrology, *Nature* **464**, 1170–1173 (2010).
- [88] D. Kajtoch, K. Pawłowski, and E. Witkowska, Metrologically useful states of spin-1 Bose condensates with macroscopic magnetization, *Phys. Rev. A* **97**, 023616 (2018).
- [89] J. Czajkowski, K. Pawłowski, and R. Demkowicz-Dobrzański, Many-body effects in quantum metrology, *New J. Phys.* **21**, 053031 (2019).
- [90] G. Barontini and M. Paternostro, Ultra-cold single-atom quantum heat engines, *New J. Phys.* **21**, 063019 (2019).
- [91] W. Niedenzu, I. Mazets, G. Kurizki, and F. Jendrzejewski, Quantized refrigerator for an atomic cloud, *Quantum* **3**, 155 (2019).
- [92] Q. Bouton, J. Nettersheim, S. Burgardt, D. Adam, E. Lutz, and A. Widera, A quantum heat engine driven by atomic collisions, *Nat. Commun.* **12**, 2063 (2021).

- [93] N. M. Myers, F. J. Peña, O. Negrete, P. Vargas, G. De Chiara, and S. Deffner, Boosting engine performance with Bose–Einstein condensation, *New J. Phys.* **24**, 025001 (2022).
- [94] J. Fraxanet, T. Salamon, and M. Lewenstein, The coming decades of quantum simulation, in *Sketches of Physics: The Celebration Collection*, edited by R. Citro, M. Lewenstein, A. Rubio, W. P. Schleich, J. D. Wells, and G. P. Zank (Springer International Publishing, Cham, CH, 2023) pp. 85–125.
- [95] I. Bloch, J. Dalibard, and S. Nascimbène, Quantum simulations with ultracold quantum gases, *Nature Phys.* **8**, 267–276 (2012).
- [96] T. Byrnes, K. Wen, and Y. Yamamoto, Macroscopic quantum computation using Bose-Einstein condensates, *Phys. Rev. A* **85**, 040306 (2012).
- [97] T. Byrnes, D. Rosseau, M. Khosla, A. Pyrkov, A. Thomasen, T. Mukai, S. Koyama, A. Abdelrahman, and E. Ilo-Okeke, Macroscopic quantum information processing using spin coherent states, *Opt. Commun.* **337**, 102 (2015).
- [98] E. Ghasemian, Dissipative quantum computation and quantum state preparation based on BEC qubits, *J. Opt. Soc. Am. B* **40**, 247 (2023).
- [99] G. Fujii, Measurement-based quantum computation using two-component BECs, *Phys. Scr.* **98**, 065109 (2023).
- [100] M. Crăciun and T. Harko, Testing Bose–Einstein condensate dark matter models with the SPARC galactic rotation curves data, *Eur. Phys. J. C* **80**, 8 (2020).
- [101] E. Poli, T. Bland, S. J. M. White, M. J. Mark, F. Ferlaino, S. Trabucco, and M. Mannarelli, Glitches in rotating supersolids, *Phys. Rev. Lett.* **131**, 223401 (2023).
- [102] J. Steinhauer, Observation of quantum Hawking radiation and its entanglement in an analogue black hole, *Nature Phys.* **12**, 959–965 (2016).
- [103] J. R. Muñoz de Nova, K. Golubkov, V. I. Kolobov, and J. Steinhauer, Observation of thermal Hawking radiation and its temperature in an analogue black hole, *Nature* **569**, 688–691 (2019).
- [104] V. I. Kolobov, K. Golubkov, J. R. Muñoz de Nova, and J. Steinhauer, Observation of stationary spontaneous Hawking radiation and the time evolution of an analogue black hole, *Nature Phys.* **17**, 362–367 (2021).
- [105] Z. Hadzibabic and M. Köhl, Low-dimensional atomic Bose gases, in *Ultracold Bosonic and Fermionic Gases*, Contemporary Concepts of Condensed Matter Science, Vol. 5, edited by K. Levin, A. L. Fetter, and D. M. Stamper-Kurn (Elsevier, 2012) pp. 95–120.
- [106] E. H. Lieb and W. Liniger, Exact analysis of an interacting Bose Gas. I. the general solution and the ground state, *Phys. Rev.* **130**, 1605 (1963).
- [107] Z. Ristivojevic, Conjectures about the ground-state energy of the Lieb-Liniger model at weak repulsion, *Phys. Rev. B* **100**, 081110 (2019).
- [108] G. Lang, F. Hekking, and A. Minguzzi, Ground-state energy and excitation spectrum of the Lieb-Liniger model: Accurate analytical results and conjectures about the exact solution, *SciPost Phys.* **3**, 003 (2017).
- [109] S. Prolhac, Ground state energy of the δ -Bose and Fermi gas at weak coupling from double extrapolation, *J. Phys. A: Math. Theor.* **50**, 144001 (2017).

- [110] L. P. Pitaevskii, Vortex lines in an imperfect Bose gas, *Sov. Phys. JETP* **13**, 646 (1960), [*Zh. Eksp. Teor. Fiz.*, **40**, 451 (1961)].
- [111] E. P. Gross, Structure of a quantized vortex in boson systems, *Nuovo Cim.* **20**, 454 (1961).
- [112] F. Dalfovo, S. Giorgini, L. P. Pitaevskii, and S. Stringari, Theory of Bose-Einstein condensation in trapped gases, *Rev. Mod. Phys.* **71**, 463 (1999).
- [113] G. Baym and C. J. Pethick, Ground-state properties of magnetically trapped Bose-condensed rubidium gas, *Phys. Rev. Lett.* **76**, 6 (1996).
- [114] A. D. Jackson, G. M. Kavoulakis, and C. J. Pethick, Solitary waves in clouds of Bose-Einstein condensed atoms, *Phys. Rev. A* **58**, 2417 (1998).
- [115] H.-J. Miesner, D. M. Stamper-Kurn, M. R. Andrews, D. S. Durfee, S. Inouye, and W. Ketterle, Bosonic stimulation in the formation of a Bose-Einstein condensate, *Science* **279**, 1005 (1998).
- [116] D. A. Butts and D. S. Rokhsar, Predicted signatures of rotating Bose-Einstein condensates, *Nature* **397**, 327–329 (1999).
- [117] Z. Dutton, M. Budde, C. Slowe, and L. V. Hau, Observation of quantum shock waves created with ultra-compressed slow light pulses in a Bose-Einstein condensate, *Science* **293**, 663 (2001).
- [118] E. Gershnabel, N. Katz, E. Rowen, and N. Davidson, The Bogoliubov excitation spectrum in anharmonic traps, *New J. Phys.* **6**, 127–127 (2004).
- [119] M. S. Pindzola and B. Sun, Collective modes of ground and excited states of Bose-Einstein condensates in axially symmetric anisotropic traps, *J. Phys. B: At. Mol. Opt. Phys.* **43**, 235302 (2010).
- [120] M. T. Reeves, T. P. Billam, B. P. Anderson, and A. S. Bradley, Inverse energy cascade in forced two-dimensional quantum turbulence, *Phys. Rev. Lett.* **110**, 104501 (2013).
- [121] W. Kohn and L. J. Sham, Self-consistent equations including exchange and correlation effects, *Phys. Rev.* **140**, A1133 (1965).
- [122] J. P. Perdew and S. Kurth, Density functionals for non-relativistic Coulomb systems in the new century, in *A Primer in Density Functional Theory*, edited by C. Fiolhais, F. Nogueira, and M. A. L. Marques (Springer Berlin Heidelberg, Berlin, Heidelberg, DE, 2003) pp. 1–55.
- [123] M. Girardeau, Relationship between systems of impenetrable bosons and fermions in one dimension, *J. Math. Phys.* **1**, 516–523 (1960).
- [124] M. D. Girardeau, Permutation symmetry of many-particle wave functions, *Phys. Rev.* **139**, B500 (1965).
- [125] E. B. Kolomeisky, T. J. Newman, J. P. Straley, and X. Qi, Low-dimensional Bose liquids: Beyond the Gross-Pitaevskii approximation, *Phys. Rev. Lett.* **85**, 1146 (2000).
- [126] J. Friedel, Metallic alloys, *Nuovo Cim.* **7**, 287–311 (1958).
- [127] M. D. Girardeau and E. M. Wright, Breakdown of time-dependent mean-field theory for a one-dimensional condensate of impenetrable bosons, *Phys. Rev. Lett.* **84**, 5239 (2000).
- [128] P. Öhberg and L. Santos, Dynamical transition from a quasi-one-dimensional Bose-Einstein condensate to a Tonks-Girardeau gas, *Phys. Rev. Lett.* **89**, 240402 (2002).
- [129] S. Peotta and M. D. Ventra, Quantum shock waves and population inversion in collisions of ultracold atomic clouds, *Phys. Rev. A* **89**, 013621 (2014).

- [130] S. Choi, V. Dunjko, Z. D. Zhang, and M. Olshanii, Monopole excitations of a harmonically trapped one-dimensional Bose gas from the ideal gas to the Tonks-Girardeau regime, *Phys. Rev. Lett.* **115**, 115302 (2015).
- [131] M. L. Chiofalo, S. Succi, and M. P. Tosi, Ground state of trapped interacting Bose-Einstein condensates by an explicit imaginary-time algorithm, *Phys. Rev. E* **62**, 7438 (2000).
- [132] N. N. Bogoljubov, On a new method in the theory of superconductivity, *Nuovo Cim.* **7**, 794–805 (1958).
- [133] I. Barashenkov, A. Gocheva, V. Makhankov, and I. Puzynin, Stability of the soliton-like “bubbles”, *Phys. D* **34**, 240 (1989).
- [134] R. Kanamoto, H. Saito, and M. Ueda, Quantum phase transition in one-dimensional Bose-Einstein condensates with attractive interactions, *Phys. Rev. A* **67**, 013608 (2003).
- [135] L. Santos, G. V. Shlyapnikov, and M. Lewenstein, Roton-maxon spectrum and stability of trapped dipolar Bose-Einstein condensates, *Phys. Rev. Lett.* **90**, 250403 (2003).
- [136] D. H. J. O’Dell, S. Giovanazzi, and G. Kurizki, Rotons in gaseous Bose-Einstein condensates irradiated by a laser, *Phys. Rev. Lett.* **90**, 110402 (2003).
- [137] C. Pethick and H. Smith, Bose-Einstein condensation in dilute gases (Cambridge University Press, Cambridge, UK, 2008) Chap. 12. Mixtures and spinor condensates, 2nd ed.
- [138] M. Tylutki, G. E. Astrakharchik, B. A. Malomed, and D. S. Petrov, Collective excitations of a one-dimensional quantum droplet, *Phys. Rev. A* **101**, 051601 (2020).
- [139] D. S. Petrov and G. E. Astrakharchik, Ultradilute low-dimensional liquids, *Phys. Rev. Lett.* **117**, 100401 (2016).
- [140] C. N. Yang, Some exact results for the many-body problem in one dimension with repulsive delta-function interaction, *Phys. Rev. Lett.* **19**, 1312 (1967).
- [141] M. Gaudin, Un système à une dimension de fermions en interaction, *Phys. Lett. A* **24**, 55 (1967).
- [142] N. J. Robinson and R. M. Konik, Excitations in the Yang–Gaudin Bose gas, *J. Stat. Mech.* **2017**, 063101 (2017).
- [143] P. J. Reynolds, J. Tobochnik, and H. Gould, Diffusion quantum Monte Carlo, *Comput. Phys.* **4**, 662–668 (1990).
- [144] L. Parisi, G. E. Astrakharchik, and S. Giorgini, Liquid state of one-dimensional Bose mixtures: A quantum Monte Carlo study, *Phys. Rev. Lett.* **122**, 105302 (2019).
- [145] L. Parisi and S. Giorgini, Quantum droplets in one-dimensional Bose mixtures: A quantum Monte Carlo study, *Phys. Rev. A* **102**, 023318 (2020).
- [146] H. Hu, J. Wang, and X.-J. Liu, Microscopic pairing theory of a binary Bose mixture with interspecies attractions: Bosonic BEC-BCS crossover and ultradilute low-dimensional quantum droplets, *Phys. Rev. A* **102**, 043301 (2020).
- [147] M. Ota and G. E. Astrakharchik, Beyond Lee-Huang-Yang description of self-bound Bose mixtures, *SciPost Phys.* **9**, 020 (2020).
- [148] F. Wächtler and L. Santos, Quantum filaments in dipolar Bose-Einstein condensates, *Phys. Rev. A* **93**, 061603 (2016).

- [149] M. Edmonds, T. Bland, and N. Parker, Quantum droplets of quasi-one-dimensional dipolar Bose–Einstein condensates, *J. Phys. Commun.* **4**, 125008 (2020).
- [150] P. Zin, M. Pylak, T. Wasak, M. Gajda, and Z. Idziaszek, Quantum Bose-Bose droplets at a dimensional crossover, *Phys. Rev. A* **98**, 051603 (2018).
- [151] P. Zin, M. Pylak, T. Wasak, K. Jachymski, and Z. Idziaszek, Quantum droplets in a dipolar Bose gas at a dimensional crossover, *J. Phys. B: At. Mol. Opt. Phys.* **54**, 165302 (2021).
- [152] R. M. Ziff, G. E. Uhlenbeck, and M. Kac, The ideal Bose-Einstein gas, revisited, *Phys. Rep.* **32**, 169 (1977).
- [153] J. T. Lewis, Why do bosons condense?, in *Statistical Mechanics and Field Theory: Mathematical Aspects*, edited by T. C. Dorlas, N. M. Hugenholtz, and M. Winnink (Springer Berlin Heidelberg, Berlin, Heidelberg, DE, 1986) pp. 234–256.
- [154] A. Trautmann, P. Ilzhöfer, G. Durastante, C. Politi, M. Sohmen, M. J. Mark, and F. Ferlaino, Dipolar quantum mixtures of erbium and dysprosium atoms, *Phys. Rev. Lett.* **121**, 213601 (2018).
- [155] G. Durastante, C. Politi, M. Sohmen, P. Ilzhöfer, M. J. Mark, M. A. Norcia, and F. Ferlaino, Feshbach resonances in an erbium-dysprosium dipolar mixture, *Phys. Rev. A* **102**, 033330 (2020).
- [156] R. N. Bisset, L. A. Peña Ardila, and L. Santos, Quantum droplets of dipolar mixtures, *Phys. Rev. Lett.* **126**, 025301 (2021).
- [157] Y. S. Kivshar and B. Luther-Davies, Dark optical solitons: physics and applications, *Phys. Rep.* **298**, 81 (1998).
- [158] L. Khaykovich, F. Schreck, G. Ferrari, T. Bourdel, J. Cubizolles, L. D. Carr, Y. Castin, and C. Salomon, Formation of a matter-wave bright soliton, *Science* **296**, 1290 (2002).
- [159] T. Karpiuk, P. Deuar, P. Bienias, E. Witkowska, K. Pawłowski, M. Gajda, K. Rzążewski, and M. Brewczyk, Spontaneous solitons in the thermal equilibrium of a quasi-1D Bose gas, *Phys. Rev. Lett.* **109**, 205302 (2012).
- [160] J. Denschlag, J. E. Simsarian, D. L. Feder, C. W. Clark, L. A. Collins, J. Cubizolles, L. Deng, E. W. Hagley, K. Helmerson, W. P. Reinhardt, S. L. Rolston, B. I. Schneider, and W. D. Phillips, Generating solitons by phase engineering of a Bose-Einstein condensate, *Science* **287**, 97 (2000).
- [161] B. Wu, J. Liu, and Q. Niu, Controlled generation of dark solitons with phase imprinting, *Phys. Rev. Lett.* **88**, 034101 (2002).
- [162] L. D. Landau and E. M. Lifshitz, *Fluid mechanics*, 2nd ed. (Pergamon Press, Oxford, UK, 1987).
- [163] K. Pawłowski and K. Rzążewski, Dipolar dark solitons, *New J. Phys.* **17**, 105006 (2015).
- [164] M. Edmonds, Dark quantum droplets and solitary waves in beyond-mean-field Bose-Einstein condensate mixtures, *Phys. Rev. Res.* **5**, 023175 (2023).
- [165] E. H. Lieb, Exact analysis of an interacting Bose gas. II. The excitation spectrum, *Phys. Rev.* **130**, 1616 (1963).
- [166] A. D. Jackson and G. M. Kavoulakis, Lieb mode in a quasi-one-dimensional Bose-Einstein condensate of atoms, *Phys. Rev. Lett.* **89**, 070403 (2002).

- [167] R. Kanamoto, L. D. Carr, and M. Ueda, Topological winding and unwinding in metastable Bose-Einstein condensates, *Phys. Rev. Lett.* **100**, 060401 (2008).
- [168] T. Karpiuk, T. Sowiński, M. Gajda, K. Rzażewski, and M. Brewczyk, Correspondence between dark solitons and the type II excitations of the Lieb-Liniger model, *Phys. Rev. A* **91**, 013621 (2015).
- [169] N. D. Mermin, The topological theory of defects in ordered media, *Rev. Mod. Phys.* **51**, 591 (1979).
- [170] W. H. Zurek, Causality in condensates: Gray solitons as relics of BEC formation, *Phys. Rev. Lett.* **102**, 105702 (2009).
- [171] J. R. Grover, Shell-model calculations of the lowest-energy nuclear excited states of very high angular momentum, *Phys. Rev.* **157**, 832 (1967).
- [172] J. Sato, R. Kanamoto, E. Kaminishi, and T. Deguchi, Quantum states of dark solitons in the 1D Bose gas, *New J. Phys.* **18**, 075008 (2016).
- [173] A. Bulgac, Dilute quantum droplets, *Phys. Rev. Lett.* **89**, 050402 (2002).
- [174] F. Ferlaino, A. Zenesini, M. Berninger, B. Huang, H. C. Nägerl, and R. Grimm, Efimov resonances in ultracold quantum gases, *Few-Body Syst.* **51**, 113–133 (2011).
- [175] D. S. Petrov, Three-body interacting bosons in free space, *Phys. Rev. Lett.* **112**, 103201 (2014).
- [176] F. Böttcher, J.-N. Schmidt, J. Hertkorn, K. S. H. Ng, S. D. Graham, M. Guo, T. Langen, and T. Pfau, New states of matter with fine-tuned interactions: quantum droplets and dipolar supersolids, *Rep. Prog. Phys.* **84**, 012403 (2020).
- [177] L. Chomaz, S. Baier, D. Petter, M. J. Mark, F. Wächtler, L. Santos, and F. Ferlaino, Quantum-fluctuation-driven crossover from a dilute Bose-Einstein condensate to a macrodroplet in a dipolar quantum fluid, *Phys. Rev. X* **6**, 041039 (2016).
- [178] R. Ołdziejewski, W. Górecki, K. Pawłowski, and K. Rzażewski, Strongly correlated quantum droplets in quasi-1D dipolar Bose gas, *Phys. Rev. Lett.* **124**, 090401 (2020).
- [179] L. Dong, K. Shi, and C. Huang, Internal modes of two-dimensional quantum droplets, *Phys. Rev. A* **106**, 053303 (2022).
- [180] D. Baillie, R. M. Wilson, and P. B. Blakie, Collective excitations of self-bound droplets of a dipolar quantum fluid, *Phys. Rev. Lett.* **119**, 255302 (2017).
- [181] A. Boudjemâa, Two-dimensional quantum droplets in dipolar Bose gases, *New J. Phys.* **21**, 093027 (2019).
- [182] M. Łebek, J. Kopyciński, W. Górecki, R. Ołdziejewski, and K. Pawłowski, Elementary excitations of dipolar Tonks-Girardeau droplets (2022), [arXiv:2209.01887](https://arxiv.org/abs/2209.01887).
- [183] M. Pylak, F. Gampel, M. Płodzień, and M. Gajda, Manifestation of relative phase in dynamics of two interacting Bose-Bose droplets, *Phys. Rev. Res.* **4**, 013168 (2022).
- [184] G. C. Katsimiga, S. I. Mistakidis, B. A. Malomed, D. J. Frantzeskakis, R. Carretero-Gonzalez, and P. G. Kevrekidis, Interactions and dynamics of one-dimensional droplets, bubbles and kinks, *Condens. Matter* **8**, 67 (2023).
- [185] G. Potel, F. Barranco, E. Vigezzi, and R. A. Broglia, Quantum entanglement in nuclear Cooper-pair tunneling with γ rays, *Phys. Rev. C* **103**, L021601 (2021).
- [186] P. Magierski, A. Makowski, M. C. Barton, K. Sekizawa, and G. Wlazłowski, Pairing dynamics and solitonic excitations in collisions of medium-mass, identical nuclei, *Phys. Rev. C* **105**,

064602 (2022).

- [187] E. Orignac, S. D. Palo, L. Salasnich, and R. Citro, Breathing mode of a quantum droplet in a quasi-one-dimensional dipolar Bose gas (2024), [arXiv:2401.03918](#).
- [188] D. Edler, C. Mishra, F. Wächtler, R. Nath, S. Sinha, and L. Santos, Quantum fluctuations in quasi-one-dimensional dipolar Bose-Einstein condensates, *Phys. Rev. Lett.* **119**, 050403 (2017).
- [189] V. Dunjko, V. Lorent, and M. Olshanii, Bosons in cigar-shaped traps: Thomas-Fermi regime, Tonks-Girardeau regime, and in between, *Phys. Rev. Lett.* **86**, 5413 (2001).
- [190] B. Damski, Formation of shock waves in a Bose-Einstein condensate, *Phys. Rev. A* **69**, 043610 (2004).
- [191] R. Ołdziejewski, W. Górecki, K. Pawłowski, and K. Rzażewski, Roton in a few-body dipolar system, *New J. Phys.* **20**, 123006 (2018).
- [192] W. Kao, K.-Y. Li, K.-Y. Lin, S. Gopalakrishnan, and B. L. Lev, Topological pumping of a 1D dipolar gas into strongly correlated prethermal states, *Science* **371**, 296 (2021).
- [193] G. E. Astrakharchik and B. A. Malomed, Dynamics of one-dimensional quantum droplets, *Phys. Rev. A* **98**, 013631 (2018).
- [194] A. I. Gudyma, G. E. Astrakharchik, and M. B. Zvonarev, Reentrant behavior of the breathing-mode-oscillation frequency in a one-dimensional Bose gas, *Phys. Rev. A* **92**, 021601 (2015).
- [195] H. Berestycki and P.-L. Lions, Nonlinear scalar field equations. I. Existence of a ground state, *Arch. Ration. Mech. Anal.* **82**, 313 (1983).
- [196] Z. Lin, Stability and instability of traveling solitonic bubbles, *Adv. Differ. Equ.* **7**, 897 (2002).
- [197] S. De Palo, E. Orignac, R. Citro, and L. Salasnich, Effect of transverse confinement on a quasi-one-dimensional dipolar Bose gas, *Condens. Matter* **8**, 26 (2023).
- [198] J. Stuhler, A. Griesmaier, T. Koch, M. Fattori, and T. Pfau, Magnetostriction in a degenerate quantum gas, *Journal of Magn. Magn. Mater.* **316**, 429 (2007).

Part II.
Publications

1. [J. Kopyciński *et al.*, Beyond Gross-Pitaevskii equation for 1D gas: Quasiparticles and solitons, SciPost Phys. 12, 023 (2022)]

Beyond Gross-Pitaevskii equation for 1D gas: Quasiparticles and solitons

Jakub Kopyciński^{1*}, Maciej Łebek^{1,2}, Maciej Marciniak¹,
Rafał Ołdziejewski^{3,4}, Wojciech Górecki² and Krzysztof Pawłowski¹

¹ Center for Theoretical Physics, Polish Academy of Sciences,
Al. Lotników 32/46, 02-668 Warsaw, Poland

² Faculty of Physics, University of Warsaw, Pasteura 5, 02-093 Warsaw, Poland

³ Max Planck Institute of Quantum Optics, 85748 Garching, Germany

⁴ Munich Center for Quantum Science and Technology,
Schellingstrasse 4, 80799 Munich, Germany

* jkopycinski@cft.edu.pl

Abstract

Describing properties of a strongly interacting quantum many-body system poses a serious challenge both for theory and experiment. In this work, we study excitations of one-dimensional repulsive Bose gas for arbitrary interaction strength using a hydrodynamic approach. We use linearization to study particle (type-I) excitations and numerical minimization to study hole (type-II) excitations. We observe a good agreement between our approach and exact solutions of the Lieb-Liniger model for the particle modes and discrepancies for the hole modes. Therefore, the hydrodynamical equations find to be useful for long-wave structures like phonons and of a limited range of applicability for short-wave ones like narrow solitons. We discuss potential further applications of the method.



Copyright J. Kopyciński *et al.*

This work is licensed under the Creative Commons

[Attribution 4.0 International License](https://creativecommons.org/licenses/by/4.0/).

Published by the SciPost Foundation.

Received 20-07-2021

Accepted 24-11-2021

Published 14-01-2022

doi:[10.21468/SciPostPhys.12.1.023](https://doi.org/10.21468/SciPostPhys.12.1.023)



Check for
updates

Contents

1	Introduction	2
2	Models	4
3	Phonons and quasiparticles	7
4	Solitons	9
4.1	Comparison between solitons of GPE and LLGPE	10
4.2	Comparison between solitons and the type-II excitations	11
5	Validity range of LLGPE and solitons	14
6	Conclusions	15

A Accurate approximations for e_{LL}	15
B Numerical implementation of (LL)GPE	16
C Phase imprinting method	17
References	20

1 Introduction

In weakly interacting ultracold Bose gas, the mean-field approach given by a single particle non-linear Schrodinger equation, which is also known as the Gross-Pitaevski equation (GPE), has explained and predicted a large swathe of phenomena [1]. Interestingly, the GPE derives from the complete neglecting of the mutual quantum correlations between the particles, and yet it describes non-linear phenomena that originate from interactions between them. The most known are solitons observed in experiments with an ultracold gas confined in a steep cigar-shaped harmonic trap [2–4]. In the repulsive gas, the solitons are density dips travelling with a constant speed, robust due to the balance between interaction and dispersion. The dark solitons predicted by the GPE correspond to hole excitations in the many-body system described by the linear Lieb-Liniger model [5]. The above correspondence has been debated for many years before being fully justified only recently by works of different authors in Refs. [6–14]. Should the correspondence hold for stronger interactions, however, remains an open question.

The original GPE may overlook interesting physics even for weakly interacting systems with quantum depletion [15, 16] still being very small. In the presence of both repulsive and attractive interparticle forces of comparable interaction strength, the mean-field contributions to the total energy almost cancel each other out and become of the same order as low-energy quantum fluctuations. Their sudden prominence has given rise to the discovery of quantum droplets and supersolids that have been recently studied at length both in experiment and theory [17]. In three dimensions, one can easily add the effective term describing quantum fluctuations, called the Lee-Huang-Yang (LHY) correction, to the GPE leading to its extended version both for Bose-Bose mixtures [18] and dipolar Bose gas [19, 20], that resolves the initial problem. For the dipolar case in one or two dimensions, however, such an approach is more challenging to justify [21]. Nevertheless, in one dimension, both dipolar and Bose-Bose mixtures have been investigated already by using ab-initio approaches like Monte-Carlo or exact diagonalization, for example in Refs. [22–25].

The widely-used GPE, even supplemented by the LHY correction, becomes unreliable for the strong interaction, especially in lower dimensions where quantum effects are enhanced. A question arises whether there exists a better effective non-linear model that would be useful to study quasi-1D Bose gas also for strongly correlated systems. The simplest system to study is the uniform one and interacting only via short-range repulsive forces. The underlying many-body model describing such a system with N particles is given by the exactly solvable Lieb-Liniger (LL) model [26–28]. Nowadays, the LL model is a testbed for many-body methods, a starting point of subsequent theoretical frameworks (like Luttinger liquid) but also an active research area in mathematical physics. [29, 30].

Although the LL model describes uniform repulsive 1D Bose gas completely, an effective framework, somehow similar to the GPE, has been sought that would be suitable also for

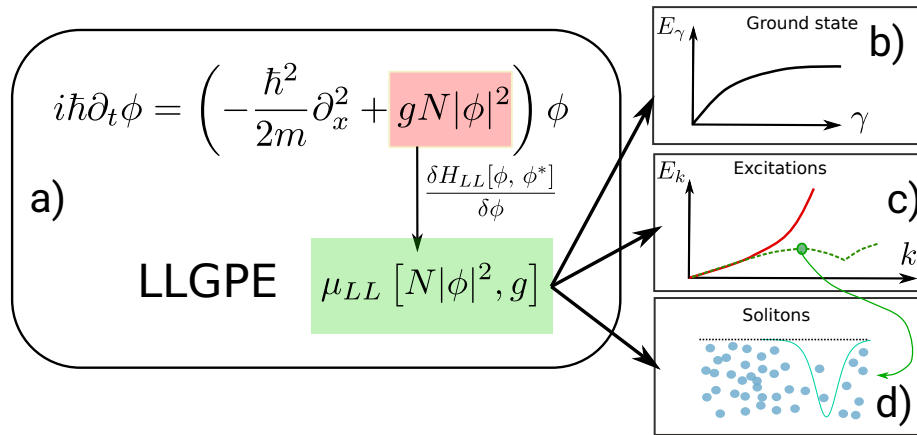


Figure 1: Graphical abstract: a) We describe 1D repulsive Bose gas using an equation called here the LLGPE. The LLGPE differs from the GPE only by the interaction energy term, which, according to the explanation given in this work, is replaced with the chemical potential of the Lieb-Liniger model. b) We study the energy of the ground state. c) We analyse the dispersion relations of both types of the Lieb-Liniger elementary excitations: the type-I excitations (Bogoliubov-like, solid red line) and type-II excitations (solitonic branch, dashed green). d) We study spatial properties of the type-II excitations that correspond to the black solitons and compare them with solitonic solutions of the GPE and LLGPE equations.

In all these tasks (b-d), we benchmark our findings with the GPE and exact solutions of the Lieb-Liniger model for all interaction regimes, from the weakly interacting gas up to the Tonks-Girardeau limit.

strongly correlated systems with additional trapping potential or different interaction type. In the extreme case of trapped 1D gas in the Tonks-Girardeau limit, Kolomeisky et al. [31] already proposed a non-linear equation with higher-order nonlinearity than the GPE. Despite the initial critics by Girardeau and Wright [32], the equation was generalized in [33,34] to any interaction strength and successfully applied to a problem of an expanding 1D cloud. Similar extensions served to study ground state properties as well as collective excitations of strongly interacting gas in a harmonic trap [35,36] and dynamics of shock waves [37,38]. Finally, alternatives of the GPE for strongly interacting dipolar systems have been proposed [23,39] and have already shown usefulness in timely topics like dipolar quantum droplets [23,40].

To assess the validity scope of the effective approach employed in this work, we focus on the system described by the LL model. We will benchmark the ground state and its elementary excitations inferred from the effective non-linear approach [23,31,34], called here the Lieb-Liniger Gross-Pitaevski equation (LLGPE), against the corresponding solutions of the LL model [26,27] to test the validity range of the former. Our equation has the form of the GPE but with the nonlinearity from the exact results for the Lieb-Liniger model, see Fig. 1. It has appeared in the literature under the names the Modified Non-linear Schrödinger Equation [41] and the Generalized Non-linear Schrödinger Equation [42]. Here, we will focus on two branches of elementary excitations in the LL, i.e. particle (type-I) and hole (type-II) modes that correspond to phonons and solitons respectively. Their hallmarks are their dispersion relations and, for the type-II excitations, their spatial dependence. We will discuss the interpretation of solitons as the many-body excitations for strong and intermediate interaction strength. In this way, we will test the scope of the non-linear model, which is the cornerstone of the quantum droplet description employed in [23] and an analysis of breathing modes in [40].

The paper and the main results are organized as follows. In Sec. 2 we introduce all impor-

tant models: the LL model, the standard non-linear equation and finally the main subject of this paper, i.e. the generalized non-linear equation. We discuss its derivation and the ground state wave-function. In Sec. 3, we focus on particle excitations. Linearizing the generalized non-linear equation, we calculate the excitation spectrum and the sound velocity for all γ that coincide with many-body results of the LL model. Subsequently, we compare our results to the standard GPE and examine its validity range. In Sec. 4, we analyse dark solitons predicted by the generalized non-linear model. In the first step, we compare our findings with solitons obtained for two limiting cases of $\gamma \rightarrow 0$ and $\gamma \rightarrow \infty$ within corresponding effective, non-linear models. Our model reproduces the preceding results and predicts solitons for intermediate values of γ . Later, we examine the correspondence between hole excitations in the LL model and the dark solitons from the generalized non-linear equation for any γ . As γ increases, narrow solitons predicted by the hydrodynamical approach lose their connection with the hole excitations in the LL model. In Sec. 5, we predict the scope of validity of the generalized equation. The hydrodynamical equations find to be useful for long-wave structures like phonons and of a limited range of applicability for short-wave ones like narrow solitons. In Sec. 6, we summarize the main findings of the work and discuss further applications of the generalized non-linear equation.

2 Models

In this Section, we introduce different models of N bosons moving along a circle of length L and interacting via delta potential $V(x) = g\delta(x)$, where x is a distance between particles and g is a coupling strength.

The fundamental model is expressed by the following many-body Hamiltonian:

$$\hat{H} = -\frac{\hbar^2}{2m} \sum_{j=1}^N \partial_{x_j}^2 + g \sum_{\substack{j,l \\ j < l}}^N \delta(x_j - x_l), \quad (1)$$

where x_j denotes position of the j -th particle. The Hamiltonian (1) equals to the Lieb-Liniger Hamiltonian, with physical constants written explicitly.

The seminal papers of Lieb and Liniger [26,27] present the general form of all eigenstates of the Hamiltonian (1) in the case of repulsive interactions, i.e. $g > 0$. A useful dimensionless parameter is:

$$\gamma := \frac{m g L}{\hbar^2 N}, \quad (2)$$

known as the Lieb parameter. In particular, the energy of the ground state E_0 in the thermodynamic limit ($N \rightarrow \infty, L \rightarrow \infty, N/L = \text{const}$) is given by:

$$E_0[N, L] = \frac{\hbar^2 N^3}{2m L^2} e_{\text{LL}}(\gamma), \quad (3)$$

that defines the pressure [43]:

$$P_{\text{LL}}[N/L] = -\frac{\partial E_0[N, L]}{\partial L} = \frac{\hbar^2 N^3}{2m L^3} (2e_{\text{LL}}(\gamma) - \gamma e'_{\text{LL}}(\gamma)), \quad (4)$$

and the chemical potential:

$$\mu_{\text{LL}}[N/L] = \frac{\partial E_0[N, L]}{\partial N} = \frac{\hbar^2 N^2}{2m L^2} (3e_{\text{LL}}(\gamma) - \gamma e'_{\text{LL}}(\gamma)), \quad (5)$$

as well. Here, $e_{\text{LL}}(\gamma)$ does not have a known explicit analytical form^{1,2}. Although the explicit expression for the function $e_{\text{LL}}(\gamma)$ is missing, its very expansions for small and large γ are known. In particular, for small γ , it reads $e_{\text{LL}}(\gamma) \approx \gamma - 4\gamma^{3/2}/(3\pi)$. The first term of the expansion leads to the mean-field energy, whereas the second negative term can be identified with the LHY correction. Note that, unlike the total energy, the pressure and chemical potential as intensive properties depend only on the ratio N/L .

Unfortunately, the many-body eigenstates of the LL model [26] are often impractical to use straightforwardly due to the number of permutations of the N -particle bosonic state. One has to resort to approximate models, from which the easiest one comprises the GPE. A typical derivation of GPE is based on an Ansatz in the form of the Hartree product, in which a many-body solution of the Schrödinger equation $\psi(x_1, \dots, x_N, t)$ is approximated by a product state $\prod_{j=1}^N \phi(x_j, t)$. The LL Hamiltonian (1) averaged in such Ansatz gives the mean energy³:

$$E_{\text{GPE}}[\phi] = \frac{N}{2} \int dx \left[\frac{\hbar^2}{m} \left| \frac{d\phi}{dx} \right|^2 + gN|\phi|^4 \right]. \quad (6)$$

The least action principle applied to the energy functional above leads to the Gross-Pitaevskii equation for an optimal orbital $\phi(x, t)$:

$$i\hbar\partial_t \phi(x, t) = \left(-\frac{\hbar^2}{2m} \partial_x^2 + gN|\phi(x, t)|^2 \right) \phi(x, t). \quad (7)$$

Most of the phenomena observed in the first years of research on the Bose-Einstein condensate were sufficiently well described by this equation. Despite its indisputable role, however, the GPE equation is only an approximation. For weak interactions, it does not include effects related to the depletion of condensate by interactions, e.g. quantum depletion (including the LHY correction). For stronger interactions, due to the resulting correlations between atoms, the system state is no longer a product state, and the GPE equation (7) is no more justified. On the other hand, there might exist another model that would be able to capture the essentials of the system even in the strongly interacting regime. Indeed, such models for fermions are being derived routinely in the frame of the density functional theory.

Here, we use the hydrodynamical approach to extend approximate models beyond weak interactions. The classical hydrodynamic equations⁴ read:

$$\frac{\partial}{\partial t} \rho + \frac{\partial}{\partial x} (\rho v) = 0, \quad (8)$$

$$\frac{\partial}{\partial t} v + v \frac{\partial}{\partial x} v = \frac{1}{m\rho} \frac{\partial}{\partial x} P, \quad (9)$$

where $m \cdot \rho(x, t)$, with $\int \rho(x, t) = N$, is the gas density, $v(x, t)$ denotes the velocity field, and $P(x, t)$ indicates pressure. We treat an atomic cloud as composed of small 'volume' elements, which are still large enough that comprise many particles. Following Ref. [33], we assume local equilibrium, i.e. in each 'volume' element the energy density, pressure and chemical potential are fixed by the corresponding values of the many-body energy of the ground state (3) (after replacing N/L by $\rho(x, t)$ everywhere).

¹The values of $e_{\text{LL}}(\gamma)$ can be determined by solving the Fredholm equations given in [26] (where it is denoted as $e(\gamma)$ without subscripts).

²Please do not confuse with e_{LL} introduced in Ref. [23], where it had a meaning of the total energy per volume unit. Moreover, it used a crude approximation of the total energy.

³We consider $N \gg 1$ therefore we replace $N - 1$ with N .

⁴The quantum hydrodynamic equation might consist of the quantum pressure term. Its role and flows in the considered system are discussed in [37].

Comparing (4) and (5), one may check by direct calculation that the Euler equation (9) may be rewritten as:

$$\frac{\partial}{\partial t} v + v \frac{\partial}{\partial x} v = -\frac{1}{m} \frac{\partial}{\partial x} (\mu_{\text{LL}}[\rho]). \quad (10)$$

Note that Eq. (10) may be derived in an alternative, more intuitive way. Suppose the fluid consists of many particles and consider the trajectory $(x(t), t)$ of one of them. As the potential energy for the particle at any point is given by a chemical potential μ_{LL} , one has directly from Newton's law of motion:

$$\frac{d}{dt} m v(x(t), t) = -\frac{\partial}{\partial x} \mu_{\text{LL}}[\rho(x, t)], \quad (11)$$

which, after a straightforward applying of $\frac{d}{dt}$, gives Eq. (10).

Introducing

$$\phi(x) = \sqrt{\rho/N} e^{i\varphi}, \quad (12)$$

with $\hbar \partial_x \varphi = m v$, the two hydrodynamical equations (8),(10) can be written, up to a quantum pressure term, in a compact form [37, 44]:

$$i\hbar \frac{\partial}{\partial t} \phi = -\frac{\hbar^2}{2m} \frac{\partial^2 \phi}{\partial x^2} + \mu_{\text{LL}}[N|\phi|^2] \phi, \quad (13)$$

with

$$\mu_{\text{LL}}[N|\phi|^2] = \frac{\hbar^2}{2m} N^2 |\phi|^4 \left(3e_{\text{LL}} \left(\frac{\kappa}{N|\phi|^2} \right) - \frac{\kappa}{N|\phi|^2} e'_{\text{LL}} \left(\frac{\kappa}{N|\phi|^2} \right) \right), \quad (14)$$

where $\kappa := \frac{gm}{\hbar^2}$ denotes a parameter of inverse length dimension.

The equation (13) is our main subject of interest. In particular, one can rewrite it also as

$$i\hbar \frac{\partial}{\partial t} \phi = \frac{\delta \mathcal{H}_{\text{LL}}[\phi, \phi^*]}{\delta \phi^*}, \quad (15)$$

where

$$\mathcal{H}_{\text{LL}}[\phi, \phi^*] := \frac{\hbar^2}{2m} \left| \frac{d\phi}{dx} \right|^2 + \frac{\hbar^2}{2m} N^2 |\phi|^6 e_{\text{LL}} \left(\frac{\kappa}{N|\phi|^2} \right), \quad (16)$$

is the energy density. Thus the LLGPE can be derived using the least action principle for the energy functional:

$$E[\phi] = N \int dx \mathcal{H}[\phi, \phi^*] = \frac{N\hbar^2}{2m} \int dx \left[\left| \frac{d\phi}{dx} \right|^2 + N^2 |\phi|^6 e_{\text{LL}} \left(\frac{\kappa}{N|\phi|^2} \right) \right]. \quad (17)$$

Notably, ϕ does not have interpretation of a macroscopically occupied orbital as in the derivation of GPE.

For $\gamma \ll 1$, the function $e_{\text{LL}}(\gamma)$ may be approximated in the first order as $e_{\text{LL}}(\gamma) \approx \gamma$, and then the resulting dynamical equation (13) coincides with the GPE for $\gamma \ll 1$. In this regime, the pressure (4) $P_{\text{LL}}[\rho] = \frac{g}{2} \rho^2$ appearing in the hydrodynamical equation corresponds to the pressure of classical interacting gas.

For the opposite limit of $\gamma \rightarrow \infty$, fermionization occurs in one-dimensional Bose gas – the value of $e_{\text{LL}}(\gamma)$ converges to a constant $\frac{\pi^2}{3}$, so (13) coincides with the equation proposed in [31]:

$$i\hbar \frac{\partial}{\partial t} \phi = -\frac{\hbar^2}{2m} \frac{\partial^2 \phi}{\partial x^2} + \frac{\hbar^2 \pi^2}{2m} N^2 |\phi|^4 \phi. \quad (18)$$

In such a case, the pressure (4) $P_{\text{LL}}[\rho] = \frac{4\pi^2}{3} \frac{\hbar^2}{2m} \rho^3$ should be understood rather like an analogy of fermion degeneracy pressure.

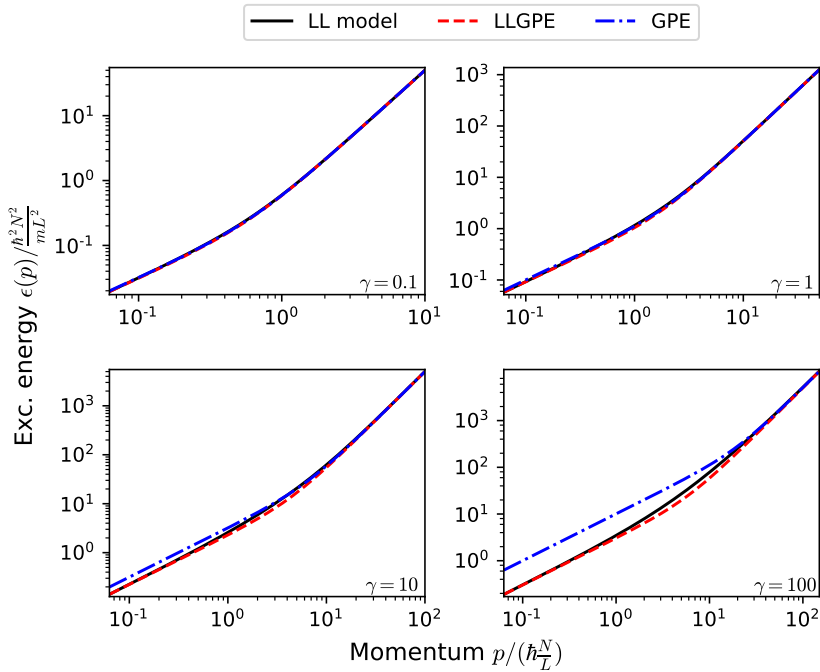


Figure 2: Energy of type-I excitations as a function of the momentum for different values of the interparticle interaction γ . Following Lieb’s recipe [27], excitation energies for the LL model were obtained directly from solutions of the Bethe equations for $N = 100$ particles. On the other hand, red and blue dashed lines correspond to the excitation spectrum calculated from linearization of the GPE (7) and LLGPE, respectively.

From the construction, the minimal value of the energy function (17), obtained for the constant function

$$\phi_{\text{GS}}(x) = \frac{1}{\sqrt{L}}, \tag{19}$$

equals to the actual ground state energy $E_0[N, L]$ for any interaction strength γ . The ground state of the GPE equals to the function (19) also, but its GPE energy, $E_{\text{GPE}}[\phi_{\text{GS}}] = \frac{1}{2}N^2g/L$, approximates E_0 well in the weakly interacting regime only.

In the following sections, we will benchmark the underlying Lieb-Liniger model with the approximated ones, the GPE and the LLGPE, elaborating the advantages of the latter. In our numerical analysis, we approximate the function e_{LL} , which does not have a known exact and compact form, with a very accurate approximation presented in [45] (compare with Ref. [46]) and repeated here in the Appendix A.

3 Phonons and quasiparticles

Sound propagation, superfluidity, normal modes, stiffness — all these depend on the quasiparticles properties in a many-body system. In the case of weak interaction strength, the dispersion relation of excitations was computed by Bogoliubov [47], before the general solution of Lieb. The very notion of quasiparticles, natural in the approximated treatment of Bogoliubov, required a new formulation in the exact many-body theory. Surprisingly, the elementary excitations defined by E. Lieb form two excitation branches instead of one. One of them, the

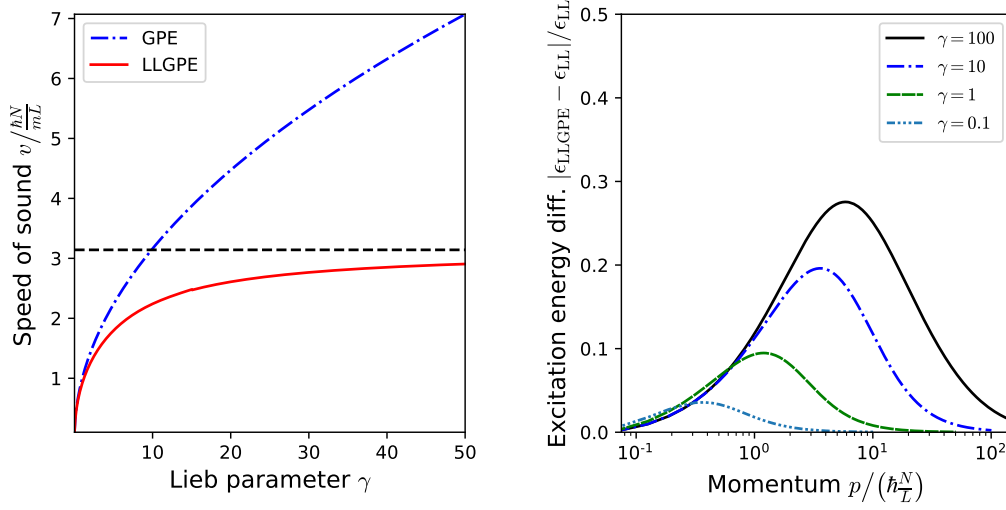


Figure 3: Left: The speed of sound as a function of the Lieb interaction parameter γ for two different approaches: LLGPE and GPE. In the former case, the speed of sound has an asymptote $\lim_{\gamma \rightarrow \infty} v_{LLGPE} = \frac{\pi h\bar{N}}{mL}$, which is marked with the black dashed line. Right: Relative excitation energy difference $\frac{|\epsilon_{LLGPPE} - \epsilon_{LL}|}{\epsilon_{LL}}$ as a function of momentum for different Lieb interaction parameters γ .

branch of the so-called type-I excitations, has almost the same dispersion relation $E_I(p)$ as the Bogoliubov modes (in the weak interaction regime). For low momenta, their energy scales linearly with momentum,

$$E_I(p) \stackrel{p \rightarrow 0}{\approx} v |p|, \tag{20}$$

where v stands for the speed of sound. These excitations, responsible for superfluidity, are the carriers of sound and are known as phonons.

The fast quasiparticles have the dispersion relation of free particles:

$$E_I(p) \stackrel{p \rightarrow \infty}{\approx} p^2/(2m). \tag{21}$$

As shown in Ref. [48], linearization around the ground state in the frame of the GPE leads to the same dispersion relation as using Bogoliubov quasiparticles. Therefore, we recall and apply this method to both approximate models, the GPE and the LLGPE, to trace the differences between, similarly to Ref. [35].

Linearization. — We consider a small perturbation to the stationary solution (19). Following Ref. [49], we restrict ourselves to linearized dynamics and propose an Ansatz for a time-dependent solution in the form:

$$\phi(x, t) = \left(\frac{1}{\sqrt{L}} + \delta\phi(x, t) \right) e^{-i\mu_{LL}[N/L]t/\hbar}, \tag{22}$$

where $\delta\phi(x, t) = \sum_p u_p(x) e^{-i\epsilon_p t/\hbar} + v_p^*(x) e^{i\epsilon_p t/\hbar}$ is assumed to be a small correction to the stationary solution (19). Hence, after substituting the Ansatz to the LLGPE, we keep terms at most linear in $\delta\phi$ and obtain

$$i\hbar\partial_t\delta\phi = \left[-\frac{\hbar^2}{2m}\partial_x^2 + mv_{LL}^2[N/L] \right] \delta\phi + mv_{LL}^2[N/L]\delta\phi^*, \tag{23}$$

where $v_{\text{LL}}[N/L] = \frac{\hbar N}{mL} \sqrt{3e_{\text{LL}}(\gamma) - 2\gamma e'_{\text{LL}}(\gamma) + \frac{1}{2}\gamma^2 e''_{\text{LL}}(\gamma)}$ determines an exact expression for the speed of sound in LL model [27, 50]. We use our ansatz for $\delta\phi(x, t)$ getting:

$$\epsilon_p u_p(x) = \left(-\frac{\hbar^2}{2m} \partial_x^2 + m v_{\text{LL}}^2 [N/L] \right) u_p(x) + m v_{\text{LL}}^2 [N/L] v_p(x), \quad (24)$$

$$-\epsilon_p v_p(x) = \left(-\frac{\hbar^2}{2m} \partial_x^2 + m v_{\text{LL}}^2 [N/L] \right) v_p(x) + m v_{\text{LL}}^2 [N/L] u_p(x). \quad (25)$$

Owing to the translational invariance of our system, we consider $u_p(x) = u_p e^{ipx/\hbar}$ and $v_p(x) = v_p e^{ipx/\hbar}$ simplifying our equations to the form:

$$\epsilon_p u_p = \frac{p^2}{2m} u_p + (u_p + v_p) m v_{\text{LL}}^2 [N/L], \quad (26)$$

$$-\epsilon_p v_p = \frac{p^2}{2m} v_p + (u_p + v_p) m v_{\text{LL}}^2 [N/L]. \quad (27)$$

We solve the above equations, finally obtaining the excitation spectrum:

$$\epsilon(p) = \sqrt{(v_{\text{LL}}[N/L]p)^2 + \left(\frac{p^2}{2m}\right)^2}. \quad (28)$$

The formula (28) is the main result of this section. In the low momenta limit, one gets $\epsilon(p) \stackrel{p \rightarrow 0}{\approx} v_{\text{LL}}[N/L] |p|$, i.e. the phononic relation with the correct speed of sound; the same as in the many-body approach. Interestingly, we recover also the correct limit (up to the second order) for large momenta (cf. (21)). Thus the linearization of the LLGPE gives a dispersion relation that coincides with the dispersion relation of type-I elementary excitations at low and high energy limit and for any interaction strength. In Fig. 2, we show a comparison between (28) and the exact many-body solutions. The deviations are present only for the intermediate momenta. For completeness, we also show the dispersion relation based on linearization of the GPE. It reads $\epsilon_{\text{GP}}(p) = \sqrt{(v_{\text{GP}}[N/L]p)^2 + \left(\frac{p^2}{2m}\right)^2}$, with a modification in the speed of sound which equals $v_{\text{GP}}[N/L] := \sqrt{gN/mL}$ and tends to infinity in the Tonks-Girardeau limit. This is illustrated in the left panel of Fig. 3. In the right panel we show relative error between the LLGPE excitations and the type-I excitations. The discrepancies are visible mostly for the intermediate momenta.

The results presented in this section show how well the LLGPE works concerning type-I excitations for all interaction regimes. This leads us to more subtle questions about non-linear effects. Such effects, observed in a number of experiments, appear naturally in the GPE, which is based on the linear equation but are more difficult to identify in the frame of the many-body approach. In the next sections, we shall focus on solitons and their relations with the type-II elementary excitations.

4 Solitons

The GPE appears to be very convenient to study non-linear phenomena like solitons. Generally speaking, a soliton is a solution of a non-linear equation in the form of a moving wave, $\phi_S(x, t) = \phi_S(x - v_s t)$, that preserves its shape in dynamics due to the balance between kinetic energy and nonlinearity. In the case of the GPE with repulsive interaction, a soliton has a form of a density dip, as shown by a blue dashed line in Fig. 4. Such solitonic dips, predicted by the

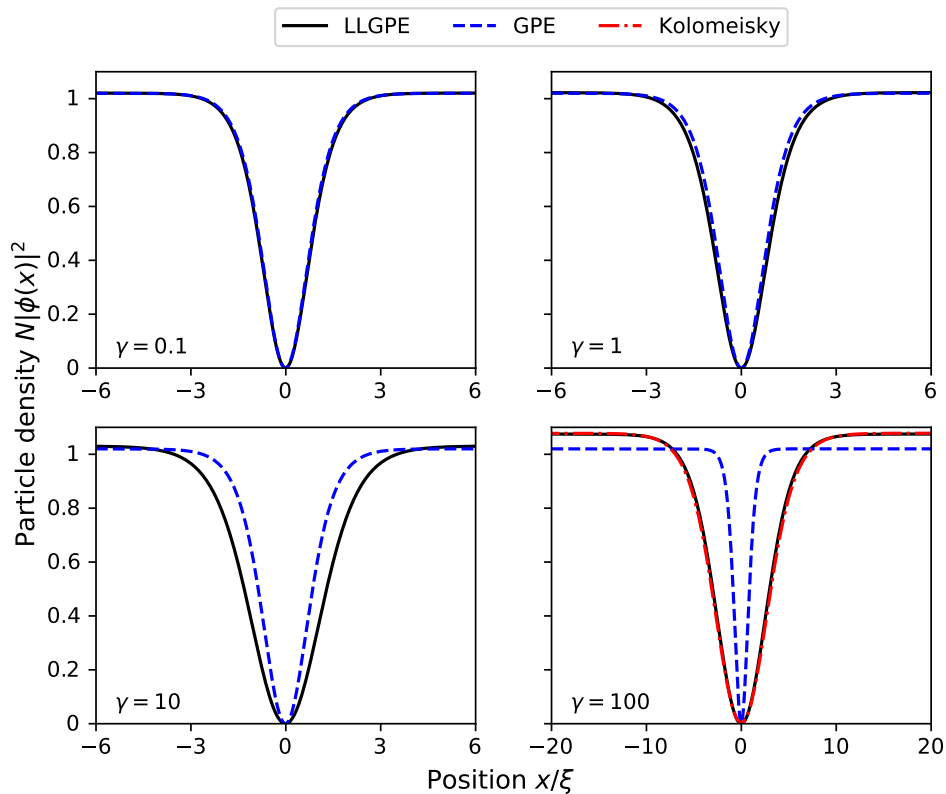


Figure 4: Black soliton density profiles for different equations and interaction strengths. Note the GPE and the LLGPE solutions for $\gamma = 0.1$ as well as LLGPE and Kolomeisky (cf. Ref. [31]) solutions for $\gamma = 100$ overlap each other. In all cases the box size $L = 100\xi$, where ξ is the healing length (which corresponds to $N = 100\sqrt{1/\gamma}$).

GPE, were demonstrated experimentally [2, 3]. Here, we shall focus on a special case, namely solitons with the density dip touching 0, called the *black solitons*.

Besides, the black soliton has a π phase jump in the very point of the density minimum. In an infinite box, the black soliton is motionless $v_s = 0$ (the situation in the box with periodic boundary conditions is described in Appendix C). These features are the same as in the solitons in the weakly interacting regime [51].

In this chapter, we discuss i.a. the differences in shape (focusing on the soliton width) between solitons within GPE and LLGPE.

4.1 Comparison between solitons of GPE and LLGPE

As discussed above, the linearization of the LLGPE leads to the correct speed of sound in the 1D gas of bosons with short-range interaction, even for the intermediate and strong interaction regime. A natural question arises whether the LLGPE has a solitonic solution beyond the weakly interacting regime.

Here, following the reasoning presented in Ref. [14], we find candidates for solitons in LLGPE numerically for any interaction strength, as the minimal energy states constraint to a π jump of phase at the origin. We tested numerically that these states do not move and do preserve their shape in dynamics, as the solitons should do (cf. Figs. 8 and 9 in Appendix C).

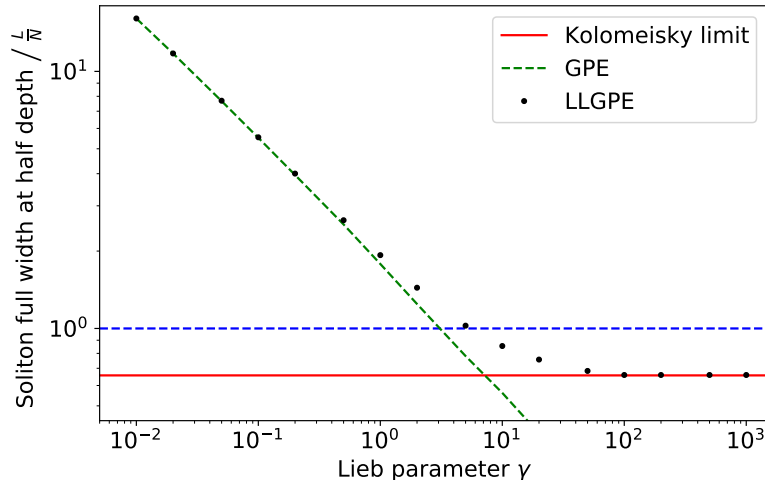


Figure 5: Widths of black LLGPE (black dots) and GPE (green dashed line) solitons found with the ITE method as a function of the Lieb parameter γ . The dashed blue line corresponds to the average interparticle distance L/N and the solid red line to the Kolomeisky limit for $\gamma \rightarrow \infty$ (cf. [31]).

That is the most fundamental property of solitons. The technical details of our method and references to our codes are given in Appendices B and C. The results for the LLGPE are shown in Fig. 4 with the solid black lines, together with the GPE solitons (blue dashed lines). The width of a GPE soliton, which is of the order of the healing length $\xi := \hbar/\sqrt{mNg/L}$, vanishes in the limit of large g . This is an unphysical effect: in reality, the gas reaches the Tonks-Girardeau limit, at which the further increase of interaction strength does not affect the system anymore. In the LLGPE, this saturation effect is accounted for by the relation $e_{LL}(\gamma) \xrightarrow{\gamma \rightarrow \infty} \pi^2/3$, and the width of LLGPE solitons converges to a constant. In Fig. 5 we present the widths in the logarithmic scale. As shown in Fig. 4, already for $\gamma = 100$, the LLGPE soliton is indistinguishable from the solitons that are analytically derived in the Tonks-Girardeau limit $\gamma \rightarrow \infty$ (red dashed line) [31].

4.2 Comparison between solitons and the type-II excitations

It was observed in Ref. [5] that for weak interactions, the GPE solitons have the same dispersion relation as the many-body eigenstates forming the second branch of elementary excitations in the solution of Lieb called in the literature yrast states or type-II excitations or the lowest energy states at fixed momentum. This coincidence was rather unexpected: why the dispersion relation of the solutions of a dynamical, non-linear GPE should match the dispersion of some static solutions of the linear many-body model, distinguished by E. Lieb as the type-II elementary excitations?

There has been a lot of effort devoted to understanding better this relation [6–14, 52, 52–55]. It has been pointed out that the GPE soliton emerges in the high order correlation function computed for the type-II excitation [9, 10, 55, 56]. The other observation points that the solitonic shape appears also in the single-body reduced density matrix evaluated in the appropriate superpositions of the type-II excitations [8, 11–13, 54]. These two different viewpoints were recently unified in Ref. [14]. The agreement holds, however, for weak interactions only, where the GPE is reliable. Here, we address a question whether the relation between solitons and the type-II excitations remains valid for stronger interaction, provided that we use the

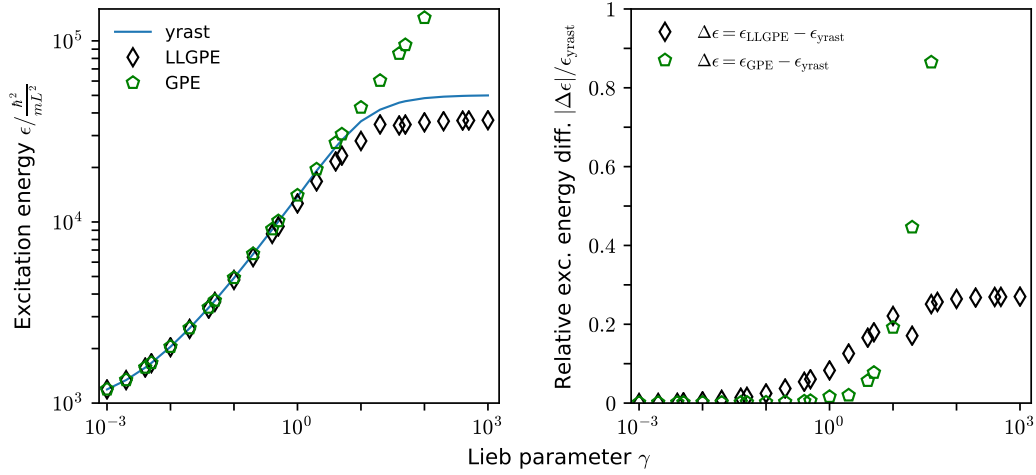


Figure 6: Left: Yrast state excitation energy in the Lieb-Liniger model (blue line) vs dark soliton excitation energy obtained with the LLGPE (black diamonds) and the GPE (green pentagons) as a function of the Lieb parameter γ . Right: Relative excitation energy $\Delta\epsilon$ of dark solitons within the LLGPE (black diamonds) and GPE (green pentagons). Parameters used in all simulations: $N = 100$.

LLGPE solitons for comparison.

In Fig. 6, we compare the energy of the black GPE and LLGPE solitons with the energies of the type-II excitations evaluated from the exact solution [27] for $N = 100$ particles. For comparison, we use the type-II excitations with the total momentum $\hbar\pi N/L$ that has the same momentum per atom as a black soliton. For a fair comparison, we present the excitation energy being the total energy of the GPE (6) or the LLGPE (17) soliton reduced by the energy of the ground state⁵. The excitation energy of GPE solitons, marked with green pentagons, tends to the infinity with increasing γ . This is a residue of the vanishing width of the GPE soliton that gives a simple estimation of their kinetic energy by $\frac{\hbar^2}{mw^2}$, where w is the soliton width. In the strong interaction limit, the excitation energy of the LLGPE solitons converges to a constant because the system enters the Tonks-Girardeau phase. The latter dispersion relation qualitatively agrees with the dispersion relation of the type-II excitation, although differences are clearly visible. We show the discrepancies between the energies in the right panel of Fig. 6. The figure shows that in the considered example ($N = 100$), there are significant differences in the relative energies of LLGPE solitons and the type-II excitations, which reach up to 25% in the Tonks-Girardeau limit. Importantly, this divergence is not an artefact of the small number of atoms used in the comparison. In fact, in the thermodynamic limit and for $\gamma \rightarrow \infty$, the excitation energy of the yrast state equals $E_{\text{yrast}} - E_{\text{GS}} = \frac{\pi^2 \hbar^2 N^2}{2mL^2}$, whereas the LLGPE soliton has the energy equal to $\frac{\pi^2 \hbar^2 N^2}{2mL^2} [\sqrt{3} \log(2 + \sqrt{3}) / \pi]$ [31]. That gives relative difference between energies around 28%.

It is not obvious how to reveal the GPE or LLGPE solitonic density profiles with characteristic dip directly from the type-II "solitonic" excitations. Due to the translational symmetry, the single body density

$$\rho(x) = \int dx_2 \int dx_3 \dots \int dx_N |\psi_E(x, x_2, x_3 \dots x_N)|^2, \quad (29)$$

of any eigenstate ψ_E of the LL model, including the type-II elementary excitations, is uniform.

⁵The subtracted ground state energy differs between the GPE and the LLGPE.

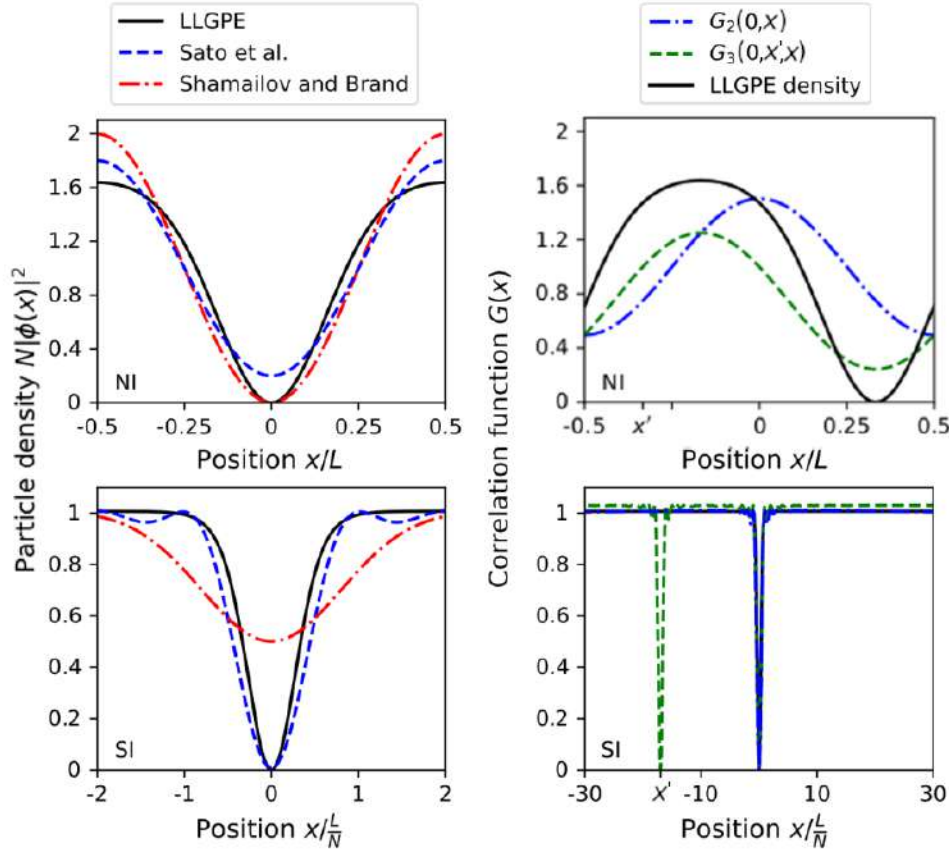


Figure 7: Left panels: Single particle density of the yrast state superpositions (Sato et al. - based on [54], Shamailov and Brand - based on [11] with the dispersion $\Delta P = 0.2\hbar\pi N/L$ used to generate a Gaussian superposition). Right panels: $G_2(0, x)$ and $G_3(0, x', x)$ correlation functions evaluated for the yrast state with the total momentum $\hbar\pi N/L$. NI - non-interacting gas, SI - strongly interacting gas ($\gamma \rightarrow \infty$). The G_2 function, one dip in G_3 and the LLGPE solution overlap each other in the strong interaction limit. The length scales used on the horizontal axes reflect that the soliton width depends only on L in the non-interacting regime, and only on L/N in the strongly interacting regime. The value of x' is chosen randomly.

Therefore, the differences in spatial properties of eigenstates are visible only in typical relations between atoms' positions. Following [9] we study such relations using the families of correlation functions

$$G_m(x_m|x_1, \dots, x_{m-1}) := \mathcal{N} \left\langle \prod_{i=1}^m \hat{\Psi}^\dagger(x_i) \prod_{i=1}^m \hat{\Psi}(x_i) \right\rangle, \tag{30}$$

evaluated in the type II eigenstates. The correlation function (30) is a probability density of measuring m -th particle at a position x_m provided that $m - 1$ particles has been already detected at the random points x_1, \dots, x_{m-1} , and \mathcal{N} stands for a normalization factor. It has been shown in [9, 14] that for weak interactions and large m , the functions $G_m(x|x_1, \dots, x_{m-1})$ have spatial profiles close to densities of the GPE solitons. This coincidence is observed for typical positions of other particles x_1, x_2, \dots, x_{m-1} , namely positions drawn according to G_1, G_2, \dots, G_{m-1} respectively.

The other way to reveal mean-field solitons out of the type II excitations was suggested in [8, 11–13, 54]. The Authors studied a wavepacket of the type-II excitations instead of a single one. In this approach, the GPE solitons appear in the single-body density matrix (29). In this approach, different wave packets were proposed.

Here we would like to use these ways, but in the regime of strong-interactions, and compare the results with LLGPE solitons instead of the GPE ones.

In Fig. 7, we recapitulate findings of these two approaches at two extreme regimes: in the limit of non-interacting gas (NI) and the strong-interaction regime (SI). In all panels, we also present LLGPE black solitons marked by a solid black line. The left panels of Fig. 7 show a comparison between the density of the LLGPE soliton and the single-body densities of superpositions of the type-II excitations, as studied in Refs. [11, 12, 54]. These results are not unique in the sense that the reduced density depends on the choice of the superposition.

The right panels of Fig. 7 present benchmarks between LLGPE solitons and $G_m(x_m|x_1, \dots, x_{m-1})$. Here, we show results for $m = 2$ and $m = 3$ only. A situation in the TG limit (bottom right of Fig. 7) is very different. In the limit $\gamma \rightarrow \infty$, the correlation functions assume a simple structure. Owing to the fermionization, the atoms have to be at different places. Thus the probability of finding the m -th particle, provided that $m - 1$ particles were already measured, has zeros at the locations of already measured particles. Therefore, although the LLGPE soliton seems similar to the G_2 function of the yrast state (compare the solid black and blue dashed line in Fig. 7), it has to differ from the higher order correlation functions that have m local minima and not a single one likewise the soliton. Actually, the fact that the LLGPE soliton is close to G_2 of the fermionized gas is striking in the context of the hydrodynamical origin of the LLGPE.

5 Validity range of LLGPE and solitons

The LLGPE equation derives from the hydrodynamical description, assuming that locally the gas is at equilibrium. However, what *locally* means has to be specified. In the theory of continuous media, one introduces fluid elements consisting of many atoms but spanned over the lengths much shorter than the length scale associated with the density changes. It means that we should restrict our analysis to such solitons for which the latter length, of the order of the soliton width w , is much larger than the typical distance between particles, here roughly approximated by L/N . The width w can be estimated from the condition that the kinetic energy of a soliton, which is of the order of $\hbar^2/(2mw^2)$, balances the non-linear term in Eq. (13), which is of the order of $\mu_{LL}[N/L]$. This balance leads to an estimate $w \approx \hbar/\sqrt{2m\mu_{LL}[N/L]}$. In the case of the weakly interacting limit, i.e. $\mu_{LL} \approx gN/L$, one gets $w_{\text{GPE}} \approx \hbar/\sqrt{2mgN/L}$, which gives the correct length scale of the GPE soliton width. The hydrodynamical analysis relies on the assumption $w \gg L/N$, which can be expressed as $1 \gg 2\gamma$. Indeed, these qualitative considerations are confirmed by the numerical analysis of the solitonic width illustrated in Fig. 5. The width of the GPE soliton, shown with the dashed green line crosses the typical distance between atoms L/N (blue line) around $\gamma \approx 1$. Apparently, the situation does not significantly change for LLGPE solitons (black dots).

The qualitative discussion of the length scales leads to the conclusion that the solitons presented in the previous section fulfil the assumptions underlying the LLGPE only for weakly interacting gas. In particular, the analytical solutions given in Ref. [31] can go beyond the validity range of the LLGPE. In the Tonks-Girardeau limit considered in Ref. [31], the solitonic width equals the typical distance between particles that, owing to the fermionization, is of the order of L/N . In that situation, one cannot define elements of fluid consisting of many atoms with a smooth density profile as assumed in the derivation of the LLGPE. This will be also the

case of other states involving length scales shorter than interparticle distance, for example, two interfering atomic clouds [32] or shock waves [37]. The question of whether solitons exist in the intermediate and strongly interacting regimes may be difficult to resolve on theoretical grounds. We leave the question about their existence open as a challenge for experimentalists.

6 Conclusions

The purpose of this work has been to benchmark the generalization of GPE, called here the LLGPE on the well-studied case of gas with solely contact interactions trapped in a 1D box with the periodic boundary conditions. Our analysis support the credibility of this equation, giving the stronger foundations for the further extension, like the one presented in Ref. [23] about quantum droplets in 1D.

In introducing the LLGPE, we invoke the hydrodynamic interpretation. We expect that the equation works in cases where the gas density is slowly varying in space. Indeed, the linearization of the LLGPE leads to the analytical formula for phononic spectra that coincides with the exact formulas known for type-I excitations of the Lieb-Liniger model, even in the limit of infinite interactions. We also find solitonic solutions of the LLGPE and compare their dispersion relation and the spatial dependence to type-II excitations of the Lieb-Liniger model forming a 'solitonic' branch. The correspondence between LLGPE solitons and type-II excitations is limited to weak interaction $\gamma \lesssim 1$. For stronger interaction, the LLGPE solitons do not meet assumptions underlying the LLGPE. The question of whether solitons exist in the 1D gas beyond the weakly interacting regime remains open. The problem might be addressed by experimenters with the technique that was successfully employed for the weakly interacting gas.

To conclude, the LLGPE offers an alternative tool to the GPE, useful in a wide class of smooth solutions even in the strongly interacting 1D Bose gas. In principle, one could also apply it to a gas confined by a slowly varying external potential or for atoms interacting via smooth non-local potential.

Acknowledgements

We thank G. Astrakharchik and B. Julia-Diaz for fruitful discussions. We wish to thank Z. Ristivojevic for pointing Refs. [46] and [57] to us. Center for Theoretical Physics of the Polish Academy of Sciences is a member of the National Laboratory of Atomic, Molecular and Optical Physics (KL FAMO).

Funding information J.K., M.L., M.M., K.P. acknowledges support from the (Polish) National Science Center Grant No. 2019/34/E/ST2/00289. This research was supported in part by PLGrid Infrastructure.

A Accurate approximations for e_{LL}

The equation studied in this paper is based on the function $e_{LL}(\gamma)$, part of the ground state energy in the LL model. There is no simple compact formula for this function, but there are known accurate analytical [46] and numerical [45] approximations. In our numerical tools we have used the approximation of e_{LL} as given in Ref. [45]. In the regime of weak interactions

$\gamma < 1$ we have

$$e_{\text{LL}}(\gamma) = \gamma - \frac{4}{3\pi}\gamma^{3/2} + \left[\frac{1}{6} - \frac{1}{\pi^2}\right]\gamma^2 - 0.0016\gamma^{5/2} + O(\gamma^3). \quad (31)$$

For intermediate interactions $1 \leq \gamma < 15$

$$e_{\text{LL}}(\gamma) \approx \gamma - \frac{4}{3\pi}\gamma^{3/2} + \left[\frac{1}{6} - \frac{1}{\pi^2}\right]\gamma^2 - 0.002005\gamma^{5/2} + 0.000419\gamma^3 - 0.000284\gamma^{7/2} + 0.000031\gamma^4. \quad (32)$$

Finally, nearly the fermionized regime $\gamma \geq 15$

$$\begin{aligned} e_{\text{LL}}(\gamma) \approx & \frac{\pi^2}{3} \left(1 - \frac{4}{\gamma} + \frac{12}{\gamma^2} - \frac{10.9448}{\gamma^3} - \frac{130.552}{\gamma^4} + \frac{804.13}{\gamma^5} - \frac{910.345}{\gamma^6} - \frac{15423.8}{\gamma^7} \right. \\ & + \frac{100559.}{\gamma^8} - \frac{67110.5}{\gamma^9} - \frac{2.64681 \times 10^6}{\gamma^{10}} + \frac{1.55627 \times 10^7}{\gamma^{11}} + \frac{4.69185 \times 10^6}{\gamma^{12}} \\ & - \frac{5.35057 \times 10^8}{\gamma^{13}} + \frac{2.6096 \times 10^9}{\gamma^{14}} + \frac{4.84076 \times 10^9}{\gamma^{15}} - \frac{1.16548 \times 10^{11}}{\gamma^{16}} \\ & + \frac{4.35667 \times 10^{11}}{\gamma^{17}} + \frac{1.93421 \times 10^{12}}{\gamma^{18}} - \frac{2.60894 \times 10^{13}}{\gamma^{19}} + \frac{6.51416 \times 10^{13}}{\gamma^{20}} \\ & \left. + O\left(\frac{1}{\gamma^{21}}\right)\right). \quad (33) \end{aligned}$$

After having prepared our manuscript we got aware of better, analytical expansions for weak interaction, given in Ref. [46]

$$\begin{aligned} e_{\text{LL}}(\gamma) \approx & \gamma - \frac{4}{3\pi}\gamma^{3/2} + \frac{\pi^2 - 6}{6\pi^2}\gamma^2 - \frac{4 - 3\zeta(3)}{8\pi^3}\gamma^{5/2} - \frac{4 - 3\zeta(3)}{24\pi^4}\gamma^3 \\ & - \frac{45\zeta(5) - 60\zeta(3) + 32}{1024\pi^5}\gamma^{7/2} - \frac{3[15\zeta(5) - 4\zeta(3) - 6\zeta^2(3)]}{2048\pi^6}\gamma^4 \\ & - \frac{8505\zeta(7) - 2520\zeta(5) + 4368\zeta(3) - 6048\zeta^2(3) - 1024}{786432\pi^7}\gamma^{9/2} \\ & - \frac{9[273\zeta(7) - 120\zeta(5) + 16\zeta(3) - 120\zeta(3)\zeta(5)]}{131072\pi^8}\gamma^5 + O(\gamma^{11/2}). \quad (34) \end{aligned}$$

It has been shown in [57] that Eq. (34) (with expansion cut after the sixth term [the one with $\gamma^{7/2}$]) taken for $\gamma \ll 1$ matches asymptotically Eq. (33) taken for $\gamma \gg 1$.

B Numerical implementation of (LL)GPE

The (LL)GPE (cf. Eq. 7 for GPE and Eq. 15 for LLGPE) is a complex, non-linear partial differential equation. In order to solve it, we use the imaginary time evolution (ITE) method. The function ϕ is represented on a one-dimensional spatial lattice with N_x fixed points with lattice constant $\text{DX} = \frac{L}{N_x}$.

The algorithm is built in such way that we choose an initial guess. Generally, it can be any function. We further evolve the initial guess in imaginary time $t \mapsto -i\tau$. It is done with the use of split-step numerical method. The evolution in kinetic energy term is done in the momentum domain, the self-interaction term is calculated in the spatial domain.

No external potential is used. The solution is being found in a box with periodic boundary conditions $\phi\left(\frac{-L}{2}\right) = \phi\left(\frac{L}{2}\right)$.

The program implementing the algorithm above is available here: <https://gitlab.com/jakkop/mudge/-/tags/v01Jun2021>. The program uses W-DATA format dedicated to store data in numerical experiments with ultracold Bose and Fermi gases. The W-DATA project is a part of the W-SLDA toolkit [58–60].

C Phase imprinting method

We use phase imprinting to generate solutions of black solitons; in every iteration ϕ is modified in such a way that $\arg \phi(x) = \pi \cdot (\frac{x}{L} + 0.5)$ for $x \in \langle -\frac{L}{2}, 0 \rangle$ and $\arg \phi(x) = \pi \cdot (\frac{x}{L} - 0.5)$ for $x \in \langle 0, \frac{L}{2} \rangle$. One can easily see that there is a π phase jump for $x = 0$. Moreover, the periodic boundary conditions in terms of phase, i.e. $\arg \phi(\frac{-L}{2}) = \arg \phi(\frac{L}{2})$, are fulfilled. The soliton moves with constant velocity $v_s = \frac{\hbar}{m} \frac{\pi}{L}$.

It is worth mentioning that the healing length ξ is the proper soliton width scale for $\gamma \ll 1$ (as in the GPE), whereas for $\gamma \gg 10$ (fermionized regime) soliton width scales with average interparticle distance L/N .

The resulting soliton profile remains unchanged in the course of the real-time evolution, as can be seen in Figs. 8 and 9.

On the other hand, when we initialize the real time evolution within LLGPE, but with the soliton from GPE, we immediately see it gets distorted. It is shown in Figs. 10 and 11.

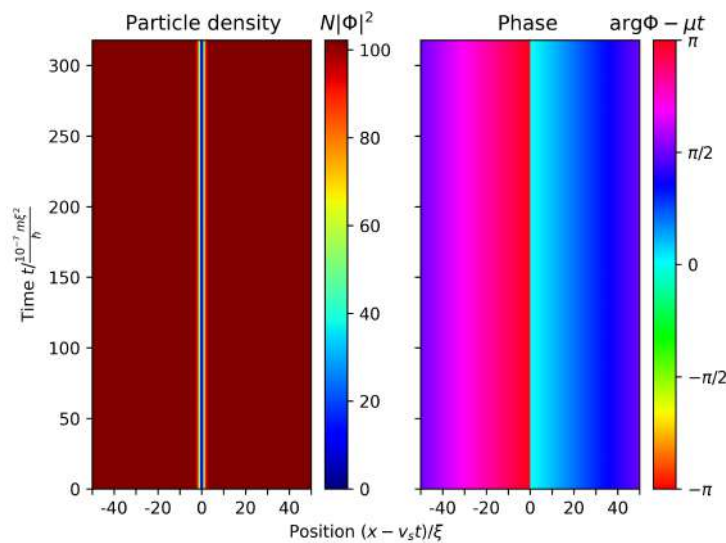


Figure 8: Particle density (left) and phase $\arg \phi$ (right) during the real-time evolution of the LLGPE approach for $\gamma = 1$. Other parameters as in Fig. 4.

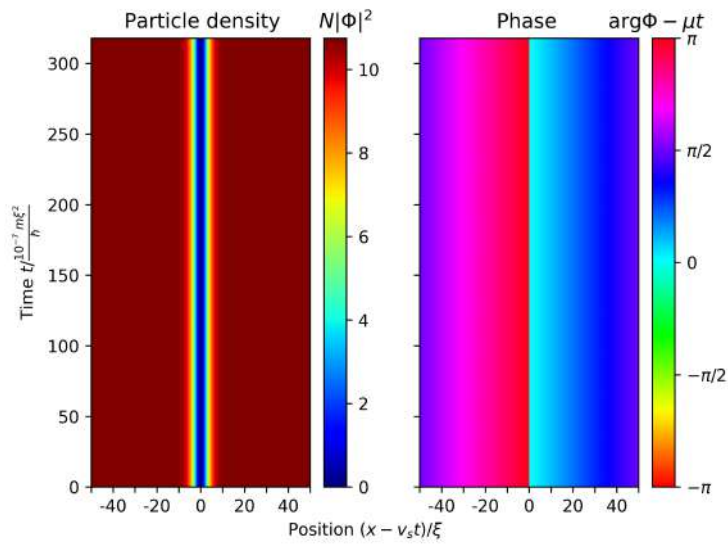


Figure 9: Particle density (left) and phase $\arg \phi$ (right) during the real time evolution of the LLGPE approach for $\gamma = 100$. Other parameters as in Fig. 4.

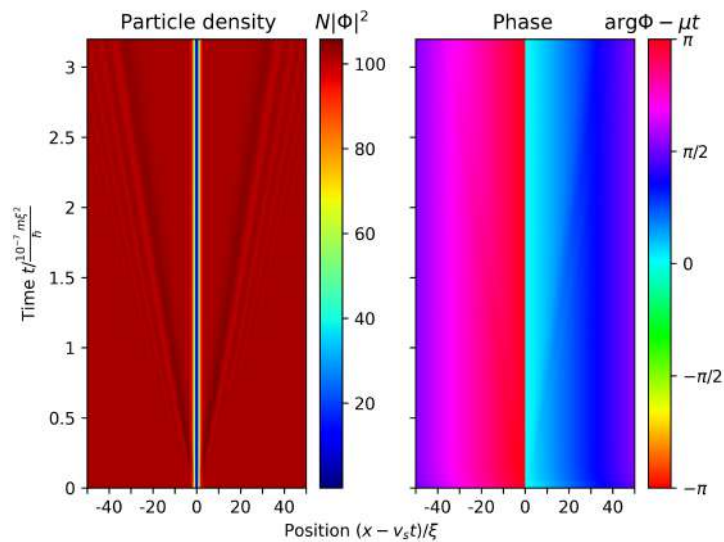


Figure 10: Particle density (left) and phase $\arg \phi$ (right) during the real time evolution of GPE solitonic solution within the LLGPE soliton for $\gamma = 1$. Other parameters as in Fig. 4.

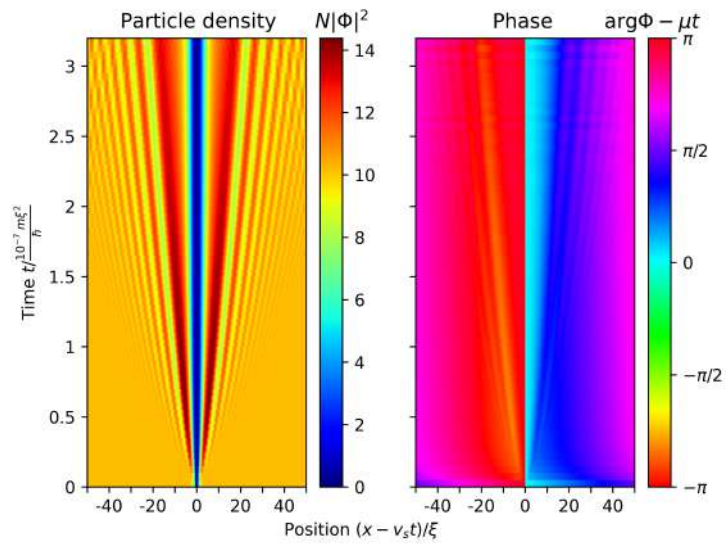


Figure 11: Particle density (left) and phase $\arg \phi$ (right) during the real time evolution of GPE solitonic solution within the LLGPE approach for $\gamma = 100$. Other parameters as in Fig. 4.

References

- [1] C. J. Pethick and H. Smith, *Bose–Einstein condensation in dilute gases*, Cambridge University Press, Cambridge, UK, (2008).
- [2] J. Denschlag et al., *Generating solitons by phase engineering of a Bose-Einstein condensate*, *Science* **287**, 97 (2000), doi:[10.1126/science.287.5450.97](https://doi.org/10.1126/science.287.5450.97).
- [3] S. Burger, K. Bongs, S. Dettmer, W. Ertmer, K. Sengstock, A. Sanpera, G. V. Shlyapnikov and M. Lewenstein, *Dark solitons in Bose-Einstein condensates*, *Phys. Rev. Lett.* **83**, 5198 (1999), doi:[10.1103/PhysRevLett.83.5198](https://doi.org/10.1103/PhysRevLett.83.5198).
- [4] A. Weller, J. P. Ronzheimer, C. Gross, J. Esteve, M. K. Oberthaler, D. J. Frantzeskakis, G. Theocharis and P. G. Kevrekidis, *Experimental observation of oscillating and interacting matter wave dark solitons*, *Phys. Rev. Lett.* **101**, 130401 (2008), doi:[10.1103/PhysRevLett.101.130401](https://doi.org/10.1103/PhysRevLett.101.130401).
- [5] P. P. Kulish, S. V. Manakov and L. D. Faddeev, *Comparison of the exact quantum and quasiclassical results for a nonlinear Schrödinger equation*, *Th. Math. Phys.* **28**, 615 (1976), doi:[10.1007/BF01028912](https://doi.org/10.1007/BF01028912).
- [6] R. Kanamoto, L. D. Carr and M. Ueda, *Topological winding and unwinding in metastable Bose-Einstein condensates*, *Phys. Rev. Lett.* **100**, 060401 (2008), doi:[10.1103/PhysRevLett.100.060401](https://doi.org/10.1103/PhysRevLett.100.060401).
- [7] R. Kanamoto, L. D. Carr and M. Ueda, *Metastable quantum phase transitions in a periodic one-dimensional Bose gas: Mean-field and Bogoliubov analyses*, *Phys. Rev. A* **79**, 063616 (2009), doi:[10.1103/PhysRevA.79.063616](https://doi.org/10.1103/PhysRevA.79.063616).
- [8] J. Sato, R. Kanamoto, E. Kaminishi and T. Deguchi, *Exact relaxation dynamics of a localized many-body state in the 1D Bose gas*, *Phys. Rev. Lett.* **108**, 110401 (2012), doi:[10.1103/PhysRevLett.108.110401](https://doi.org/10.1103/PhysRevLett.108.110401).
- [9] A. Syrwid and K. Sacha, *Lieb-Liniger model: Emergence of dark solitons in the course of measurements of particle positions*, *Phys. Rev. A* **92**, 032110 (2015), doi:[10.1103/PhysRevA.92.032110](https://doi.org/10.1103/PhysRevA.92.032110).
- [10] A. Syrwid, M. Brewczyk, M. Gajda and K. Sacha, *Single-shot simulations of dynamics of quantum dark solitons*, *Phys. Rev. A* **94**, 023623 (2016), doi:[10.1103/PhysRevA.94.023623](https://doi.org/10.1103/PhysRevA.94.023623).
- [11] S. S. Shamaïlov and J. Brand, *Quantum dark solitons in the one-dimensional Bose gas*, *Phys. Rev. A* **99**, 043632 (2019), doi:[10.1103/PhysRevA.99.043632](https://doi.org/10.1103/PhysRevA.99.043632).
- [12] E. Kaminishi, R. Kanamoto, J. Sato and T. Deguchi, *Exact yrast spectra of cold atoms on a ring*, *Phys. Rev. A* **83**, 031601 (2011), doi:[10.1103/PhysRevA.83.031601](https://doi.org/10.1103/PhysRevA.83.031601).
- [13] E. Kaminishi, T. Mori and S. Miyashita, *Construction of quantum dark soliton in one-dimensional Bose gas*, [arXiv:1811.00211](https://arxiv.org/abs/1811.00211).
- [14] W. Golletz, W. Górecki, R. Ołdziejewski and K. Pawłowski, *Dark solitons revealed in Lieb-Liniger eigenstates*, *Phys. Rev. Research* **2**, 033368 (2020), doi:[10.1103/PhysRevResearch.2.033368](https://doi.org/10.1103/PhysRevResearch.2.033368).

- [15] R. Lopes, C. Eigen, N. Navon, D. Clément, R. P. Smith and Z. Hadzibabic, *Quantum depletion of a homogeneous Bose-Einstein condensate*, Phys. Rev. Lett. **119**, 190404 (2017), doi:[10.1103/PhysRevLett.119.190404](https://doi.org/10.1103/PhysRevLett.119.190404).
- [16] R. Chang, Q. Bouton, H. Cayla, C. Qu, A. Aspect, C. I. Westbrook and D. Clément, *Momentum-resolved observation of thermal and quantum depletion in a Bose gas*, Phys. Rev. Lett. **117**, 235303 (2016), doi:[10.1103/PhysRevLett.117.235303](https://doi.org/10.1103/PhysRevLett.117.235303).
- [17] F. Böttcher, J.-N. Schmidt, J. Hertkorn, K. S. H. Ng, S. D. Graham, M. Guo, T. Langen and T. Pfau, *New states of matter with fine-tuned interactions: quantum droplets and dipolar supersolids*, Rep. Prog. Phys. **84**, 012403 (2021), doi:[10.1088/1361-6633/abc9ab](https://doi.org/10.1088/1361-6633/abc9ab).
- [18] D. Petrov, *Quantum mechanical stabilization of a collapsing Bose-Bose mixture*, Phys. Rev. Lett. **115**, 155302 (2015), doi:[10.1103/PhysRevLett.115.155302](https://doi.org/10.1103/PhysRevLett.115.155302).
- [19] A. R. Lima and A. Pelster, *Quantum fluctuations in dipolar Bose gases*, Phys. Rev. A. **84**, 041604 (2011), doi:[10.1103/PhysRevA.84.041604](https://doi.org/10.1103/PhysRevA.84.041604).
- [20] A. R. Lima and A. Pelster, *Beyond mean-field low-lying excitations of dipolar Bose gases*, Phys. Rev. A. **86**, 063609 (2012), doi:[10.1103/PhysRevA.86.063609](https://doi.org/10.1103/PhysRevA.86.063609).
- [21] K. Jachymski and R. Ołdziejewski, *Nonuniversal beyond-mean-field properties of quasi-two-dimensional dipolar Bose gases*, Phys. Rev. A **98**, 043601 (2018), doi:[10.1103/PhysRevA.98.043601](https://doi.org/10.1103/PhysRevA.98.043601).
- [22] L. Parisi, G. E. Astrakharchik and S. Giorgini, *Liquid state of one-dimensional Bose mixtures: A quantum Monte Carlo study*, Phys. Rev. Lett. **122**, 105302 (2019), doi:[10.1103/PhysRevLett.122.105302](https://doi.org/10.1103/PhysRevLett.122.105302).
- [23] R. Ołdziejewski, W. Górecki, K. Pawłowski and K. Rzażewski, *Strongly correlated quantum droplets in quasi-1D dipolar Bose gas*, Phys. Rev. Lett. **124**, 090401 (2020), doi:[10.1103/PhysRevLett.124.090401](https://doi.org/10.1103/PhysRevLett.124.090401).
- [24] L. Parisi and S. Giorgini, *Quantum droplets in one-dimensional Bose mixtures: A quantum Monte Carlo study*, Phys. Rev. A **102**, 023318 (2020), doi:[10.1103/PhysRevA.102.023318](https://doi.org/10.1103/PhysRevA.102.023318).
- [25] S. I. Mistakidis, T. Mithun, P. G. Kevrekidis, H. R. Sadeghpour and P. Schmelcher, *Formation and quench of homonuclear and heteronuclear quantum droplets in one dimension*, Phys. Rev. Research **3**, 043128 (2021), doi:[10.1103/PhysRevResearch.3.043128](https://doi.org/10.1103/PhysRevResearch.3.043128).
- [26] E. H. Lieb and W. Liniger, *Exact analysis of an interacting Bose gas. I. The general solution and the ground state*, Phys. Rev. **130**, 1605 (1963), doi:[10.1103/PhysRev.130.1605](https://doi.org/10.1103/PhysRev.130.1605).
- [27] E. H. Lieb, *Exact analysis of an interacting Bose gas. II. The excitation spectrum*, Phys. Rev. **130**, 1616 (1963), doi:[10.1103/PhysRev.130.1616](https://doi.org/10.1103/PhysRev.130.1616).
- [28] E. H. Lieb, R. Seiringer and J. Yngvason, *One-dimensional bosons in three-dimensional traps*, Phys. Rev. Lett. **91**, 150401 (2003), doi:[10.1103/PhysRevLett.91.150401](https://doi.org/10.1103/PhysRevLett.91.150401).
- [29] J. Mossel and J.-S. Caux, *Exact time evolution of space- and time-dependent correlation functions after an interaction quench in the one-dimensional Bose gas*, New J. Phys. **14**, 075006 (2012), doi:[10.1088/1367-2630/14/7/075006](https://doi.org/10.1088/1367-2630/14/7/075006).
- [30] M. Panfil and J.-S. Caux, *Finite-temperature correlations in the Lieb-Liniger one-dimensional Bose gas*, Phys. Rev. A **89**, 033605 (2014), doi:[10.1103/PhysRevA.89.033605](https://doi.org/10.1103/PhysRevA.89.033605).

- [31] E. B. Kolomeisky, T. J. Newman, J. P. Straley and X. Qi, *Low-dimensional Bose liquids: Beyond the Gross-Pitaevskii approximation*, Phys. Rev. Lett. **85**, 1146 (2000), doi:[10.1103/PhysRevLett.85.1146](https://doi.org/10.1103/PhysRevLett.85.1146).
- [32] M. D. Girardeau and E. M. Wright, *Breakdown of time-dependent mean-field theory for a one-dimensional condensate of impenetrable bosons*, Phys. Rev. Lett. **84**, 5239 (2000), doi:[10.1103/PhysRevLett.84.5239](https://doi.org/10.1103/PhysRevLett.84.5239).
- [33] V. Dunjko, V. Lorent and M. Olshanii, *Bosons in cigar-shaped traps: Thomas-Fermi regime, Tonks-Girardeau regime, and in between*, Phys. Rev. Lett. **86**, 5413 (2001), doi:[10.1103/PhysRevLett.86.5413](https://doi.org/10.1103/PhysRevLett.86.5413).
- [34] P. Öhberg and L. Santos, *Dynamical transition from a quasi-one-dimensional Bose-Einstein condensate to a Tonks-Girardeau gas*, Phys. Rev. Lett. **89**, 240402 (2002), doi:[10.1103/PhysRevLett.89.240402](https://doi.org/10.1103/PhysRevLett.89.240402).
- [35] Y. E. Kim and A. L. Zubarev, *Density-functional theory of bosons in a trap*, Phys. Rev. A **67**, 015602 (2003), doi:[10.1103/PhysRevA.67.015602](https://doi.org/10.1103/PhysRevA.67.015602).
- [36] I. Bouchoule, S. S. Szigeti, M. J. Davis and K. V. Kheruntsyan, *Finite-temperature hydrodynamics for one-dimensional Bose gases: Breathing-mode oscillations as a case study*, Phys. Rev. A **94**, 051602 (2016), doi:[10.1103/PhysRevA.94.051602](https://doi.org/10.1103/PhysRevA.94.051602).
- [37] B. Damski, *Formation of shock waves in a Bose-Einstein condensate*, Phys. Rev. A **69**, 043610 (2004), doi:[10.1103/PhysRevA.69.043610](https://doi.org/10.1103/PhysRevA.69.043610).
- [38] B. Damski, *Shock waves in a one-dimensional Bose gas: From a Bose-Einstein condensate to a Tonks gas*, Phys. Rev. A **73**, 043601 (2006), doi:[10.1103/PhysRevA.73.043601](https://doi.org/10.1103/PhysRevA.73.043601).
- [39] B. B. Baizakov, F. Kh Abdullaev, B. A. Malomed and M. Salerno, *Solitons in the Tonks-Girardeau gas with dipolar interactions*, J. Phys. B: At. Mol. Opt. Phys. **42**, 175302 (2009), doi:[10.1088/0953-4075/42/17/175302](https://doi.org/10.1088/0953-4075/42/17/175302).
- [40] S. De Palo, E. Orignac, M. L. Chiofalo and R. Citro, *Polarization angle dependence of the breathing mode in confined one-dimensional dipolar bosons*, Phys. Rev. B **103**, 115109 (2021), doi:[10.1103/PhysRevB.103.115109](https://doi.org/10.1103/PhysRevB.103.115109).
- [41] S. Choi, V. Dunjko, Z. D. Zhang and M. Olshanii, *Monopole excitations of a harmonically trapped one-dimensional Bose gas from the ideal gas to the Tonks-Girardeau regime*, Phys. Rev. Lett. **115**, 115302 (2015), doi:[10.1103/PhysRevLett.115.115302](https://doi.org/10.1103/PhysRevLett.115.115302).
- [42] S. Peotta and M. Di Ventra, *Quantum shock waves and population inversion in collisions of ultracold atomic clouds*, Phys. Rev. A **89**, 013621 (2014), doi:[10.1103/PhysRevA.89.013621](https://doi.org/10.1103/PhysRevA.89.013621).
- [43] F. Mancarella, G. Mussardo and A. Trombettoni, *Energy-pressure relation for low-dimensional gases*, Nucl. Phys. B **887**, 216 (2014), doi:[10.1016/j.nuclphysb.2014.08.007](https://doi.org/10.1016/j.nuclphysb.2014.08.007).
- [44] I. Bialynicki-Birula, M. Cieplak and J. Kaminski, *Theory of quanta*, Oxford University Press, Oxford, UK, (1992).
- [45] G. Lang, F. Hekking and A. Minguzzi, *Ground-state energy and excitation spectrum of the Lieb-Liniger model: Accurate analytical results and conjectures about the exact solution*, SciPost Phys. **3**, 003 (2017), doi:[10.21468/SciPostPhys.3.1.003](https://doi.org/10.21468/SciPostPhys.3.1.003).

- [46] Z. Ristivojevic, *Conjectures about the ground-state energy of the Lieb-Liniger model at weak repulsion*, Phys. Rev. B **100**, 081110 (2019), doi:[10.1103/PhysRevB.100.081110](https://doi.org/10.1103/PhysRevB.100.081110).
- [47] N. N. Bogoliubov, *On the theory of superfluidity*, J. Phys. **11**, 23 (1947).
- [48] Y. Castin, *Bose-Einstein condensates in atomic gases: Simple theoretical results*, in Les Houches - Ecole d'Ete de Physique Theorique, Springer Berlin Heidelberg, doi:[10.1007/3-540-45338-5_1](https://doi.org/10.1007/3-540-45338-5_1).
- [49] L. P. Pitaevskii and S. Stringari, *Bose-Einstein condensation*, Int. Ser. Monogr. Phys., Clarendon Press, Oxford, UK (2003).
- [50] Z. Ristivojevic, *Excitation spectrum of the Lieb-Liniger model*, Phys. Rev. Lett. **113**, 015301 (2014), doi:[10.1103/PhysRevLett.113.015301](https://doi.org/10.1103/PhysRevLett.113.015301).
- [51] A. D. Jackson, G. M. Kavoulakis and C. J. Pethick, *Solitary waves in clouds of Bose-Einstein condensed atoms*, Phys. Rev. A **58**, 2417 (1998), doi:[10.1103/physreva.58.2417](https://doi.org/10.1103/physreva.58.2417).
- [52] A. D. Jackson, J. Smyrnakis, M. Magiropoulos and G. M. Kavoulakis, *Solitary waves and yrast states in Bose-Einstein condensed gases of atoms*, Europhys. Lett. **95**, 30002 (2011), doi:[10.1209/0295-5075/95/30002](https://doi.org/10.1209/0295-5075/95/30002).
- [53] O. Fialko, M.-C. Delattre, J. Brand and A. R. Kolovsky, *Nucleation in finite topological systems during continuous metastable quantum phase transitions*, Phys. Rev. Lett. **108**, 250402 (2012), doi:[10.1103/PhysRevLett.108.250402](https://doi.org/10.1103/PhysRevLett.108.250402).
- [54] J. Sato, R. Kanamoto, E. Kaminishi and T. Deguchi, *Quantum states of dark solitons in the 1D Bose gas*, New J. Phys. **18**, 075008 (2016), doi:[10.1088/1367-2630/18/7/075008](https://doi.org/10.1088/1367-2630/18/7/075008).
- [55] A. Syrwid, *Quantum dark solitons in ultracold one-dimensional Bose and Fermi gases*, J. Phys. B: At. Mol. Opt. Phys. **54**, 103001 (2021), doi:[10.1088/1361-6455/abd37f](https://doi.org/10.1088/1361-6455/abd37f).
- [56] A. Syrwid and K. Sacha, *Quantum dark solitons in a Bose gas confined in a hard-wall box*, Phys. Rev. A **96**, 043602 (2017), doi:[10.1103/PhysRevA.96.043602](https://doi.org/10.1103/PhysRevA.96.043602).
- [57] S. Prolhac, *Ground state energy of the δ -Bose and Fermi gas at weak coupling from double extrapolation*, J. Phys. A: Math. Theor. **50**, 144001 (2017), doi:[10.1088/1751-8121/aa5e00](https://doi.org/10.1088/1751-8121/aa5e00).
- [58] *W-SLDA Toolkit*, <https://wsllda.fizyka.pw.edu.pl>.
- [59] G. Wlazłowski, K. Sekizawa, M. Marchwiany and P. Magierski, *Suppressed solitonic cascade in spin-imbalanced superfluid Fermi gas*, Phys. Rev. Lett. **120**, 253002 (2018), doi:[10.1103/PhysRevLett.120.253002](https://doi.org/10.1103/PhysRevLett.120.253002).
- [60] A. Bulgac, M. M. Forbes, M. M. Kelley, K. J. Roche and G. Wlazłowski, *Quantized superfluid vortex rings in the unitary Fermi gas*, Phys. Rev. Lett. **112**, 025301 (2014), doi:[10.1103/PhysRevLett.112.025301](https://doi.org/10.1103/PhysRevLett.112.025301).

2. [J. Kopyciński *et al.*, Ultrawide dark solitons and droplet-soliton coexistence in a dipolar Bose gas with strong contact interactions, *Phys. Rev. Lett.* **130**, 043401 (2023)]

PHYSICAL REVIEW LETTERS **130**, 043401 (2023)

Ultrawide Dark Solitons and Droplet-Soliton Coexistence in a Dipolar Bose Gas with Strong Contact Interactions

Jakub Kopyciński^{1,*}, Maciej Łebek¹, Wojciech Górecki², and Krzysztof Pawłowski¹

¹*Center for Theoretical Physics, Polish Academy of Sciences, Al. Lotników 32/46, 02-668 Warsaw, Poland*

²*Faculty of Physics, University of Warsaw, Pasteura 5, 02-093 Warsaw, Poland*

(Received 14 July 2022; revised 10 November 2022; accepted 19 December 2022; published 25 January 2023)

We look into dark solitons in a quasi-1D dipolar Bose gas and in a quantum droplet. We derive the analytical solitonic solution of a Gross-Pitaevskii-like equation accounting for beyond mean-field effects. The results show there is a certain critical value of the dipolar interactions, for which the width of a motionless soliton diverges. Moreover, there is a peculiar solution of the motionless soliton with a nonzero density minimum. We also present the energy spectrum of these solitons with an additional excitation subbranch appearing. Finally, we perform a series of numerical experiments revealing the coexistence of a dark soliton inside a quantum droplet.

DOI: [10.1103/PhysRevLett.130.043401](https://doi.org/10.1103/PhysRevLett.130.043401)

Introduction.—In this Letter, we wish to address two vital topics in the field of ultracold atoms: the investigation of quantum droplets and the subject of dipolar dark solitons (Fig. 1).

The early experiments with attractive dipolar Bose-Einstein condensates (BEC) reported the gas collapse dubbed Bose-nova [1–4]. Later on, opening doors to some new species with a high magnetic dipole moment [5–7] offered more possibilities. Apart from the next evidence of the collapse [8–10], a state with a broken symmetry was unexpectedly brought to light [11]. Subsequently, the novel states of matter—quantum droplets [12–14] and super-solids [15,16], were observed in dipolar systems and Bose-Bose mixtures.

The collapse-preventing mechanism in mixtures [17] and dipolar BECs [18] is due to the quantum fluctuations, not accounted for in the seminal Gross-Pitaevskii equation (GPE). Therefore, one may look for an extended Gross-Pitaevskii equation (EGPE). For instance, the Kolomeisky equation [19] was proposed to describe the Tonks-Girardeau gas [20], but suffered an immediate criticism [21]. Another example of an EGPE is the generalized nonlocal nonlinear Schrödinger equation [22–24] employing the Lee-Huang-Yang (LHY) correction [25,26]. GPE extended by the LHY correction only, does not provide us with a quantitative agreement with quantum Monte Carlo predictions for strong interactions [27,28].

The gap of strong interactions seems to be filled with a hydrodynamic-based approach resulting in the Lieb-Liniger GPE (LLGPE), which we use in this Letter. The equation in question was used to investigate BECs in Refs. [29–37], including the prediction of dipolar quantum droplets in a quasi-1D configuration [38].

Typically, these waves due their existence to nonlinear effects and have been already studied in various physical

systems [39–47], including BECs with contact interactions [48–50], dipolar interactions [51,52], and also beyond the mean-field description [19,34]. It was shown that in the Tonks-Girardeau gas, thanks to the Bose-Fermi mapping, one can find stable solitonlike solutions in many-body calculations [53].

Dark solitons are routinely produced via phase imprinting [54,55], but they are predicted to appear spontaneously during heating as well [56]. Unfortunately, the solitons are

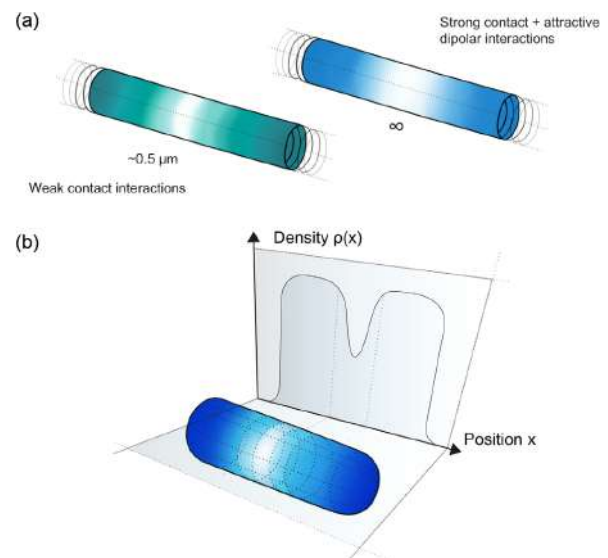


FIG. 1. Graphical abstract. (a) We demonstrate that in a dipolar gas, there are solutions of infinitely wide dark solitons due to an interplay between short- and long-range interactions. (b) Artistic vision of a dark soliton existing inside a quantum droplet.

too narrow to be observed *in situ*, which makes an obstacle to investigate them properly.

The aim of this Letter is to find out whether or not dark solitons exist in a dipolar Bose gas with strong contact interactions and if such solitons can coexist with quantum droplets. As far as we are concerned, the necessary ingredients, namely strong contact interactions, quasi-1D geometry, and dipolar interactions, have been present in the experiment [57].

Nonlocal Lieb-Liniger Gross-Pitaevskii equation.—We study a dipolar Bose gas in a quasi-1D configuration, i.e., with unconfined atoms of mass m in the x direction (box of a size L with periodic boundary conditions or an infinite system), but tightly trapped in the transverse y and z directions. We assume a harmonic trap with frequency ω_{\perp} and introduce the aspect ratio $\sigma = l_{\perp}/L$ with $l_{\perp} = \sqrt{\hbar/m\omega_{\perp}}$. The excitation energies in the perpendicular directions are assumed to be relatively large in comparison to those in the longitudinal one, therefore unoccupied and neglected here.

We consider a head-to-tail configuration of the dipoles. This implies the attractive character of the dipole-dipole interaction (DDI). The dipolar interaction coefficient $g_{\text{dd}} \equiv (\mu_0\mu_D^2/2l_{\perp}^2)$ depends on the atom magnetic moment μ_D .

To understand the dynamics of the system, we start with classical hydrodynamical Euler conservation equations

$$\frac{\partial \rho}{\partial t} + \frac{\partial(\rho v)}{\partial x} = 0, \quad (1a)$$

$$\frac{\partial v}{\partial t} + v \frac{\partial v}{\partial x} = \frac{1}{m\rho} \frac{\partial P_{\text{LL}}}{\partial x} + f, \quad (1b)$$

where P_{LL} is the pressure and f contains body accelerations. We assume further that all fields change sufficiently slow such that locally the gas remains in the ground state of the Lieb-Liniger model with energy E_{LL} , and therefore $P_{\text{LL}} = -(\partial E_{\text{LL}}/\partial L)$ (which we calculate only in the thermodynamic limit [58]), while dipolar magnetic forces are included in f .

We introduce a pseudo-wave function $\Phi(x, t)$, which has to obey the above set of hydrodynamic equations via the density field $\rho(x, t) = |\Phi(x, t)|^2$ and velocity field $v(x, t) = (\hbar/m)\partial_x[\arg \Phi(x, t)]$. This, up to the quantum pressure term, leads to the nonlocal LLGPE [59]:

$$i\hbar\partial_t\Phi(x, t) = \left(-\frac{\hbar^2}{2m}\partial_{xx} + \mu_{\text{LL}}[g, |\Phi(x, t)|^2] \right) \Phi(x, t) - g_{\text{dd}} \int |\Phi(x', t)|^2 v_{\text{dd}}^{\sigma}(|x-x'|)\Phi(x, t) dx', \quad (2)$$

where g is the contact interaction coefficient, $v_{\text{dd}}^{\sigma}(u) = (1/\sigma)v_{\text{dd}}(u/\sigma)$ is the effective quasi-1D dipolar potential [60] with $v_{\text{dd}}(u) = \frac{1}{4}[-2|u| + \sqrt{2\pi(1+u^2)}]e^{u^2/2}$

$\text{Erfc}(|u|/\sqrt{2})$ and μ_{LL} is the Lieb-Liniger chemical potential [61]. The latter can be easily evaluated numerically basing on Refs. [62,63]. The parameter σ acquires another meaning of the effective dipolar interaction range here.

For the weak contact interactions the subsequent terms of μ_{LL} expanded in the Taylor series give rise to the GPE and EGPE (that is, GPE with LHY term). Keeping in (2) the full μ_{LL} , without cutting the Taylor series, makes the equation useful for strong short-range interactions [34] and a tool to study the 1D quantum droplets [38].

Approximation of infinitely strong contact interactions with zero-range dipolar ones.—Following the notation from the Lieb-Liniger model, we will use a dimensionless parameter $\gamma \equiv (m/\hbar^2)(g/\rho_0)$ to describe the contact interaction strength, where $\rho_0 = N/L$ is the average gas density. Let us now consider Eq. (2) in the limit of the infinite contact and zero-range dipolar interactions (i.e., $\gamma \rightarrow \infty$ and $\sigma \rightarrow 0$):

$$i\hbar\partial_t\Phi(x, t) = \frac{\hbar^2}{2m}[-\partial_{xx} + \pi^2|\Phi(x, t)|^4]\Phi(x, t) - g_{\text{dd}}|\Phi(x, t)|^2\Phi(x, t), \quad (3)$$

which is the very equation from Ref. [64]. As it can be immediately seen, the part of this equation responsible for the short-range interactions becomes the same as in the Kolomeisky equation [19]. On the other hand, the dipolar part acquires the nonlinear form known from the GPE. This approximation works well when the interaction range σ is smaller than the typical length scale over which density can change, but still much larger than the average interparticle distance. According to Ref. [51], the solitonic solution in the repulsive dipolar gas in this limit is convergent to the one in the gas with contact interactions only.

One of the solutions of Eq. (3), $\Phi_{\text{MS}}(x)$ was found in Ref. [64]. It was initially thought to be a family of bright solitons. However, as some solutions have a flattop density profile and the energy linear in N , we refer to these objects as quantum droplets. Such crossovers, from a bright soliton to a quantum droplet, were seen in dipolar systems [38] and mixtures [65,66].

Speed of sound and stability of the constant density profile.—We introduce a dimensionless parameter $\gamma_{\text{dd}} \equiv (m/\hbar^2)(g_{\text{dd}}/\rho_0)$ describing the dipolar interaction strength, mimicking the Lieb parameter γ .

First, we linearize Eq. (3) for a homogenous system and solve Bogoliubov-de Gennes equations [67] to get the excitation energy $\epsilon(k) = \sqrt{(\hbar^4 k^4/4m^2) + \hbar^2 k^2[(\hbar^2 \pi^2 \rho_0^2/m^2) - (g_{\text{dd}}\rho_0/m)]}$ as a function of the wave vector k . For low momenta the spectrum is linear, i.e., it contains phonons with the speed of sound $c = \sqrt{(\hbar^2 \rho_0^2/m^2)(\pi^2 - \gamma_{\text{dd}})}$. When $\gamma_{\text{dd}} > \pi^2$, the Bogoliubov excitation energy becomes complex for low

momenta, manifesting the phonon instability in this region. Such an instability is present in a Bose gas with attractive interactions, where the ground state breaks the translational symmetry to form a bright soliton [68]. In our case, however, the symmetry-broken ground state appears as soon as $\gamma_{dd} > \frac{2}{3}\pi^2$ where the pressure $P = -(\partial E_0/\partial L) = (\hbar^2\rho_0^3/m)[(\pi^2/3) - (\gamma_{dd}/2)]$ [34], with E_0 being the homogeneous state energy, becomes negative. Thus, pressure is the very parameter which determines the emergence of quantum droplets.

Dark soliton solution.—We look for a family of Eq. (3) solutions such that $\Phi_s(x, t) \equiv \psi(x - vt) \exp(-i\mu t/\hbar)$ and $\psi(\zeta) = \sqrt{\rho(\zeta)} e^{i\phi(\zeta)}$. Real-valued functions ρ and ϕ are interpreted as the density and phase, respectively. Parameter v is the soliton velocity, $\zeta = x - vt$ is the comoving coordinate, and μ is the chemical potential. When we apply $\Phi_s(x, t)$ to Eq. (3), we obtain the soliton density and phase profiles

$$\rho(\zeta) = \rho_\infty - \frac{(\rho_\infty - \rho_{\min})(1 + D)}{1 + D \cosh(W\zeta)}, \quad (4a)$$

$$\phi(\zeta) = \frac{2mv(D+1)(\frac{\rho_{\min}}{\rho_\infty} - 1)}{\hbar DW \sqrt{1 - a^2}} \times \arctan\left(\frac{(a-1) \tanh(\frac{W\zeta}{2})}{\sqrt{1 - a^2}}\right), \quad (4b)$$

where $a \equiv (\rho_{\min}/\rho_\infty) + (\rho_{\min}/D\rho_\infty) - 1$, $D \equiv [(\rho_{\min} - \rho_1)/(2\rho_\infty - \rho_1 - \rho_{\min})]$, and $W \equiv 2\sqrt{(\pi^2/3)(\rho_\infty - \rho_{\min})(\rho_\infty - \rho_1)}$. Constants $\rho_{\min} = (3mg_{dd}/2\hbar^2\pi^2) - \rho_\infty + (\sqrt{\Delta}/2)$ with $\Delta = [2\rho_\infty - (3mg_{dd}/\hbar^2\pi^2)]^2 + (12m^2v^2/\hbar^2\pi^2)$ is interpreted as the soliton density minimum and ρ_∞ is the background density [$\lim_{\zeta \rightarrow \pm\infty} \rho(\zeta) = \rho_\infty$]. There is no clear interpretation for $\rho_1 = (3mg_{dd}/2\hbar^2\pi^2) - \rho_\infty - (\sqrt{\Delta}/2)$, though. In the thermodynamic limit $\rho_\infty = \rho_0$.

One can notice an interesting feature analyzing solely the soliton density minimum as a function of the dipolar interaction strength γ_{dd} . As we can see it in Fig. 2(a), the density of the motionless soliton ($\beta \equiv v/c = 0$) above $\gamma_{dd} > \frac{2}{3}\pi^2$ is not vanishing. Moreover, the phase of such a solution is constant.

Another vital property of the soliton in question is its full width at half depth $X_{\text{FWHD}} = (2/W) \text{arccosh}[(1 + 2D)/D]$ such that $\rho(X_{\text{FWHD}}/2) = [(\rho_\infty + \rho_{\min})/2]$. Figure 2(b) shows the motionless soliton width diverges logarithmically when $\gamma_{dd} \rightarrow \frac{2}{3}\pi^2$. Even if $0 < \beta \ll 1$, we can see the soliton size at $\gamma_{dd} = \frac{2}{3}\pi^2$ is larger than the interparticle distance $1/\rho_\infty$ and might be easier to detect in the experiment.

The soliton width also diverges when $\gamma_{dd} \rightarrow \pi^2$ but in that case $X_{\text{FWHD}} \propto |\gamma_{dd} - \pi^2|^{-\nu}$ with the critical exponent $\nu = 1/2$.

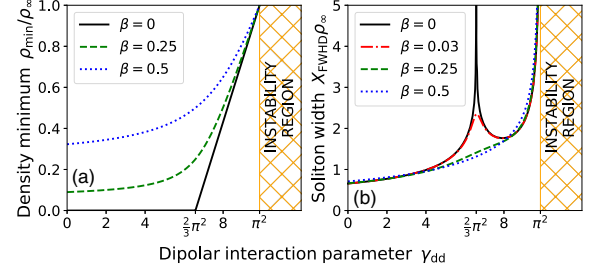


FIG. 2. (a) Soliton density minima ρ_{\min} as functions of the dipolar interaction strength γ_{dd} for different relative velocities β . (b) Soliton full width at half depth X_{FWHD} as functions of the dipolar interaction strength γ_{dd} for different relative velocities β .

One can also notice the phase difference $\Delta\phi_{\max} = \max[\lim_{\zeta \rightarrow \infty} \phi(\zeta) - \lim_{\zeta \rightarrow -\infty} \phi(\zeta)]$ is equal to π when $\gamma_{dd} < \frac{2}{3}\pi^2$, but it is smaller than π otherwise [69]. We hypothesize a phase imprint of $\Delta\phi > \Delta\phi_{\max}$ on a droplet may lead to its splitting rather than a soliton formation. We investigate this case later in this Letter.

Dispersion relation: We calculate and show in Fig. 3 the dispersion relation $\mathcal{E}(\mathcal{P})$ [70,71] of the soliton renormalized energy \mathcal{E} and momentum \mathcal{P} .

In the range $0 \leq \gamma_{dd} < \frac{2}{3}\pi^2$, the dispersion relation behaves qualitatively the same as the one coming from the Kolomeisky solution ($\gamma_{dd} = 0$) [19], whereas, when $\gamma_{dd} > \frac{2}{3}\pi^2$, we observe a new subbranch formed. From now on, we refer to these solutions as anomalous solitons.

Obviously, it may be more difficult to phase imprint the anomalous solitons just because their excitation energy is higher than the one corresponding to the solution with the same phase difference $\Delta\phi$, but situated on the lower subbranch. We cannot also perform a phase imprint of a motionless anomalous soliton.

Another problem may be encountered when trying to calculate the effective soliton mass $m^* = \hbar^2(d^2\mathcal{E}/dk^2)^{-1}$. It is not well defined due to the presence of a cusp in the spectrum.

Dark soliton generation inside a quantum droplet.—Last but not least, we want to find out whether or not dark solitons may coexist with quantum droplets. We prepared

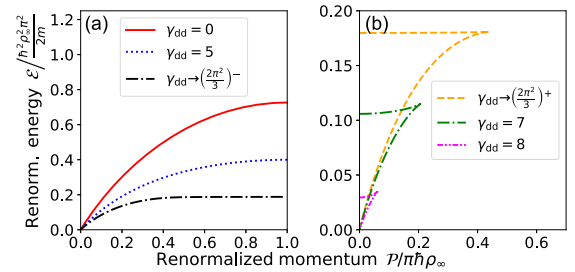


FIG. 3. (a) Soliton dispersion relation $\mathcal{E}(\mathcal{P})$ for $\gamma_{dd} < \frac{2}{3}\pi^2$. (b) Soliton dispersion relation $\mathcal{E}(\mathcal{P})$ for $\gamma_{dd} > \frac{2}{3}\pi^2$.

two series of numerical experiments using the MUDGE toolkit [71,72]. Assuming the soliton width is much smaller than the droplet size, one can treat the droplet bulk density ρ_{eq} as ρ_{∞} and expect that after a phase imprint of $\Delta\phi$ phase difference, the imprinted state is similar to the analytical solitonic solution.

Note that then, due to the interplay between the short-range and dipole interaction, consequently rescaled interaction parameter $(\rho_0/\rho_{\text{eq}})\gamma_{\text{dd}}$ does not depend on the actual value of γ_{dd} and is equal to $\frac{2}{3}\pi^2[1 - \text{sech}(\pi\sqrt{N}/3)]^{-1}$ [71], which corresponds to the left edge of the anomalous region in Fig. 2.

We use the fidelity $F = |\langle \psi_{\text{num}}^{\sigma} | \psi \rangle|^2$ between the numerically evaluated phase-imprinted state $\psi_{\text{num}}^{\sigma}$ and the solitonic solution $\psi = \sqrt{\rho}e^{i\phi}$ with density and phase given by Eqs. (4a) and (4b). We have $\sigma = 0$ and $\gamma \rightarrow \infty$ in the first series of numerical experiments and $\sigma = 0.05$ and $\gamma = 50$ in the other one. We set the number of particles $N = 20$ just like in one of the experimental configurations in the strong interaction regime [57].

As we have mentioned earlier, one can think that above a certain value $\Delta\phi_{\text{max}}$, the droplet will not coexist with a soliton, but split into two. In such a case, the fidelity should drop rapidly in the vicinity of $\Delta\phi_{\text{max}}$. Droplet splitting is shown in Ref. [76], when a droplet is released from an

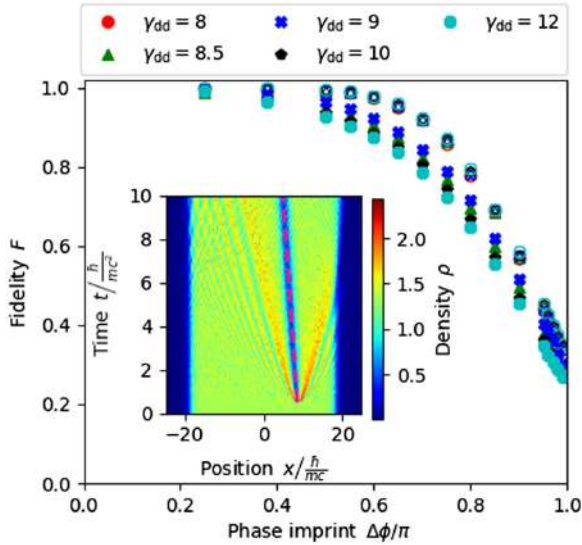


FIG. 4. Fidelity F between a state that appears dynamically after phase imprinting and the analytical solitonic solution. Empty markers: $\gamma \rightarrow \infty$ and $\sigma = 0$; filled markers: $\gamma = 50$ and $\sigma = 0.05$. Inset: evolution of a quantum droplet given by Eq. (3) with dipolar interaction strength $\gamma_{\text{dd}} = 9$ after a phase imprint $\Delta\phi = \pi/2$ at $t \approx (mc^2/\hbar)$. The dashed line marks a trajectory of an object moving with velocity $\beta = 0.3684(4)$, which was predicted from the shape of the soliton in accordance with Fig. 2. The visible emerging high-density structures are the shock waves induced in the phase-imprinting process.

external confinement and in Ref. [77] as a result of an interaction quench.

Nevertheless, as we can see in Fig. 4, no such behavior is present there. Obviously, the fidelities are smaller in the case with finite both DDI range and contact interaction strength as compared to the other case.

The inset of Fig. 4 shows us the time evolution of the droplet. We imprint a phase difference of $\Delta\phi = \pi/2$ on a quarter of the droplet. From this moment on, we can observe a dark soliton moving with a relative velocity $\beta \approx 0.37$ and accompanied by shock waves.

Conclusions.—All in all, the results shown in this Letter corroborate both the existence of dark solitons in the dipolar Bose gases with strong contact interactions and the possibility of quantum droplet-dark soliton coexistence.

We put our focus on the strong contact interaction regime, where the quantum droplets emerge in quasi-1D. In this regime, where the system can be modeled with the nonlocal LLGPE, we deal with a competence between two different types of nonlinearities, the quintic and the cubic one. In the limit of infinite contact interaction strength ($\gamma \rightarrow \infty$) and zero-range dipolar interactions ($\sigma = 0$), we found an analytical solution for the dark solitons given by Eqs. (4a) and (4b). The motionless soliton width diverges when $\gamma_{\text{dd}} = \frac{2}{3}\pi^2$. As a consequence, the solitons will be ultrawide and easy to observe experimentally in large quasi-1D systems.

We show that in the droplet regime, due to the interplay between different nonlinearities, the soliton exhibits anomalous behavior—there exists a gray, but a motionless one. The anomaly is also apparent in the soliton dispersion relation, which contains an additional subbranch.

We complement our analytical considerations with the numerical simulation of an experimental procedure used to generate solitons, i.e., the phase imprinting. We showed the procedure causes the formation of a dark soliton on top of the droplet, even for large phase jumps, finite γ and σ . This fact disfavors the idea that the phase-imprinting method can lead to an instantaneous droplet splitting.

We acknowledge support from Center for Theoretical Physics of the Polish Academy of Sciences, which is a member of KL FAMO. J. K., M. Ł., and K. P. acknowledge support from the (Polish) National Science Center Grant No. 2019/34/E/ST2/00289. W. G. was supported by the Foundation for Polish Science (FNP) via the START scholarship.

J. K. performed the numerical and analytical calculations with help from M. Ł. (linearization) and W. G. (energy renormalization). K. P. designed and supervised the project. J. K. wrote the manuscript with input of all authors.

*jkopycinski@cft.edu.pl

[1] C. A. Sackett, J. M. Gerton, M. Welling, and R. G. Hulet, *Phys. Rev. Lett.* **82**, 876 (1999).

- [2] J. M. Gerton, D. Strekalov, I. Prodan, and R. G. Hulet, *Nature (London)* **408**, 692 (2000).
- [3] E. A. Donley, N. R. Claussen, S. L. Cornish, J. L. Roberts, E. A. Cornell, and C. E. Wieman, *Nature (London)* **412**, 295 (2001).
- [4] J. L. Roberts, N. R. Claussen, S. L. Cornish, E. A. Donley, E. A. Cornell, and C. E. Wieman, *Phys. Rev. Lett.* **86**, 4211 (2001).
- [5] A. Griesmaier, J. Werner, S. Hensler, J. Stuhler, and T. Pfau, *Phys. Rev. Lett.* **94**, 160401 (2005).
- [6] K. Aikawa, A. Frisch, M. Mark, S. Baier, A. Rietzler, R. Grimm, and F. Ferlaino, *Phys. Rev. Lett.* **108**, 210401 (2012).
- [7] M. Lu, N. Q. Burdick, and B. L. Lev, *Phys. Rev. Lett.* **108**, 215301 (2012).
- [8] T. Lahaye, J. Metz, B. Fröhlich, T. Koch, M. Meister, A. Griesmaier, T. Pfau, H. Saito, Y. Kawaguchi, and M. Ueda, *Phys. Rev. Lett.* **101**, 080401 (2008).
- [9] J. Metz, T. Lahaye, B. Fröhlich, A. Griesmaier, T. Pfau, H. Saito, Y. Kawaguchi, and M. Ueda, *New J. Phys.* **11**, 055032 (2009).
- [10] T. Lahaye, C. Menotti, L. Santos, M. Lewenstein, and T. Pfau, *Rep. Progr. Phys.* **72**, 126401 (2009).
- [11] H. Kadau, M. Schmitt, M. Wenzel, C. Wink, T. Maier, I. Ferrier-Barbut, and T. Pfau, *Nature (London)* **530**, 194 (2016).
- [12] M. Schmitt, M. Wenzel, F. Böttcher, I. Ferrier-Barbut, and T. Pfau, *Nature (London)* **539**, 259 (2016).
- [13] C. R. Cabrera, L. Tanzi, J. Sanz, B. Naylor, P. Thomas, P. Cheiney, and L. Tarruell, *Science* **359**, 301 (2018).
- [14] G. Semeghini, G. Ferioli, L. Masi, C. Mazzi, L. Wolski, F. Minardi, M. Modugno, G. Modugno, M. Inguscio, and M. Fattori, *Phys. Rev. Lett.* **120**, 235301 (2018).
- [15] M. Wenzel, F. Böttcher, T. Langen, I. Ferrier-Barbut, and T. Pfau, *Phys. Rev. A* **96**, 053630 (2017).
- [16] M. Sohmen, C. Politi, L. Klaus, L. Chomaz, M. J. Mark, M. A. Norcia, and F. Ferlaino, *Phys. Rev. Lett.* **126**, 233401 (2021).
- [17] D. S. Petrov, *Phys. Rev. Lett.* **115**, 155302 (2015).
- [18] I. Ferrier-Barbut, H. Kadau, M. Schmitt, M. Wenzel, and T. Pfau, *Phys. Rev. Lett.* **116**, 215301 (2016).
- [19] E. B. Kolomeisky, T. J. Newman, J. P. Straley, and X. Qi, *Phys. Rev. Lett.* **85**, 1146 (2000).
- [20] M. Girardeau, *J. Math. Phys. (N.Y.)* **1**, 516 (1960).
- [21] M. D. Girardeau and E. M. Wright, *Phys. Rev. Lett.* **84**, 5239 (2000).
- [22] F. Wächtler and L. Santos, *Phys. Rev. A* **93**, 061603(R) (2016).
- [23] F. Wächtler and L. Santos, *Phys. Rev. A* **94**, 043618 (2016).
- [24] R. N. Bisset, R. M. Wilson, D. Baillie, and P. B. Blakie, *Phys. Rev. A* **94**, 033619 (2016).
- [25] T. D. Lee and C. N. Yang, *Phys. Rev.* **105**, 1119 (1957).
- [26] T. D. Lee, K. Huang, and C. N. Yang, *Phys. Rev.* **106**, 1135 (1957).
- [27] F. Böttcher, M. Wenzel, J.-N. Schmidt, M. Guo, T. Langen, I. Ferrier-Barbut, T. Pfau, R. Bombín, J. Sánchez-Baena, J. Boronat, and F. Mazzanti, *Phys. Rev. Res.* **1**, 033088 (2019).
- [28] L. Parisi, G. E. Astrakharchik, and S. Giorgini, *Phys. Rev. Lett.* **122**, 105302 (2019).
- [29] V. Dunjko, V. Lorent, and M. Olshanii, *Phys. Rev. Lett.* **86**, 5413 (2001).
- [30] Y. E. Kim and A. L. Zubarev, *Phys. Rev. A* **67**, 015602 (2003).
- [31] B. Damski, *Phys. Rev. A* **69**, 043610 (2004).
- [32] B. Damski, *Phys. Rev. A* **73**, 043601 (2006).
- [33] P. Öhberg and L. Santos, *Phys. Rev. Lett.* **89**, 240402 (2002).
- [34] J. Kopyciński, M. Łebek, M. Marciniak, R. Oldziejewski, W. Górecki, and K. Pawłowski, *SciPost Phys.* **12**, 23 (2022).
- [35] S. Peotta and M. Di Ventra, *Phys. Rev. A* **89**, 013621 (2014).
- [36] S. Choi, V. Dunjko, Z. D. Zhang, and M. Olshanii, *Phys. Rev. Lett.* **115**, 115302 (2015).
- [37] S. De Palo, E. Orignac, M. L. Chiofalo, and R. Citro, *Phys. Rev. B* **103**, 115109 (2021).
- [38] R. Oldziejewski, W. Górecki, K. Pawłowski, and K. Rzazewski, *Phys. Rev. Lett.* **124**, 090401 (2020).
- [39] G. Poy, A. J. Hess, A. J. Seracuse, M. Paul, S. Žumer, and I. I. Smalyukh, *Nat. Photonics* **16**, 454 (2022).
- [40] X. Chai, D. Lao, K. Fujimoto, R. Hamazaki, M. Ueda, and C. Raman, *Phys. Rev. Lett.* **125**, 030402 (2020).
- [41] T. M. Bersano, V. Gokhroo, M. A. Khomehchi, J. D'Ambroise, D. J. Frantzeskakis, P. Engels, and P. G. Kevrekidis, *Phys. Rev. Lett.* **120**, 063202 (2018).
- [42] M. A. Hoefer, J. J. Chang, C. Hamner, and P. Engels, *Phys. Rev. A* **84**, 041605(R) (2011).
- [43] G. Theocharis, A. Weller, J. P. Ronzheimer, C. Gross, M. K. Oberthaler, P. G. Kevrekidis, and D. J. Frantzeskakis, *Phys. Rev. A* **81**, 063604 (2010).
- [44] C. Becker, S. Stellmer, P. Soltan-Panahi, S. Dörscher, M. Baumert, E.-M. Richter, J. Kronjäger, K. Bongs, and K. Sengstock, *Nat. Phys.* **4**, 496 (2008).
- [45] A. Weller, J. P. Ronzheimer, C. Gross, J. Esteve, M. K. Oberthaler, D. J. Frantzeskakis, G. Theocharis, and P. G. Kevrekidis, *Phys. Rev. Lett.* **101**, 130401 (2008).
- [46] C. Rotschild, B. Alfassi, O. Cohen, and M. Segev, *Nat. Phys.* **2**, 769 (2006).
- [47] Y. S. Kivshar and B. Luther-Davies, *Phys. Rep.* **298**, 81 (1998).
- [48] V. E. Zakharov and A. B. Shabat, *Sov. Phys. JETP* **37**, 823 (1973).
- [49] A. D. Jackson, G. M. Kavoulakis, and C. J. Pethick, *Phys. Rev. A* **58**, 2417 (1998).
- [50] J. Sato, R. Kanamoto, E. Kaminishi, and T. Deguchi, *New J. Phys.* **18**, 075008 (2016).
- [51] K. Pawłowski and K. Rzazewski, *New J. Phys.* **17**, 105006 (2015).
- [52] M. Beau, A. del Campo, D. J. Frantzeskakis, T. P. Horikis, and P. G. Kevrekidis, *Phys. Rev. A* **105**, 023323 (2022).
- [53] M. Tettamanti and A. Parola, *Phys. Rev. A* **104**, 043325 (2021).
- [54] S. Burger, K. Bongs, S. Dettmer, W. Ertmer, K. Sengstock, A. Sanpera, G. V. Shlyapnikov, and M. Lewenstein, *Phys. Rev. Lett.* **83**, 5198 (1999).
- [55] J. Denschlag, J. E. Simsarian, D. L. Feder, C. W. Clark, L. A. Collins, J. Cubizolles, L. Deng, E. W. Hagley, K. Helmerson, W. P. Reinhardt, S. L. Rolston, B. I. Schneider, and W. D. Phillips, *Science* **287**, 97 (2000).

3. [J. Kopyciński *et al.*, Quantum Monte Carlo-based density functional for one-dimensional Bose-Bose mixtures, *Phys. Rev. Res.* **5**, 023050 (2023)]

PHYSICAL REVIEW RESEARCH **5**, 023050 (2023)

Quantum Monte Carlo-based density functional for one-dimensional Bose-Bose mixtures

Jakub Kopyciński ^{1,2,*}, Luca Parisi,² Nick G. Parker,² and Krzysztof Pawłowski ¹

¹*Center for Theoretical Physics, Polish Academy of Sciences, Al. Lotników 32/46, 02-668 Warsaw, Poland*

²*Joint Quantum Centre (JQC) Durham-Newcastle, School of Mathematics, Statistics and Physics, Newcastle University, Newcastle upon Tyne NE1 7RU, United Kingdom*



(Received 20 January 2023; accepted 7 April 2023; published 24 April 2023)

We propose and benchmark a Gross-Pitaevskii-like equation for two-component Bose mixtures with competing interactions in 1D. Our approach follows the density functional theory with the energy functional based on the exact quantum Monte Carlo (QMC) simulations. Our model covers, but goes beyond, the popular approach with the Lee-Huang-Yang corrections. We first benchmark our approach against available QMC data in all interaction regimes and then study dynamical properties, inaccessible by *ab initio* many-body simulations. Our analysis includes a study of monopole modes and reveals the presence of anomalous dark solitons.

DOI: [10.1103/PhysRevResearch.5.023050](https://doi.org/10.1103/PhysRevResearch.5.023050)

I. INTRODUCTION

Recent studies of ultracold gases with competing interactions have led to a major change in the field. They undermined the validity of the mean-field approximation when attractive and repulsive interactions in the system almost cancel each other.

The first predictions indicated that systems with dominating three-body interactions were bound to hold quantum droplets [1,2]. We shall focus, however, on the stabilising effect of quantum fluctuations [3]. To account for it, one can include Lee-Huang-Yang (LHY) corrections [4,5] to the mean-field equation using a local density approximation. One then derives a generalized Gross-Pitaevskii (GGP) equation. It has been widely used to theoretically investigate the ground-state properties and excitations of Bose-Bose mixtures with particular attention given to the compressional mode (known also as the monopole or breathing mode) [6–9]. The GGP theory predicts the existence of self-bound objects—ultradilute quantum droplets made of ultracold atoms [3]. The emergence of a liquid phase is marked by the presence of a local minimum in the energy density functional.

Soon after having been proposed theoretically, quantum droplets were experimentally observed [10–14]. Some theoretical predictions indicate even the possibility of finding quantum droplets [15] in recently obtained heteronuclear dipolar condensates [16,17]. Despite its remarkable usefulness, there are still factors not included in the GGP theory. For instance, *ab initio* calculations show a liquid-gas transition in two-component mixtures [18], whereas the GGP does

not. Moreover, the same work demonstrates a quantitative disagreement of the homogeneous state energy. Quite unexpectedly, the monopole mode frequencies happen to match the QMC calculations, though [19]. The nature of the liquid-gas transition still remains an open question. It is an especially interesting in the light of the Mermin-Wagner theorem [20,21]. Unfortunately, such a question cannot be answered in a purely numerical model we are about to present.

Several attempts have been made to overcome the existing imperfections of the GGP equation. One of the ideas that follows the density functional theory was to build an equation, which would quantitatively reproduce the spatially uniform state energy from a chosen *ab initio* method for any interaction strength. In this regard the 1D Bose contact gas is a special system as its ground-state energy has been already derived in the analytical *ab initio* calculations by E. Lieb and E. Liniger [22,23].

Using this exact energy functional one gets the single-particle equation here referred to as the Lieb-Liniger Gross-Pitaevskii (LLGP) equation that was used in Refs. [24–31]. The equation proved to correctly describe the ground state and low-lying excitations in all regimes—from the weakly-interacting one (which, contrary to the 3D case happens at high gas densities) up to the Tonks-Girardeau regime (at low gas densities). The LLGP equation was recently used to study Bose gas with repulsive short-range and attractive dipolar interactions [32–36] to show the existence and properties of the dipolar quantum droplets. Concerning the droplets in quantum mixtures, a similar approach was employed to construct a quantum Monte Carlo (QMC)-based energy density functional for bosonic mixtures in 3D [37], but so far the 1D Bose mixture was not investigated in such framework. For the latter system it was shown [18] that GGP fails to reproduce the phase diagram in certain regimes, in particular at low densities when atoms bind together into interacting dimers.

In this article, we aim to formulate and benchmark the QMC-based single-orbital density functional theory that is applicable to two-component Bose mixtures with repulsive

*jkopycinski@cft.edu.pl

intra- and attractive intercomponent interactions. We later refer to it as Lieb-Liniger Gross-Pitaevskii for mixtures (mLLGP). Our theoretical approach using a single orbital ψ and a QMC-based energy density functional \mathcal{E} results in an equation of the following form:

$$i\hbar\partial_t\psi(x,t) = -\frac{\hbar^2}{2m}\partial_x^2\psi(x,t) + \frac{\delta\mathcal{E}}{\delta n}\psi(x,t), \quad (1)$$

where n is the particle density. We want it to be applicable to two-component Bose mixtures with repulsive intra- and attractive intercomponent interactions. To do this, we analyze the phase diagram of the system and numerically study the static properties and monopole mode of quantum droplets. We use data from Ref. [18] to construct the energy density functional and Ref. [19] to benchmark our approach.

In lower-dimensional systems, we can name two substantial beyond-LHY approaches. One of them is a pairing theory for bosons [38]. The other one is based on the inclusion of higher-order corrections to the GGP equation [39]. Both of them generally give only a qualitative agreement with QMC calculations.

Our approach shares similarities with a density functional theory [40] for Fermi systems at unitarity [41]. The resulting density functional has been employed multiple times to look into strongly interacting fermions [42–46], revealing a remarkable consistency with the experiments [47,48].

A great advantage of having a Gross-Pitaevskii-like equation, in comparison to the QMC methods, is the possibility of studying nonlinear and time-dependent effects like the existence of dark solitons. This subject is particularly interesting as we may expect fundamentally different results than the solitons we know from single-species systems [49] or dark-dark solitons occurring in miscible bosonic mixtures [50,51].

Very recently there have been reports on wide soliton-like objects, both in mixtures [52] and in dipolar Bose gases [31]. As such, last but not least, we show density and phase profiles of solitary waves evaluated with our theory.

II. FRAMEWORK

A. System

We consider a one-dimensional Bose gas consisting of two components $\sigma = \{\uparrow, \downarrow\}$ in a box of size L . We assume that the components have equal atomic masses $m_\uparrow = m_\downarrow = m$. We also assume that the short-range interaction coupling constants are the same in the intracomponent case $g_{\uparrow\uparrow} = g_{\downarrow\downarrow} = g$, whereas the intercomponent interactions can be independently tuned with a coupling constant $g_{\uparrow\downarrow}$. Atoms of the same species repel each other while the intercomponent interactions are attractive. The binding energy of an atomic pair in vacuum $\varepsilon_b = -(mg_{\uparrow\downarrow}^2/4\hbar^2)$ is a relevant energy scale in the system, while for the length scale we choose the intracomponent scattering length $a = 2\hbar^2/mg$. In experimental setups, such a system can be realised as a spin-balanced gas of a single bosonic isotope, where spins σ correspond to two different hyperfine levels and the interaction strengths can be tuned with magnetic field via Feshbach interactions.

We assume that we are in the miscible regime. The single-component densities are locked according to the condition

$n_\downarrow/n_\uparrow = \sqrt{g_{\uparrow\uparrow}/g_{\downarrow\downarrow}}$ [3], which holds even in inhomogeneous cases. In our system this implies that there are equal number of atoms in each component $N_\uparrow = N_\downarrow = N/2$ and that the single-component densities are half of the total density $n_\uparrow = n_\downarrow = n/2$. If the system is homogeneous, the overall density is equal to $n = N/L$.

B. Generalized Gross-Pitaevskii and quantum Monte Carlo approaches

In the weakly-interacting limit (corresponding to high densities $na \gg 1$), one may expect the generalized GGP approach to be valid. The GGP energy density functional has the following part corresponding to interactions [18]:

$$\mathcal{E}_{\text{GGP}}[n; g, g_{\uparrow\downarrow}] = \frac{(g - g_{\uparrow\downarrow})n^2}{4} - \frac{mn^{3/2}}{3\sqrt{2}\pi\hbar}[(g - g_{\uparrow\downarrow})^{3/2} + (g + g_{\uparrow\downarrow})^{3/2}]. \quad (2)$$

The first term in Eq. (2) corresponds to the mean-field contribution to the interaction energy and the other to the correction for quantum fluctuations, widely known as the LHY term. If we compare, however, the results from GGP equation and *ab initio* calculations from diffusion Monte Carlo in a wide range of densities and interaction ratios, we observe discrepancies at low ratios. It is due to one of the peculiarities of one-dimensional systems—the lower the density, the higher the interaction. Thus, the GGP model is correct in the high-density limit but cannot be trusted in the opposite case.

First of all, the GGP predicts the existence of stable quantum droplets for any ratio $g_{\uparrow\downarrow}/g < 1$. In other words, there is always a local minimum present in the energy density functional $\mathcal{E}_{\text{GGP}}[n; g, g_{\uparrow\downarrow}]$ as long as $g_{\uparrow\downarrow}/g < 1$. QMC predicts a certain critical value of the interaction ratio, below which the minimum disappears and we have a liquid-gas transition at $(g_{\uparrow\downarrow}/g)_{\text{cr}} = 0.47(2)$ [18].

Although there are other methods, like a general extension to the LHY theory proposed in Ref. [39] or a pairing theory for bosons introduced in [38], which are able to predict such a transition, they do not enable us to quantitatively compute the homogeneous gas energy with their use. Neither does the GGP, which results in an inaccurate estimate of a quantum droplet size and bulk density.

Lastly, the GGP is not applicable to the strongly-interacting regime. When $na \ll 1$, the gas energy quickly approaches half of the binding energy of a dimer, i.e., $-\varepsilon_b/2$, indicating that the system could be understood as a weakly-interacting gas of dimers [38]. The energy per dimer approaches $-\varepsilon_b$ in the limit of vanishing density, while according to the GGP theory it tends to zero.

C. Lieb-Liniger Gross-Pitaevskii equation for two-component 1D bosonic mixtures (mLLGP equation)

We aim to construct a energy density functional to study bosonic mixtures in 1D, which gives (i) a quantitative agreement with QMC in terms of a homogeneous gas energy $E(n; g, g_{\uparrow\downarrow})$ in a wide range of interaction ratios [53], (ii) a proper limit of a uniform gas energy, i.e., $\lim_{n \rightarrow 0} E(n; g, g_{\uparrow\downarrow}) = -N\varepsilon_b/2$, and (iii) a correct value for

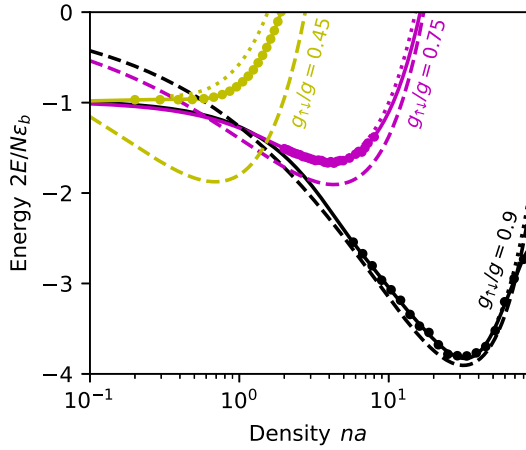


FIG. 1. Energy per particle as a function of density; comparison of different models. QMC from Ref. [18] (markers), our density functional dubbed mLLGP (solid line), GGP (dashed line), pairing theory (dotted line); and interaction ratios $g_{\uparrow\downarrow}/g = 0.45$ (yellow [light grey]), 0.75 (magenta [grey]) and 0.9 (black). The QMC error bars are smaller than the marker sizes.

the critical interaction ratio $(g_{\uparrow\downarrow}/g)_{cr}$, at which a liquid-gas transition occurs. It is more accurate than both the GGP and pairing theory, but, unlike QMC, enables us to study nonlinear and time-dependent effects, e.g., the properties of dark solitons.

To do that, we fit QMC data from Ref. [18] to get a spline representation of the energy functional $\mathcal{E}_{mLLGP}[n; g, g_{\uparrow\downarrow}]$ and construct a single-orbital density functional theory for bosonic mixtures. To do this, we extrapolate the data in the low- and high-density regimes with two separate functions. This is necessary because the QMC data is covering only a part of densities, omitting the low- and high-density regions. Afterwards, we interpolate the data with a spline in densities and linearly in interaction ratios. In this way, we obtain $\mathcal{E}_{mLLGP}[n; g, g_{\uparrow\downarrow}]$ in a form that is convenient for numerical evaluation. This whole procedure is described in detail in Appendix A.

We decided to use a numerical representation of $\mathcal{E}_{mLLGP}[n; g, g_{\uparrow\downarrow}]$ after having checked a few simpler representations, including polynomials, but these representations did not fulfill the conditions (i)–(iii) we have listed earlier.

Figure 1 shows us the energy per particle of a homogeneous Bose-Bose mixture. For interaction ratios $g_{\uparrow\downarrow}/g \simeq 1$ all three theories (GGP, pairing theory, and mLLGP) are consistent with QMC calculations. In the case of the GGP and pairing theory, the smaller the ratio becomes, the higher the discrepancy is. For ratio $g_{\uparrow\downarrow}/g = 0.45$, the energy per particle from the GGP model still possesses a pronounced minimum, whereas QMC, mLLGP, and the pairing theory predict a lack thereof. The latter deviates from the QMC data and matches it only qualitatively in this region. One can see the energy functional \mathcal{E}_{mLLGP} is constructed to fulfill all the conditions from the list above.

The analysis of the energy functional in a state can provide us with important thermodynamic quantities. For instance,

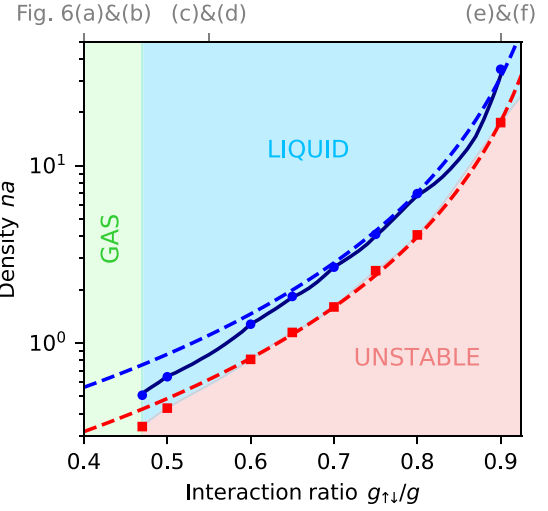


FIG. 2. Phase diagram of a homogeneous two-component mixture. The unstable region is demarcated by spinodal densities, predicted from GGP (red [light grey] dashed line) and QMC (square markers). Equilibrium density given by the mLLGP (navy [dark grey] solid line), GGP (blue [grey] dashed line), and QMC from Ref. [18] (round markers). The ticks on top correspond to the interaction ratios used in Fig. 6.

$\mu_{mLLGP}[n_0; g, g_{\uparrow\downarrow}] = \delta\mathcal{E}_{mLLGP}[n; g, g_{\uparrow\downarrow}]/\delta n|_{n=n_0}$ is the chemical potential evaluated at density n_0 , and the speed of sound c is given by the following relation $c = \sqrt{\frac{n}{m} \frac{d\mu}{dn}}$. The position of the energy per particle minimum plays a vital role in the context of quantum droplet studies: the equilibrium density n_{eq} where $d(E/N)/dn = 0$ is the value of the density in the droplet bulk, assuming the droplet is sufficiently large, i.e., $N \gg 1$ and possesses a flat-top profile. In this limit, we may approximate the properties of the droplet bulk to be the same as those of a homogeneous system with density n_{eq} .

With that knowledge we are able to explore the phase diagram and compare it to the one created with the QMC approach. We show it in Fig. 2. We are able to distinguish three phases: gaseous, liquid, and unstable. The gaseous one corresponds to the region where the minimum in the energy density functional is located at the vanishing density. It happens when the interaction ratio $g_{\uparrow\downarrow}/g < 0.47$. Above that value, the minimum exists and we enter the liquid phase. Nevertheless, in the region $g_{\uparrow\downarrow}/g > 0.47$, there is a range of densities for which the speed of sound is complex. This signals a phonon instability.

The unstable and stable liquid phases are demarcated by spinodal densities n_{ins} , where $d^2\mathcal{E}/dn^2 = 0$. At this border, the compressibility is infinite. The nature of the unstable liquid phase in a weakly interacting bosonic mixtures was discussed in Ref. [54]. In Fig. 2 we also plot equilibrium densities n_{eq} (see solid navy line for mLLGP and a dashed blue one for GGP). The two comparisons QMC vs GGP and QMC vs mLLGP favor the latter approach. Wherever we have data from QMC simulations, the mLLGP predicts the same equilibrium density as *ab initio* calculations [55]. On the other

hand, the GGP extends both liquid and unstable regions far beyond the critical interaction ratio $(g_{\uparrow\downarrow}/g)_{\text{cr}}$.

For low interaction ratios $g_{\uparrow\downarrow}/g \ll 1$, the equilibrium densities are located in the low-density region. However, in this limit of densities, the gas cannot be treated anymore as weakly interacting. The GGP approach, contrary to QMC, gives us a rough estimate of n_{eq} only.

Having established that the constructed energy functional reproduces the phase diagram according the QMC theory, we can now use this to construct an equation of the form of Eq. (1), which allows for modeling time dependence and inhomogeneity of the effective single particle orbital. We now write this equation as

$$i\hbar\partial_t\psi(x,t) = -\frac{\hbar^2}{2m}\partial_x^2\psi(x,t) + \mu_{\text{mLLGP}}[|\psi(x,t)|^2; g, g_{\uparrow\downarrow}] \times \psi(x,t). \quad (3)$$

The square modulus of this orbital is interpreted as the particle density $n(x)$. Next, in Sec. III A, we will numerically solve the mLLGP equation (3), with the use of imaginary time propagation to find broken-symmetry states in Bose-Bose mixtures. Following this, in Sec. III B we will additionally solve the equation in real time to simulate the breathing modes of a perturbed droplet. Our toolkit is provided on GitLab [56].

III. QUANTUM DROPLETS

A. Static properties

The ground state (GS) of a two-component mixture in the liquid regime takes a form of a quantum droplet. Typical density profiles of one-dimensional droplets are shown in the inset of Fig. 3. The quantum droplets evaluated with the mLLGP (see Appendix A for numerical details) exhibit a flat-top bulk when the number of particles exceeds 20. For $N = 60$ and 100, we can observe a prominent plateau with the same density as the equilibrium value n_{eq} given by QMC calculations. We juxtaposed these density profiles with analogous ones given by the GGP equation. As we can see, their bulk densities do not match the QMC prediction. The discrepancy for $g_{\uparrow\downarrow}/g = 0.6$ is equal to 14%, but grows up to 48% at the critical ratio $(g_{\uparrow\downarrow}/g)_{\text{cr}} = 0.47(2)$ (cf. Fig. 2).

As the number of particles in the droplet N , its bulk density n_{eq} and its width $\sqrt{\langle x^2 \rangle - \langle x \rangle^2}$ are connected (in the first approximation $n_{\text{eq}} \propto N/\sqrt{\langle x^2 \rangle - \langle x \rangle^2}$), the difference between the estimations of the equilibrium density should be also visible when we plot the droplet width against the interaction ratio, but keeping a fixed number of atoms in the system. We show it in the main panel of Fig. 3.

As we can see, the droplet width is a decreasing function of $g_{\uparrow\downarrow}/g$. When $g_{\uparrow\downarrow}$ becomes larger, the interparticle attraction gets more pronounced and the droplet contracts. As expected, the GGP gives a qualitative agreement of the droplet width with the mLLGP. However, the lower the interaction ratio, the higher the discrepancy between the models.

In classical physics the total energy of the droplet can be divided into the volume and surface terms $E_{\text{tot}} = E_V + E_S$. In a one-dimensional system, the surface term should be N independent and the volume term (for $N \gg 1$) should be proportional to the number of particles in the droplet as we show

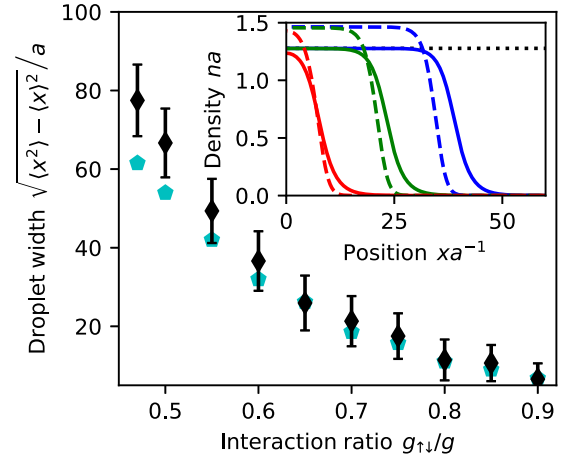


FIG. 3. Droplet width $\sqrt{\langle x^2 \rangle - \langle x \rangle^2}$ as a function of the interaction ratio $g_{\uparrow\downarrow}/g$. Pentagonal cyan markers correspond to the GGP prediction, diamond black ones to the mLLGP estimation. Number of particles forming the droplet $N = 100$. Inset: Density profiles of quantum droplet evaluated at a ratio $g_{\uparrow\downarrow}/g = 0.6$ using the mLLGPE (solid) and GGP (dashed) for different number of particles $N = 20$ (red [innermost]), 60 (green [middle]), and 100 (blue [outermost]). Black dotted line corresponds to the equilibrium density given by the QMC calculations from Ref. [18].

it in the inset of Fig. 4. We are particularly interested in the value of the surface term. If a droplet gets split, the energy in the system increases by E_S . Low values of the surface energy may be considered an issue in the experiment. Namely, thermal excitations might cause a fission of the droplet.

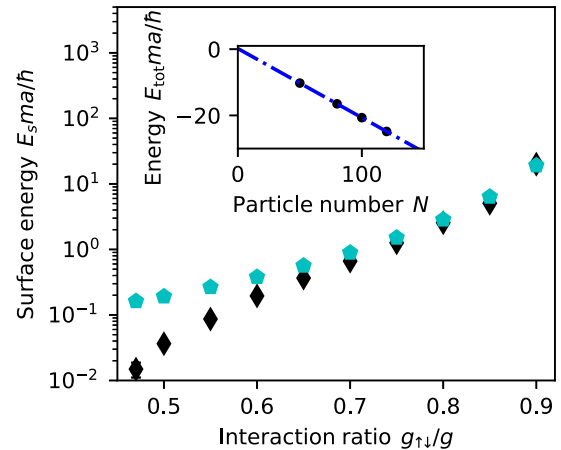


FIG. 4. Surface energies of quantum droplets for different interaction ratios $g_{\uparrow\downarrow}/g$. Pentagonal cyan markers correspond to the GGP results, diamond black ones to the mLLGP prediction. Inset: Total energy of a quantum droplet obtained with Eq. (3) for high particle numbers $N \gg 1$ and $g_{\uparrow\downarrow}/g = 0.6$. The dash-dotted line corresponds to a linear fit $E_{\text{tot}} = \bar{e}N + E_S$. The main contribution to the uncertainty of the surface energy is due to the linear fit and in most cases, the error bars are smaller than the marker size.

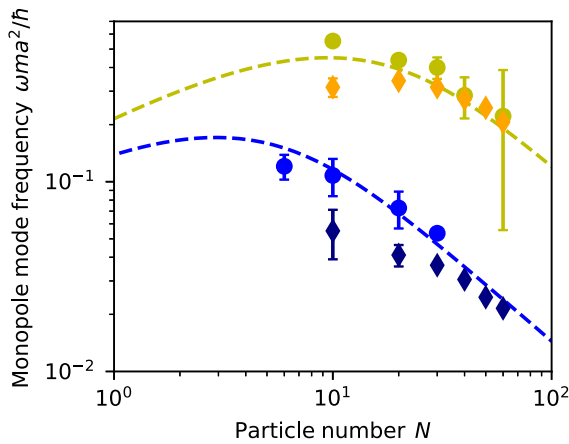


FIG. 5. Monopole mode frequency as a function of the number of particles in the droplet. Round markers correspond to the linear response theory prediction based on QMC data from Ref. [19], diamonds to the mLLGP, and the dashed lines to the GGP predictions. Frequencies evaluated at a ratios $g_{\uparrow\downarrow}/g = 0.6$ (blue [dark grey]) and 0.8 (yellow [light grey]).

Figure 4 depicts the surface energy of the droplet as a function of the interaction ratio $g_{\uparrow\downarrow}/g$. In the case of mLLGP, the diminishing surface energy when approaching $(g_{\uparrow\downarrow}/g)_{\text{cr}}$ is a signature of the liquid-gas transition proximity. The surface tension slowly decreases until it vanishes below the critical interaction ratio. The GGP does not predict such a transition, so the surface tension does not go to zero according to this theory.

One may ask here on the contribution from gradient corrections to the energy functional and their influence on the results. As the analysis conducted in Ref. [19] shows a quantitative agreement of the surface energy of the droplet between the QMC and GGP in the weakly interacting regime, we do not include them into $\mathcal{E}_{\text{mLLGP}}$.

B. Monopole mode excitation

We now look into how the ground state reacts to a small perturbation. We choose to study the monopole mode. We evolve in real time a quantum droplet perturbed by a factor $\exp(-i\epsilon x^2/a^2)$, where ϵ is a small constant. It corresponds to a situation when the initial velocity field in a droplet has the form $v(x) = -2\hbar\epsilon x/ma^2$ (further details are provided in Appendix A). At the beginning, the droplet is squeezed and at some point it expands again. This process is periodic and has its characteristic frequency, which we measure by looking at the standard deviation of the droplet width $\sqrt{\langle x^2 \rangle - \langle x \rangle^2}$ in time.

We show the results of this numerical analysis in Fig. 5 altogether with the monopole mode frequencies evaluated with the GGP [6] and linear response theory predictions based on QMC data [19], i.e., the data, which were not used in to fit $\mathcal{E}_{\text{mLLGP}}$. All three approaches give consistent results in the large particle number limit. The monopole mode frequency scales like $\omega \propto N^{-1}$ there [6]. Surprisingly, the QMC data also agree with the GGP-based results, even though the GGP

equation is not expected to be accurate for small N , due to the breakdown of the local density approximation (LDA), which requires fulfilling the condition $N \gg 1$.

The mLLGP simulations agree in most cases within the range of 2 uncertainties. The dominating source of uncertainty is the form of $\mathcal{E}_{\text{mLLGP}}$ in the low-density regions $n \ll n_{\text{eq}}$. As we lack Monte Carlo data there, we cannot control the quality of the fit below the equilibrium density. It is clearly visible when the number of particles in the droplet is low. The bulk density is lower than n_{eq} there (cf. the inset of Fig. 3), especially after a slight expansion happening due to the perturbation we apply.

Thus, an accurate measurement of monopole mode frequencies seems to be the best choice to experimentally verify the validity of mLLGP-based study. It might be a daunting task, though. The difference is most striking in the small-droplet limit, which might be difficult to achieve in an experimental setup.

IV. DARK SOLITONS

We supplement our study of Bose-Bose mixtures with a numerical analysis of dark solitons. They are an example of nonlinear effects, which are beyond the range of QMC.

We look for solitonic solutions of the mLLGP equation (3) in the thermodynamic limit. By dark soliton we understand a density depletion traveling at a constant velocity v_s without changing its shape. We may classify these solitons as grey solitons if $v_s > 0$ and they have a nonzero density minimum, and as black solitons if they are motionless and their density minimum is equal to zero [49].

We assume that the density and phase of the orbital $\varphi = \arg \psi$ far from the soliton are constant and equal to n_∞ and φ_∞ . Our numerical methods (see Appendix B for details) enable us to find both motionless and moving dark solitons. We use a velocity relative to the speed of sound $\beta = v_s/c$ to characterize the soliton.

If we take a look at the dark solitonic solutions in the weakly-interacting single-component Bose gas, we encounter both moving and motionless solutions.

Figure 6 presents the solitonic density minima $\min n(x)$ and full widths at half depths X_{FWHD} as functions of the density n_∞ for three values of the interaction ratio $g_{\uparrow\downarrow}/g$. The motionless solitons in the gaseous phase n_{eq} can be classified as standard ones—their density reaches zero [cf. black solid line in Fig. 6(a)]. Moreover, the density minima of grey solitons increase with their velocity. Figure 6(b) shows the soliton width, which diverges as $n_\infty \rightarrow 0$.

The situation changes when we cross the critical interaction ratio and enter the liquid phase. In the high-density limit the soliton minimum density is zero, but below n_{eq} we enter a region where the minimum density starts to increase [see Figs. 6(c) and 6(e)]. One may say the motionless solitons greyen. These solitons have been first described in Ref. [31] and arise due to nonlinearities. The presence of a local minimum at a finite value of the density in E/N plays a crucial role here. Due to their uncanny features, described at length later in this section, we call them anomalous. We have confirmed that these solutions maintain their form and phase profile during

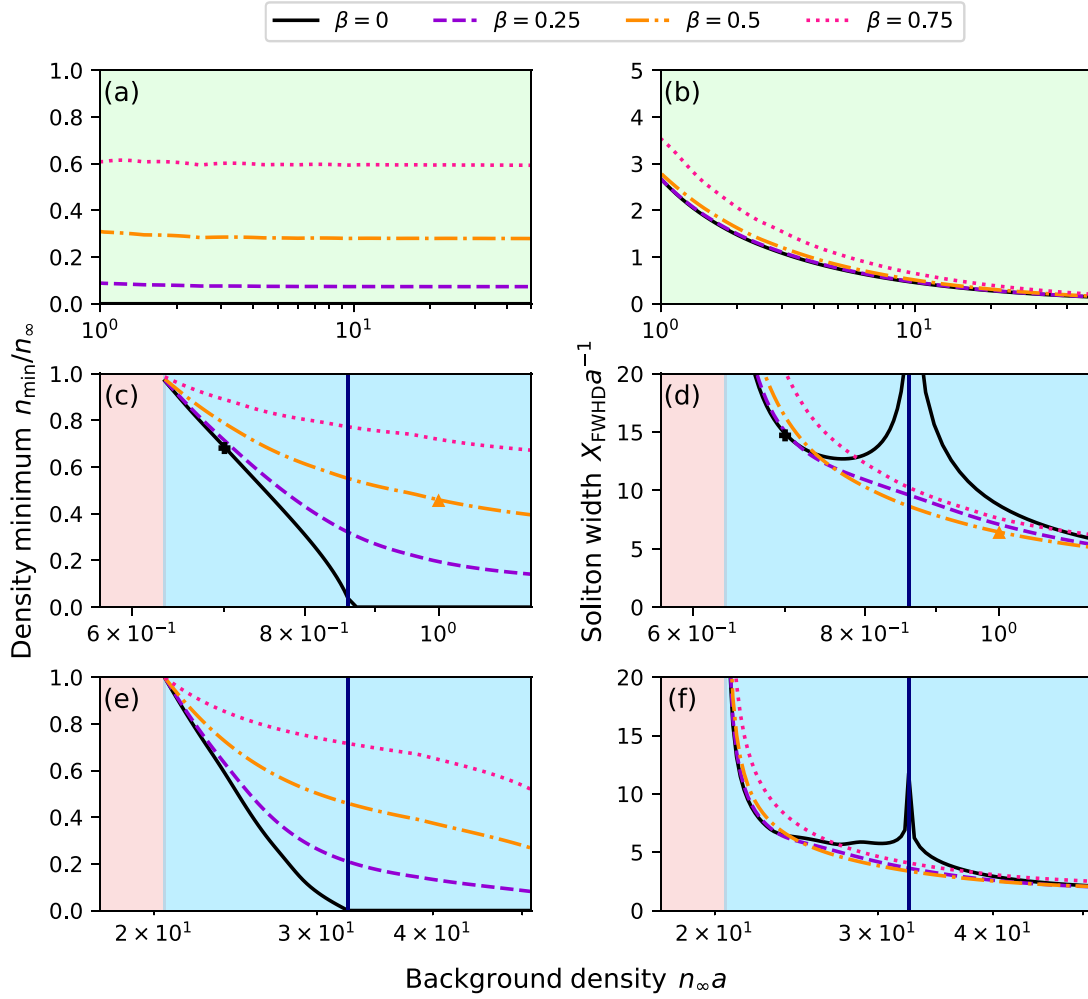


FIG. 6. Minimum densities n_{\min} [(a),(c),(e)] and full widths at half depth X_{FWHDA} [(b),(d),(f)] of dark solitons for different relative velocities of the soliton β and interaction ratios $g_{\uparrow\downarrow}/g = 0.4$ [(a),(b)], 0.55 [(c),(d)], and 0.9 [(e),(f)]. Green shading corresponds to gaseous phase, blue to the liquid one and red to the unstable regime (cf. Fig. 2). The vertical blue line marks the equilibrium density value. The black plus-shaped markers in (c) and (d) correspond to the soliton shown in Figs. 7(a) and 7(c) and the orange triangles to the soliton from Figs. 7(b) and 7(d).

real time propagation in the presence of low-amplitude noise, confirming their stability.

The solitonic solution [as shown in Figs. 6(d) and 6(f)] widens in two places. Once when $n_{\infty} \rightarrow n_{\text{eq}}$, both in the standard ($n_{\infty} \rightarrow n_{\text{eq}}^+$) and anomalous ($n_{\infty} \rightarrow n_{\text{eq}}^-$) regimes and another time, while approaching the instability region. The most interesting regime to realize experimentally is in the vicinity of n_{eq} . The solitonic solutions there are both wide and deep, which may be easier to detect with *in situ* imaging procedure.

Grey solitons also become shallower with decreasing density n_{∞} . For $\beta > 0$, it is a gradual change though [cf. Figs. 6(c) and 6(e)]. Another difference is that the grey soliton width does not diverge when $n_{\infty} \rightarrow n_{\text{eq}}$, it does so in the vicinity of the unstable regime only [cf. Figs. 6(d) and 6(f)].

In Figs. 7(a) and 7(c) we show the density and phase profiles of motionless solitons evaluated at a ratio $g_{\uparrow\downarrow}/g = 0.6$ and density fulfilling the inequality $n_{\text{ins}} < n_{\infty} < n_{\text{eq}}$. This soliton has a nonzero density minimum, normally characteristic to moving (grey) solitons. Moreover, there is no π -phase jump, as in a standard motionless (black) solitonic solution in the GPE [49].

On the other hand, when $n_{\infty} > n_{\text{eq}}$, no anomalous solutions are found. In this regime, solitons are similar to standard dark solitons. We show density and phase profiles of a grey soliton moving with velocity $\beta = 0.5$ in Figs. 7(b) and 7(d).

To gain some insight into the large width of the solitons when $n_{\infty} \approx n_{\text{eq}}$, we shall consider again a homogeneous gas. We can define the pressure as $P = -dE/dL$. Above the value of n_{eq} , the pressure is positive. But below the equilibrium density, the pressure becomes negative. Thus, if we break

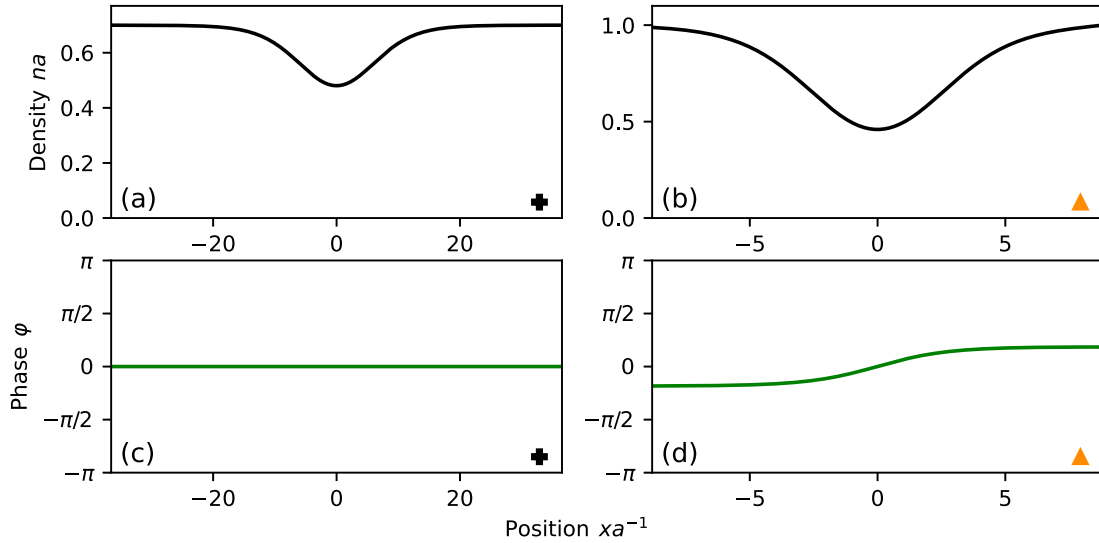


FIG. 7. Motionless anomalous soliton density (a) and phase (c) profiles. Standard grey soliton density (b) and phase (d). The grey soliton is moving with relative velocity $\beta = 0.5$. Both solitons were evaluated at a ratio $g_{\uparrow\downarrow}/g = 0.55$ using the mLLGPE. Black plus-shaped and orange triangle markers show a correspondence between this figure and Figs. 6(c) and 6(d)

the symmetry in the system by rarefying the density in one point, the pressure will make the gas on the sides of the defect contract and form a structure with wide density depletion.

V. SUMMARY

To conclude, we have presented a QMC-based single-orbital density functional theory for a two-component bosonic mixture in one dimension, which we call the mLLGP model. From construction, our approach provides a quantitative agreement in terms of the energy and chemical potential of a homogeneous state with the *ab initio* QMC model from Ref. [19].

We benchmark our equation by comparing the results with the original QMC data. This comparison shows the mLLGP can quantitatively predict the bulk density of a quantum droplet and the monopole mode frequency in the limit of a large number of particles in the droplet with a characteristic $\omega \propto N^{-1}$ dependency. It also predicts a correct phase diagram of Bose-Bose mixtures, including a transition from liquid to gas, not predicted by the mean-field model supplemented with the LHY correction. Since our approach relies on fitting an energy functional to QMC data, it is limited by the range of underpinning QMC data, which is only currently available in the literature for densities close to the equilibrium density and for specific interaction ratios. Should QMC data become available over a larger parameter space of density and interaction ratio, the model could be refined with an improved energy functional.

Our paper is limited to the specific case where the intraspecies interactions are equal, $g_{\downarrow\downarrow} = g_{\uparrow\uparrow}$, which leads to the density profile of each component being equal to each other, $n_{\downarrow}(x) = n_{\uparrow}(x)$. In principle the approach could be extended to the more general case where $g_{\downarrow\downarrow} \neq$

$g_{\uparrow\uparrow}$ and $n_{\downarrow}(x) \neq n_{\uparrow}(x)$, however this would require QMC data over a wider parameter space. Given the computational intensity of QMC calculations, this is not tractable at the present time but may become possible in the future.

Lastly, we provide a brief study of solitonic solutions of the mLLGP equation, where we find ultrawide solitonic solutions. Moreover, anomalous motionless solitons were found as well. These solitons are characterized by the lack of a π jump in the phase and a nonzero density minimum.

The presence of such wide solitons can be an advantage for experimenters who would like to perform an *in situ* imaging of these objects. As far as we are concerned, the measurement of the monopole mode frequency for small droplets may be helpful to verify the validity of the mLLGP equation too. It would demand creating droplets consisting of very few particles, though, making such an experiment tougher to design and conduct. An avenue for further work would be to use the mLLGP model to study the dynamical properties of dark solitons in 1D Bose-Bose mixtures, particularly the anomalous solitons, including their collisions, stability and experimental generation.

The supporting data for this paper are available in the Supplemental Material [57].

ACKNOWLEDGMENTS

The authors acknowledge discussions with Dr Thomas Billam and Mr Thomas Flynn (Newcastle University). L.P. and N.G.P. acknowledge support from the UK Engineering and Physical Sciences Research Council (Grant No. EP/T015241/1). J.K. and K.P. acknowledge support from the (Polish) National Science Center Grant No. 2019/34/E/ST2/00289. Center for Theoretical Physics of the

Polish Academy of Sciences is a member of the National Laboratory of Atomic, Molecular and Optical Physics (KL FAMO).

L.P. prepared the energy density functional, J.K. conducted the numerical simulations. K.P. and N.G.P. conceptualized and supervised the research. J.K. wrote the manuscript with input of all authors.

APPENDIX A: DETAILS OF THE NUMERICAL PROCEDURES

1. Energy density functional

In order to find the energy density functional $\mathcal{E}_{\text{mLLGP}}[n; g, g_{\uparrow\downarrow}]$, we use the QMC data from Ref. [18], namely the energy per particle $E/N \equiv e(n; g, g_{\uparrow\downarrow})$ for the following interaction ratios $g_{\uparrow\downarrow}/g = \{0.3, 0.4, 0.45, 0.5, 0.6, 0.65, 0.7, 0.75, 0.8, 0.9\}$. The data are extrapolated in the low density limit with a function $f_L(n) = -1 + c_1 n^{3/2} + c_2 n^{5/2} + c_3 n^3$ and $f_H(n) = c_4 n^{1/2} + c_5 n + c_6 n^{3/2}$ [in units of $\varepsilon_b/2$], where c_i for $i = \{1, 2, \dots, 6\}$ are constants to be fitted. Then, we perform a spline interpolation of the augmented QMC data and perform a linear interpolation between the ratios. The energy density functional is connected to the energy per particle function $e(n; g, g_{\uparrow\downarrow})$ via a simple relation: $\mathcal{E}_{\text{mLLGP}}[n; g, g_{\uparrow\downarrow}] = ne(n; g, g_{\uparrow\downarrow})$.

2. Imaginary and real time evolution details

The mLLGP equation is a complex, nonlinear partial differential equation. The orbital $\psi(x)$ is discretized on a spatial mesh with N_x fixed points and lattice spacing $DX = L/N_x$, where L is the box size. We assume periodic boundary conditions, i.e., $\psi(-L/2) = \psi(L/2)$. The real-time evolution is done with the use of the split-step numerical method. The evolution with the kinetic term is done in the momentum domain, whereas the contact interaction term is calculated in the spatial domain. No external potential is used. The quantum droplet is obtained with the use of imaginary time evolution, where we use Wick rotation $t \rightarrow -i\tau$ to find the ground state. The program written

in C++ implementing the algorithm above is publicly available [56].

The program uses the W-DATA format dedicated to store data in numerical experiments with ultracold Bose and Fermi gases. The W-DATA project is a part of the W-SLDA toolkit [58].

When measuring the monopole mode frequency ω , we perturb the ground state by multiplying it by a factor $\exp(-i\epsilon x^2/a^2)$, where ϵ is of the order of 10^{-6} in our simulations. Afterwards, we fit the droplet width $\sqrt{\langle x^2 \rangle - \langle x \rangle^2}(t)$ to a function $f(t) = A + B \cos(\omega t + C)$, where A , B , C , and ω are fitted constants.

In order to estimate the uncertainty due to the quality of the energy density functional, we repeat the simulations with alternative spline representations of $\mathcal{E}_{\text{mLLGP}}$. Namely we reduce the number of points we use to extrapolate the data with $f_L(n)$ and redo the whole procedure with a slightly different spline.

APPENDIX B: DARK SOLITONS IN THE MLLGP EQUATION

To find the dark solitonic solutions of the mLLGP equation, we go to the thermodynamic limit, i.e., $L \rightarrow \infty, N \rightarrow \infty$ and $N/L = \text{const}$. We plug the following Ansatz for a wave traveling through the system at a constant velocity v_s , i.e., $\psi(x, t) = \tilde{\psi}(\zeta)$, where $\zeta = x - v_s t$ is a comoving coordinate, to Eq. (3) and obtain

$$\mu_s \tilde{\psi} - imv_s \tilde{\psi}' = -\frac{\hbar^2}{2m} \tilde{\psi}'' + \mu_{\text{mLLGP}}[|\tilde{\psi}|^2; g, g_{\uparrow\downarrow}] \tilde{\psi}. \quad (\text{B1})$$

If we assume that far away from the soliton, the density and phase are constant $\lim_{\zeta \rightarrow \infty} |\tilde{\psi}(\zeta)|^2 = n_\infty$ and $\lim_{\zeta \rightarrow \infty} \arg \tilde{\psi}(\zeta) = \varphi_\infty$, we can find the value of the chemical potential $\mu_s = \mu_{\text{mLLGP}}[n_\infty; g, g_{\uparrow\downarrow}]$. Then, we rewrite the equation above in a discretized form, assuming that we start from two points far away from the soliton $\tilde{\psi}_0 = (1 - \epsilon_1)\sqrt{n_\infty}$ and $\tilde{\psi}_1 = (1 - \epsilon_2)\sqrt{n_\infty}$ with $\epsilon_{1,2} \ll 1$ (typically $\sim 10^{-4}$) and $\epsilon_1 > \epsilon_2$.

We have also checked that solitonic solutions are dynamically stable.

-
- [1] A. Bulgac, Dilute Quantum Droplets, *Phys. Rev. Lett.* **89**, 050402 (2002).
- [2] D. S. Petrov, Three-Body Interacting Bosons in Free Space, *Phys. Rev. Lett.* **112**, 103201 (2014).
- [3] D. S. Petrov, Quantum Mechanical Stabilization of a Collapsing Bose-Bose Mixture, *Phys. Rev. Lett.* **115**, 155302 (2015).
- [4] T. D. Lee, K. Huang, and C. N. Yang, Eigenvalues and eigenfunctions of a Bose system of hard spheres and its low-temperature properties, *Phys. Rev.* **106**, 1135 (1957).
- [5] T. D. Lee and C. N. Yang, Many-body problem in quantum mechanics and quantum statistical mechanics, *Phys. Rev.* **105**, 1119 (1957).
- [6] G. E. Astrakharchik and B. A. Malomed, Dynamics of one-dimensional quantum droplets, *Phys. Rev. A* **98**, 013631 (2018).
- [7] D. S. Petrov and G. E. Astrakharchik, Ultradilute Low-Dimensional Liquids, *Phys. Rev. Lett.* **117**, 100401 (2016).
- [8] M. Tylutki, G. E. Astrakharchik, B. A. Malomed, and D. S. Petrov, Collective excitations of a one-dimensional quantum droplet, *Phys. Rev. A* **101**, 051601(R) (2020).
- [9] T. A. Flynn, L. Parisi, T. P. Billam, and N. G. Parker, Quantum droplets in imbalanced atomic mixtures [arXiv:2209.04318](https://arxiv.org/abs/2209.04318).
- [10] C. R. Cabrera, L. Tanzi, J. Sanz, B. Naylor, P. Thomas, P. Cheiney, and L. Tarruell, Quantum liquid droplets in a mixture of Bose-Einstein condensates, *Science* **359**, 301 (2018).
- [11] P. Cheiney, C. R. Cabrera, J. Sanz, B. Naylor, L. Tanzi, and L. Tarruell, Bright Soliton to Quantum Droplet Transition in a Mixture of Bose-Einstein Condensates, *Phys. Rev. Lett.* **120**, 135301 (2018).
- [12] G. Semeghini, G. Ferioli, L. Masi, C. Mazzinghi, L. Wolswijk, F. Minardi, M. Modugno, G. Modugno, M. Inguscio,

- and M. Fattori, Self-Bound Quantum Droplets of Atomic Mixtures in Free Space, *Phys. Rev. Lett.* **120**, 235301 (2018).
- [13] G. Ferioli, G. Semeghini, L. Masi, G. Giusti, G. Modugno, M. Inguscio, A. Galletti, A. Recati, and M. Fattori, Collisions of Self-Bound Quantum Droplets, *Phys. Rev. Lett.* **122**, 090401 (2019).
- [14] C. D'Errico, A. Burchianti, M. Prevedelli, L. Salasnich, F. Ancilotto, M. Modugno, F. Minardi, and C. Fort, Observation of quantum droplets in a heteronuclear bosonic mixture, *Phys. Rev. Res.* **1**, 033155 (2019).
- [15] R. N. Bisset, L. A. Peña Ardila, and L. Santos, Quantum Droplets of Dipolar Mixtures, *Phys. Rev. Lett.* **126**, 025301 (2021).
- [16] A. Trautmann, P. Ilzhöfer, G. Durastante, C. Politi, M. Sohmen, M. J. Mark, and F. Ferlaino, Dipolar Quantum Mixtures of Erbium and Dysprosium Atoms, *Phys. Rev. Lett.* **121**, 213601 (2018).
- [17] G. Durastante, C. Politi, M. Sohmen, P. Ilzhöfer, M. J. Mark, M. A. Norcia, and F. Ferlaino, Feshbach resonances in an erbium-dysprosium dipolar mixture, *Phys. Rev. A* **102**, 033330 (2020).
- [18] L. Parisi, G. E. Astrakharchik, and S. Giorgini, Liquid State of One-Dimensional Bose Mixtures: A Quantum Monte Carlo Study, *Phys. Rev. Lett.* **122**, 105302 (2019).
- [19] L. Parisi and S. Giorgini, Quantum droplets in one-dimensional Bose mixtures: A quantum Monte Carlo study, *Phys. Rev. A* **102**, 023318 (2020).
- [20] N. D. Mermin and H. Wagner, Absence of Ferromagnetism or Antiferromagnetism in One- or Two-Dimensional Isotropic Heisenberg Models, *Phys. Rev. Lett.* **17**, 1133 (1966).
- [21] P. C. Hohenberg, Existence of long-range order in one and two dimensions, *Phys. Rev.* **158**, 383 (1967).
- [22] E. H. Lieb and W. Liniger, Exact analysis of an interacting Bose gas. I. The general solution and the ground state, *Phys. Rev.* **130**, 1605 (1963).
- [23] E. H. Lieb, Exact analysis of an interacting Bose gas. II. The excitation spectrum, *Phys. Rev.* **130**, 1616 (1963).
- [24] V. Dunjko, V. Lorent, and M. Olshanii, Bosons in Cigar-Shaped Traps: Thomas-Fermi Regime, Tonks-Girardeau Regime, and In Between, *Phys. Rev. Lett.* **86**, 5413 (2001).
- [25] P. Öhberg and L. Santos, Dynamical Transition from a Quasi-One-Dimensional Bose-Einstein Condensate to a Tonks-Girardeau Gas, *Phys. Rev. Lett.* **89**, 240402 (2002).
- [26] Y. E. Kim and A. L. Zubarev, Density-functional theory of bosons in a trap, *Phys. Rev. A* **67**, 015602 (2003).
- [27] B. Damski, Formation of shock waves in a Bose-Einstein condensate, *Phys. Rev. A* **69**, 043610 (2004).
- [28] B. Damski, Shock waves in a one-dimensional Bose gas: From a Bose-Einstein condensate to a Tonks gas, *Phys. Rev. A* **73**, 043601 (2006).
- [29] S. Peotta and M. DiVentra, Quantum shock waves and population inversion in collisions of ultracold atomic clouds, *Phys. Rev. A* **89**, 013621 (2014).
- [30] S. Choi, V. Dunjko, Z. D. Zhang, and M. Olshanii, Monopole Excitations of a Harmonically Trapped One-Dimensional Bose Gas from the Ideal Gas to the Tonks-Girardeau Regime, *Phys. Rev. Lett.* **115**, 115302 (2015).
- [31] J. Kopyciński, M. Łebek, W. Górecki, and K. Pawłowski, Ultrawide Dark Solitons and Droplet-Soliton Coexistence in a Dipolar Bose Gas with Strong Contact Interactions, *Phys. Rev. Lett.* **130**, 043401 (2023).
- [32] R. Oldziejewski, W. Górecki, K. Pawłowski, and K. Rzażewski, Strongly Correlated Quantum Droplets in Quasi-1D Dipolar Bose Gas, *Phys. Rev. Lett.* **124**, 090401 (2020).
- [33] S. De Palo, E. Orignac, M. L. Chiofalo, and R. Citro, Polarization angle dependence of the breathing mode in confined one-dimensional dipolar bosons, *Phys. Rev. B* **103**, 115109 (2021).
- [34] J. Kopyciński, M. Łebek, M. Marciniak, R. Oldziejewski, W. Górecki, and K. Pawłowski, Beyond Gross-Pitaevskii equation for 1D gas: Quasiparticles and solitons, *SciPost Phys.* **12**, 023 (2022).
- [35] S. De Palo, E. Orignac, and R. Citro, Formation and fragmentation of quantum droplets in a quasi-one-dimensional dipolar Bose gas, *Phys. Rev. B* **106**, 014503 (2022).
- [36] M. Łebek, J. Kopyciński, W. Górecki, R. Oldziejewski, and K. Pawłowski, Elementary excitations of dipolar Tonks-Girardeau droplets, [arXiv:2209.01887](https://arxiv.org/abs/2209.01887).
- [37] V. Cikojević, L. V. Markić, M. Pi, M. Barranco, and J. Boronat, Towards a quantum Monte Carlo-based density functional including finite-range effects: Excitation modes of a ^{39}K quantum droplet, *Phys. Rev. A* **102**, 033335 (2020).
- [38] H. Hu, J. Wang, and X.-J. Liu, Microscopic pairing theory of a binary Bose mixture with interspecies attractions: Bosonic BEC-BCS crossover and ultradilute low-dimensional quantum droplets, *Phys. Rev. A* **102**, 043301 (2020).
- [39] M. Ota and G. E. Astrakharchik, Beyond Lee-Huang-Yang description of self-bound Bose mixtures, *SciPost Phys.* **9**, 020 (2020).
- [40] C. Fiolhais, F. Nogueira, and M. Marques (eds.), *A Primer in Density Functional Theory*, 2003rd ed., Lecture Notes in Physics (Springer, Berlin, 2003).
- [41] A. Bulgac, M. M. Forbes, and P. Magierski, The unitary Fermi gas: From Monte Carlo to density functionals, in *The BCS-BEC Crossover and the Unitary Fermi Gas*, edited by W. Zwerger (Springer, Berlin, 2012), pp. 305–373.
- [42] A. Bulgac and S. Yoon, Large Amplitude Dynamics of the Pairing Correlations in a Unitary Fermi Gas, *Phys. Rev. Lett.* **102**, 085302 (2009).
- [43] G. Włazłowski, K. Sekizawa, M. Marchwiany, and P. Magierski, Suppressed Solitonic Cascade in Spin-Imbalanced Superfluid Fermi Gas, *Phys. Rev. Lett.* **120**, 253002 (2018).
- [44] P. Magierski, B. Tüzemen, and G. Włazłowski, Spin-polarized droplets in the unitary Fermi gas, *Phys. Rev. A* **100**, 033613 (2019).
- [45] M. Tylutki and G. Włazłowski, Universal aspects of vortex reconnections across the BCS-BEC crossover, *Phys. Rev. A* **103**, L051302 (2021).
- [46] P. Magierski, G. Włazłowski, A. Makowski, and K. Kobuszewski, Spin-polarized vortices with reversed circulation, *Phys. Rev. A* **106**, 033322 (2022).
- [47] M. W. Zwierlein, A. Schirotzek, C. H. Schunck, and W. Ketterle, Fermionic superfluidity with imbalanced spin populations, *Science* **311**, 492 (2006).
- [48] M. J. H. Ku, B. Mukherjee, T. Yefsah, and M. W. Zwierlein, Cascade of Solitonic Excitations in a Superfluid Fermi gas: From Planar Solitons to Vortex Rings and Lines, *Phys. Rev. Lett.* **116**, 045304 (2016).

- [49] A. D. Jackson, G. M. Kavoulakis, and C. J. Pethick, Solitary waves in clouds of Bose-Einstein condensed atoms, *Phys. Rev. A* **58**, 2417 (1998).
- [50] I. Morera, A. M. Mateo, A. Polls, and B. Juliá-Díaz, Dark-dark-soliton dynamics in two density-coupled Bose-Einstein condensates, *Phys. Rev. A* **97**, 043621 (2018).
- [51] P. Kevrekidis and D. Frantzeskakis, Solitons in coupled nonlinear Schrödinger models: A survey of recent developments, *Rev. Phys.* **1**, 140 (2016).
- [52] M. Edmonds, Dark quantum droplets in beyond-mean-field Bose-Einstein condensate mixtures, [arXiv:2209.00790](https://arxiv.org/abs/2209.00790).
- [53] Just as the original Lieb-Liniger Gross-Pitaevskii equation gives a quantitative agreement with the Lieb-Liniger model—the homogeneous system energy, chemical potential and speed of sound are the same from construction.
- [54] G. De Rosi, G. E. Astrakharchik, and P. Massignan, Thermal instability, evaporation, and thermodynamics of one-dimensional liquids in weakly interacting Bose-Bose mixtures, *Phys. Rev. A* **103**, 043316 (2021).
- [55] It is a benchmark of a correctly prepared fit.
- [56] <https://gitlab.com/jakkop/mudge/-/releases/v07Mar2023>.
- [57] See Supplemental Material at <http://link.aps.org/supplemental/10.1103/PhysRevResearch.5.023050> for the numerical data necessary to reproduce figures, including QMC data and the results of simulations with the MUDGE toolkit.
- [58] W-SLDA Toolkit, <https://wsllda.fizyka.pw.edu.pl/>.

4. [J. Kopyciński *et al.*, Propagation properties and stability of dark solitons in weakly interacting Bose–Bose droplets, *J. Phys. B: At. Mol. Opt. Phys.* **57**, 035302 (2024)]

Propagation properties and stability of dark solitons in weakly interacting Bose–Bose droplets

Jakub Kopyciński^{1,*} , Buğra Tüzemen¹ , Wojciech Górecki² , Krzysztof Pawłowski¹ 
and Maciej Łebek^{1,2} 

¹ Center for Theoretical Physics, Polish Academy of Sciences, Al. Lotników 32/46, 02-668 Warsaw, Poland

² Faculty of Physics, University of Warsaw, Pasteura 5, 02-093 Warsaw, Poland

E-mail: jkopycinski@cft.edu.pl

Received 11 October 2023, revised 7 December 2023

Accepted for publication 1 February 2024

Published 12 February 2024



CrossMark

Abstract

We investigate dark solitons in two-component Bose systems with competing interactions in one dimension. Such a system hosts a liquid phase stabilized by the beyond-mean field corrections. Using the generalized Gross–Pitaevskii equation, we reveal the presence of two families of solitonic solutions. The solitons in both of them can be engineered to be arbitrarily wide. One family of solutions, however, has an anomalous dispersion relation, and our analyses show one of its branches is unstable. We find a critical velocity that demarcates the stable from unstable solutions. Nonetheless, gray anomalous solitons can exist inside quantum droplets and can be treated as solitonic excitations thereof.

Keywords: quantum droplets, dark solitons, Bose–Bose mixtures

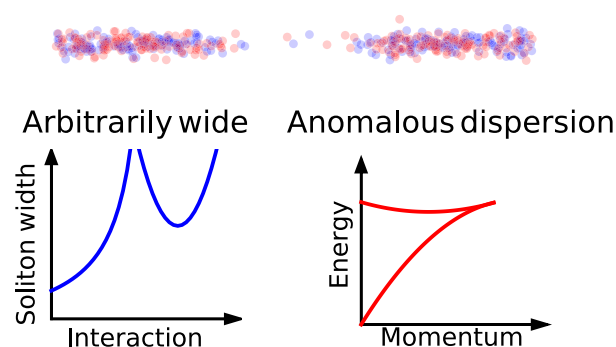


Figure 1. Graphical abstract: we look into dark solitons in two-component Bose gases (species colored red and blue) with a beyond mean-field approach. Our studies show that dark solitons can be arbitrarily wide in such systems. Moreover, we find a class of solutions with an anomalous dispersion relation and perform a stability analysis of these solutions. We predict the moving solitons can exist in the quantum droplets as their excitations.

* Author to whom any correspondence should be addressed.



Original Content from this work may be used under the terms of the [Creative Commons Attribution 4.0 licence](https://creativecommons.org/licenses/by/4.0/). Any further distribution of this work must maintain attribution to the author(s) and the title of the work, journal citation and DOI.

1. Introduction

Ultracold atomic systems with competing interactions have been the subject of extensive theoretical research powered up by various experiments. The addition of corrections for quantum fluctuations [1] to the mean-field theory led to the correct description of the emergence of self-bound objects called quantum droplets in two-component systems [2–6]. A quite unexpected appearance of droplets in dipolar gases [7–9] also became explicable by this effect. All in all, the mean-field approach tumbled down in these two regimes, and the use of its version with Lee-Huang-Yang (LHY) corrections [10, 11]—known as the generalized Gross–Pitaevskii equation (GGP), became crucial.

The GGP [12] proves its usefulness in the weakly-interacting regime [13] of Bose–Bose mixtures. It has been employed to study the properties of quantum droplets [14, 15], including elementary excitations [16] like breathing modes [17], even in the case of unequal number of bosons of each species [18, 19].

Besides quantum droplets, bosonic mixtures may also uncover bright solitons [20], mixed bubbles [21] near the miscible–immiscible threshold, experimentally seen dark–bright solitons [22, 23], also predicted for highly magnetic species [24].

There is a variety of already known dark-soliton-like solutions of the GGP in the miscible regime, such as kink-type solitons [25], dark quantum droplets [26] and standard dark solitons [27].

Let us briefly describe the most important properties of these excitations. The kink-type soliton density profile has two different asymptotic values with a rapidly varying region located at its origin. In this case, the phase of the wave function remains constant.

Dark quantum droplets, on the other hand, have the shape of an inverted quantum droplet. Their phase pattern is non-trivial, with $-\pi/2$ phase on one side of the depletion and $\pi/2$ on the other with an intermediate step in the wide depleted density region of phase equal to 0. All three regions are smoothly connected.

Standard dark solitons can be divided into fully and partially depleted—black and gray correspondingly. Black solitons have a π -jump in their phase. The phase of gray solitons changes smoothly, and the total phase difference is smaller than π . All in all, they share the features of dark solitons in single-component Bose gases [28, 29].

Yet, there is still another type of solitons, so far found only in a beyond-LHY description called LLGPE of 1D Bose–Bose mixtures [30] and dipolar Bose gases [31], but had been retrieved as the solutions of some differential equations [32] and called ‘solitonlike bubbles’ there. These anomalous solitons can be arbitrarily wide, are never fully depleted, and have a constant phase profile. Moreover, they have a peculiar dispersion relation with an additional sub-branch and a cusp. As they were not found in [26], one may think they appear due to beyond-LHY contributions to the method.

In this article, we derive the solitonic solution of the GGP and reveal the presence of anomalous solitons. We also check the stability of the solutions and show that dark solitons can exist inside quantum droplets (see figure 1).

2. Framework

We look into a weakly interacting two-component gas of \tilde{N} bosons in 1D. The intraspecies interaction is repulsive, whereas the intercomponent ones are attractive. Their masses are the same, i.e. $m_\uparrow = m_\downarrow = m$ with $\sigma = \{\uparrow, \downarrow\}$ denoting the component. The energy density functional for this system is given by [12]:

$$\begin{aligned} \mathcal{E}_{\text{int}}[\tilde{\rho}_\uparrow, \tilde{\rho}_\downarrow] = & \frac{(\sqrt{g_{\uparrow\uparrow}}\tilde{\rho}_\uparrow - \sqrt{g_{\downarrow\downarrow}}\tilde{\rho}_\downarrow)^2}{2} + (g_{\uparrow\downarrow}\sqrt{g_{\uparrow\uparrow}g_{\downarrow\downarrow}} + g_{\uparrow\uparrow}g_{\downarrow\downarrow}) \\ & \times \frac{(\sqrt{g_{\uparrow\uparrow}}\tilde{\rho}_\uparrow + \sqrt{g_{\downarrow\downarrow}}\tilde{\rho}_\downarrow)^2}{(g_{\uparrow\uparrow} + g_{\downarrow\downarrow})^2} - \frac{2\sqrt{m}}{3\pi\hbar} (g_{\uparrow\downarrow}\tilde{\rho}_\downarrow + g_{\downarrow\downarrow}\tilde{\rho}_\downarrow)^{3/2}, \end{aligned} \quad (1)$$

where $\tilde{\rho}_\sigma$ is the σ -component density and $g_{\sigma\sigma'}$ for $\sigma = \sigma'$ is the intracomponent interaction strength and the intercomponent interaction strength otherwise, i.e. when $\sigma \neq \sigma'$.

In the miscible system without any external confinement, the densities are tied up via the condition $\tilde{\rho}_\uparrow/\tilde{\rho}_\downarrow = \sqrt{g_{\downarrow\downarrow}/g_{\uparrow\uparrow}}$ [1]. This leads to a simplification of the energy density functional \mathcal{E}_{int} . An approach based on the local density approximation enables us to use \mathcal{E}_{int} and write the GGP equation for the wave function $\Phi(\tilde{x}, \tilde{t})$ as follows [12]:

$$\begin{aligned} i\hbar\partial_{\tilde{t}}\tilde{\Phi} = & -\frac{\hbar^2}{2m}\partial_{\tilde{x}}^2\tilde{\Phi} + \frac{2\sqrt{g_{\uparrow\uparrow}g_{\downarrow\downarrow}}\delta g}{(\sqrt{g_{\uparrow\uparrow}} + \sqrt{g_{\downarrow\downarrow}})^2}|\tilde{\Phi}|^2\tilde{\Phi} \\ & - \frac{\sqrt{m}}{\pi\hbar} (g_{\uparrow\uparrow}g_{\downarrow\downarrow})^{3/4}|\tilde{\Phi}|\tilde{\Phi}, \end{aligned} \quad (2)$$

where $\tilde{\Phi}(\tilde{x}, \tilde{t})$ is related to single-component wave functions $\tilde{\Phi}_\sigma$ via $\tilde{\Phi}_\sigma(\tilde{x}, \tilde{t}) = g_{\sigma\sigma}^{1/4}\tilde{\Phi}(\tilde{x}, \tilde{t})\sqrt{\sqrt{g_{\uparrow\uparrow}} + \sqrt{g_{\downarrow\downarrow}}}$, where $\tilde{\uparrow} = \downarrow$ and $\tilde{\downarrow} = \uparrow$. Moreover, we have defined $\delta g = g_{\uparrow\downarrow} + \sqrt{g_{\uparrow\uparrow}g_{\downarrow\downarrow}}$, which is assumed to be positive throughout the work.

We now introduce the units of length $x_0 \equiv \frac{\pi\hbar^2}{m}\frac{\sqrt{2\delta g}}{\sqrt{g_{\uparrow\uparrow}g_{\downarrow\downarrow}}(\sqrt{g_{\uparrow\uparrow}} + \sqrt{g_{\downarrow\downarrow}})}$, time $t_0 = \hbar/mx_0^2$, energy $E_0 = \hbar/t_0$ and normalization factor of the wave function $\Phi_0 = \frac{(\sqrt{g_{\uparrow\uparrow}} + \sqrt{g_{\downarrow\downarrow}})^{3/2}}{\sqrt{\pi x_0 (2\delta g)^{3/4}}}$ [16]. With $\tilde{t} = t_0 t$, $\tilde{x} = x_0 x$, $\tilde{\Phi} = \Phi_0 \Phi$ and $\tilde{E} = E_0 E$, we can rewrite (2) in the dimensionless form [14]:

$$i\partial_t\Phi(x, t) = -\frac{1}{2}\partial_x^2\Phi(x, t) + |\Phi(x, t)|^2\Phi(x, t) - |\Phi(x, t)|\Phi(x, t). \quad (3)$$

The normalization condition of the wave function Φ is related to the real number of atom in the system \tilde{N} via $N = \int_{-L/2}^{L/2} |\Phi|^2 dx = \tilde{N}\pi(2\delta g)^{3/2}/(\sqrt{g_{\uparrow\uparrow}} + \sqrt{g_{\downarrow\downarrow}})^3$ [16], assuming a box of size L with periodic boundary conditions.

3. Results

3.1. Speed of sound and equilibrium density

The stable and unstable liquid phases in Bose–Bose mixtures are demarcated by the point where the speed of sound becomes imaginary [13]. We use the following time-dependent ansatz to linearize (3):

$$\Phi(x, t) = [\Phi_0 + \delta\Phi(x, t)]e^{-i\mu_0 t}, \quad (4)$$

where $\Phi_0 = \sqrt{N/L}$, $\mu_0 = \frac{N}{L} - \sqrt{\frac{N}{L}}$ is the chemical potential corresponding to the constant density profile and $\delta\Phi$ is a small perturbation. Then, with $\omega_\rho = \rho_0 - \frac{1}{2}\sqrt{\rho_0}$, we obtain a set of Bogoliubov–de Gennes (BdG) equations

$$i\partial_t \begin{pmatrix} \delta\Phi \\ \delta\Phi^* \end{pmatrix} = \begin{pmatrix} -\partial_x^2/2 + \omega_\rho & \omega_\rho \\ -\omega_\rho & -(\partial_x^2/2 + \omega_\rho) \end{pmatrix} \begin{pmatrix} \delta\Phi \\ \delta\Phi^* \end{pmatrix}. \quad (5)$$

Assuming that $\delta\Phi = ue^{(ikx - i\omega t)} + v^*e^{-(ikx - i\omega t)}$ [33], we diagonalize the Hamiltonian matrix and obtain the following eigenfrequencies

$$\omega = \sqrt{\frac{k^4}{4} + k^2 \left(\rho_0 - \frac{1}{2}\sqrt{\rho_0} \right)}. \quad (6)$$

The spectrum is linear in the limit of low momenta, well approximated by the phonon dispersion law $\omega = ck$, where

$$c = \sqrt{\rho_0 - \frac{1}{2}\sqrt{\rho_0}} \quad (7)$$

is the speed of sound. On the other hand, when $k \gg 1$, (6) reduces to the free particle spectrum $\omega = k^2/2$.

From (7), we see the speed of sound is imaginary when $\rho_0 < 1/4$. It indicates that the stable-to-unstable liquid transition happens when $\rho_0 = 1/4 \equiv \rho_{\text{ins}}$, and this is a phonon instability.

The liquid phase is characterized by the presence of a minimum in the energy per particle function [13, 14]

$$E/N = \frac{1}{2}\rho_0 - \frac{2}{3}\rho_0^{1/2}. \quad (8)$$

This minimum occurs when $\rho_0 = 4/9$, and we will further refer to this value as the equilibrium density ρ_{eq} .

Assuming that $N \gg 1$ and without the constraint on the uniformity of the system, we can have two cases. When $N/L < \rho_{\text{eq}}$, the system prefers to form a quantum droplet with a bulk density equal to ρ_{eq} . In such a case, the surface energy needed to form the droplet density profile is small in comparison to the bulk energy and, therefore, negligible. Otherwise, when $N/L > \rho_{\text{eq}}$, the system prefers to be uniform.

3.2. Solitonic solutions

We now look for a solution of a dispersionless wave moving with velocity v through an infinite constant background density. Such an object is represented by the following wave function:

$$\Phi(x, t) \equiv \psi(x - vt) \exp(-i\mu t), \quad (9a)$$

where

$$\psi(\zeta) = \sqrt{\rho(\zeta)} \exp[i\phi(\zeta)] \quad (9b)$$

and ζ is the comoving coordinate $\zeta = x - vt$.

One can insert (9a) to the GGP equation (3). Then, we split a single complex non-linear differential equation into two—the real part

$$\mu\sqrt{\rho} - v\phi'\sqrt{\rho} + \frac{1}{2}(\sqrt{\rho})'' - \frac{1}{2}(\phi')^2\sqrt{\rho} - \sqrt{\rho}^3 + \sqrt{\rho}^2 = 0 \quad (10a)$$

and the imaginary one:

$$\phi''\sqrt{\rho}^2 + 2\phi'(\sqrt{\rho})'\sqrt{\rho} - 2v(\sqrt{\rho})'\sqrt{\rho} = 0, \quad (10b)$$

where $(\cdot)' := \frac{d}{d\zeta}(\cdot)$.

Assuming that the density and phase are constant far away from the soliton, i.e. $\lim_{\zeta \rightarrow \pm\infty} \rho(\zeta) = \rho_\infty$ and $\lim_{\zeta \rightarrow \pm\infty} \phi(\zeta) = \pm\phi_\infty$ enables us to simplify the set of equations (10a) and (10b) to:

$$\left(\frac{\rho'}{2}\right)^2 + U(\rho) = 0 \quad (11a)$$

$$\phi' = v \left(1 - \frac{\rho_\infty}{\rho}\right), \quad (11b)$$

with $U(\rho)$ given by:

$$U(\rho) = (\rho - \rho_\infty)^2 \left[v^2 - \rho + \frac{2\rho(2\sqrt{\rho} + \sqrt{\rho_\infty})}{3(\sqrt{\rho} + \sqrt{\rho_\infty})^2} \right]. \quad (12)$$

We numerically³ solve (11a) for a given ρ_∞ and v first and then use it to solve (11b).

Figure 2 shows the density minimum $\min \rho(x, t = 0)$ and root mean square width $\sqrt{\langle x^2 \rangle}$ (assuming $\langle x \rangle = 0$) of the solitonic excitations as functions of the background density. One can distinguish three regions there: (i) unstable liquid, (ii) anomalous, and (iii) the standard one.

In the unstable region, when $\rho_\infty < \rho_{\text{ins}}$, even a small perturbation to a uniform density can cause violent dynamics in the system. Thus, it is no surprise that there are no solitonic solutions there.

Otherwise, when $\rho_{\text{ins}} < \rho_\infty < \rho_{\text{eq}}$, we are in the anomalous regime. The inequality fulfills the necessary condition for the existence of an anomalous soliton [32, 34], namely $0 < \rho_{\text{min}} < \rho_\infty < \rho_{\text{eq}}$ such that $U(\rho_{\text{min}}) = U(\rho_\infty) = 0$ and $U(\rho) < 0 \forall \rho_{\text{min}} \leq \rho \leq \rho_\infty$ as well as the stability of a uniform system, i.e. $c^2 > 0$. A motionless anomalous soliton is shown in the inset of figure 2(a). Its characteristic feature is a partial depletion of density even if the soliton is motionless ($\beta \equiv v/c = 0$). Another important property of the motionless soliton in the

³ In principle, it is possible to proceed with the analytical calculations. Nevertheless, the solution is very complex and does not give much insight into the problem.

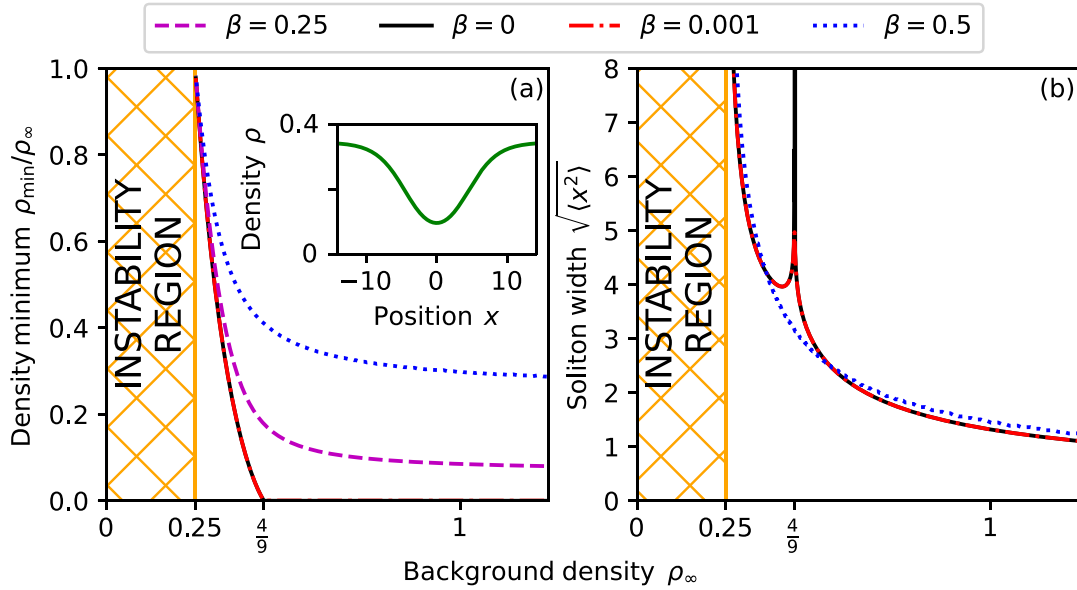


Figure 2. Dark soliton (a) density minima and (b) RMS widths as functions of the background density ρ_∞ for different relative velocities $\beta = \{0, 0.001, 0.25, 0.5\}$. Inset in (a): density profile of an anomalous soliton ($\beta = 0$ and $\rho_\infty = 0.345$). The solitonic properties of $\beta = 0.001$ will be important when we consider the coexistence of a quantum droplet and a dark soliton.

anomalous regime is a constant phase profile $\phi(\zeta; \beta = 0) = \text{const}$. The comparison of the properties of motionless solitons shows the most evident differences between the standard and anomalous regimes.

In the last regime, $\rho_\infty > \rho_{\text{eq}}$, the solitons have standard properties in terms of their density minimum and phase profile. Namely, the density of a black ($\beta = 0$) soliton reaches zero, and there is a typical π -jump in the phase.

As one can see in figure 2(b), the motionless solitons—both anomalous and standard ones—become ultrawide when $\rho_\infty \rightarrow \rho_{\text{eq}}$. It gives an opportunity to steer their size with the number of atoms in the system and interaction strengths $g_{\sigma\sigma'}$. The presence of arbitrarily wide solitons with a substantial density depletion in weakly interacting Bose–Bose mixtures is an opportunity for taking an *in situ* absorption image of a dark soliton in such systems.

It is worth mentioning the kink-type solitons described in [25] occur exactly at ρ_{eq} , i.e. $\lim_{\zeta \rightarrow \infty} \rho_{\text{kink}}(\zeta) = \rho_{\text{eq}}$ and $\lim_{\zeta \rightarrow -\infty} \rho_{\text{kink}}(\zeta) = 0$.

Another distinct property of the anomalous solitons, already described in [31], is the appearance of a subbranch in the dispersion relation. In figures 3(a) and (c), we present the relation of the renormalized⁴ energy [26]:

$$\mathcal{E} = \int_{-\infty}^{\infty} \left[\frac{1}{2} \left| \frac{d\psi}{d\zeta} \right|^2 + \frac{1}{2} (\rho_\infty - \rho)^2 - \frac{2}{3} \left(\rho^{3/2} - \frac{3}{2} \rho_\infty^{1/2} \rho + \frac{1}{2} \rho_\infty^{3/2} \right) \right] d\zeta \quad (13)$$

⁴ We need this renormalization to properly evaluate the difference in energy between the homogeneous profile and the one with a soliton. Namely, we have to compute it in a finite box and only then go to the thermodynamic limit.

and regularized momentum [35]:

$$\mathcal{P} = v \int_{-\infty}^{\infty} (\rho - \rho_\infty) d\zeta - 2\rho_\infty \phi_\infty. \quad (14)$$

Also, in this case, there is a violent change in the energy spectrum when we cross $\rho_\infty = 4/9$ from above and enter the anomalous region. Namely, an additional subbranch altogether with a cusp appears.

It makes the effective mass $m_{\text{eff}} = (d^2\mathcal{E}/d\mathcal{P}^2)^{-1}$ not properly defined due to the lack of derivative.

The stability analysis reveals another meaning of the two subbranches. The soliton is stable when $d\mathcal{P}/d\beta < 0$ [36]. In our case, this condition is fulfilled only for the lower branch of anomalous solitons. It means there is a critical velocity β_{cr} below which the anomalous soliton is unstable.

In figure 3(d) we show the stability criterion and see the solitons are stable only above a certain velocity β_{cr} , marked with a red circle. If we compare this picture with figure 3(c), the upper subbranch corresponds to solitons moving with $\beta \leq \beta_{\text{cr}}$ (also marked with a red circle). Thus, the upper branch is the unstable one.

On the other hand, standard solitons with $\rho_\infty > \rho_{\text{eq}}$, are always stable, which we can see in figure 3(b), namely $\beta_{\text{cr}} = 0$. On the anomalous side, when we approach the standard regime ($\rho_\infty \rightarrow \rho_{\text{eq}}^-$), we have $\beta_{\text{cr}} \rightarrow 0$, whereas while getting closer to the unstable one ($\rho_\infty \rightarrow \rho_{\text{ins}}^+$), $\beta_{\text{cr}} \rightarrow 1/2$, which we show in figure 4.

To give further evidence on the matter of the soliton stability, we numerically perform a BdG analysis of solitonic wave functions (see appendix B for technical details). The lowest-state eigenenergy ω indicates whether or not the soliton is stable. We extract the critical velocity by finding the soliton

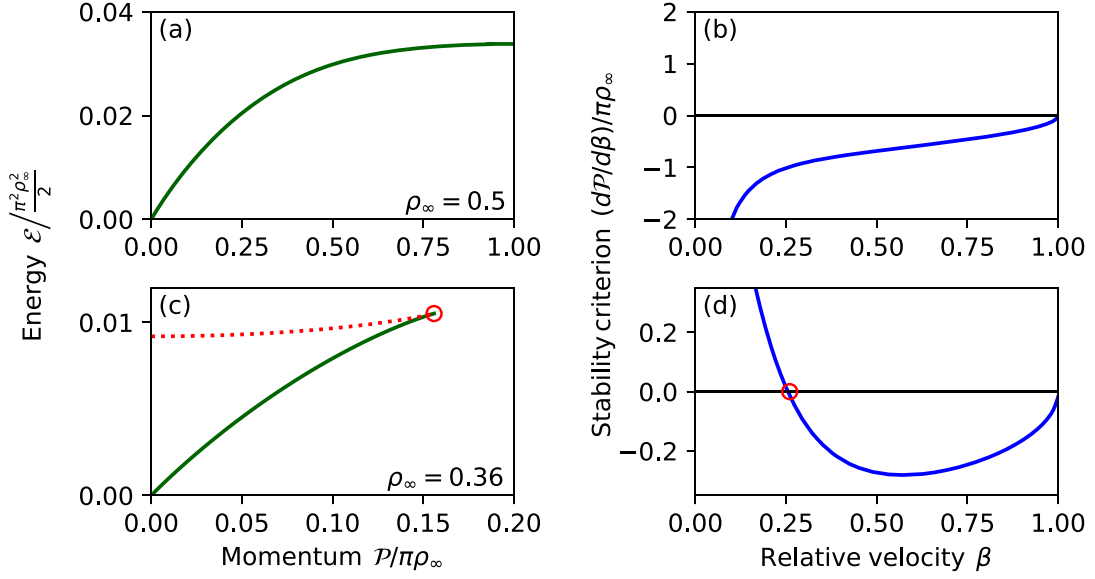


Figure 3. (a) and (c) Dispersion relation of solitons (standard—top row, anomalous—bottom row). The red dashed line shows the upper subbranch. (b) and (d) Soliton stability criterion. Solitons are stable when $d\mathcal{P}/d\beta < 0$. In the standard regime, the solitons are stable everywhere. In the anomalous one—only above the critical velocity, which in this case of $\rho_\infty = 0.36$ is numerically evaluated to be $\beta_{cr} = 0.2550(29)$. (Red circles in panels (c) and (d) mark the place where the velocity of solitons equals the critical velocity β_{cr} .)

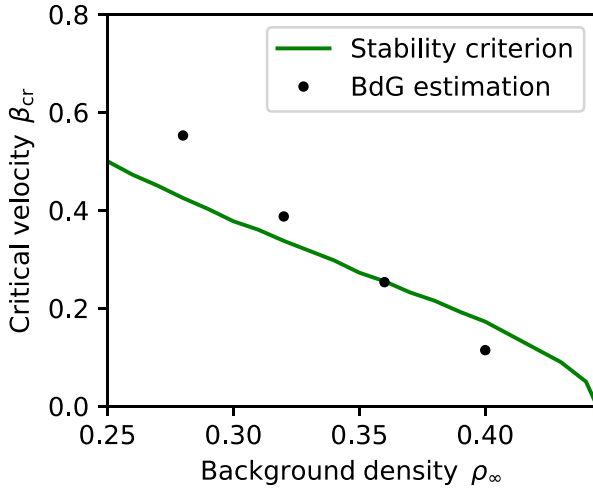


Figure 4. Critical velocity based on the stability criterion $d\mathcal{P}/d\beta < 0$ (solid green line) and its estimation based on the Bogoliubov–de Gennes analysis of solitonic wave function.

velocity for which the BdG eigenvalue becomes real. The results are qualitatively consistent with the analysis based on the stability criterion from [36] (see figure 4).

4. Dark soliton in a quantum droplet

The analysis of Bogoliubov excitations in quantum Bose–Bose droplets has revealed the presence of phonon modes [16]. We now check whether solitons are present in quantum droplets

as well. As the droplet is an inhomogeneous object, we use methods previously applied to trapped gases [37]. We describe this approach below.

We take the following solution for a quantum droplet [12]

$$\psi_{\text{QD}}(x) = \frac{\sqrt{\rho_{\text{eq}}\mu/\mu_{\text{eq}}}}{1 + \sqrt{1 - \mu/\mu_{\text{eq}}} \cosh(\sqrt{-2\mu}x)}, \quad (15)$$

where $\mu_{\text{eq}} = \rho_{\text{eq}} - \sqrt{\rho_{\text{eq}}}$ is the chemical potential corresponding to a homogeneous density profile with density $\rho = \rho_{\text{eq}}$ and the number of particles in the droplet N as a function of the chemical potential μ is given by [16]:

$$N = \rho_{\text{eq}} \sqrt{\frac{-2}{\mu_{\text{eq}}}} \left[\ln \left(\frac{1 + \sqrt{\mu/\mu_{\text{eq}}}}{\sqrt{1 - \mu/\mu_{\text{eq}}}} \right) - \sqrt{\mu/\mu_{\text{eq}}} \right]. \quad (16)$$

Next, we modify the droplet wave function in order to get a dark soliton inside it. We achieve it by simply multiplying (15) by the solitonic wave function $\psi(x) = \sqrt{\rho(x)}e^{i\phi(x)}$, where $\rho(x)$ and $\phi(x)$ are the solutions of equations (11a) and (11b) for $\rho_\infty = \max|\psi_{\text{QD}}(x)|^2$ and a given non-zero velocity $\beta \neq 0$. We will comment on the case $\beta = 0$ later. Then, we normalize the overall wave function $\psi(x)\psi_{\text{QD}}(x)$, impose periodic boundary conditions on the phase, and numerically evolve in real-time (see appendix A for more details).

Figure 5 shows us the results of these simulations. The initial density and phase profiles of a moving soliton inside a droplet are shown in figures 5(a) and (b) correspondingly.

The space-time diagram in figure 5(c) shows us how the anomalous moving soliton behaves in a quantum droplet. The dynamics are very stable. We do not see any phonons or shock waves appearing. The gray soliton in figure 5(c) indeed travels

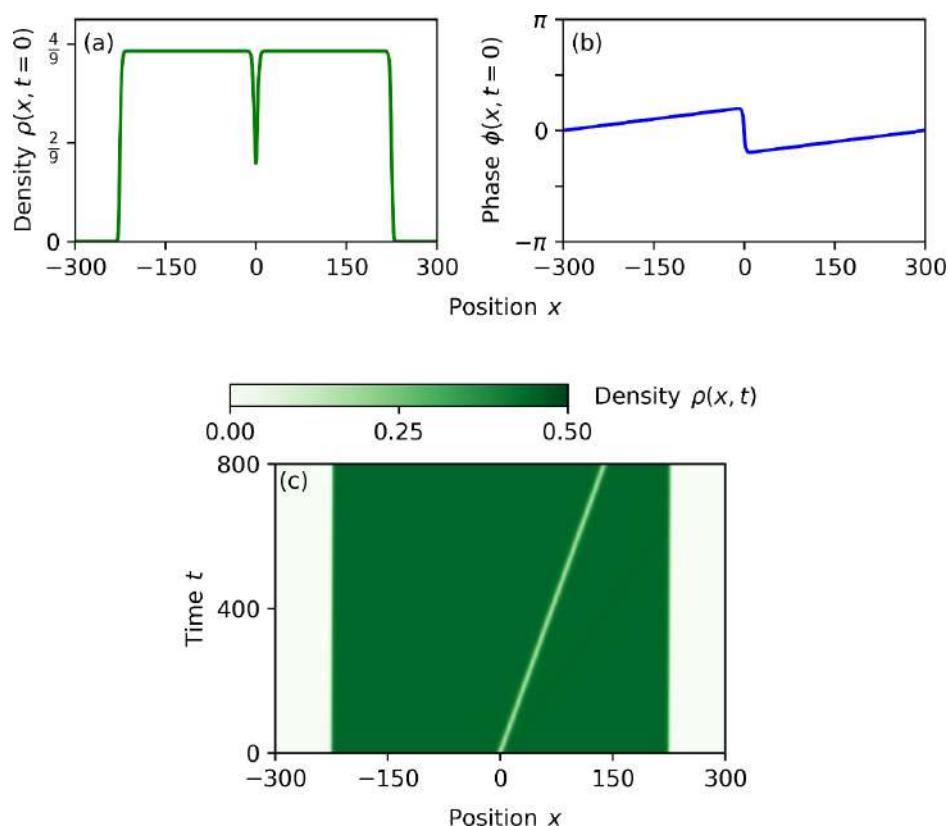


Figure 5. Dark soliton in a quantum droplet. Initial density (a) and phase (b) profiles as well as a space-time diagram of evolution (c) of a quantum droplet with a gray ($\beta = 0.5$) soliton inside. The number of particles in the system $N = 198.079$.

at $\beta = 0.5$. When the droplet bulk is much larger than the soliton width, one should be able to use (16) along with the solution of equations (11a) and (11b) to construct the wave function of a dark soliton-quantum droplet system.

Let us now return to the condition we made earlier about the non-zero soliton velocity. Are the motionless solitons not able to exist inside quantum droplets? According to our stability analysis, the motionless solitons are bound to be unstable. We emphasize, however, that one still can achieve very wide stable solitons inside quantum droplets having a small but finite velocity β (like the case of $\beta = 0.001$ shown in figure 2), as $\lim_{\rho_\infty \rightarrow \rho_{\text{eq}}^-} \beta_{\text{cr}} = 0$.

5. Conclusions

We have shown the basic properties of a single dark soliton in a weakly interacting Bose–Bose mixture. There are two types of solitons: standard and anomalous ones. The standard motionless solitons are black and have a π -jump in the phase, whereas the anomalous motionless ones do not have a fully depleted density nor a phase jump. In the anomalous regime, the solitons also have a peculiar dispersion relation with a cusp and subbranch. We found there is a critical velocity of the solitons β_{cr} , below which the solitons are unstable.

The stability analysis plays a crucial role in the possible experimental realization of solitons in quantum droplets. First, the unstable solitons will be suppressed in a potential experiment. Second, it is an opportunity to study the instability mechanism.

Our study disfavors the hypothesis that anomalous solitons are a beyond-LHY feature. Our observations [30, 31] are consistent with the condition for the presence of anomalous solitons [32, 34], where a preferred equilibrium density ρ_{eq} plays a key role in the existence of these objects.

Most importantly, we show that this uncanny type of solitons can exist inside a quantum droplet. According to our numerical simulations, the stable anomalous gray solitons might be experimentally observable in the droplets.

A theoretical study of multiple-soliton systems is a natural way to extend our research, especially if it goes for two-soliton interactions.

Data availability statement

The MUDGE toolkit is available under <https://gitlab.com/jakkop/mudge/-/releases/v03Apr2023>.

The data that support the findings of this study are openly available at the following URL/DOI: <https://doi.org/10.5281/zenodo.8427527>.

Acknowledgments

J K, B T, K P, and M Ł acknowledge support from the (Polish) National Science Center Grant No. 2019/34/E/ST2/00289.

We acknowledge the assistance from Center for Theoretical Physics of the Polish Academy of Sciences, which is a member of the National Laboratory of Atomic, Molecular, and Optical Physics (KL FAMO).

J K conducted the numerical simulations and analytical calculations with help from M Ł and W G; B T and J K performed the stability analysis of solitons. M Ł conceptualized the research and co-supervised it with K P; K P was responsible for project administration and acquisition of financial support. All authors took part in the discussion of the results. J K wrote the first draft of the manuscript with help from M Ł.

Appendix A. Numerical tools

We solve the GGP equation for a complex orbital $\psi(x)$ discretized on a spatial grid with N_x points and spacing $DX = L/N_x$. Parameter L is the box size. We use periodic boundary conditions by imposing $\psi(-L/2) = \psi(L/2)$ in every iteration. When we simulate dark solitons inside the droplet, we change the phase $\phi(x)$ to $\phi(x) + \frac{2\phi_\infty}{L}x$. The real-time evolution is done with the split-step method. The evolution with the kinetic term is done in the momentum domain, whereas the contact interaction term is calculated in the spatial domain. We do not use any external potential. The program MUDGE, written in C++ and implementing the algorithm above, is publicly available (see [Data availability](#) for link). The W-DATA format dedicated to storing data in numerical experiments with ultracold Bose and Fermi gases is used. The W-DATA project is a part of the W-SLDA toolkit [38].

Appendix B. Bogoliubov–de Gennes analysis of the solitonic profiles

In order to examine the stability of the solitonic solutions as in (9a), we linearize the dimensionless generalized Gross–Pitaevskii equation (3) using the following ansatz

$$\Phi(x, t) = [\Phi_0(x) + \delta\Phi(x, t)]e^{-i\mu t}, \quad (B1)$$

where $\Phi_0(x)$ is the solitonic wave function, obtained numerically from equations (11a) and (11b). We look for solutions having the form:

$$\delta\Phi(x, t) = u(x, t)e^{-i\omega t} + v^*(x, t)e^{i\omega t}. \quad (B2)$$

The linearization of (3) yields a set of equations that are formally equivalent to Bogoliubov–de Gennes equations:

$$\begin{pmatrix} \hat{h}(x) & \chi(x) \\ -\chi^*(x) & -\hat{h}(x) \end{pmatrix} \begin{pmatrix} u_n(x) \\ v_n(x) \end{pmatrix} = \omega_n \begin{pmatrix} u_n(x) \\ v_n(x) \end{pmatrix}. \quad (B3)$$

Here, $\hat{h}(x) = -\partial_x^2/2 - \mu + 2|\Phi_0(x)|^2 - \frac{3}{2}|\Phi_0(x)|$, and $\chi(x) = \Phi_0^2(x) - \frac{\Phi_0^3(x)}{2|\Phi_0(x)|}$. Note that the term $\Phi_0(x)$ should

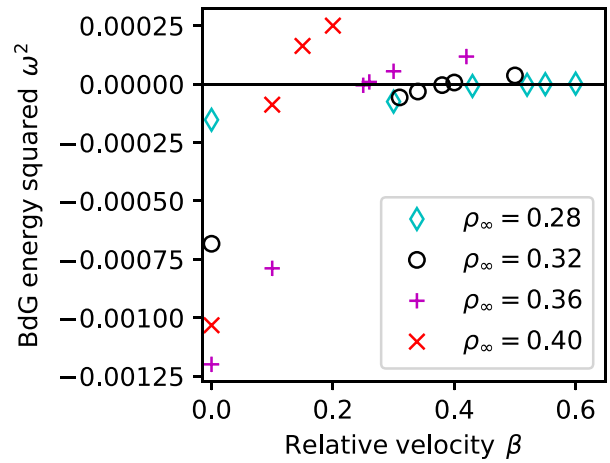


Figure 6. BdG energy squared ω^2 as a function of the soliton relative velocity for different background densities ρ_∞ .

be treated carefully due to the non-zero imaginary part of the solitonic wave function. The operator ∂_x^2 is evaluated using the discrete variable representation [39, 40]. The BdG Hamiltonian in (B3) is not Hermitian. Therefore, it may result in imaginary eigenvalues, which indicate instability. In figure 6, we examine lowest eigenvalues ω , as a function of soliton velocity for a series of different densities in order to estimate the transition from an unstable profile to a stable one; a negative value of ω^2 indicates the solitonic profile is unstable. It is worth noting the values obtained for $\beta = 0$ are consistent with [41].

The lack of quantitative agreement in figure 4 might be caused by the numerical imperfections, especially related to the numerical grid size. Here, we show results for a numerical grid with 2048 nodes, i.e. resulting in a 4096×4096 matrix to diagonalize. However, it is noteworthy to mention that the results obtained with grid sizes of 512 and 1024 nodes exhibited comparatively poorer performance. This suggests that the choice of a coarser grid significantly impacted the accuracy of the outcomes, reinforcing the importance of an appropriately refined numerical grid for obtaining more reliable numerical results. As the grid size increases, so does the dimension of the matrix that needs to be diagonalized. This relationship highlights that larger grids entail more complex computational processes due to the higher-dimensional nature of the underlying matrices. This seems to be the main limitation of our BdG analysis.

ORCID iDs

Jakub Kopyciński <https://orcid.org/0000-0002-7530-8945>
 Buğra Tüzemen <https://orcid.org/0000-0002-8619-754X>
 Wojciech Górecki <https://orcid.org/0000-0001-9912-9186>
 Krzysztof Pawłowski <https://orcid.org/0000-0001-6412-4457>
 Maciej Łebek <https://orcid.org/0000-0003-4858-2460>

References

- [1] Petrov D S 2015 *Phys. Rev. Lett.* **115** 155302
- [2] Cabrera C R, Tanzi L, Sanz J, Naylor B, Thomas P, Cheiney P and Tarruell L 2018 *Science* **359** 301
- [3] Cheiney P, Cabrera C R, Sanz J, Naylor B, Tanzi L and Tarruell L 2018 *Phys. Rev. Lett.* **120** 135301
- [4] Semeghini G, Ferioli G, Masi L, Mazzinghi C, Wolswijk L, Minardi F, Modugno M, Modugno G, Inguscio M and Fattori M 2018 *Phys. Rev. Lett.* **120** 235301
- [5] Ferioli G, Semeghini G, Masi L, Giusti G, Modugno G, Inguscio M, Gallemí A, Recati A and Fattori M 2019 *Phys. Rev. Lett.* **122** 090401
- [6] D'Errico C, Burchianti A, Prevedelli M, Salasnich L, Ancilotto F, Modugno M, Minardi F and Fort C 2019 *Phys. Rev. Res.* **1** 033155
- [7] Kadau H, Schmitt M, Wenzel M, Wink C, Maier T, Ferrier-Barbut I and Pfau T 2016 *Nature* **530** 194
- [8] Schmitt M, Wenzel M, Böttcher F, Ferrier-Barbut I and Pfau T 2016 *Nature* **539** 259
- [9] Ferrier-Barbut I, Kadau H, Schmitt M, Wenzel M and Pfau T 2016 *Phys. Rev. Lett.* **116** 215301
- [10] Lee T D and Yang C N 1957 *Phys. Rev.* **105** 1119
- [11] Lee T D, Huang K and Yang C N 1957 *Phys. Rev.* **106** 1135
- [12] Petrov D S and Astrakharchik G E 2016 *Phys. Rev. Lett.* **117** 100401
- [13] Parisi L, Astrakharchik G E and Giorgini S 2019 *Phys. Rev. Lett.* **122** 105302
- [14] Astrakharchik G E and Malomed B A 2018 *Phys. Rev. A* **98** 013631
- [15] Luo Z-H, Pang W, Liu B, Li Y-Y and Malomed B A 2020 *Front. Phys.* **16** 32201
- [16] Tylutki M, Astrakharchik G E, Malomed B A and Petrov D S 2020 *Phys. Rev. A* **101** 051601
- [17] Parisi L and Giorgini S 2020 *Phys. Rev. A* **102** 023318
- [18] Flynn T A, Parisi L, Billam T P and Parker N G 2023 *Phys. Rev. Res.* **5** 033167
- [19] Flynn T A, Keeper N A, Parker N G and Billam T P 2023 Trapped imbalanced quantum droplets (arXiv:2309.04300 [cond-mat.quant-gas])
- [20] Liu X and Zeng J 2022 *Chaos Solitons Fractals* **160** 112240
- [21] Stürmer P, Tengstrand M N and Reimann S M 2022 *Phys. Rev. Res.* **4** 043182
- [22] Yan D, Tsitoura F, Kevrekidis P G and Frantzeskakis D J 2015 *Phys. Rev. A* **91** 023619
- [23] Kevrekidis P and Frantzeskakis D 2016 *Rev. Phys.* **1** 140
- [24] Adhikari S K 2014 *Phys. Rev. A* **89** 043615
- [25] Shukla A, Neeraj and Panigrahi P K 2021 *J. Phys. B: At. Mol. Opt. Phys.* **54** 165301
- [26] Edmonds M 2023 *Phys. Rev. Res.* **5** 023175
- [27] Katsimiga G C, Mistakidis S I, Koutsokostas G N, Frantzeskakis D J, Carretero-González R and Kevrekidis P G 2023 *Phys. Rev. A* **107** 063308
- [28] Jackson A D, Kavoulakis G M and Pethick C J 1998 *Phys. Rev. A* **58** 2417
- [29] Sato J, Kanamoto R, Kaminishi E and Deguchi T 2016 *New J. Phys.* **18** 075008
- [30] Kopyciński J, Parisi L, Parker N G and Pawłowski K 2023 *Phys. Rev. Res.* **5** 023050
- [31] Kopyciński J, Lebek M, Górecki W and Pawłowski K 2023 *Phys. Rev. Lett.* **130** 043401
- [32] Berestycki H and Lions P L 1983 *Arch. Ration. Mech. Anal.* **82** 313
- [33] Pitaevskii L and Stringari S 2016 *Bose-Einstein Condensation and Superfluidity* (Oxford University Press)
- [34] Lin Z 2002 *Adv. Differ. Equ.* **7** 897
- [35] Kivshar Y S and Luther-Davies B 1998 *Phys. Rep.* **298** 81
- [36] Barashenkov I, Gocheva A, Makhankov V and Puzynin I 1989 *Physica D* **34** 240
- [37] Parker N G, Proukakis N P and Adams C S 2010 *Phys. Rev. A* **81** 033606
- [38] Nuclear Theory Group, Warsaw University of Technology 2020 W-SLDA toolkit (available at: <https://wslda.fizyka.pw.edu.pl/>)
- [39] Bulgac A and Forbes M M 2013 *Phys. Rev. C* **87** 051301
- [40] Jin S, Roche K J, Stetcu I, Abdurrahman I and Bulgac A 2021 *Comput. Phys. Commun.* **269** 108130
- [41] Katsimiga G C, Mistakidis S I, Malomed B A, Frantzeskakis D J, Carretero-Gonzalez R and Kevrekidis P G 2023 *Condens. Matter* **8** 67

COMPLETE LIST OF PHD CANDIDATE'S PUBLICATIONS

- [J. Kopyciński](#), W.R. Pudełko, and G. Wlazłowski, Vortex lattice in spin-imbalanced unitary Fermi gas, *Phys. Rev. A* **104**, 053322 (2021).
- [J. Kopyciński](#), M. Łebek, M. Marciniak, R. Ołdziejewski, W. Górecki, and K. Pawłowski, Beyond Gross-Pitaevskii equation for 1D gas: quasiparticles and solitons, *SciPost Phys.* **12**, 023 (2022).
- K. Fornalski, Ł. Adamowski, E. Bugała, R. Jarmakiewicz, M. Kirejczyk, [J. Kopyciński](#), J. Krasowska, P. Kukulski, Ł. Piotrowski, J. Ponikowska, J. Reszczyńska, I. Słonecka, P. Wysocki, and L. Dobrzyński, Biophysical modeling of the ionizing radiation influence on cells using the stochastic (Monte Carlo) and deterministic (analytical) approaches, *Dose-Response* **20**, 4 (2022).
- [J. Kopyciński](#), M. Łebek, W. Górecki, and K. Pawłowski, Ultrawide dark solitons and droplet-soliton coexistence in a dipolar Bose gas with strong contact interactions, *Phys. Rev. Lett.* **130**, 043401 (2023).
- [J. Kopyciński](#), L. Parisi, N.G. Parker, and K. Pawłowski, Quantum Monte Carlo-based density functional for one-dimensional Bose-Bose mixtures, *Phys. Rev. Res.* **5**, 023050 (2023).
- M. Marciniak, M. Łebek, [J. Kopyciński](#), W. Górecki, R. Ołdziejewski, and K. Pawłowski, Super-Tonks-Girardeau quench in the extended Bose-Hubbard model, *Phys. Rev. A* **108**, 043304 (2023).
- [J. Kopyciński](#), B. Tüzemen, W. Górecki, K. Pawłowski, and M. Łebek, Propagation properties and stability of dark solitons in weakly interacting Bose-Bose droplets, *J. Phys. B: At. Mol. Opt. Phys.* **57** 035302 (2024).
- M. Łebek, [J. Kopyciński](#), W. Górecki, R. Ołdziejewski, and K. Pawłowski, Elementary excitations of dipolar Tonks-Girardeau droplets, [arXiv:2209.01887](#).